Fire-exposed Hyperstatic Concrete Structures - An Experimental and Theoretical Study

Anderberg, Yngve

1976

LUND INSTITUTE OF TECHNOLOGY · LUND · SWEDEN · 1976
DIVISION OF STRUCTURAL MECHANICS AND CONCRETE CONSTRUCTION · BULLETIN 55

YNGVE ANDERBERG

FIRE-EXPOSED HYPERSTATIC CONCRETE STRUCTURES – AN EXPERIMENTAL AND THEORETICAL STUDY

LUND INSTITUTE OF TECHNOLOGY LUND SWEDEN 1976

DIVISION OF STRUCTURAL MECHANICS AND CONCRETE CONSTRUCTION

FIRE-EXPOSED HYPERSTATIC CONCRETE STRUCTURES - AN EXPERIMENTAL AND THEORETICAL STUDY

YNGVE ANDERBERG

LUND, AUGUST 1976

To ANITA,
NIKLAS and JESPER

CONTENTS

ACKNOWLEDGEMENTS

This paper is the final report from a research project sponsored by the Swedish Council of Building Research. The author wants to thank the Council for this support.

The author wishes to thank Professor Ove Pettersson, head of the Division of Structural Mechanics and Concrete Construction, for giving valuable views and encouraging support. Thanks are furthermore due to the whole staff of the division and in particular

Kjell Andersson, Lennart Andersson, Karl-Erik Bohlin, Sven-Ingvar Granemark, Bengt Götesson, Hans-Erik Ernstsson, Bengt Hjort, Ingvar Nohlin, Svante Bernow, Rolf Kristoffersson and Björn Paulsson for all practical help and assistance in connection to the performance of the tests,

Sven Strandberg and Ulf Wickström for assistance in making up the temperature calculating program,

Sven Norén at Lund Computer Center for converting the "Fires-RC" program and assistance in constructing a modified and extended version of the program,

Bo Zadig for skillful drawing,

Christina Norlin for her efficient typing of the manuscript, and

Lisbeth Henning for checking the English language of the manuscript.

1 INTRODUCTION

Experimental investigations, published in literature, of fire-exposed, reinforced and prestressed concrete structures all-pervadingly have been limited to fixed heating conditions according to standard fire resistance tests, ISO 834 (1975). Additionally the effect of cooling, which follows a heating phase is ignored and the objective of the experiments primarily has been a determination of the fire resistance, fire resistance time. In some cases a complementary ascertainment of the residual load-carrying capacity after fire is also done. In a very dominating extent the investigations are carried out at statically determinate support conditions.

However, during the recent years there has been a growing interest in a more thorough study of the mechanical behaviour and load-carrying capacity of structures thermally exposed, including hyperstatic structures. Among theoretical works the following ought to be mentioned: Saito (1968), Issen & Gustaferro (1970), Haksever (1975) and Klingsch (1975). Examples of standard fire resistance tests for hyperstatic concrete structures are given in Selvaggio & Carlson (1963 and 1967), Carlson et al (1965), Ehm & von Postel (1965), Gustaferro (1970), Gustaferro et al (1971) and Salse & Gustaferro (1971).

At present, in several countries, a development of design codes and regulations takes place, which leads towards an increased degree of functionally based requirements and performance criteria. This trend gives a high priority to a development of differentiated systems for a fire engineering design, based on a real, complete process of a fire development. The fire process is varying with the combustion characteristics of the fire load and the geometrical, ventilation and thermal properties of the fire compartment (Magnusson & Thelandersson (1970, 71 and 74), Harmathy (1972), Thomas (1976)). The condition precedent for such a development leading to rational and practical design methods is among other things a thorough understanding of the mechanical behaviour of structures during a whole fire process, comprising a heating and a subsequent cooling phase. Consequently, the goal

has to be analytical models for a realistic prediction of a complete structural behaviour and load-carrying capacity at different fire exposures. The models also have to be verified by experimental investigations, carried out during well-defined test conditions. If the goal is attained it decreases the need of extensive and expensive fire testings for the benefit of analytical predictions of structural response.

Any experimental studies of reinforced and prestressed concrete structures at fire - in addition to an investigation presented by the author (Anderberg (1973)) - have not been accounted for as regards the influence of practically representative fire processes. The experimental investigation reported and analyzed in the present publication is the first one of its kind. Furthermore it includes the earlier study accounted for by the author in Anderberg (1973). In another aspect the investigation is also original i.e. the structural behaviour is followed up to the residual state after cooling with respect to residual stresses and deformations, residual load-carrying capacity and flexural stiffness.

The experimental investigation is performed with regard to support conditions, for a pure type of hyperstatic structure and comprises a continuous registration of temperature-gradients, deformations, cracking formations and restraint bending moments. These measurements are carried through at a fire-exposure merely and at a combined influence of a fire and external transverse load respectively. The experimental part of the project is directly coupled to a comprehensive theoretical analysis, which comprises an evaluation of thermal and structural response of the current structure. The study of structural behaviour is based on a computer model, which can be described as a modification and further development of a model, constructed at University of California, Berkeley, for a response analysis of reinforced concrete frames in fire environments (Becker & Bresler 1974)). The most profound, new contribution to the computer model constitutes a material behaviour model of concrete valid at transient high-temperature conditions, which is recently developed in Anderberg & Thelandersson (1976). Material behaviour models of concrete

applied and accounted for earlier in literature are incomplete for use in a fire engineering design as they are based on test data obtained in high-temperature tests at steady state of load and temperature. Consequently, the new material behaviour model functionally gives a more correct description of the mechanical behaviour of fire-exposed concrete. Thus it also improves the prospects for realistic fire engineering designs not only for the structure dealt with here but also for other types of concrete structures.

2 OBJECTIVE OF THE RESEARCH PROJECT

On this general background, the main goal of the project is to derive analytical models and connected computer programs. The programs will have the capability of predicting the thermal and structural behaviour and the load-carrying capacity of hyperstatic, continuous beams and frames of reinforced concrete subjected to fire. For a verification of the analytical models with respect to the thermal and mechanical response of the fire-exposed structures, the project also contains an extensive experimental investigation. It embraces a great number of tests carried out for different fire exposure characteristics and different levels of external static load.

The experimental part of the project is mainly focused on a fundamental study of an extremely pure type of hyperstatic structure, viz. a reinforced concrete plate strip, thermally exposed on one side and restrained against rotation at both ends, with axial displacement is free to take place. The investigation is planned to give a comprehensive survey of the behaviour and load-carrying capacity of the structure during a complete fire process. It also includes a determination of the residual state with regard to stresses, deformations, load-carrying capacity and bending stiffness after fire. The investigation further covers, in a systematic manner, a wide, practically representative variation in the fire process, external load level, concrete composition and age of the specimen at testing. The laboratory tests were carried out by Anderberg et al (1969) and in three graduate thesis (Denker et al (1970), Erntsson et al (1971) and Bernow et al (1972)) under the supervision of the author.

The outline of the research project is based on the principles of a functionally based, analytical design procedure for fire-exposed, load-carrying and separating structures (Pettersson (1971), Pettersson (1973), Magnusson et al (1974), Anderberg et al (1974) and FIP/CEB (1975)). Such a design procedure refers to performance criteria and postulates that the real physical processes with respect to fire exposure, heat transfer and structural behaviour are predictable as far as possible.

A description of the test arrangement is given in the next section which then is followed by a presentation of the experimental program in section 4. The results from laboratory tests comprising temperature measurements and observed structural behaviour are accounted for and analyzed in section 5. The scope of test data is very great and therefore it cannot be accounted for in detail. However, a complete collection of these are available and can be requested from the author. The theoretical study divided into a thermal and a structural behaviour analysis including comparisons with test results is described in section 6. Complete material behaviour models of concrete and steel utilized in the computations are also given within this section. In section 7 a very brief proposal of theoretical design of fire-exposed concrete structures is made. Finally a summary and conclusions are presented. Furthermore an Appendix is embraced as a supplement to the publication. The Appendix contains further illustrations and diagrams.

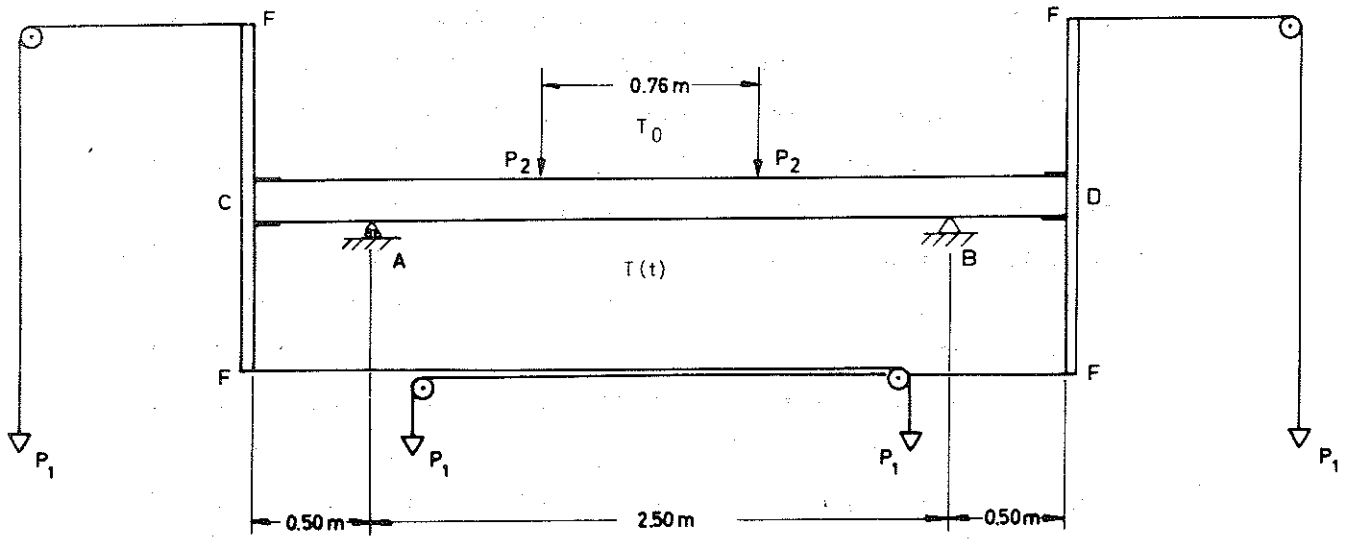

Figure 3.1 Principals of test arrangement.

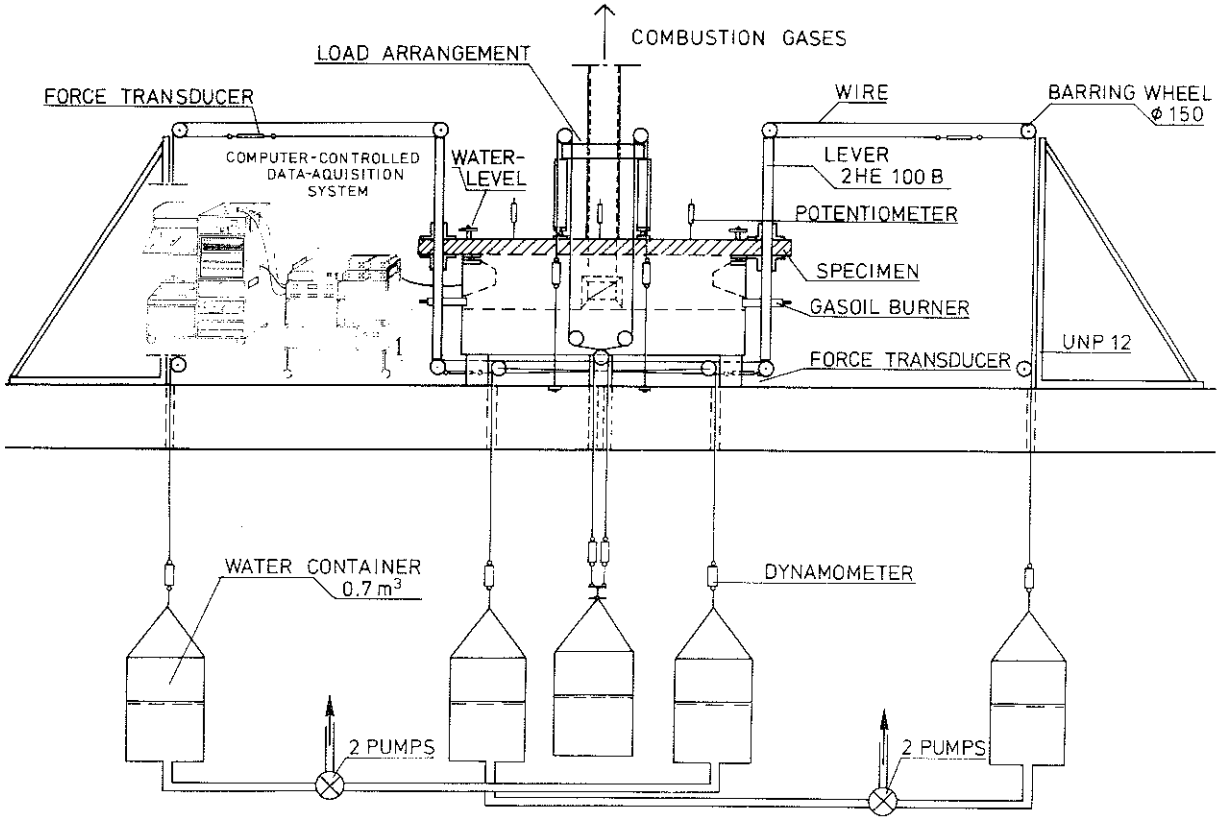

Figure 3.2 The complete testing equipment.

3 TEST ARRANGEMENT

The principal form and function of the testing facilities are shown in Fig. 3.1 and Fig. 3.2. The tests were performed for reinforced concrete plate strips which were symmetrically located on a horizontal roller-bearing at A and a hinge support at B and supplied with cantilevers AC and BD (Fig. 3.1). The plate strips were exposed to fire from below within the area AB through a gas burner system in a furnace whose longitudinal upper wall edge approximately coincided with the upper surface of the plate strips. The supports of the plate strips were directly placed against the short walls of the furnace. The prescribed degree of restraint against rotation on the supports A and B was realized by applying concentrated bending moments on the cantilever ends C and D through couples of concentrated forces P_1, introduced by means of loaded wires, fastened to the lever arms FF. During the experiment, these cantilever moments were continuously varied such as to maintain the rotation at the supports A and B at zero value, controlled by water levels which were located over the support. In three of the test series (A, B and C) the fire behaviour of the plate strips were examined without any external transverse load acting upon the strips. In a fourth test series (D), the plate strips were simultaneously exposed to a fire process and a constant transverse load, applied in the form of two symmetrically located concentrated loads P according to Fig. 3.1. Fig. 3.2 gives a more detailed description of the complete testing equipment. The experiments were computer-controlled as regards all measurements and a data-acquisition system collected all test data.

3.1 Heating arrangement

The furnace, used in the test series, is built of refractory bricks giving a wall thickness of 31 cm and externally covered by sheet-metal as protection against external wear. The detailed design of the furnace is illustrated in Fig. 3.3.

The heating of the furnace is produced by a gasoil burner system with one burner applied through an opening on each short side of

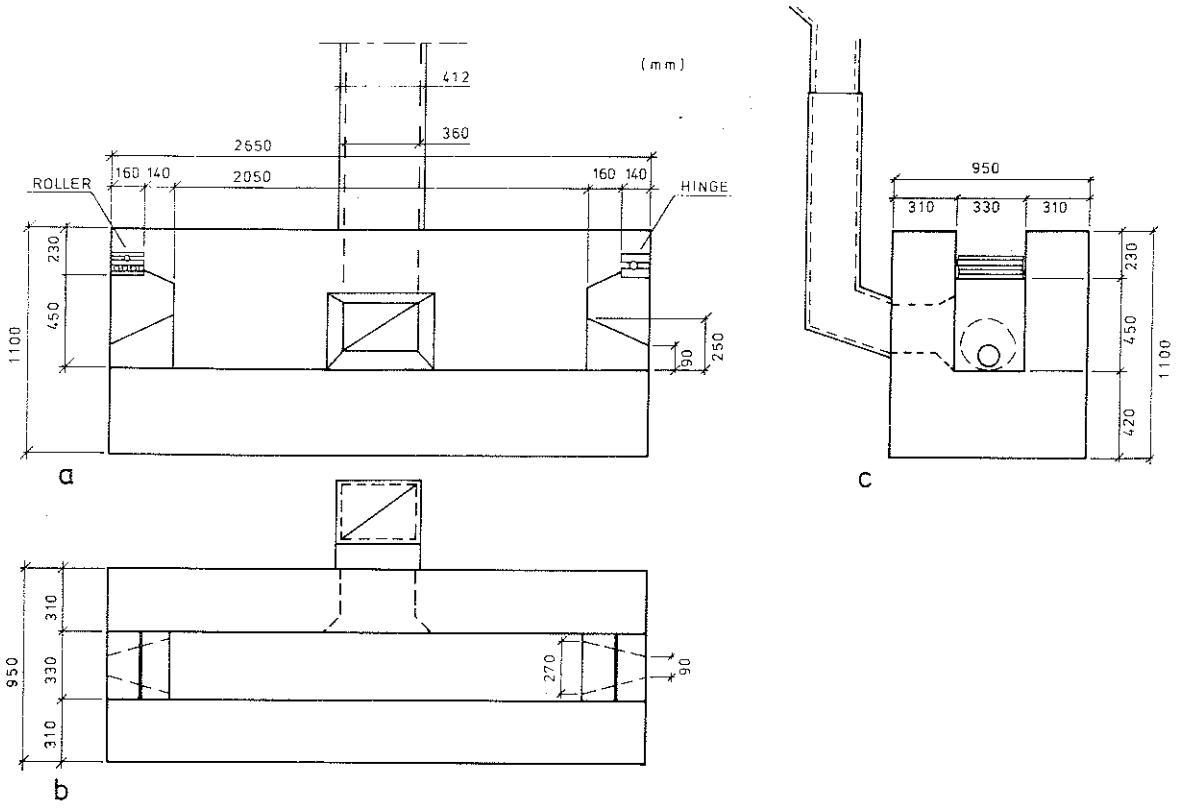

Figure 3.3 The furnace seen in three sections, viz.
a) from the long side
b) from above
c) from the short side

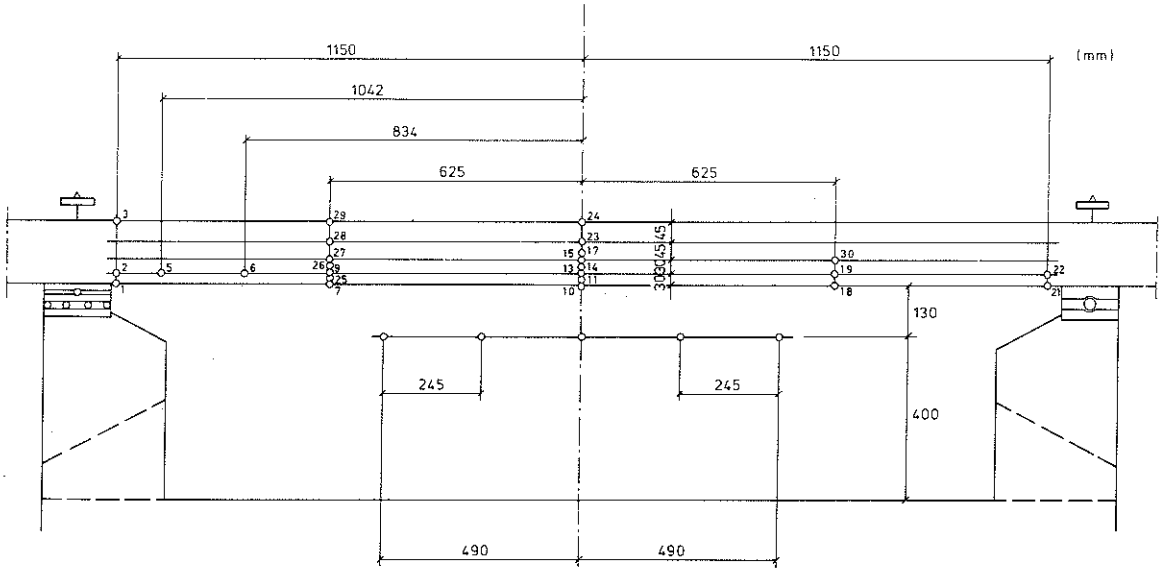

Figure 3.4 Location of thermocouples inside the furnace and the concrete plate strip.

the furnace. The burners are specially manufactured for this purpose by the Oil Consumers (OK). The maximum capacity of the burners amounts to 7 - 8 l gasoil/min, and 1 l gas corresponds to an effective heat value of 25 kJ. The gas pressure, ordinarily used, is about 0.1 MPa. The gas and air supply of the burners is controlled by a regulating system and adjustable within a wide range. The combustion products are exhausted through a chimney, setting out from one of the long sides of the furnace and discharging into the open air. By continuously adjusting the air supply of the burners and the cross sectional area of the chimney, a prescribed temperature-time curve of the furnace can be followed satisfactorily. A representative illustration of how close the measured furnace temperatures follow the prescribed curve is furthermore given in Fig. 5.2.

For fire processes with a very high or a very slow rate of heating, a risk of a sudden temperature fall of short duration was found. It was due to the fact that a burner may become extinguished by pressure changes in the furnace. Such a temperature fall could last for some minutes and may in some cases have an appreciable influence on the testing process. In the intermediate range of heating rate, most commonly used in the test series, the burners proved to operate quite satisfactorily. The furnace temperature was recorded by the data-acquisition system and measured by 5 thermocouples (4, 20, 8, 16 and 12) of chromel-alumel-type placed in kanthal pyrometer conduits. These were located in the longitudinal symmetrical section of the furnace according to Fig. 3.4. The response time of the thermocouples in the furnace is discussed in section 5.2. The design characteristics of the furnace and the location of the burners and the chimney opening rendered the highest furnace temperature within a centre region between the thermocouples 16 and 20. This region was selected as reference for regulating the furnace temperature according to the prescribed temperature-time curve. The reference temperature was defined as the mean value of the three thermocouples 20, 8 and 16. From this region the temperature decreases somewhat towards the short sides of the furnace. An example of the temperature distribution inside the furnace is given in Fig. 5.3 for the test A2:5.

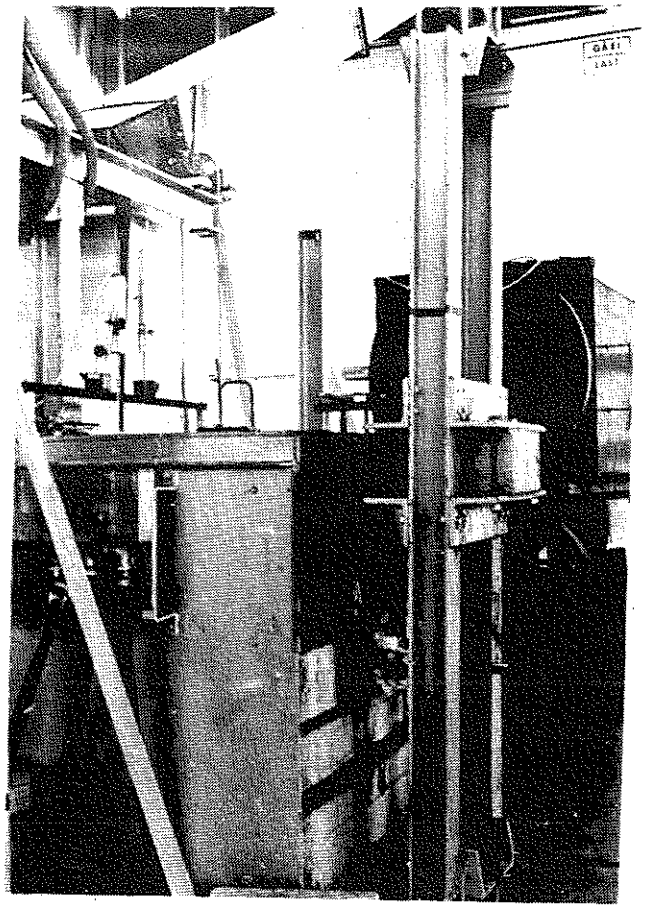

Figure 3.5 The arrangement of applying end restraint.

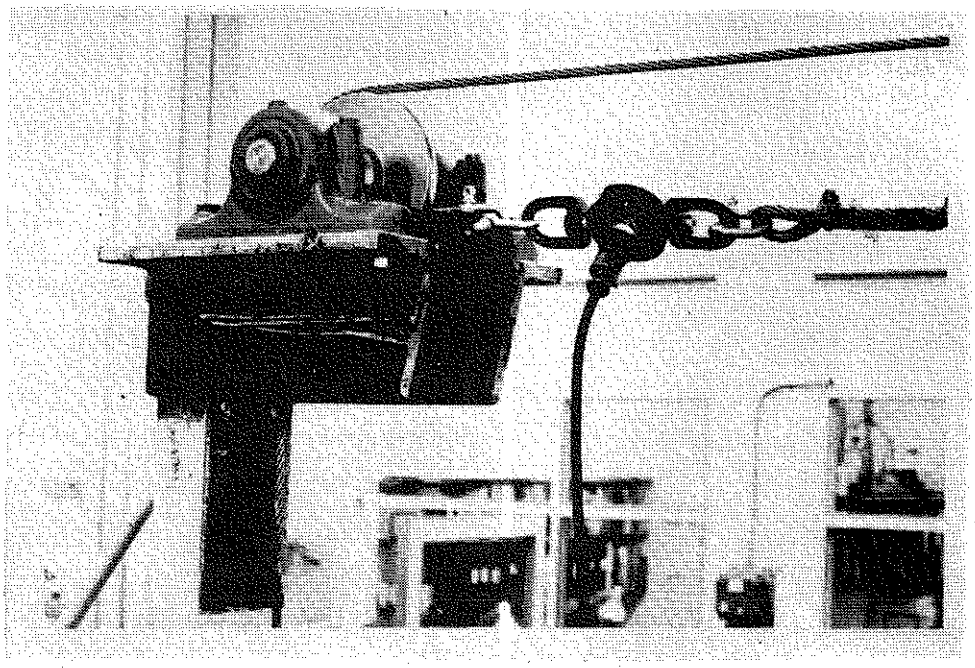

Figure 3.6 Assemblage of pulleys.

3.2 Arrangement for end restraint

In order to simulate fixed-end conditions with respect to rotation without preventing the elongation of the test specimens, levers are used, attached to the cantilever ends of the plate strips, as shown in Fig. 3.1 and Fig. 3.2. Each lever is 2.25 m long and consists of two I-beam sections (HE 100 B), threaded over the cantilever ends of the plate strip and clamped to this by means of four angle profiles (L 120) according to Fig. 3.5. A porous pad was placed between the plate strip and each angle profile in order to achieve a more uniform load transmission. As shown in Fig. 3.1 and Fig. 3.2, the couples of forces P_1, producing the cantilever bending moments, were applied through wires fastened to the ends of the levers. These wires lead over pulleys and through holes in the floor deck to the basement where they are connected to four water containers of 0.7 m^3 capacity each, serving as weights. The detailed assemblage of the pulleys is shown in Fig. 3.6, from which it is to be observed that the pulleys are firmly locked around an axis with pivoted ends, which are placed in a ball bearing cup that reduces the friction a maximum value of only 0.05 kN per pulley, which was considered acceptable for the present investigation. The final choice of the detailed pulley design was preceded by a series of loading tests for various design characteristics in order to study the different factors influencing the magnitude of friction, viz. the cross sectional area of the wire, the size of the pulley and the length of the pulley axis.

The wire forces P_1 were applied by filling the containers with water, through connected rubber tubes, to a lever, giving the required fixed-end conditions of the plate strip. The filling could be adjusted by four taps, one for each container, located nearby the furnace. Emptying of the containers is achieved by four pumps, with an individual capacity of 55 l/min. In order to obtain equal loads in the wires connected to the same lever, assuring that no longitudinal forces are introduced on the plate strip, the containers are communicating with each other two by two.

The wire forces P_1 were measured by electrical loading cells with

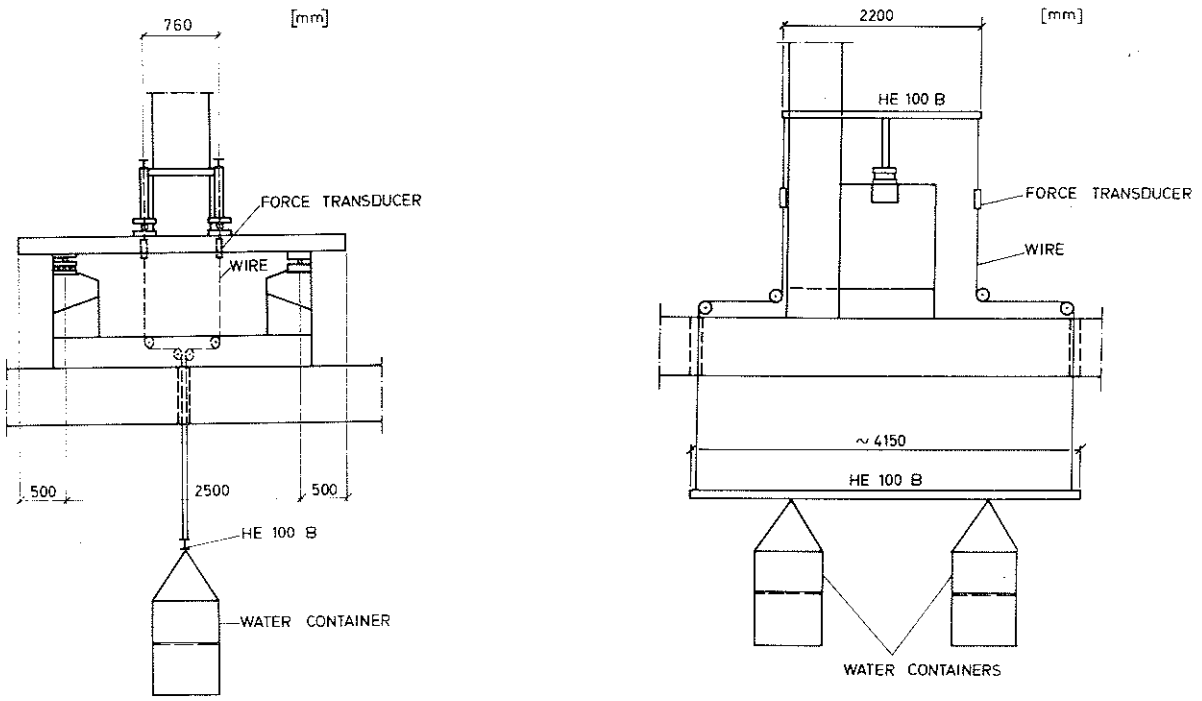

Figure 3.7 Equipment for applying lateral loading in two sections, viz.
a) through the short side of the furnace
b) through the long side of the furnace.

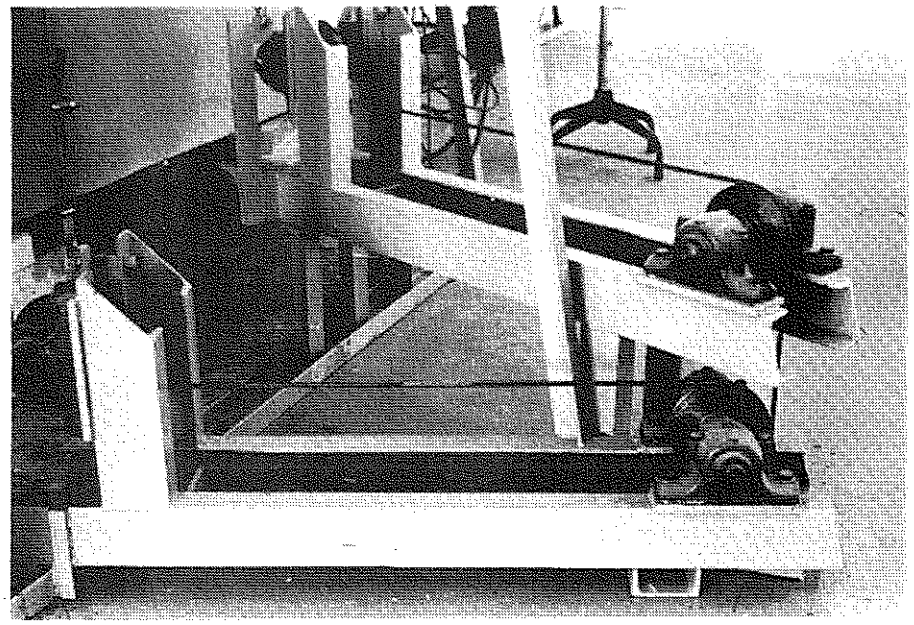

Figure 3.8 Detail of external load arrangement.

a direct registration by the data-acquisition system. For control purposes, complementary measurements were made with gauge-indicators, type KRG-4, from Bofors.

In certain cases, the restraint bending moment changes its direction during the cooling phase of the fire process. In order to enable a measurement of the restraint moment during a complete fire process also at such circumstances, an arrangement is required to reverse the direction of the lever forces P_1. For this purpose a special switching arrangement has been designed.

The fulfilment of the fixed-end conditions during the test was controlled by two water levels placed at each support section, fastened via T-profiles in the plate strip. Two parallel water levels at each support then enabled a control of a possible warping of the plate strip. This control system does not function, if a crack formation takes place during the test in a support section of the plate strip. To cope with this problem and to assure further precision, also a third water level was placed just outside each support section. This finally adopted procedure was developed after a series of less successful experiments, using other alternative arrangements for the control of prevented end rotation.

3.3 Arrangement for lateral load

Fig. 3.7 illustrates the basic equipment, used in series D, for the application of the symmetrically placed vertical loads P, shown schematically in Fig. 3.1. The arrangement consists of a loading yoke built up by means of steel beams (HE 100 B). The load is applied through wires, fastened to the loading yoke, which are passing over pulleys (Fig. 3.8) and continuing through holes in the floor deck to the basement, where they are attached to a horizontal steel beam (HE 100 B), on which an arbitrary load can be applied, for instance, in the form of a water container system (Fig. 3.7). To this load the dead weight of the load-transmitter construction, which amounts to a total of 2.3 kN, is added.

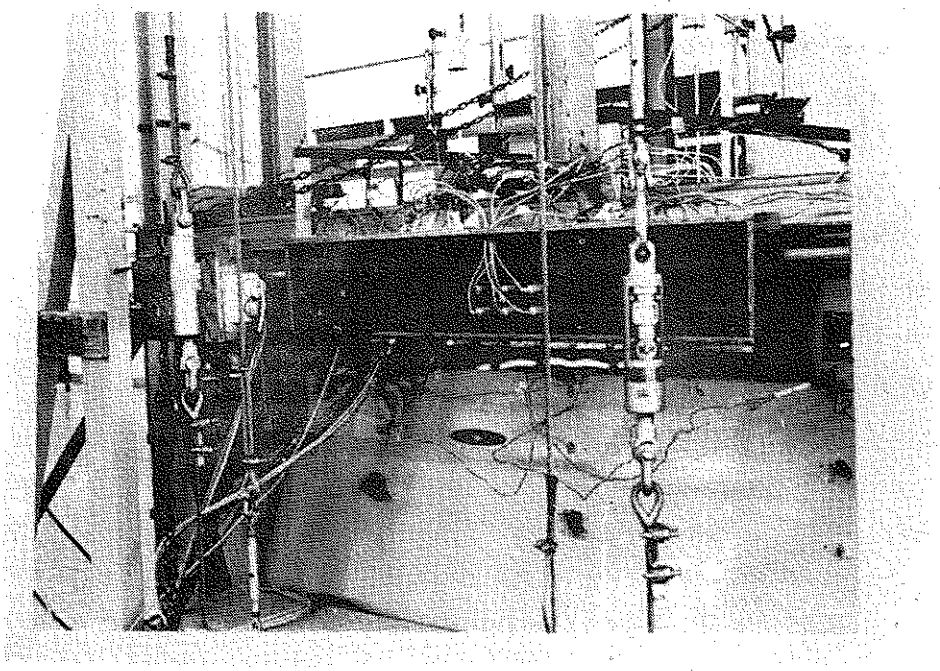

Figure 3.9 Connection box for measurements.

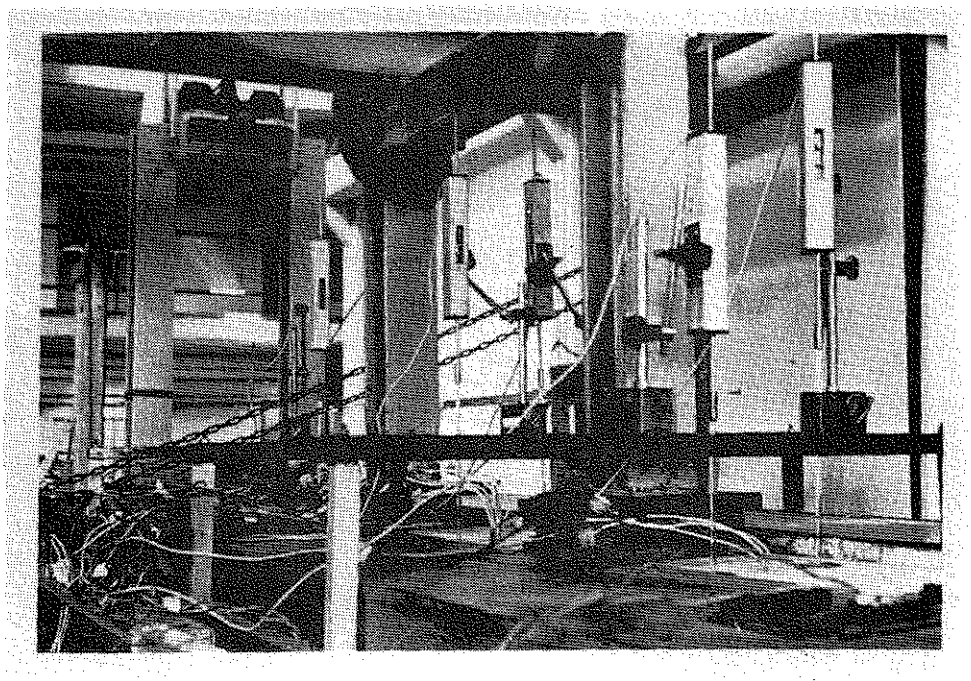

Figure 3.10 View of applicated potentiometers measuring deflections at mid- and 1/4-sections of the plate strip.

3.4 Registration of measurements

A computer-controlled data-acquisition system (Fig. 3.2) with a capacity of 200 channels was used in order to automatically and continuously collect all the test data from the different types of measurements. Test data were obtained from

themocouples, giving the temperature distribution within the furnace and the plate strip

potentiometers, giving the deflections

force transducers, rendering the lever forces which are determining the restraint bending moments.

At the front side of the furnace a connection box (Fig. 3.9) is located, to which 30 thermocouples, 6 potentiometers and 4 force transducers can be connnected. From this connection box, four gold-plate plugs are directly coupled to the scanner unit of the data-logging system. Three of these plugs, used for temperature measurements, contain 10 channels each, and the fourth plug contains 6+4 channels for deflection and force measurements, respectively.

The distribution of the furnace temperature was determined according to section 3.1. The temperature-time fields of the fire exposed plate strips were measured by 25 chromel-alumel thermocouples, located in the plate strips in accordance to Fig. 3.4. These thermocouples rendered the temperature gradients in the mid-, 1/4- and end-sections of the plate strips as well as the temperature distribution along the strip at different depths. The thermocouples, nubered 25 - 30, were only used in the last part of the investigation, embracing 14 tests. The response time of these thermocouples are also discussed in section 5.2.

The deflections were determined by 6 potentiometers, applicated two by two to the mid-span and the two 1/4-sections, as indicated in Fig. 3.10. These twin measurements were used for controlling any possible warping of the plate strips. In order to preserve the accuracy of the potentiometers (precision 0.05 mm) it was necessary to protect them from heat transfer and vapour diffusion from the

plate strips. This was achieved by inserting 0.25 m long quartz-rods between the upper surface of the plate strips and the mechanical stroke of the potentiometers and by installing a fan for cooling.

The restraint moment was determined indirectly by measuring the wire forces P_1 by force transducers (precision 0.2 kN) attached to the 4 wires for the levers (Fig. 3.5).

The registration of the different measurements was carried out at prescribed times, regulated by an external digital clock connected to the computer- controlled system. The computer program was so constructed that, some seconds after each recording, selected results were printed out on the teletype in order that the furnace temperature and the behaviour process in general could be followed intermittently. In conjunction with the printing, the complete results were punched in order to facilitate a subsequent computer analysis.

3.5 Computer and data-acquisition system

During the last part of the investigation, which embraces 14 tests, a computer-controlled data-acquistition system was available and therefore incorporated in the tests. These facilities are illustrated in FIg. 3.11, which shows the Hewlett-Packard computer and the data-logging system, containing scanner with scanner control and multifunctionmeter "DVM" and signal conditioning unit "SCU", and the units such as tape punch Facit 4070, optical high-speed punched tape reader and teletype. Some data about the different units are as follows.

Computer: Hewlett-Packard 2114 A
8.000 words 16 bits
(later 2116 C with 16 K words memory)

Software: Available languages are assembler, basic, algol and fortran.

Handware: Data acquisition system: Hewlett-Packard 2321 A

Scanner: Scanner control: 200 channels, speed = 10 channels/s and a resolution of 1 μ V

DVM multifunctionmeter: five full digits 20% overrange

Tapepunch: Facit 4070, 75 characters/s

Optical high-speed punched tape reader

Hewlett-Packard 2748, 415 characters/s

Teletype: ASR 33 10 characters/s

A complete description of the equipment and its possibilities of application is given in Christiansson (1974).

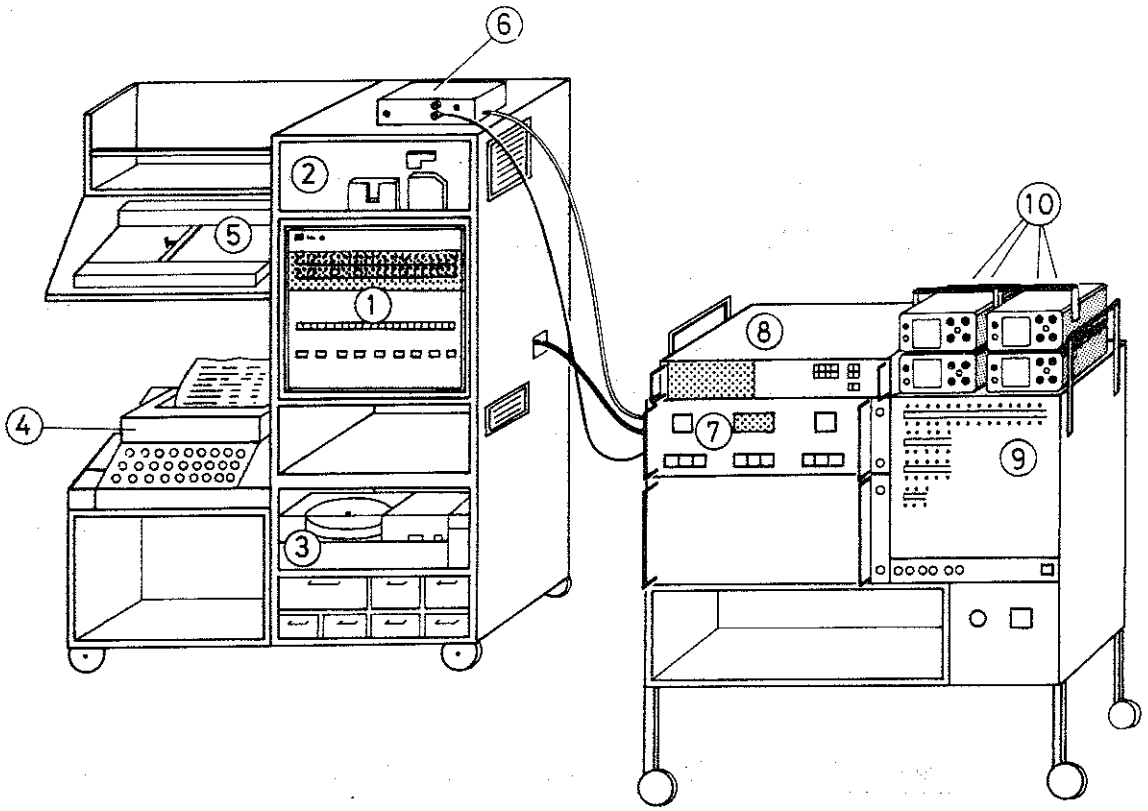

Figure 3.11 Computer-controlled data-acquisition system

(1) HP-Computer	(6) Digital clock
(2) Tape-reader	(7) Scanner with scanner control
(3) Tape-punch	(8) Digital-voltmeter
(4) Teletype	(9) Signal conditioning unit
(5) Plotter	(10) Gauge indicators.

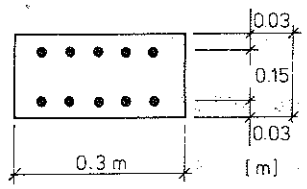

Reinforcement
ϕ 10 mm Ks 40

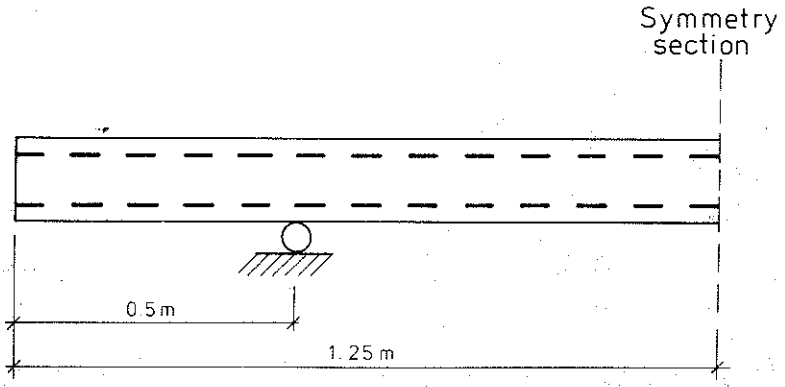

Figure 4.1 Reinforced concrete plate strip used in fire tests.

4 TEST PROGRAM

4.1 General description on the investigation

The experimental investigation contains 81 tests, divided into 6 test series (A1, A2, A3, B, C and D). All tests were performed on reinforced concrete plate strips with a span of 2.5 m and a total length of 3.5 m which gives a cantilever length of 0.5 m outside the two supports according to Fig. 4.1. The strips had a cross-sectional area, bxh, of 0.3x0.15 m^2 and a longitudinal reinforcement in the tension as well as the compression zone of each with a concrete cover of 0.025 m (Fig. 4.1). Each of the cantilevers was furthermore strengthened with 5 stirrups ϕ10 KS 40.

The reinforced concrete plate strips were tested as fixed against rotation at both supports and free to deform in the longitudinal direction.

Tests were accomplished with varying characteristics of the fire exposure, the concrete composition, the age of the plate strips at testing and the external transverse load.

The fire exposure was applied unilaterally from below over the whole span length. The gastemperature-time curve of the fire exposure was varied within the test series according to the current Swedish Standard Specification, SBN 75, as specified for a fire compartment, type A, having surrounding structures made of a material with a thermal conductivity λ = 0.81 W/m^{o}C and a heat capacity ρc_p = 1.67 MJ/m$^{3\,o}$C - cf. Magnusson & Thelandersson (1970). The gastemperature-time curves are exemplified in Fig. 4.2. Entrance parameters are the ventilation charactersitics of the fire compartment, expressed by the opening factor $A\sqrt{H}/A_t$, and the fire load density q, given by the formula

$$q = \frac{1}{A_t} \Sigma m_\nu H_\nu \qquad (MJ/m^2) \qquad 4.1$$

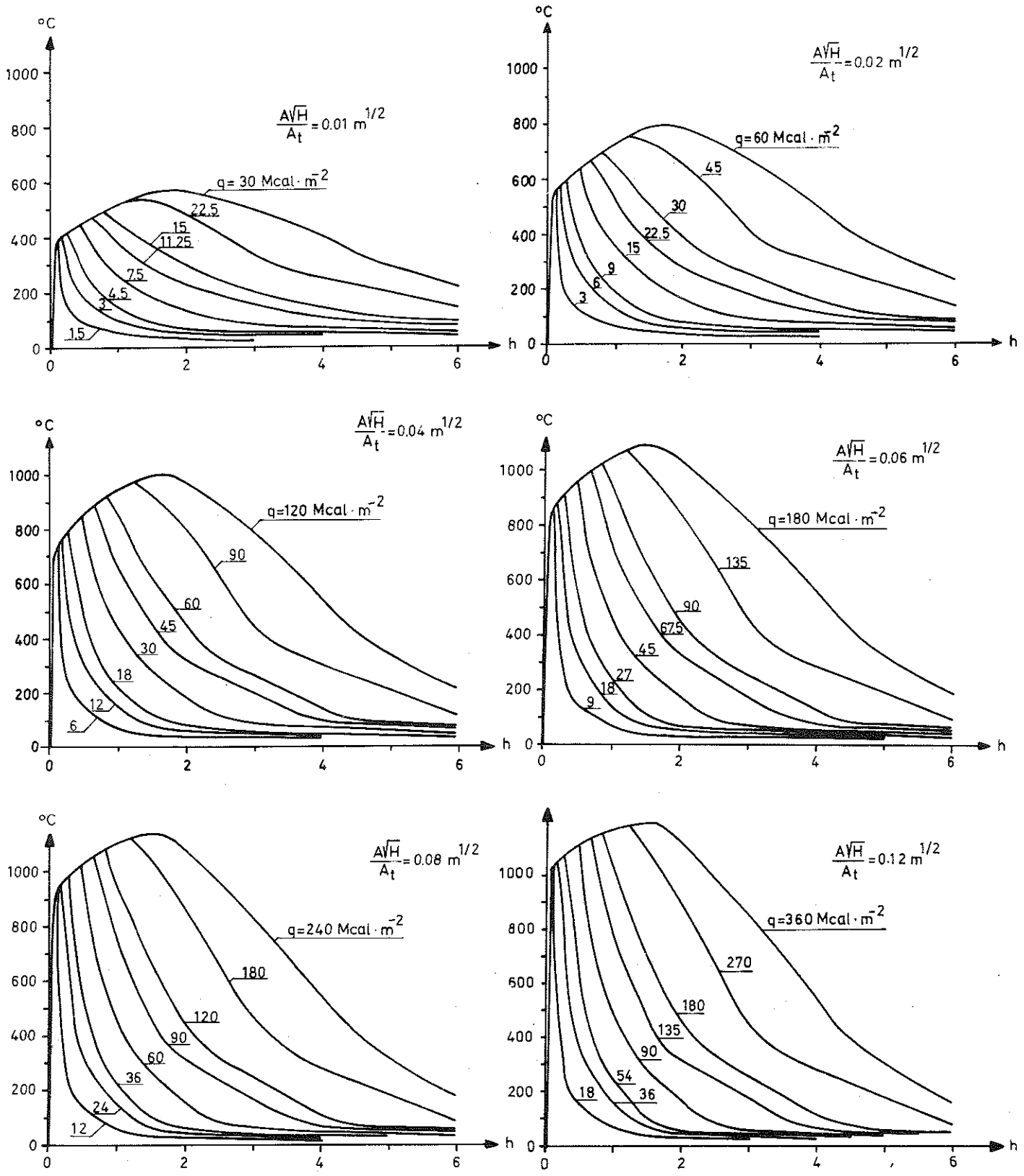

Figure 4.2 Gastemperature-time curves for type A of enclosed space at different opening factors: $A\sqrt{H}/A_t$ = 0.01, 0.02, 0.04, 0.06, 0.08 and 0.12 $m^{1/2}$.

From Magnusson & Thelandersson (1970)

Mcal·m^{-2}	MJ·m^{-2}	Mcal·m^{-2}	MJ·m^{-2}
7.5	31	120	502
15	63	180	754
30	126	240	1005
60	251	(cf. Table 4.4)	

where A = total area of the window and door openings (m^2)

H = mean value of the heights of the window and door openings, weighed with respect to each individual opening area (m),

A_t = total interior area of the surfaces bounding the fire compartment, opening areas included (m^2),

m_ν = total weight of combustible material ν (kg), and

H_ν = effective heat value of combustible material ν within the fire compartment (MJ/kg).

In a design procedure, fire compartments having surrounding structures with other thermal properties than for fire compartment, type A, can be transferred to the fire compartment, type A, according to simple rules, based on fictitious values of the opening factor $(A\sqrt{H}/A_t)_f$ and the fire load density q_f - see Anderberg et al (1974) and Pettersson (1976).

All tests embraced in the investigation, except those belonging to the test series D, were carried out with the strips having no lateral load. From this type of tests, basic informations are given regarding the structural response of a hyperstatic concrete structure due to the fire exposure alone. The additional influence of a simultaneous constant load is then studied in test series D. The load is made up by two symmetrically applied concentrated loads 0.76 m apart from each other cf. Fig. 3.1. The loading levels 1/4, 1/2, 3/4 and 1/1 of P_{all} were used, where P_{all} = 16 kN denotes the allowable load at ambient conditions according to Swedish Concrete Standards. Furthermore P_{all} amounts to about half the theoretical ultimate value of the plate strips.

As stated, the experimental investigation generally comprised for all tests, a continuous determination of the temperature gradient, the restraint bending moment and the bending moment distribution, the vertical deflection, and the crack formation of the plate strips during a complete fire process. In test series A2 and A3, the change in the flexural stiffness during the fire exposure was investigated as well by measuring the deflection response from an instantaneous load application.

Information concerning the residual state characteristics are of fundamental importance for structures with a requirement on re-serviceability after fire and generally for an estimation of the condition of a fire-damaged, load-bearing structure. Consequently, a complementary study was carried through for a determination of the residual restraint bending moment as well as the residual bending moment capacity and the residual flexural stiffness of the fire exposed plate strips after cooling down to ordinary room temperature conditions. Also an investigation of the residual stress-strain relationship of the reinforcement of the plate strips was included in this complementary study.

4.2 Material data

This section deals with some basic material data at room temperature as concerns the material properties of the concrete and the reinforcement steel, the concrete composition and the age of the plate strips at testing. Also a summary report is given of the residual ultimate strength of the reinforcement steel after fire exposure. The concrete was made from Standard Portland Cement, gravel ($\leq$ 8 mm) of glacial origin and macadam (8 - 16 mm) of quartzite. Information about the concrete mix proportions is given in Anderberg (1973). The detailed mechanical behaviour of concrete and reinforcement steel at transient high temperature conditions will be dealt with in connection to the presentation of the material models, used in the theoretical calculation in section 6.2.2.

For every test specimen, the concrete quality was controlled by determining the compressive, tensile (test series A1 only) and flexural strength on specimens, poured for these purposes. Six cubes, 0.15 m in length were used for the compressive and split-cube test and two non-reinforced beams, bxlxh, 0.8x0.15x0.10 m^3 for the flexural test. The specimens were cured 5 days in water and then in air at 20°C and 50% relative humidity up to the time when the fire test was carried out. Mean value and relative standard deviation of the strength data as concerns compressive and tensile strength are summarized in Table 4.1 for all tests. Furthermore the water-cement-ratio, the amount of cement paste and

Table 4.1 Material data for concrete at room temperature

Test	Compressive strength		Tensile strength		Tensile bending strength	Water-cement ratio	Amount of cement-paste	Testing age
	Mean value	Relative standard deviation	Mean value	Relative standard deviation	Mean value			
	MN/m^2	%	MN/m^2	%	MN/m^2		ℓ	months
A1:1	35.0	3	2.2	68	4.3	0.63	280	2
A1:2	39.0	5	2.4	25	4.5	"	"	2
A1:3	38.0	3	2.1	14	4.1	"	"	2
A1:4	40.0	5	2.5	32	4.5	"	"	2
A1:5	40.0	4	2.5	36	5.3	"	"	2
A1:6	35.0	3	2.1	62	4.5	"	"	2
A1:7	39.0	4	2.4	42	5.3	"	"	2
A1:8	38.5	-	-	-	3.8	"	277	2
A1:9	-	-	-	-	-	"	"	2
A1:10	45.0	3	-	-	5.1	"	"	5
A1:11	46.0	5	-	-	6.0	"	"	6
A1:12	38.8	2	-	-	4.1	"	"	1
A2:1	28.6	2	-	-	3.3	0.63	277	1
A2:2	28.0	4	-	-	3.5	"	"	1
A2:3	29.1	2	-	-	3.5	"	"	1
A2:4	25.2	2	-	-	2.8	"	"	1
A2:5	30.7	5	-	-	3.6	"	"	1
A2:6	27.9	3	-	-	3.5	"	"	1
A2:7	27.9	5	-	-	3.1	"	"	1
A2:8	28.2	4	-	-	2.5	"	"	1
A2:9	27.8	4	-	-	3.7	"	"	1
A2:10	29.7	2	-	-	3.5	"	"	1
A3:1	38.6	2	-	-	5.0	0.63	277	1
A3:2	34.0	6	-	-	4.7	"	"	1
A3:3	35.0	3	-	-	4.5	"	"	1
A3:4	36.3	2	-	-	4.3	"	"	1
A3:5	36.1	1	-	-	4.1	"	"	1
A3:6	33.7	7	-	-	4.2	"	"	1
A3:7	39.6	1	-	-	4.7	"	"	1
A3:8	34.5	3	-	-	4.3	"	"	1
A3:9	38.0	1	-	-	4.5	"	"	1
A3:10	35.2	2	-	-	4.2	"	"	1

Table 4.1 cont. Material data for concrete at room temperature

Test	Compressive strength		Tensile strength		Tensile bending strength	Water-cement ratio	Amount of cement-paste	Testing age
	Mean value	Relative standard deviation	Mean value	Relative standard deviation				
	MN/m^2	%	MN/m^2	%	MN/m^2		ℓ	months
B 1	42.0	-	-	-	5.3	0.63	277	3
B 2	53.0	-	-	-	5.5	0.52	"	3
B 3	22.0	-	-	-	3.5	0.77	"	3
B 4	36.0	5	-	-	3.9	0.63	"	1
B 5	22.0	3	-	-	2.9	0.77	"	1
B 6	40.0	5	-	-	4.4	0.52	"	1
B 7	45.0	4	-	-	4.0	0.52	"	1/2
B 8	26.0	3	-	-	2.7	0.77	"	1/2
B 9	35.0	4	-	-	4.1	0.63	"	1/2
B 10	32.3	5	-	-	4.5	0.77	"	12
B 11	52.4	4	-	-	5.0	0.52	"	12
C 1	49.0	4	-	-	4.6	0.63	277	1
C 2	46.0	3	-	-	4.9	"	257	1
C 3	43.0	2	-	-	4.4	"	296	1
C 4	42.2	8	-	-	6.0	"	277	3
C 5	45.5	5	-	-	6.3	"	257	3
C 6	34.2	6	-	-	4.8	"	296	3
C 7	41.5	7	-	-	5.8	"	277	4
C 8	35.6	6	-	-	5.5	"	257	4
C 9	49.2	5	-	-	6.2	"	296	6
D 1	32.8	6	-	-	4.0	0.63	277	1
D 2	30.6	3	-	-	3.3	"	"	1
D 3:1	35.4	9	-	-	4.0	"	"	1
D 3:2	35.3	2	-	-	4.1	"	"	1
D 4	37.1	5	-	-	4.4	"	"	1
D 5:1	37.2	2	-	-	3.9	"	"	1
D 6:1	36.4	4	-	-	4.6	"	"	1
D 7:1	42.4	9	-	-	5.4	"	"	1
D 8:1	38.8	3	-	-	5.0	"	"	12
D 5:2	37.9	15	-	-	4.5	"	"	1
D 6:2	30.9	11	-	-	3.7	"	"	1
D 7:2	45.1	4	-	-	4.3	"	"	1
D 8:2	46.0	5	-	-	4.7	"	"	1
D 9	32.8	6	-	-	3.4	"	"	12
D 10	34.5	2	-	-	3.5	"	"	1
D 11:1	36.6	5	-	-	3.5	"	"	1
D 11:2	43.0	5	-	-	5.4	"	"	1
D 12:1	33.5	2	-	-	3.3	"	"	1
D 12:2	46.9	2	-	-	5.3	"	"	1
D 13	34.7	9	-	-	4.9	"	"	2
D 14	42.4	4	-	-	4.5	"	"	1
D 15	25.9	19	-	-	3.4	"	"	1
D 16	30.3	15	-	-	3.5	"	"	1
D 17	33.0	9	-	-	4.8	"	"	2
D 18	37.4	19	-	-	3.4	"	"	1
D 19	30.2	6	-	-	4.1	"	"	1
D 20	35.2	5	-	-	3.5	"	"	1
D 21	49.4	16	-	-	5.6	"	"	1
D 22	46.8	5	-	-	5.2	"	"	1

the age of the plate strips at testing are also given in the table.

The longitudinal reinforcement of the strips is characterized in Table 4.2 by the yield strength, $\sigma_y^{20^oC}$, and the ultimate strength, $\sigma_u^{20^oC}$, at ambient conditions.

Table 4.2 Material data for reinforcement steel at room temperature

Test series	Reinforcement $\sigma_y^{20^oC}$ MN/m^2	$\sigma_u^{20^oC}$ MN/m^2	Remarks Mean value of
A1	470	704	6 tests
A2	490	766	6 tests
A3	458	681	1 test
B and C	508	751	2 tests
D	458	681	1 test

The residual strength of the longitudinal reinforcement of the plate strips after having been exposed to fire was determined in five cases (tests D3, D11:2, D12:2, D21 and D22). This was made in order to roughly estimate if any significant influence from the thermal exposure could be noticed. For this purpose two pieces of the reinforcement bars located at the bottom and at the top of the mid-section of each of the five plate strips were cut off afterwards. During the fire tests this part of the bottom reinforcement was exposed to a maximum temperature within the region 400 to 700^{o}C. Owing to that the bottom reinforcement steel was thermally exposed under load its stress-strain relationship was significantly altered when compared with the virgin relationship. If this kind of steel is only thermally exposed it, however, more or less gets back to its virgin stress-strain relationship. For the residual ultimate strength, the thermal exposure only gave rise to an inconsiderable decrease in comparison to the original ultimate strength at ambient conditions, cf. Table 4.3.

Table 4.3 Residual ultimate strength of the bottom reinforcement

Test	% of $\sigma_u^{20^oC}$	Max. temperature at fire exposure	Remark
D 3	100	400	2 tests
D 11:2	100	510	2 tests
D 12:2	95	510	2 tests
D 21	99	625	2 tests
D 22	97	700	2 tests

For the top reinforcement, no noticeable decrease in ultimate strength from the thermal exposure could be measured. The temperature level for these reinforcement bars had however as a maximum been only 300^oC.

Summing up it can be established that the decrease in the residual ultimate strength of the reinforcement steel of the actual type subjected to temperatures up to about 700^oC, is in practise of no importance. The stress-strain curve, however, will be influenced in a not negligible extent by the combined effect of the load and temperature history from the fire test, especially when the temperature exceeds about 350^oC.

4.3 Main tests

The testing scheme of the main tests divided into 6 test series, is described summarily in Table 4.4, which gives the characteristic of the different tests as regards the fire exposure, concrete mixture, the age at testing and the level of applied, transverse load.

The fire exposure then is specified over the gastemperature-time curves in Fig. 4.2 by the fire load density q, defined according to Eq. 4.1, the opening factor of the fire compartment $A\sqrt{H}/A_t$ and

Table 4.4 Characteristics of main tests.

Test No.	Duration of heating phase	Fire load density	Opening-factor	Water-cement ratio	Amount of cement-paste	Testing age	Load
	h	MJ/m^2	$m^{1/2}$		ℓ/m^3	months	P/P_{all}
Test series A1							
1, 3 & 8	4	251	0.01	0.63	277	2	0
2, 4, (9), 11	4	502	0.02	"	"	2,,,6	0
5	1	251	0.04	"	"	2	0
6, 12*	2	502	0.04	"	"	2	0
7	4	1005	0.04	"	"	2	0
10	8	2010	0.04	"	"	5	0
Test series A2							
1	4	251	0.01	0.63	277	1	0
2	2	"	0.02	"	"	1	0
3	1	"	0.04	"	"	1	0
4	2/3	"	0.06	"	"	1	0
5	1/2	"	0.08	"	"	1	0
6	1/2	31	0.01	"	"	1	0
7	1	63	0.01	"	"	1	0
8	2	126	0.01	"	"	1	0
9	1/2	63	0.02	"	"	1	0
10	1	126	0.02	"	"	1	0
Test series A3							
1	1/2	126	0.04	0.63	277	1	0
2	3	754	0.04	"	"	1	0
3	4	1005	0.04	"	"	1	0
4	1/3	126	0.06	"	"	1	0
5	1 1/3	502	0.06	"	"	1	0
6	2	754	0.06	"	"	1	0
7	2 2/3	1005	0.06	"	"	1	0
8	1	502	0.08	"	"	1	0
9	1 1/2	754	0.08	"	"	1	0
10	2	1005	0.08	"	"	1	0
Test series B							
1	2	502	0.04	0.63	277	3	0
2	"	"	"	0.52	"	3	0
3	"	"	"	0.77	"	3	0
4	"	"	"	0.63	"	1	0
5	"	"	"	0.77	"	1	0
6	"	"	"	0.52	"	1	0
7	"	"	"	0.52	"	1/2	0
8	"	"	"	0.77	"	1/2	0
9	"	"	"	0.63	"	1/2	0
10*	"	"	"	0.77	"	24	0
11*	"	"	"	0.52	"	24	0
Test series C							
1	2	502	0.04	0.63	277	1	0
2	"	"	"	"	257	1	0
3	"	"	"	"	296	1	0
4	"	"	"	"	277	3	0
5	"	"	"	"	257	3	0
6	"	"	"	"	296	3	0
7	"	"	"	"	277	4	0
8	"	"	"	"	257	4	0
9	"	"	"	"	296	6	0
Test series D							
1	1/2	251	0.08	0.63	277	1	1/4
2	"	"	"	"	"	1	1/2
3*	"	"	"	"	"	1	3/4
4	"	"	"	"	"	1	1
5	1	"	0.04	"	"	1	1/4
6	"	"	"	"	"	1	1/2
7	"	"	"	"	"	1	3/4
8	"	"	"	"	"	1	1
9	4	"	0.01	"	"	1	1/4
10	"	"	"	"	"	1	1/2
11*	"	"	"	"	"	1	3/4
12*	"	"	"	"	"	1	1
13	2	502	0.04	"	"	2	1/4
14	"	"	"	"	"	1	1/2
15*	"	"	"	"	"	1	3/4
16*	"	"	"	"	"	1	1
17	1	"	0.08	"	"	2	1/4
18	"	"	"	"	"	1	1/2
19*	"	"	"	"	"	1	3/4
20*	"	"	"	"	"	1	1
21*	2 2/3	1005	0.06	"	"	1	1
22*	4	1506	"	"	"	1	1

* computer-controlled data-aquisition system used.

Notation: For fire exposures characterized by the fire load densities 1005 and 1506 MJ/m^2 supplementary gastemperature-time curves have been calculated.

an approximate value of the duration of the heating phase t_d, determined by the formula - Magnusson & Thelandersson (1970)

$$t_d = \frac{q}{6300(\frac{A\sqrt{H}}{A_t})} \quad (h) \qquad 4.2$$

q is to be inserted in $MJ \cdot m^{-2}$ and $A\sqrt{H}/A_t$ in $m^{1/2}$.

The main tests, except those belonging to test series A3, are accounted for in detail in section 4.2 in Anderberg (1972) and for that reason the following description excludes a lot of details. The test series A1, A2 and A3 comprise a study of the structural behaviour of non-loaded plate strips at different complete fire processes. The variation of the fire prccess is determined by the opening foctor, $A\sqrt{H}/A_t$ ranging from 0.01 to 0.08 $m^{1/2}$, and the fire load density, q, ranging from 31 to 2010 $MJ \cdot m^{-2}$. The corresponding gastemperature-time curves for the different combinations of opening factors and fire load densities are in accordance with Fig. 4.2. For some tests with a duration of the heating phase exceeding 2 hours, no curves are given in literature, as concerns the cooling phase. For these tests, the cooling was selected to a temperature decrease of $10^{o}C/min$, which is in accordance with the recommendations in the Swedish Standards Specification.

As the test series A1 was the first to be performed and the testing equipment then in a preliminary phase, the test results were partly not quite reliable and therefore not accounted in detail in section 5. The concrete composition is kept constant in the test series A1, A2 and A3, characterized by a water-cement-ratio of 0.63 and amount of cement paste of 277 l/m^3.

The purpose of the test series B and C was to find out any influence of variations in the concrete composition and the age of the specimens at testing on the thermal and structural behaviour of the plate strips during fire exposure. The temperature-time curve was kept constant, characterized by an opening factor of $0.04 m^{1/2}$ and a fire load density of 502 MJ/m^2. The concrete composition was varied by changing the water-cement-ratio - 0.52, 0.63 and 0.77 - at a constant cement paste quantity and by changing the

cement paste quantity - 257, 277 and 296 l/m^3 - at a constant water-cement-ratio for test series B and C, respectively. The age at testing was varied from 1/2 to 24 months. Due to the same reason as mentioned above for test series A1, the tests of series B and C are not fully reported in this connection.

Test series D which comprises 22 different tests extends the study to include the influence of a lateral load (see section 4.1) on the structural behaviour of the hyperstatic concrete plate strips, unilaterally fire exposed. In the first 20 tests of the test series, four load level alternatives were connected to different fire exposures. These are specified by the following combinations of the fire load density q and the opening factor $A\sqrt{H}/A_t$: (251 $MJ \cdot m^{-2}$, 0.01 $m^{1/2}$), (251, 0.04), (502, 0.04), (251, 0.08) and (502, 0.08). The tests D 21 (1005 $MJ \cdot m^{-2}$, 0.06 $m^{1/2}$) and D 22 (1506, 0.06) were primarily intended for a study up to a state quite near a collapse during an extreme fire exposure at a load level of P_{all}.

For all tests of the test series D, the concrete composition and the age of the plate strips at testing were kept constant. The divergence in the testing age for tests D 13 and D 17 then is practically negligible.

4.4 Test concerning residual state

In all main tests, the restraint bending moment and the vertical deflection were followed during a complete fire process until the residual state, attained when the plate strips had cooled down to room temperature. As a complement to these measurements, the residual flexural stiffness and the residual bending moment capacity were determined for a great number of the plate strips. For the plate strips in test series A2 and A3, additionally some experiments were carried out for a determination of the gradual change in the flexural stiffness during the fire exposure.

The gradual change in the flexural stiffness of the plate strips was measured by an instantaneous application - successively re-

peated for different times during the fire exposure - of two symmetrical transverse concentrated loads of 0.5 kN each and a simultaneous reading of the instantaneous additional vertical deflections of the plate strip in its midpoint and 1/4-point sections. The loading equipment consisted of two load-transmitters, connected to a steel beam, supported on two hydraulic jacks. By the jacks the instantaneous vertical load could be sinked down to or elevated from the plate strip in accordance to Fig. 4.3. Owing to experimental difficulties, the procedure only could be applied to plate strips, having no external transverse loading. The relatively low level chosen for the instantaneous load was dictated by the requirement of not influencing the crack formation and not disturbing the structural behaviour of the fire exposed plate strips.

The purpose of the determination of the gradual change in the flexural stiffness of the plate strips during the fire exposure was mainly to get additional informations which could facilitate and support a theoretical analysis of the tests. The change in flexural stiffness then constitutes a feasible tool to indicate, for instance, an increased crack formation and material disintegration from the fire exposure.

The residual flexural stiffness and the residual bending moment capacity of the fire-exposed plate strips were determined, about 5 months after the respective main test by loading them as simply supported with two symmetrically located transverse concentrated loads, 0.8 m apart (cf. Fig. 4.4). At every load step, characterized by a load increment of 1 - 2 kN, the vertical deflections in the midpoint and 1/4-point sections of the plate strips and the curvature between the two point loads were measured. In most of the residual tests, the plate strips were loaded in the same position as in the main test, giving the residual flexural stiffness and the residual moment capacity corresponding to a positive bending moment. In some residual tests, the plate strips were loaded in the reverse direction (cf. Anderberg (1973)).

A complementary determination of the residual strength and the re-

sidual stress-strain relationship of the reinforcing bars after fire exposure is reported in section 4.2.

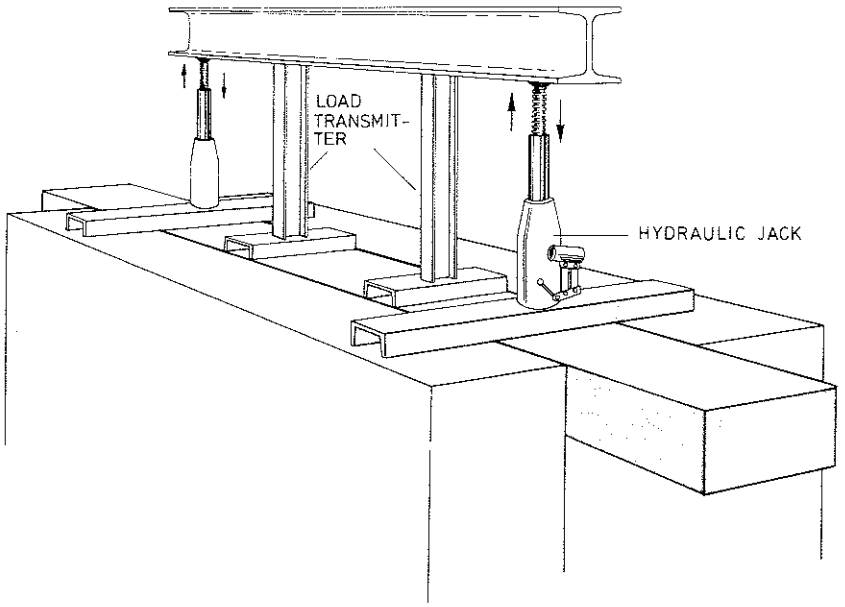

Figure 4.3 Load equipment for determining flexural stiffness during a fire test.

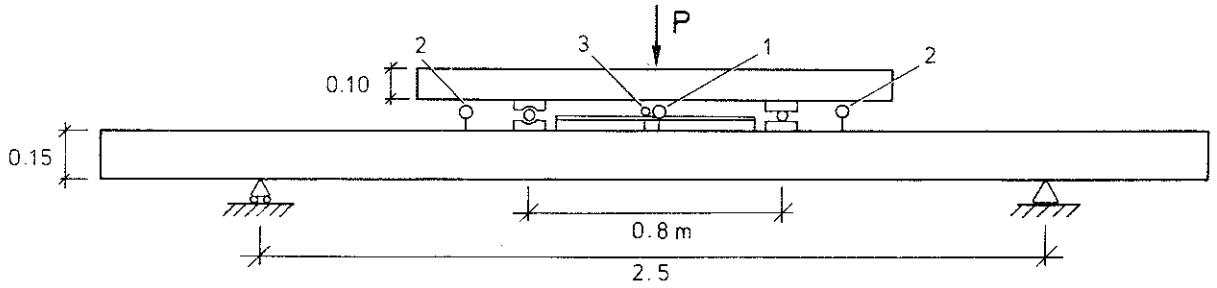

Figure 4.4 Load equipment for determining residual flexural stiffness and strength after fire test.
1 Gauge indicator at mid-section
2 Gauge indicator at 1/4-section
3 Gauge indicator for curvature measurements.

5 SOME RESULTS OF THE EXPERIMENTAL STUDY

5.1 Outline of the presentation

In Anderberg (1973), the experimental results of the majority of the tests were presented in brief, embracing an analysis of some of the most important results. Thus, the presentation was not complete, but the structural behaviour of the fire-exposed concrete plate strips was studied by selecting one illustrating test (A2:3). The detailed behaviour during the whole test then was followed thoroughly and a parallel explanation was given. In this paper, such a description is omitted and the objective is rather, as far as possible, to give a more integrated picture of the structural behaviour during fire exposure at varying conditions, accounted for in section 4. This way of presenting the test results is also caused by the intention to use the results for a control of the theoretical study in the following section 6, which deals with a thorough analysis of the structural response to fire, including the strain and stress distribution in different cross-sections. Due to the great amount of test data gathered from all the 81 tests, a fully exhaustive reporting cannot be given in this paper. A complete collection of all test results regarding the temperature measurements as well as the observed and measured structural behaviour is nevertheless available and can be obtained from the author at request.

In addition to this more over-grasping analysis with comparisons and theoretical interpretations of the results within the main study, the residual flexural stiffness and the residual strength of the plate strip are also studied in this section.

5.2 Temperature measurements

The presentation and analysis of the transient temperature state is based on measurements by 30 thermocouples where five of them (4, 8, 12, 16, 20) are giving the furnace temperature and the remaining 25 the temperature distribution of concrete plate strip in accordance with Fig. 3.4. The temperature recording of the

plate strip then comprises the surface temperature along the strip (5 points), the temperature distribution along the bottom reinforcement at 30 mm depth (7 points) and the thermal gradient at three sections, namely support section, 1/4-section and mid-section.

The accuracy in the temperature measurements was sometimes disturbed by unintentional small displacements of the thermocouples in relation to the prescribed positions, occurring when the plate strips were casted. In decisive cases the real position of the thermocouples was determined afterwards. Most sensitive to a displacement then were the thermocouples, placed immediately inside the fire-exposed surface and intended for a determination of the surface temperature. In exceptional cases, these thermocouples were found to be displaced 1/2 - 2 mm, consequently rendering a considerable error and requiring a correction. If a displacement of the surface thermocouples led to an unprotected position this was noticed immediately and the measurement was not used.

Furthermore, the response time of the thermocouples placed in the furnace and, to some extent, of the thermocouples situated at the surface of the plate strip could influence the recorded temperature.

Two different types of thermocouples were used, chromel Alumel 20 AWG, 0.81 mm in diameter, (1), within the specimen and immediatley inside its bottom surface and chromel Alumel 14AWG, 1.63 mm in diameter, isolated by a tube of ceramics and inserted in a protective tube, Ø13 - 15 mm, of Kanthal, (2), for the furnace temperature measurements. The response time of these thermocouples was determined in accordance with the manual published by ASTM Committee E-20 (1970) and is shown in Fig. 5.1 as a function of the temperature. For the smaller thermocouples (1), the delay in the measured temperature has no practical significance, apart from exceptional cases. However, the response time of the furnace thermocouples (2) is considerable, viz. 390 seconds at 80°C which drops to 48 seconds at 1000°C, but the practical consequence below about 600°C is of little importance for the heating period as the furnace temperature very quickly attains 600 -

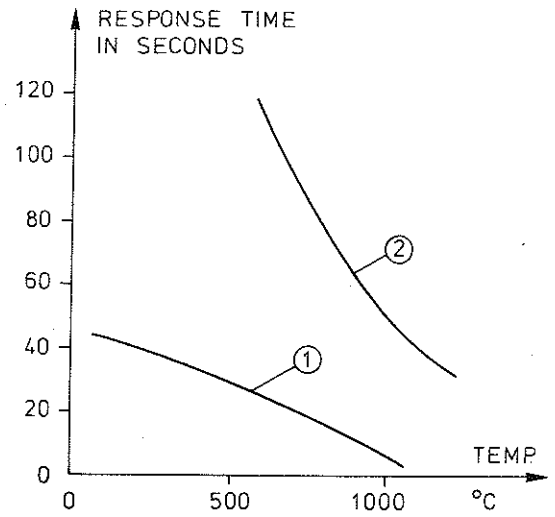

Figure 5.1 Response time of thermocouples as functions of temperature
① Chromel - Alumel 20 AWG, 0.81 mm in diameter
② Chromel - Alumel 14 AWG, 1.63 mm in diameter and insolated by a tube of cheramics and inserted in a protective tube, ϕ13 - 15 mm, of Kanthal.
Response time = time to attain $(1 - 1/e)T_f$, where T_f = furnace temperature.

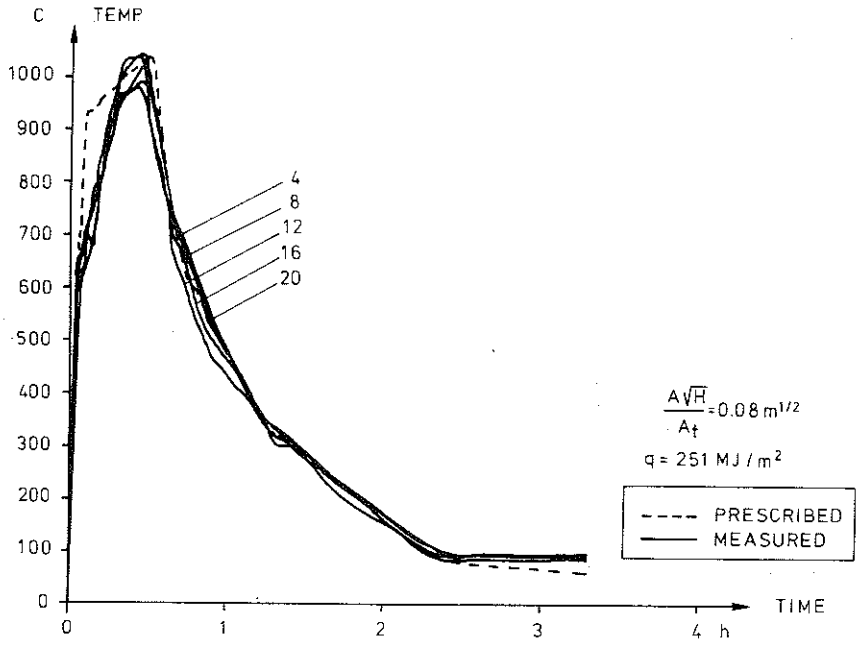

Figure 5.2 Prescribed temperature-time curve and the corresponding time curves of the furnace temperature, measured at the points 4, 8, 12, 16 and 20 for the test A2:5, chosen as representative for the tests D1 - 4 and A2:5.

800°C (already after 0.10 - 0.15 hours), when the opening factor is supposed to be greater than 0.02 $m^{1/2}$. For the cooling period, the high response time of the thermocouples (2) within the lower temperature region may have a more decisive influence. These circumstances are rendering a use of the measured furnace temperature impossible in connection with a determination of the heat transfer to the strip surface. Furthermore, the heat transfer characteristics of the furnace are insufficiently known.

Probably, a thermal calibration of the furnace could have been carried out according to the procedure developed in Paulsen (1975), comprising a thorough heat and mass balance analysis of the furnace and the thermocouples used for regulating the time variation of the gastemperature. However, such a calibration was found out to be very laborious in the present case and not necessary for a comparison between the observed and theoretically calculated, thermal and structural behaviour of the fire exposed plate strips.

The measured values of the furnace temperature were thus only used in order to control and follow a desired thermal exposure in a defined way, enabling as good a reproduction of the fire tests as possible. Consequently, the boundary conditions of the fire-exposed surface of the plate strips were formulated with a direct reference to the surface temperature.

Within this section, the illustration of the transient temperature fields will be limited to the tests D1 - 4, i.e. transversely loaded plate strips, supplemented with the test A2:5, characterized by the same thermal exposure but having no lateral load, cf. Table 4.4.

Fig. 5.2 illustrates how closely the time-curves of the furnace temperature, measured at the points 4, 8, 12, 16 and 20, follow the desired theoretical temperature-time curve, dashed in the diagram, where the test A2:5 is chosen to represent the selected five tests, characterized by the fire load density 251 $MJ \cdot m^{-2}$ and the opening factor 0.08 $m^{1/2}$. As a complement to this graph, the temperature distribution in the furnace is given at certain

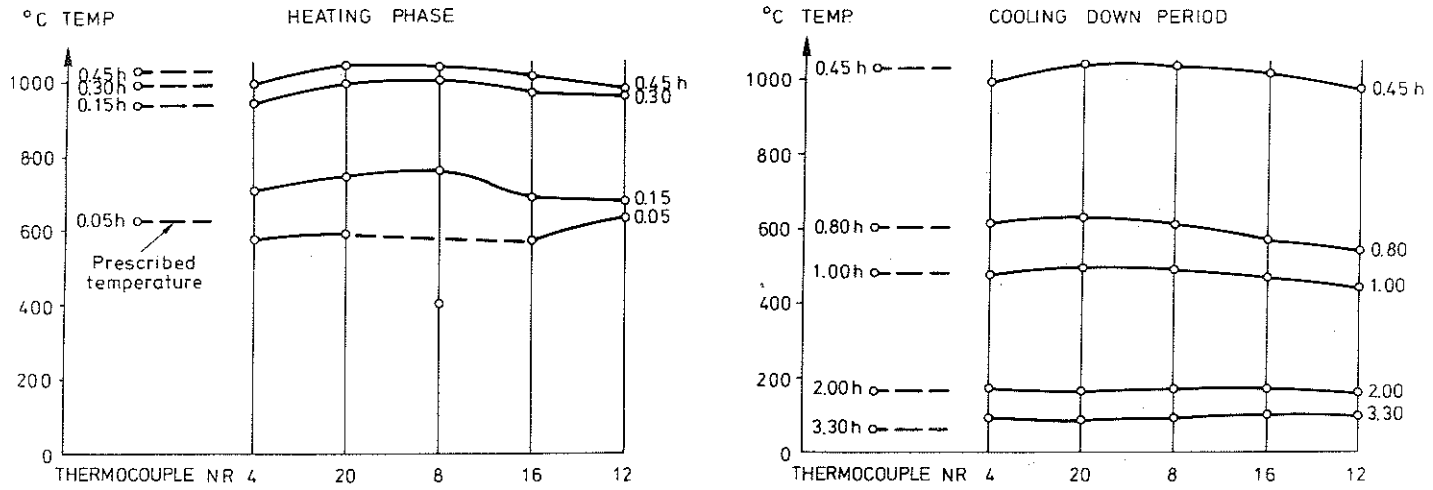

Figure 5.3 Measured temperature distribution inside the furnace during fire test A2:5 chosen as representative for the tests D1 - 4 and A2:5. Top: Heating phase. Bottom: Cooling down period.

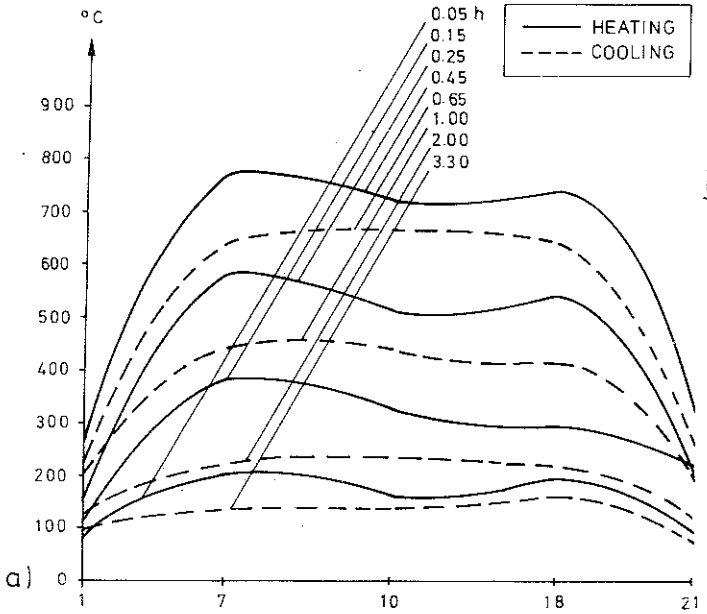

Figure 5.4a Temperature distribution of the fire-exposed surface of the plate strip A2:5 chosen as representative for the tests D1 - 4 and A2:5. The temperature is determined by thermocouples 1, 7, 10, 18 and 21.

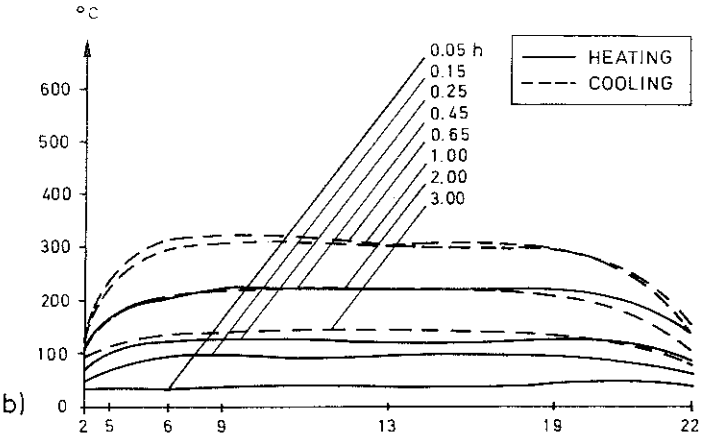

Figure 5.4b Temperature distribution of the bottom reinforcement during fire exposure in the plate strip A2:5 chosen as representative for the tests D1 - 4 and A2:5. The temperature is determined by thermocouples 2, 5, 6, 9, 13, 19 and 22.

times in Fig. 5.3, for the same group of tests. The dashed lines to the left in the figure indicate the prescribed temperature. By analyzing the results from these tests and other similar measurements, the difficulties in following the prescribed temperature-time curve can be summarized in three points.

1. At a very rapid heating ($A\sqrt{H}/A_t \geq 0.06$ $m^{1/2}$), the difficulties to reach the prescribed temperature level during the first 0.3 hours were obvious.
2. During cooling, the fluctuation of the measured temperatures was often more pronounced than during heating.
3. Sudden disturbances, due to expiring burners and attending pressure changes in the furnace, did occur in some tests.

The temperature distribution along the fire-exposed surface of the plate strip and along the bottom reinforcing steel, located 30 mm from the exposed surface, is illustrated in Fig. 5.4. The distributions are shown at selected times when the continuous curves stand for the heating period and the dashed curves for the cooling period. A characteristic feature of the temperature exposure is the rapid decrease outside the thermocouples 7 and 18 and over the supports where the surface temperature rarely reaches more than 300°C. The degree of symmetry of the laterally nonuniform thermal exposure has to be observed.

The temperature gradient at selected times, recorded by 8 thermocouples in the mid-section of the plate strip is presented in Fig. 5.5, complemented with the current temperature-time curve implying a fire load density 251 $MJ \cdot m^{-2}$ and an opening factor 0.08 $m^{1/2}$. The height of the plate strip is 0.15 m. During the heating period the temperature gradient continuously increases. After 0.45 hours, i.e. roughly at the end of the heating period, the gradient is extremely steep up to about 1/4 of the height where an evaporation plateau starts with a temperature of 100 - 110°C, indicating a moisture vapourization within this portion of the cross-section. During the subsequent cooling the gradient successively tends to be linear. The transient temperature fields of the plate strips are further illustrated in section 6 where

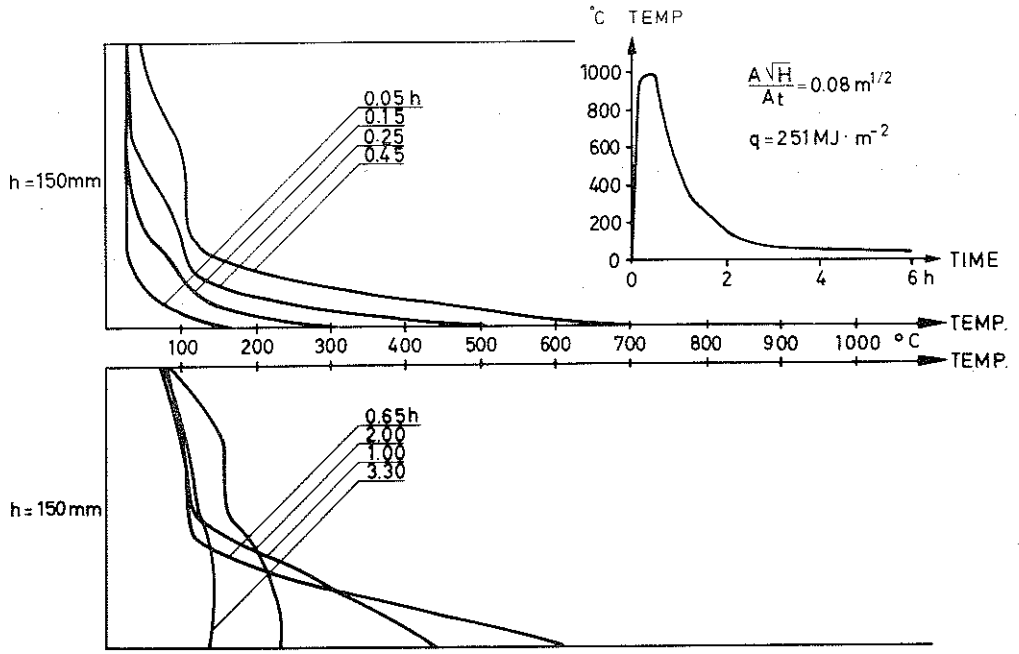

Figure 5.5 Variation in temperature gradient during fire-exposure for the mid-section of the plate strip A2:5 chosen as representative for the tests D1 - 4 and A2:5. The corresponding furnace temperature-time curve is inserted.

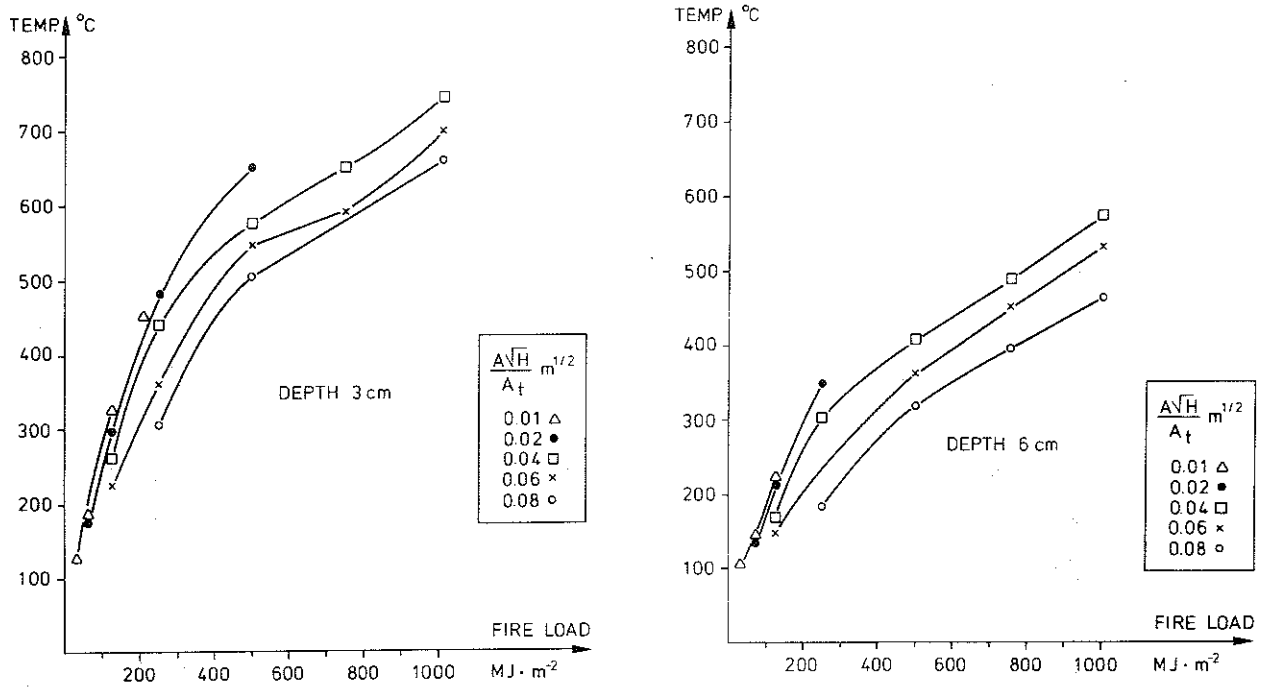

Figure 5.6 and Figure 5.7 Maximum temperature, during a complete fire process, as function of the fire load density at different opening factors.

measured temperature-time curves at different depths in mid-section, 1/4-section and support section are shown and compared with the corresponding time curves, obtained in theoretical calculations.

For structural design purposes, it is of decisive importance to know the maximum temperature, during a complete fire process, at different depths from the fire-exposed surface of a reinforced concrete structure. Applied to, for instance, a simply supported beam, where the maximum temperature achieved in the tension reinforcement has a critical influence on the collaps of the structure, this information easily can be directly transferred to the minimum load-carrying capacity during the fire exposure. Design diagrams, rendering the maximum temperature for different combinations of the fire load density and the opening factor then are very useful. Examples of such diagrams are given in Fig. 5.6 and 5.7 constructed by analyzing all relevant maximum temperatures at two different depths, 3 and 6 cm, in the accounted tests. In Fig. 5.6, the maximum temperature as a function of the fire load density at the depth of 3 cm can be found for five different opening factors (0.01, 0.02, 0.04, 0.06 and 0.08 $m^{1/2}$). A characteristic feature of the curves is the decreasing level of the maximum temperature when the opening factor increases at a constant fire load density. The same pattern can be seen in Fig. 5.7, illustrating the corresponding temperature at the depth of 6 cm.

5.3 Structural behaviour measurements

A phenomenological description of the principal behaviour of the fire-exposed structure investigated will introduce the presentation in this section, cf. for instance Fig. 5.8 and 5.9.

When the unilateral fire exposure starts, steep thermal gradients are developing in the structure according to Fig. 5.5. These gradients make the structure deflect downwards but simultaneously the rotation at the supports is prevented and consequently thermal restraint bending moments (negative sign) are induced. This characteristic behaviour is due to the large thermal expansion

effect in the external layer of the plate strips close to the fire-exposed bottom surface and which must be compensated or reduced by a change in the curvature, resulting in downwards deflection, in order to adjust for equilibrium demand. A possible lateral load has the effect of increasing these downwards deflections and restraint moments but, in principal, the structural behaviour is similar to that of a nil-loaded plate strip during the first period of heating. This period is characterized by a considerable increase in deflections and thermal restraint moments which, after a certain time, reach their maximum values about simultaneously, as far as nil-loaded plate strips are concerned. The time for reaching the maximum values depends mainly on the combination of the opening factor and the fire load density. After that time, which sometimes is shorter than the duration of the heating period, the deflections and restraint moments are decreasing and even changing their signs during the subsequent cooling, which also may occur for the laterally loaded strips but not equally accentuated. This feature in behaviour is attributed to the change in the thermal gradient towards a more linear form, the accelerating creep and transient strains (section 6.2) in the zone most strongly influenced by heat and of the cooling itself. The residual state of deflections and thermal moments of, as a rule, considerable magnitude, indicate, as a consequence, the presence of large residual stresses within the fire-exposed structure after cooling down to ambient temperature.

5.3.1 Fire-exposed plate strips without external load

The structural behaviour of the nil-loaded concrete plate strips in a fire environment will be studied in terms of the time-variation of the bending restraint moment, and the deflections in the mid-section and 1/4-section. How different fire environments, defined by varying fire process characteristics, influence the bending restraint moment and the deformation process will be shown by direct comparisons in tables and diagrams for some of the tests of the series A1, A2 and A3, which cover a wide range of heating conditions, cf. Table 4.4. The influence on the structural response by varying the concrete composition and the age

of the specimen prior to the thermal exposure is studied in test series B and C. A brief characterization of these tests will also be done.

The structural response to different fire exposure characteristics is analysed and compared, where partly the opening factor is kept constant and the fire load density varied within the range 126 - 1005 $MJ \cdot m^{-2}$, and partly the fire load density kept constant and the opening factor varied within the range 0.01 - 0.08 $m^{1/2}$.

A collation of some characteristic features of the structural response for the plate strips, accounted for in Table 4.4 is given in Table 5.1, as concerns the maximum negative bending restraint moment and the deflections at the mid-section and 1/4-section together with the times to reach these values. Also the time for the restraint moment to decrease to zero is reported.

From the detailed study of the structural behaviour of the fire-exposed plate strips belonging to the test series A1, A2 and A3, summarily characterized in Table 5.1, the following general conclusions and aspects may be accounted. This study furthermore includes penetrations of circumstances behind the various tests.

The tests, characterized by a constant opening factor ≤ 0.02 $m^{1/2}$ and a fire load density varying within the range 31 - 251 $MJ \cdot m^{-2}$, show an increase in the maximum negative restraint moment and in the maximum downward deflection when the fire load density is increased. Furthermore, the maximum moment values are reached approximately at the end of the heating phase but a similar fact is somewhat irregular for the deflection values. The same is noticed for the maximum negative restraint moment also for larger opening factors, when the fire load density ≤ 251 $MJ \cdot m^{-2}$.

However, at a constant opening factor ≥ 0.02 $m^{1/2}$ and a varying fire load density ≥ 502 $MJ \cdot m^{-2}$ the maximum restraint moment values are almost constant (70 - 80% of M_{yield}) and all attained before the end of the heating period or the start of the cooling. The

Table 5.1 Characteristic results of nil-loaded plate strips

Fire load density $MJ \cdot m^{-2}$	Duration of heating phase h	Maximum restraint moment kNm	Time h	Maximum deflection Midsection mm	Time h	1/4-section mm	Time h	Restraint moment = 0 Time h	Test
a) Opening factor 0.01 $m^{1/2}$									
31	0.50	-6.5	0.52	1.70	0.47	0.9	0.60	1.75	A2:6
63	1.00	-8.0	1.07	1.60	0.85	1.1	0.96	-3.30	A2:7
126	2.00	-9.5	2.25	3.90	2.60	2.4	2.60	-6.50	A2:8
251	4.00	-12.8	4.00	5.40	3.70	3.3	3.70	5.40	A2:1
b) Opening factor 0.02 $m^{1/2}$									
63	0.50	-7.5	0.50	2.70	0.45	1.70	0.45	3.67	A2:9
126	1.00	-9.5	0.97	3.25	1.40	2.00	1.50	3.50	A2:10
251	2.00	-12.8	1.75	4.40	1.30	2.75	1.80	5.00	A2:2
502	4.00	-14.0	2.25	4.83	1.70	3.20	1.90	5.70	A1:11
c) Opening factor 0.04 $m^{1/2}$									
126	0.50	-10.8	0.58	3.83	0.63	2.07	0.40	2.10	A3:1
251	1.00	-11.9	0.87	3.10	0.63	2.20	0.73	2.80	A2:3
502	2.00	-14.6	1.30	6.34	1.10	4.29	1.10	4.30	A1:12
754	3.00	-15.2	1.45	4.58	1.10	2.56	1.10	5.25	A3:2
1005	4.00	-15.1	1.13	5.47	1.07	3.52	1.14	6.70	A3:3
d) Opening factor 0.06 $m^{1/2}$									
126	0.33	-10.6	0.28	3.50	0.38	1.80	0.55	1.60	A3:4
251	0.67	-11.3	0.68	3.40	1.20	2.00	1.37	2.60	A2:4
502	1.33	-15.4	0.85	3.00	0.72	1.80	0.72	2.70	A3:5
754	2.00	-14.2	0.97	3.80	0.80	2.60	0.80	2.85	A3:6
1005	2.67	-15.0	1.05	3.70	0.80	2.90	0.80	4.50	A3:7
e) Opening factor 0.08 $m^{1/2}$									
251	0.50	-10.1	0.53	2.90	0.50	1.90	0.83	2.20	A2:5
502	1.00	-13.9	0.70	3.50	0.57	2.20	0.70	2.25	A3:8
754	1.50	-13.7	0.72	2.90	0.55	2.00	0.55	3.60	A3:9
1005	2.00	-14.9	0.90	2.80	0.72	1.90	0.72	3.70	A3:10

fire duration of the heating period is thus no significant parameter and additionally the deflection values indicate more or less the same feature as the restraint moment values. The maximum values of the restraint moment and the deflections are followed by a decrease before the cooling phase begins and that behaviour is due to accelerating transient and creep strains (see section 6.2) in the cross-sectional areas of concrete most strongly heated and to the successive change in the thermal gradient towards a more linear form.

The comparisons made at a constant opening factor and varying fire load densities make it possible to control the reproducability of the tests and the scattering in results as a common part of the heating period at each opening factor exists. A good reproducability is most often noticed but a dispersion in results cannot be neglected. That deviation or "error" in restraint moment and deflection values may reach values of 10% and 20 - 30% respectively. The reason for the scattering is due to the following factors:

- Deviation from desired thermal exposure depending on the success to follow the prescribed furnace temperature.
- Severe cracking over support may render unintended rotations and make it more difficult to keep the rotations over support exactly at zero.
- Any displacement of reinforcing bars and varying material characteristics.

The structural behaviour in terms of the bending restraint moment is a function of the thermal exposure and this is best shown in comparisons, where the fire load density is constant and the opening factor varied. In such comparisons, the time-curves of the restraint moment show the same pattern as the furnace temperature-time curves, i.e. the rate of moment increase is in accordance with the rate of heating, and the descending branch comes in the same order as cooling does. The structural behaviour is very sensitive to deviation in the imposed thermal gradients.

Table 5.1 and the following illustrations, supplemented with some

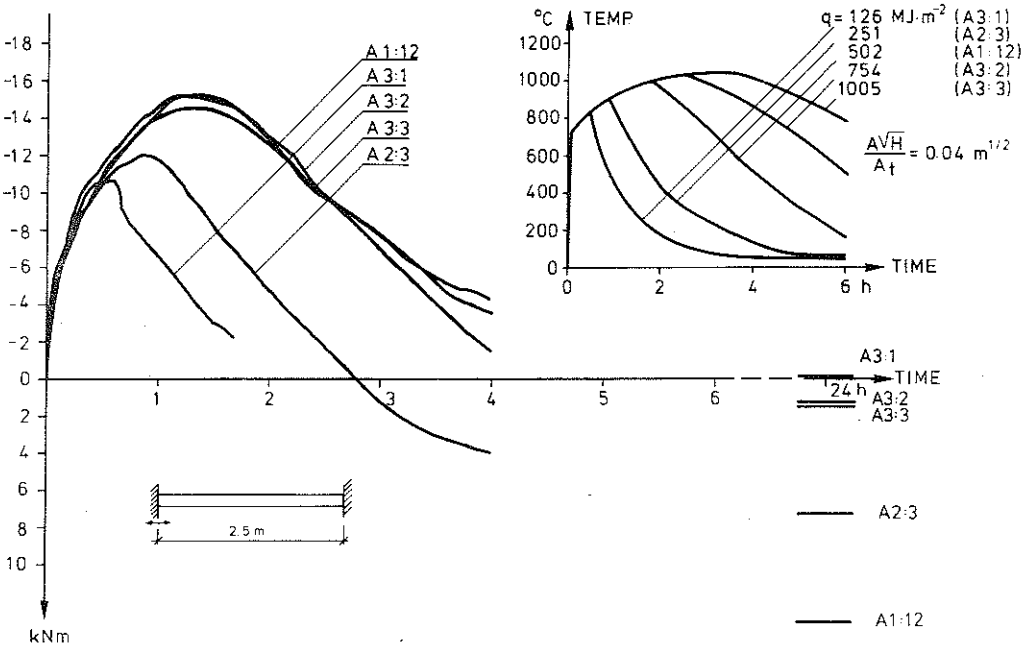

Figure 5.8 Bending restraint moment as function of time. Opening factor: 0.04 $m^{1/2}$. Fire load density within the range 126 - 1005 $MJ \cdot m^{-2}$. The corresponding furnace temperature-time curves are inserted.

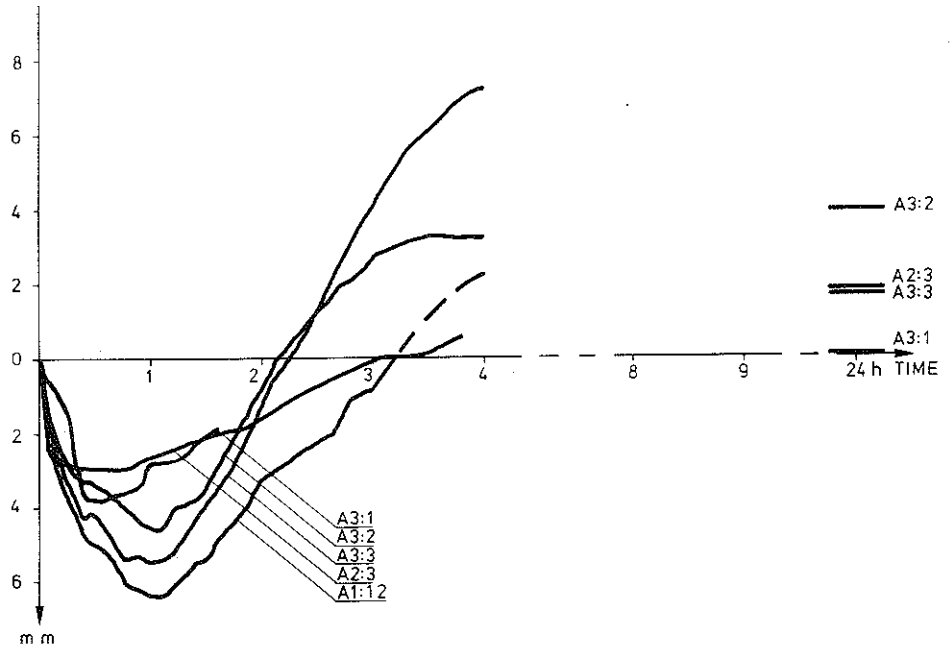

Figure 5.9 Deflection process at mid-section of the plate strip. Fire process characteristics in accordance with Fig. 5.8.

diagrams in Appendix serve to prove these statements. The time-variation of the bending restraint moment and the deflection process at the mid-section of the strips for the tests, characterized by a constant opening factor and a varying fire load density within the range 126 - 1005 $MJ \cdot m^{-2}$, are reproduced in Fig. 5.8 - 5.9. The influence of varying fire processes can be studied as well as the dispersion of the results and the reproducability of the tests during that part of the heating period which is common to the various furnace temperature-time curves.

When analyzing the reasons for the scattering in the results, explanations may be found by studying the real thermal exposure and the temperature development inside the structure. An example of such a study will be given for the tests accounted for in Table 5.1d and illustrated in Figs 5.10 - 5.12. A directly striking result in these figures is shown by the test A3:5, for which the somewhat high maximum restraint moment is followed by comparatively small deflection values as compared with the tests A3:6 and 7. An immediate cause of a pervadingly too high restraint moment should be an oversized thermal exposure. Consequently, the recorded temperatures inside the structure are shown in Fig. 5.13 at mid-section, 1/4-section and end-section for different depths, as concerns the three tests A3:5 - 7. The temperatures for the test A3:5 are thus comparably higher in all sections and this fact must have a considerable effect on the behaviour.

In order to confirm more in detail what is stated summarily in connection with Table 5.1 for tests characterized by a constant fire load density and changing opening factor within the range 0.01 - 0.08 $m^{1/2}$, Figs 5.14 - 16 are additionally shown. The pattern of the curves is recognized and for the tests A1:11 and 12 the rate of increase in the thermal restraint moment is less than for the tests A3:5 and A3:8 due to a smaller opening factor and a corresponding lower rate of heating. Inversely, larger deflection values are reached for the tests A1:11 and 12.

In all diagrams presented in Figs 5.8 - 12 and 5.14 - 16, the

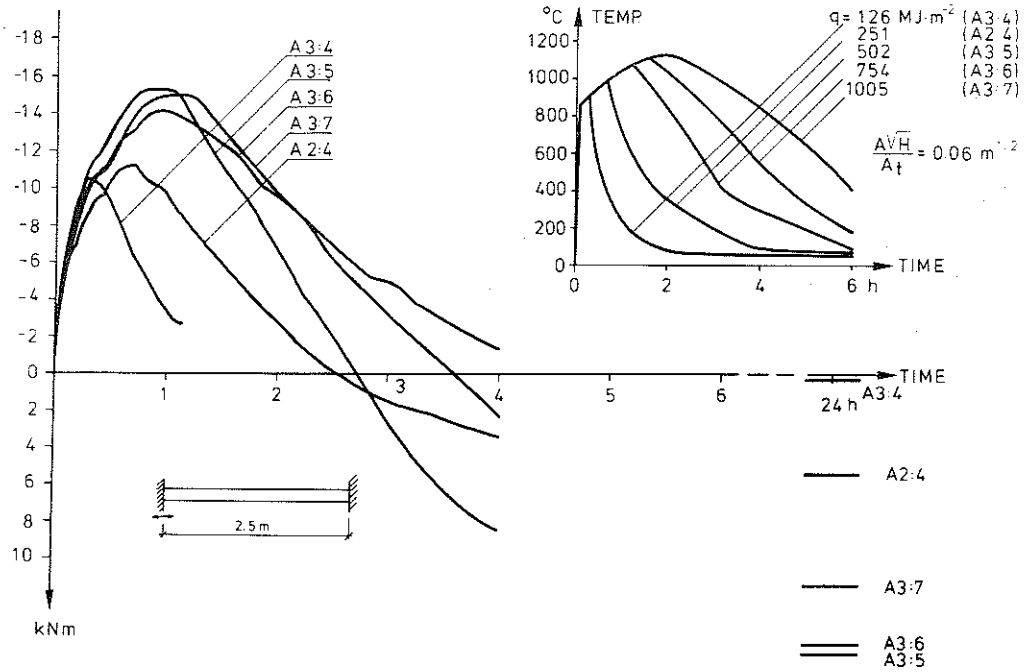

Figure 5.10 Bending restraint moment as function of time. Opening factor: 0.06 $m^{1/2}$. Fire load density within the range 126 - 1005 $MJ \cdot m^{-2}$. The corresponding furnace temperature-time curves are inserted.

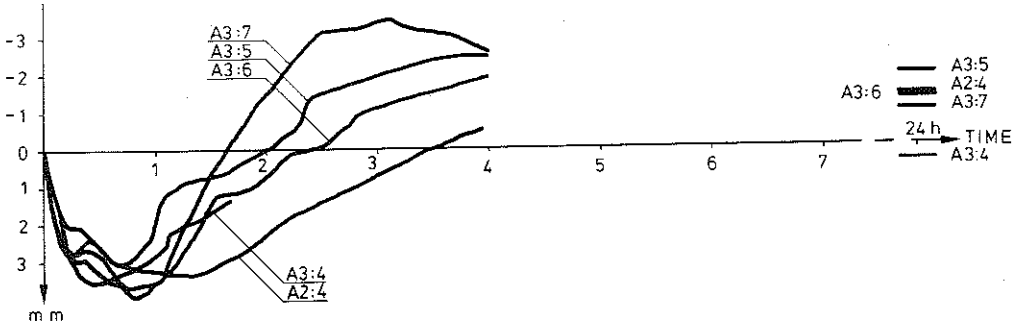

Figure 5.11 Deflection process at mid-section of the plate strip. Fire process characteristics in accordance with Fig. 5.10.

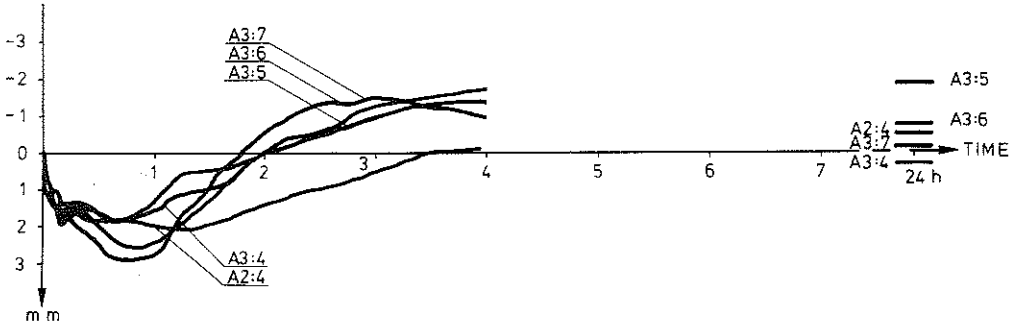

Figure 5.12 Deflection process at 1/4-section of the plate strip. Fire process characteristics in accordance with Fig. 10.

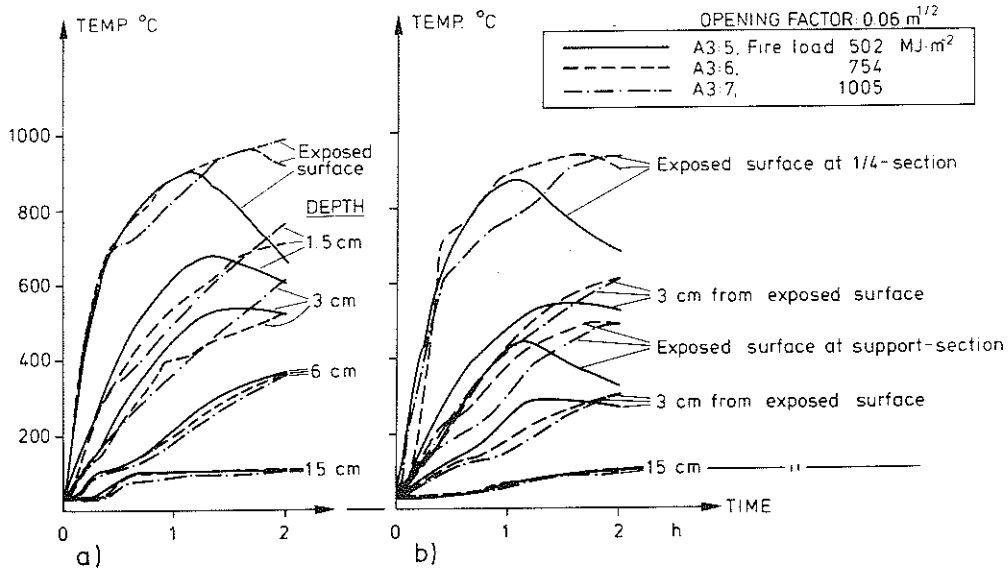

Figure 5.13 Comparison between temperature development with time at different depths of the plate strip in tests A3:5 - 7.
a) mid-section
b) 1/4- and support-sections.

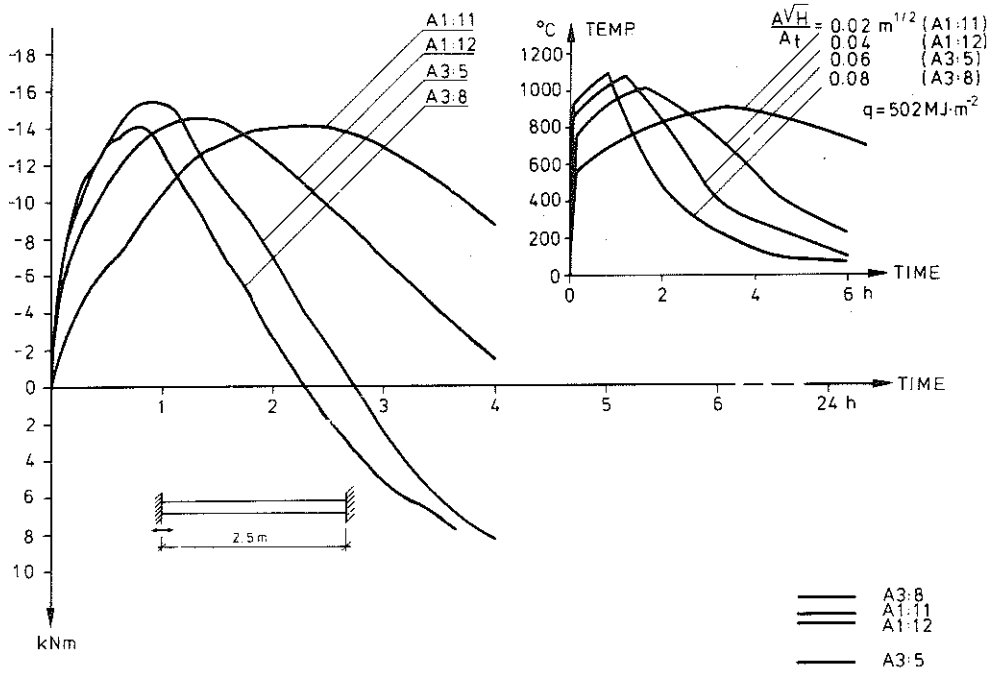

Figure 5.14 Bending restraint moment as function of time. Fire load density: 502 $MJ \cdot m^{-2}$. Opening factor within the range 0.01 - 0.08 $m^{1/2}$. The corresponding furnace temperature-time curves are inserted.

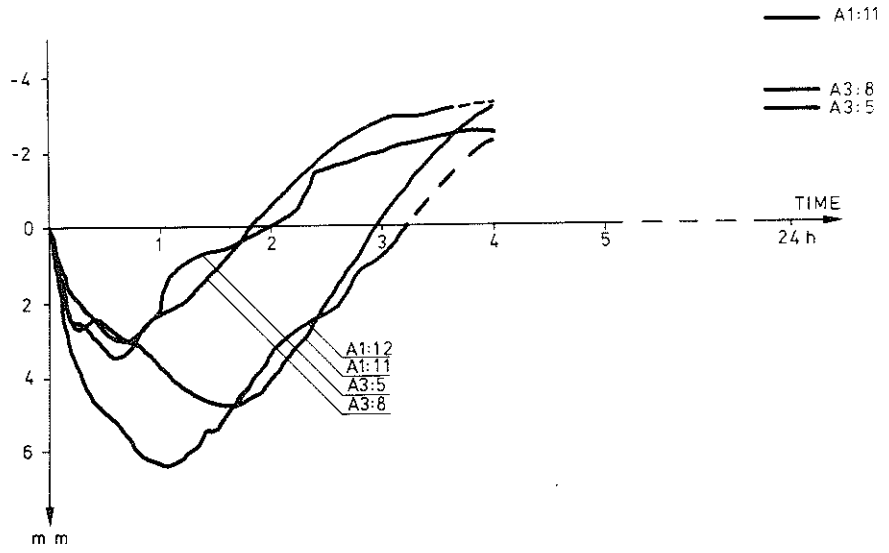

Figure 5.15 Deflection process at mid-section of the plate strip.
Fire process characteristics in accordance with Fig. 5.14.

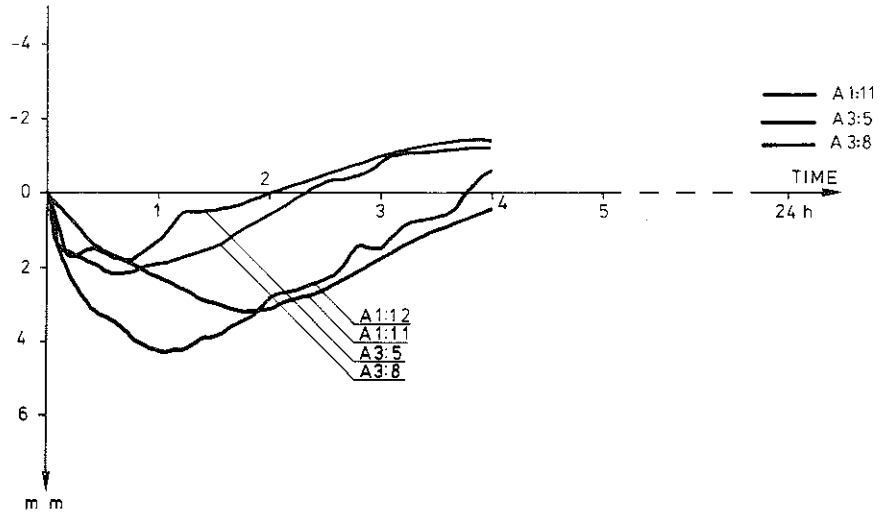

Figure 5.16 Deflection process at 1/4-section of the plate strip.
Fire process characteristics in accordance with Fig. 5.14.

residual state of restraint moment and deflections are also indicated. The residual state of the fire-tested plate strips belonging to test series A2 and A3, complemented with A1:12 is assorted in Table 5.2. A pervading feature of these tests is a positive residual restraint moment, which roughly increases with an increasing fire load density at a constant opening factor. Inversely, the influence on the residual restraint moment of variations in the opening factor at a constant fire load density is comparatively small. For lower fire load densities within the range 31 - 126 $MJ \cdot m^{-2}$, the residual deflection is close to zero. For higher fire load density values, $\geq$ 251 $MJ \cdot m^{-2}$, a residual upwards deflection occurs.

For the results of the tests in test series B and C in which the fire exposure generally was the same, q = 502 $MJ \cdot m^{-2}$ and $A\sqrt{H}/A_t$ = = 0.04 $m^{1/2}$, but the concrete composition was changed in terms of water-cement ratio and cement-paste quantity, here only some concluding remarks will be given, cf. Anderberg (1973).

A noticable influence of varying water-cement ratio is a delay in time, when the maximum restraint moment is achieved. It can also be established that an increase in cement-paste quantity shortens the time at which the restraint moment changes sign, probably due to more excessive shrinkage, creep and transient strain (cf. section 6.2) at elevated temperatures. The influence of specimen age prior to fire (1/2, 1, 3 months) was also investigated (see Table 4.4), but no significant change in the structural behaviour was noticed, except that more water transpired from the specimen of the age of 1/2 month.

The occurrence of spalling gave the impression of a random character and was noticed for about 8 of totally 50 tests and only for those which were characterized by a high rate of heating, i.e. opening factors within the range of 0.04 - 0.08 $m^{1/2}$ and fire load density $\geq$ 251 $MJ \cdot m^{-2}$. Spalling took place after about 15 - 20 min at the directly exposed corners and surface layers and appeared with irregular frequency and distribution.

Table 5.2 Residual state of fire exposed plate strips without lateral load

Test	Fire load density	Opening factor	Residual restraint moment	Residual deflections	
				mid-section	1/4-section
	$MJ \cdot m^{-2}$	$m^{1/2}$	kNm	mm	mm
	31-126				
A2:6	31	0.01	2.0	0.6	0.3
:7	63	0.01	1.2	0.2	0.2
:9	63	0.02	1.0	0.4	0.3
:8	126	0.01	1.5	0.4	0.1
:10	126	0.02	2.0	0.5	0.5
A3:1	126	0.04	0.0	0.0	0.3
:4	126	0.06	2.0	0.4	0.3
A2:1	251	0.01	4.3	-0.5	-0.3
:2	251	0.02	7.9	-2.2	-0.6
:3	251	0.04	7.3	-1.9	-0.4
:4	251	0.06	5.4	-1.3	-0.6
:5	251	0.08	5.3	-1.6	-0.2
A1:12	502	0.04	12.0	-	-
A3:5	502	0.06	15.0	-3.0	-1.9
:8	502	0.08	11.6	-3.5	-1.3
A3:2	754	0.04	13.0	-3.9	-2.0
:6	754	0.06	14.6	-1.3	-0.8
:9	754	0.08	13.2	-3.3	-2.2
A3:3	1005	0.04	14.4	-1.7	-0.1
:7	1005	0.06	13.5	-0.9	-0.2
:10	1005	0.08	14.4	-3.4	-1.9

5.3.2 Fire-exposed plate strips with lateral load

All fire-exposed plate strips, tested in the presence of a lateral load, belong to test series D, cf. Table 4.4. These tests can be combined into five groups according to Table 5.4 with each group characterized by its own fire exposure, the tests D21 and D22 excluded. At such a grouping, it is a matter of course that also the nil-loaded plate strips (P = 0), tested at the same fire exposure characteristics, are included - tests A2:5, A2:3, A2:1, A1:12 and A3:8, respectively.

As the results from the five groups of tests generally compared in section 6 with the theoretically calculated structural behaviour, the presentation here can be made very summarily. An integrated picture of the structural behaviour is given in Table 5.4, comprising only the maximum support moment and the maximum deflection in the mid-section and 1/4-section of the plate strips and the time of their occurrences. Additionally the complete structural fire behaviour of the loaded plate strips is exemplified for the tests of group 2 in terms of the time-variation of the bending restraint moment and the deflection process at the mid- and 1/4-sections. The moment distribution and the load-carrying capacity of the strips under fire will, however, not be studied until section 5.5.

Before the start of a fire test, the water-levels over the supports were adjusted to zero. Then the lateral load was applied with the plate strips restrained against rotation at the supports. The start values of the restraint moments, achieved in this way for the different tests are shown in Table 5.3a. Tests represented by the same load level show somewhat different start values of the restraint moment. This is partly due to inevitable differences from one specimen to another as regards the dimensons, location of the longitudinal reinforcement and material quality, giving a varying distribution of the flexural stiffness in the longitudinal direction of the plate strips. Also the difficulty in applying the load and simultaneously, increasing the restraint moment so that the rotation over both supports

Table 5.3 Measured and calculated start values of restraint moment and central deflection due to lateral load.

a) Measured start values

Load level	Restraint moment							
	Test kNm	Test kNm	Test kNm	Test kNm	Test kNm	Test kNm	Test kNm	Test kNm
$1/4 \cdot P_{all}$	D1 2.8	D5 2.8	D9 2.5	D13 2.5	D17 4.6			
$1/2 \cdot P_{all}$	D2 5.3	D6 4.6	D10 5.4	D14 5.0	D18 4.6			
$3/4 \cdot P_{all}$	D3 7.5	D7 6.9	D11 8.1	D15 8.0	D19 6.7			
P_{all}	D4 10.6	D8 9.8	D12 9.1	D16 8.7	D20 10.1			
P_{all}	D21 9.1	D22 9.1						

b) Calculated start values

Load level	Restraint moment		Central deflection
	Theory of elasticity kNm	FIRES-RC program kNm	FIRES-RC program mm
$1/4 \cdot P_{all}$	2.3	2.3	0.2
$1/2 \cdot P_{all}$	4.5	4.4	0.4
$3/4 \cdot P_{all}$	6.8	6.2	1.2
P_{all}	9.1	9.3	2.3

is kept at zero value, influence the start value. It thus occurred that the restraint was partly adjusted just after the total load was applied, which caused a somewhat increased cracking both at the mid- and end-sections of the plate strip.

If the start value of the restraint moment at a specified load level is calculated for the plate strip in accordance with the theory of elasticity, i.e. the flexural stiffness is assumed constant over the length of the span, the obtained values, given in Table 5.3b, are constantly lower than the measured ones. If, instead, the start value of the restraint moment is calculated according to a more sophisticated theory, based on more realistic material models, including the formation of cracks and the tensile carrying ability, and considering the moment redistribution, the result will be somewhat changed. This is also shown in Table 5.3b, which also contains the simultaneously calculated central deflection values. The FIRES-RC program, originally developed at University of California, Berkeley, indicated in the table and used in the calculation, will be presented later. Trying to interpret the results from the FIRES-RC calculation, the following can be stated. The cracking moment is about 5 kNm which is reached at the support sections for a load level between 1/2 P_{all} and 3/4 P_{all}. The calculated deflections confirm that the deflection is doubled when the load is increased from 1/4 to 1/2 P_{all}. At the next load level 3/4 P_{all}, the deflection increases considerably due to severe cracking over the supports. At the same time the moment is redistributed to the mid-section, where no cracking has taken place, which explains the somewhat smaller restraint moment value at this load level than the corresponding value according to the theory of elasticity. When the load has reached P_{all}, a considerable cracking has occurred also in the mid-section which causes a substantial increase in the deflection and a further moment redistribution.

The measured restraint moment values are pervadingly greater than the theoretical values, except in the tests D12, D21 and D22 which are to be excluded, because in these tests the applied support moment at the load level P_{all} was chosen to 9.1 kNm and

Table 5.4

Test	Fire load density	Opening factor	Duration of heating phase	Load level	Maximum support moment		Maximum deflection			
							mid-section		1/4-section	
	$MJ \cdot m^{-2}$	$m^{1/2}$	h	P_{all}	kNm	Time h	mm	Time h	mm	h
Group 1										
A2:5	251	0.08	0.5	0	-10.1	0.53	2.9	0.50	1.9	0.83
D1	"	"	"	1/4	-13.7	0.50	4.8	1.10	2.9	1.10
D2	"	"	"	1/2	-16.2	0.60	9.1	1.05	6.0	1.10
D3	"	"	"	3/4	-17.3	0.50	12.6	0.80	7.5	0.80
D4	"	"	"	1	-18.5	0.35	14.4	0.80	9.5	0.65
Group 2										
A2:3	251	0.04	1.0	0	-11.9	0.87	3.1	0.73	2.2	0.73
D5	"	"	"	1/4	-17.0	0.80	7.0	0.95	4.0	1.20
D6	"	"	"	1/2	-17.5	0.75	11.0	1.20	6.4	1.27
D7	"	"	"	3/4	-18.2	0.73	15.3	1.45	9.6	1.45
D8	"	"	"	1	-19.1	0.65	17.8	1.15	11.4	1.30
Group 3										
A2:1	251	0.01	4.0	0	-12.8	4.0	5.4	3.7	3.4	3.7
D9	"	"	"	1/4	-16.9	3.85	7.2	4.65	4.3	4.25
D10	"	"	"	1/2	-18.1	3.65	9.6	3.65	6.5	3.65
D11	"	"	"	3/4	-17.3	3.80	14.2	3.80	9.4	3.80
D12	"	"	"	1	-18.2	2.25-3.80	17.0	3.75-4.2	10.8	3.50
Group 4										
A1:12	502	0.04	2.0	0	-14.6	1.3	6.3	1.10	4.3	1.10
D13	"	"	"	1/4	-16.6	1.15	5.2	1.10	2.3	1.30
D14	"	"	"	1/2	-17.9	1.15	15.7	1.75	10.2	1.75
D15	"	"	"	3/4	-18.0	1.15	21.3	1.70	13.6	1.70
D16	"	"	"	1	-19.5	1.15	26.2	1.78	16.7	1.78
Group 5										
A3:8	502	0.08	1.0	0	-13.9	0.70	3.5	0.57	2.2	0.70
D17	"	"	"	1/4	-17.4	0.72	5.2	1.25	2.1	0.87
D18	"	"	"	1/2	-17.5	0.78	12.2	1.18	6.9	1.07
D19	"	"	"	3/4	-18.4	0.50	18.4	1.20	10.6	1.20
D20	"	"	"	1	-19.1	0.80	23.3	1.60	14.3	1.60
D21	1005	0.06	2.7	1	-19.8	1.20	34.8	5.20	21.7	4.60
D22	1506	"	4.0	1	-18.6	1.10	45.4	7.20	26.4	7.20

after that this situation was considered as the state of no rotation over the supports. The start value of the test D17 deviates too much and is accordingly too high. These deviations in the start values of the restraint moment do, however, have a little influence on the structural behaviour during fire.

Some characteristic main results of the laterally loaded plate strips at fire can be studied in Table 5.4. From this table the following may be stated:

- Increasing load level gives rise to maximum values of the restraint moment and the deflections at mid- and 1/4-sections.
- At a constant load level and a constant opening factor, the maximum deflection increases when the fire load density is increased.
- If the fire load density is constant and the opening factor is diminishing in the region above 0.04 $m^{1/2}$, the maximum deflection increase.
- The time to reach the maximum restraint moment approximately coincides with the duration of the heating period, except when the fire load density $\geq$ 502 $MJ \cdot m^{-2}$ and the opening factor $\geq$ 0.04 $m^{1/2}$. In these cases, this is shorter than the duration of the heating period.

The time variation of the structural response to fire is illustrated in Fig. 5.17 - 19 for the tests within group 2, viz. D5 - 8 complemented with A2:3, for which the fire exposure is characterized by the fire load density 251 $MJ \cdot m^{-2}$ and the opening factor 0.04 $m^{1/2}$ and the lateral load of a level varying from 0 to P_{all}. In Fig. 5.17 the restraint moment and the corresponding furnace temperature are reproduced as functions of time. The curves are characterized by a very rapid increase in restraint moment during the first 0.25 hours and the maximum moment values are reached after about 0.8 hours. The yielding moment is definitely attained at the supports for the load level $P = P_{all}$ and amounts to 19.1 kNm. Also at the load level $P = 3/4\ P_{all}$, the yielding moment may have been reached even if the

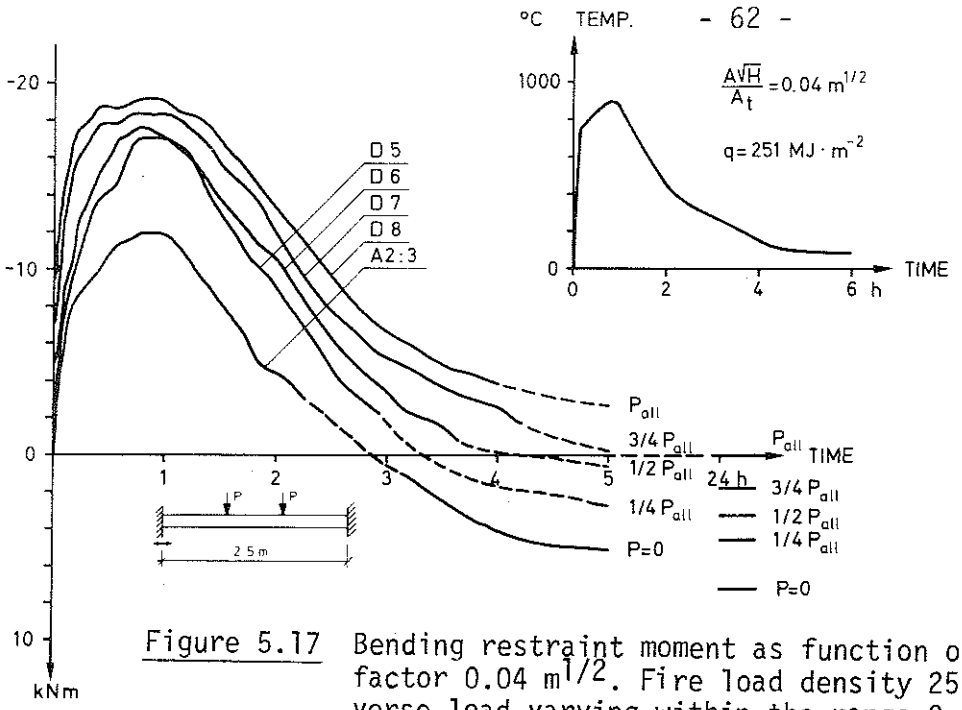

Figure 5.17 Bending restraint moment as function of time. Opening factor 0.04 $m^{1/2}$. Fire load density 251 $MJ \cdot m^{-2}$. Transverse load varying within the range 0 - P_{all}, where P_{all} = the allowable load at ambient temperature according to Swedish Concrete Standards. The corresponding temperature-time curve is inserted.

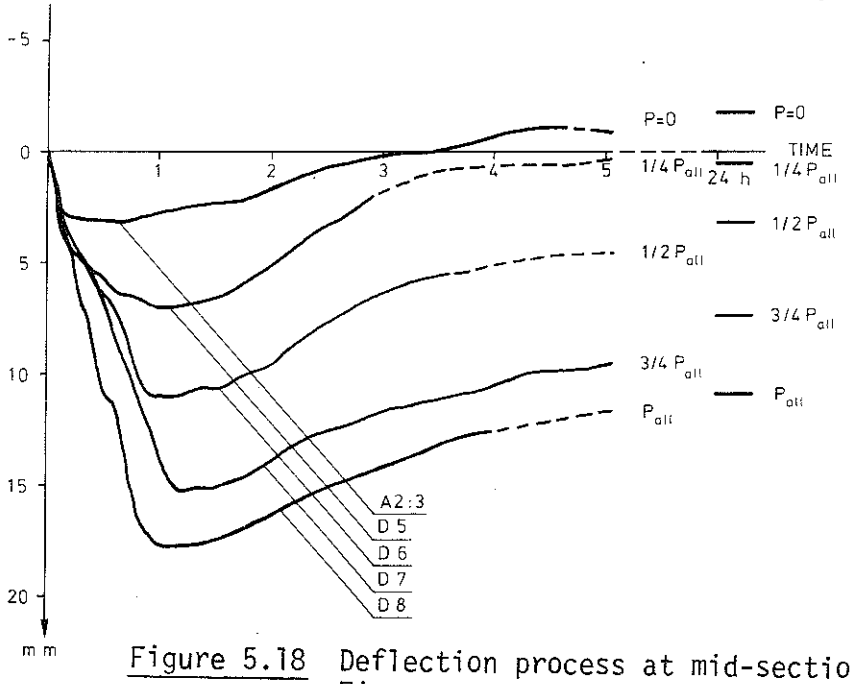

Figure 5.18 Deflection process at mid-section of the plate strip. Fire process characteristics and transverse load in accordance with Fig. 5.17.

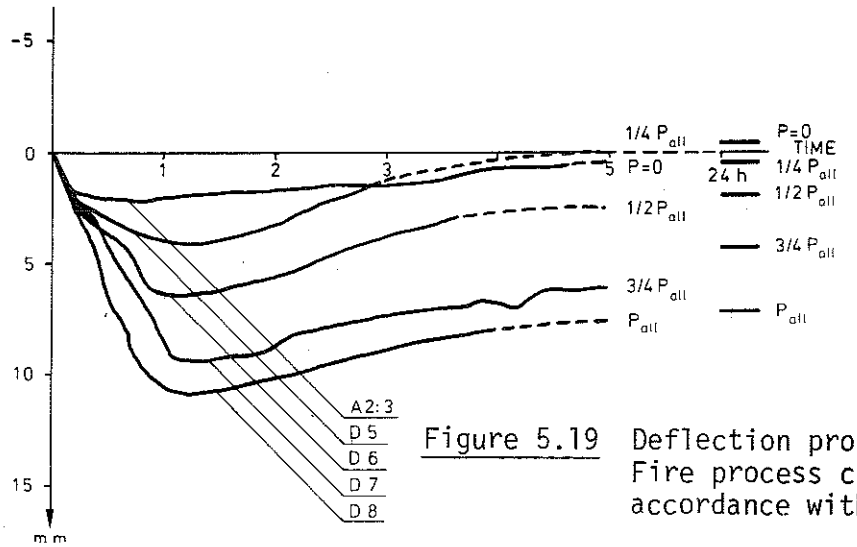

Figure 5.19 Deflection process at 1/4-section of the plate strip. Fire process characteristics and transverse load in accordance with Fig. 5.17.

maximum value only amounts to 18.2 kNm due to a possible unintensional displacement of the top reinforcement. A lowering of these reinforcing bars of 1/2 cm renders a drop in the yielding moment of about 1 kNm (cf. the calculations in 6.2.4). The rapid increase in restraint moment comes from the induced steep thermal gradient during heating, cf. Fig. 5.5, which forces the structure to find new equilibrium states resulting in a downwards deflection.

The corresponding time variation of the deflections is illustrated in Fig. 5.18 - 19 for the mid- and 1/4-sections of the strips. The initial deflections due to the application of the load prior to the fire exposure are omitted in the diagrams but are assorted in Table 5.3b. The deflections grow almost linearly until the maximum values are attained. The maximum central deflection at the load level P_{all} is 5.7 times larger than that at zero-load and corresponds to about 1/140 of the total length of the span.

During cooling, the restraint moments of the loaded plate strips (Fig. 5.17) decrease considerably and attain positive values after some hours. Also the deflections (Fig. 5.18 - 19) are continously decreasing but not changing sign during the cooling, as concerns the loaded plate strips.

As observed, an unintentional displacement of the top reinforcement influences the yielding moment at the support sections. This is further illustrated by the tests D21 and D22 in which the yielding moment attained the values -19.8 and -18.6 kNm, respectively. As pointed out before, these tests were designed to illustrate the structural behaviour up to a collapse of the plate strips during the fire process (see Table 5.4). No collapse happened, however, and the reason for that will be studied later on in section 5.5 with respect to the remaining reserve load-carrying capacity. From Table 5.4, extreme deflection values are observed and for test D22 the maximum central deflection reaches the value 45.4 mm which corresponds to 1/55 of the span length.

Table 5.5 Residual state of fire-exposed plate strips with lateral load

Test	Fire load density	Opening factor	Load level	Residual restraint moment	Residual deflection	
					mid-section	1/4-section
	$MJ \cdot m^{-2}$	$m^{1/2}$	P_{all}	kNm	mm	mm
Group 1						
A2:5	251	0.08	0	5.3	-1.6	-0.2
D1	"	"	1/4	4.0	2.7	1.3
D2	"	"	1/2	2.4	4.3	2.8
D3	"	"	3/4	-1.2	6.7	4.1
D4	"	"	1	-2.4	10.2	-
Group 2						
A2:3	251	0.04	0	7.3	-1.9	-0.5
D5	"	"	1/4	4.6	0.5	0.6
D6	"	"	1/2	3.2	3.2	2.0
D7	"	"	3/4	1.8	7.0	4.5
D8	"	"	1	0.0	10.7	7.7
Group 3						
A2:1	251	0.01	0	4.3	-0.5	-0.3
D9	"	"	1/4	3.0	-	-
D10	"	"	1/2	0.9	-	-
D11:2	"	"	3/4	1.2	-	-
D12	"	"	1	0.0	13.5	9.2
Group 4						
A1:12	502	0.04	0	12.0	-	-
D13	"	"	1/4	11.0	-0.3	-1.5
D14	"	"	1/2	8.4	7.8	-
D15	"	"	3/4	4.6	13.5	9.3
D16	"	"	1	3.4	21.0	11.8
Group 5						
A3:8	502	0.08	0	11.6	-3.5	-1.3
D17	"	"	1/4	-	-	-
D18	"	"	1/2	5.8	3.1	1.4
D19	"	"	3/4	5.7	10.0	6.2
D20	"	"	1	3.1	19.5	11.8
D21	1005	0.06	1	-2.6	33.5	19.0
D22	1506	0.06	1	-8.5	35.7	20.0

The residual state after 24 hours of the tests according to Table 5.4 is assorted in Table 5.5 and can be studied separately there. Though the plate strips are loaded vertically, considerable residual restraint moments of positive sign appear, but the residual deflections are mostly still directed downwards. This behaviour is due to the very large rotations developed during heating at the support sections of the plate strips, rendering a great inelastic deformation in concrete and reinforcing steel. These permanent deformations influence the behaviour during cooling in such a way that, when the deflections successively decrease, the restraint moment changes signs far before the deflections eventually reach zero values. As observed in Table 5.5 the residual restraint moment is decreasing at increased load level, but at the same time the residual deflection is increasing.

5.4 Change in flexural stiffness during fire exposure

The continuous change in the flexural stiffness of a reinforced concrete structure due to a thermal exposure is of a great phenomenological importance for a full understanding of the structural behaviour of a fire exposed hyperstatic structure and will hence be studied for the current type of plate strip. The effect on the flexural stiffness of a complete fire process, including the cooling phase, then will be determined for the nil-loaded plate strips belonging to the test series A2 and A3, cf. Table 4.4.

The change in the flexural stiffness, owing to a pure fire exposure, is primarily a measure and a result of the cracking formation and propagation and an eventual disintegration of the material along and within the hyperstatic plate strip, induced by the thermal gradients and the elevated temperatures. Also the reduction in the elastic moduli of the concrete and the steel reinforcement influence the flexural stiffness but not to the same extent. After fire, when ordinary room temperature is attained again, the residual flexural stiffness mainly depends on the extent of the residual cracking formation and the material

Table 5.6 Flexural stiffness of plate strips during fire

Test	Fire load density q MJ/m^2	Opening factor $\frac{A\sqrt{H}}{A_t}$ $m^{1/2}$	Duration of heating T h	Cube strength MN/m^2	Measured initial flexural stiffness MNm^2	Minimum value of flexural stiffness %x)	Time for minimum stiffness h	Flexural stiffness after fire %x)	Calculated and representative values of initial flexural stiffness MNm^2
A2:1	251	0.01	4	28.6	-	28	55	5	
A2:2	251	0.02	2	28.0	-	43	52	4	
A2:3	251	0.04	1	29.1	-	41	60	2	
A2:4	251	0.06	2/3	25.2	2.3	34	51	1-2	
A2:5	251	0.08	1/2	30.7	2.3	29	61	1	$E_c I_c = 2.34$
A2:6	31	0.01	1/2	27.9	2.6	56	75	2	$E_s I_s = 0.33$
A2:7	63	0.01	1 27.	27.9	2.8	45	64	2	
A2:8	126	0.01	2	28.2	2.7	47	69	-	$EI = E_c I_c + E_s I_s =$
A2:9	63	0.02	1/2	27.8	-	41	75	1	$= 2.67$
A2:10	126	0.02	1	29.7	-	-	-	-	
			Mean value	28.3	2.54				
A3:1	126	0.04	1/2	38.6	3.1	34	49	2	
A3:2	753	0.04	3	34.0	2.5	22	40	8	
A3:3	1004	0.04	4	35.0	2.7	20	35	8	
A3:4	126	0.06	1/3	36.3	3.0	31	52	1	$E_c I_c = 2.63$
A3:5	502	0.06	1 1/3	36.1	3.0	28	56	2	
A3:6	753	0.06	2	33.7	3.4	38	57	1.5	$E_s I_s = 0.33$
A3:7	1004	0.06	2 2/3	39.6	-	19	49	6	$EI = 2.96$
A3:8	502	0.08	1	34.5	3.1	19	41	4	
A3:9	753	0.08	1 1/2	38.0	2.8	26	49	3	
A3:10	1004	0.08	2	35.2	2.7	26	41	2	
			Mean value	36.1	2.92				

x) % of the calculated initial flexural stiffness

$E_c = 5200\ c^{1/2}\ MN/m^2$ $c = 0.8 \cdot \sigma_{cube}\ MN/m^2$

disintegration while the modulus of the steel reinforcement is fully regained.

The flexural stiffness, experimentally determined during the fire test by measuring the additional deflection response in the mid- and 1/4-sections to an instantaneous transverse load (see section 4.4) at different times, will be regarded as a fictitious stiffness of the whole plate strip. The presented results of the flexural stiffness, referred to the additional deflections, are the average of the fictitious stiffness values calculated from the mid- and 1/4-section deflections in accordance to the equations 5.6 and 5.8 in section 5.6.

As shown in Table 5.6, there is sometimes considerable discrepancy of the measured initial flexural stiffness from one plate strip to another within a test series, although the concrete mix variations are small. The concrete in each plate strip is characterized by a cube strength value, determined as the mean value from six cubes, but - as can be seen in Table 5.6 - the measured variations in the initial flexural stiffness were not in accordance with the variations in the cube strength values. A higher cube strength value did not always indicate a higher stiffness and vice versa. It must, however, be underlined that all measurements, giving the fictitious flexural stiffness, have a great uncertainty and hence the presented results are only giving a qualitative picture of the change in the flexural stiffness during a fire process.

On the basis of the difficulties, it was found appropriate to use a calculated value of the initial flexural stiffness EI as a start value for the further treatment. EI then was determined by the formula

$$EI = E_c \cdot I_c + E_s \cdot A_s \qquad 5.1$$

where

E_c = elastic modulus of concrete
I_c = moment of inertia
E_s = elastic modulus of steel reinforcement
A_s = steel reinforcement area

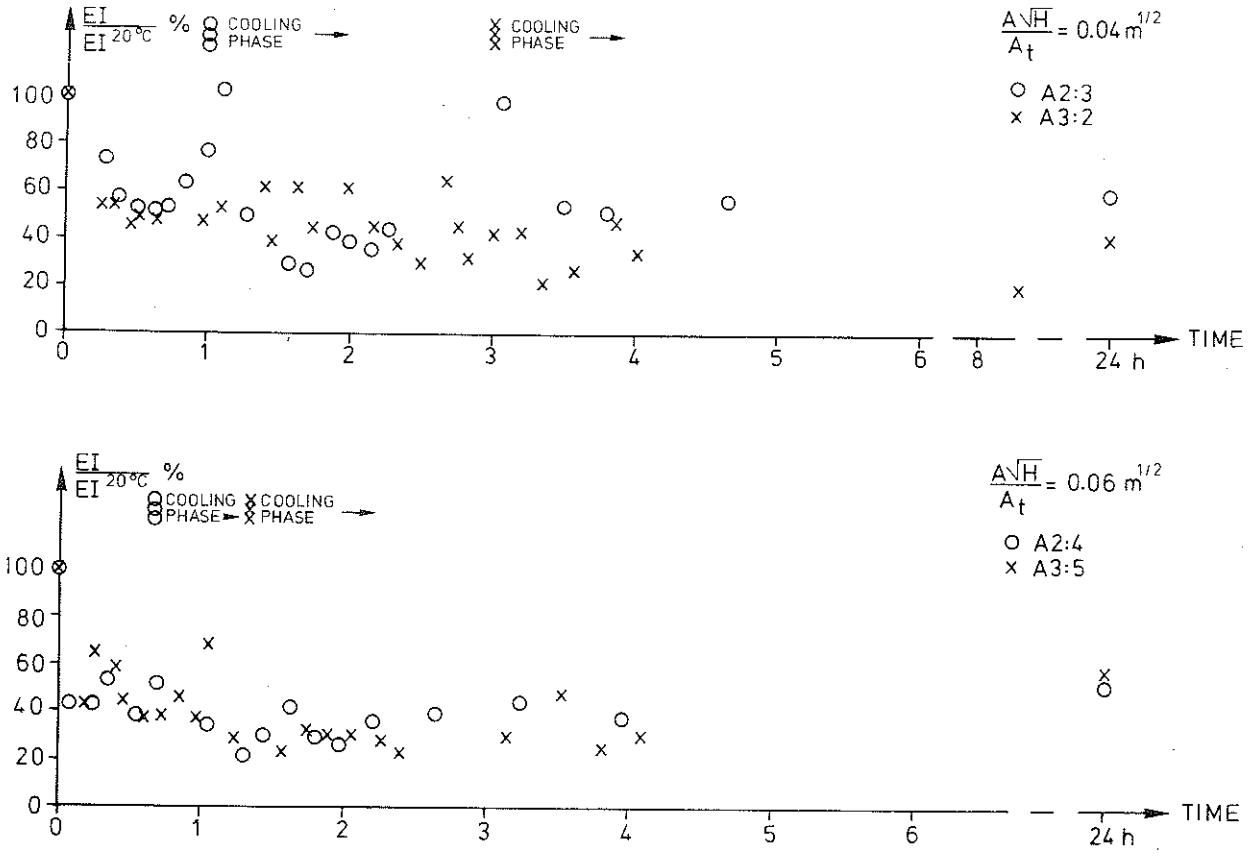

Figure 5.20 Time variation of fictitious flexural stiffness during fire of nil-loaded plate strips.

E_c is given by the formula

$$E_c = 5200 \cdot c^{1/2} \ MN/m^2 \qquad 5.2$$

where

$$c = 0.8 \cdot \sigma_{cube} \ MN/m^2 \quad (\sigma_{cube} = \text{cube strength})$$

These formulae are verified to give a good agreement with test results at ambient temperatures.

By using the average cube strength values from test series A2 and A3, which are shown in Table 5.6, EI is calculated to 2.67 and 2.96 MNm^2 respectively. These calculated values are in a reasonably good agreement with the measurements, as can be seen in the table.

As an illustration of the time-variation of the flexural stiffness, defined above, the results from the tests A2:3 and A3:2, representing the opening factor 0.04 $m^{1/2}$ and the fire load density 251 and 753 MJ/m^2, respectively, and the tests A2:4 and A3:5, representing the opening factor 0.06 $m^{1/2}$ and the fire load density 251 and 502 MJ/m^2, respectively, are reproduced in Fig. 5.20. Due to the wide dispersion in the measurements, the diagram only gives a hint of how the flexural stiffness alters. Characteristic is a great decrease of 30 - 60% of the initial value during the first 0.25 hours, followed by a more slowly continued decrease, which stops after 1 - 2 hours in the cooling phase, indicated in the figure. After that, the flexural stiffness starts to increase and attains values up to twice the minimum value after 24 hours. The minimum values and the values after fire of the flexural stiffness are gathered in Table 5.6, given in percentage of the calculated initial flexural stiffness. These values are furthermore assorted in Table 5.7, which illustrates the decrease in the minimum flexural stiffness and the flexural stiffness after fire, when the fire load density is increased. As can be noticed from the table, the minimum stiffness value may decrease to only 19% of the original value and this value represents the fictitious stiffness of the whole plate strip, whereas, for instance, the flexural stiffness at the mid-section is much less with almost the whole cross-section being cracked.

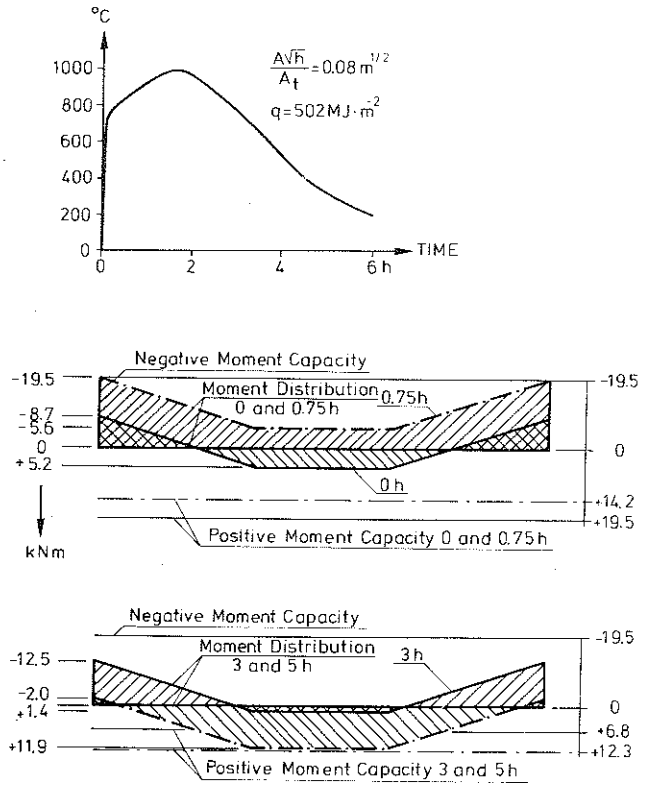

Figure 5.21 Bending moment distribution and bending moment capacity during fire-exposure for test D16. Fire load density 502 $MJ \cdot m^{-2}$. Opening factor: 0.08 $m^{1/2}$. Load level: $P = P_{all}$. The corresponding furnace temperature-time curve is inserted.

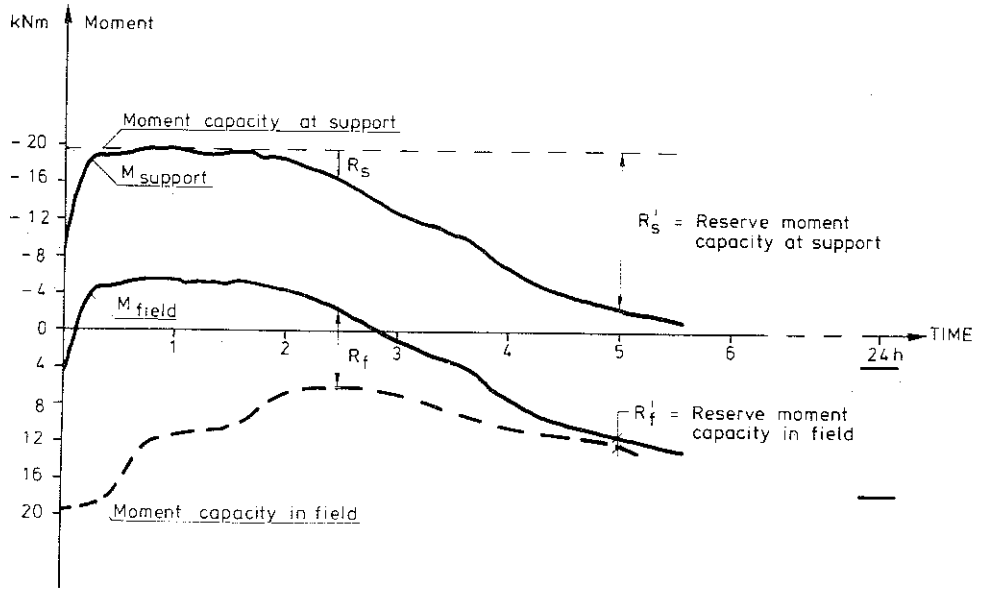

Figure 5.22 Time variation of current bending moment and calculated moment capacity at supports and in field for test D16. See further Fig. 5.21.

Table 5.7 Minimum and residual flexural stiffness of the plate strips

Number of tests	Fire load	Minimum flexural stiffness		Residual flexural stiffness	
		variation	mean value	variation	mean value
	MN/m^2	%	%	%	%
7	31 - 126	31-56	42	49-75	64
5	251	28-43	35	51-61	55
2	502	19-28	24	41-56	48
3	753	22-38	29	40-57	48
3	1004	19-26	22	35-49	45

5.5 Load-bearing capacity during and after fire exposure

In an analysis of the mechanical behaviour of a fire-exposed structure, it is of great interest to follow up the bending moment distribution, compared with the load-bearing capacity in decisive sections, in order to search into the reserve moment capacity and make conclusions about the safety to collapse. One way of illustrating this problem is shown in Fig. 5.21, giving the bending moment distribution at four different times (0, 0.75, 3.0, 5.0 h) for the plate strip in test D16, transversely loaded by $P = P_{all}$. For comparison, the corresponding values of the negative moment capacity at the supports and the positive moment capacity at the midspan are indicated. These moment capacities are evaluated for the plate strips as underreinforced on the basis of the current reinforcement temperatures at the top over the support and at the bottom in the mid-section, respectively, and no consideration is taken to any reduction in the concrete strength of the compressive zones. This is motivated by the fact that rather low temperatures are predominant in these zones as well as by the very insignificant decrease in concrete strength below

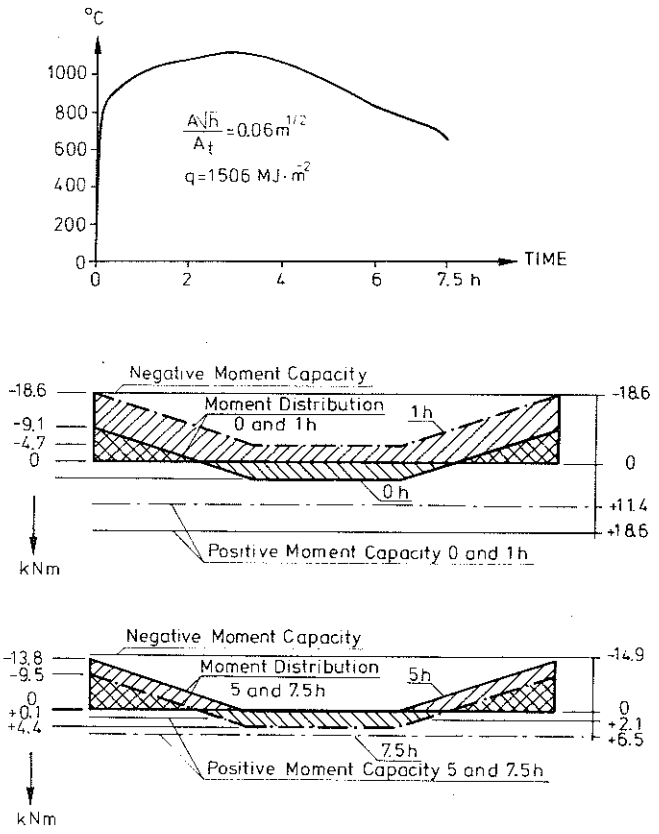

Figure 5.23 Bending moment distribution and bending moment capacity during fire exposure for test D22. Fire load density 1506 MJ·m^{-2}. Opening factor: 0.06 m$^{1/2}$. Load level: P = P_{all}. The corresponding furnace temperature-time curve is inserted.

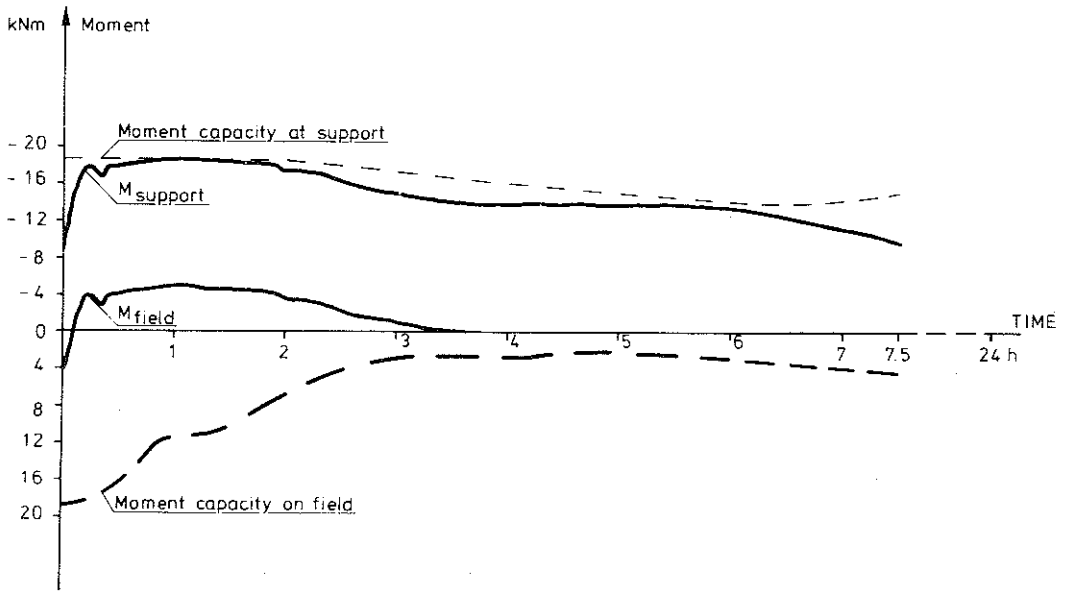

Figure 5.24 Time variation of current bending moment and calculated moment capacity at supports and in field for test D22. See further Fig. 5.23.

300 - 400°C, which temperature level never is exceeded for the investigated plate strips in the current compression zones. By measuring the temperatures in the reinforcement and using the data concerning the relationship between the yield strength and the temperature, presented in section 6.2.2.2, an approximate value of the load-bearing capacity is calculated. This way of calculating the moment capacity is further discussed in section 6.2.2.2. It may be noted from Fig. 5.21 that the initial moment capacity has the value $\pm$19.5 kNm, which is reduced in the span to only 6.8 kNm at 3 hours, at the supports, the corresponding reduction can be disregarded. At 5 hours, i.e. about 3 hours after the end of the heating phase the current moment in span is 11.9 kNm and the positive moment capacity 12.3 kNm, which means that the moment capacity in field is made full use of up to 97%. If the moment capacity is attained either in the span or at the supports, the strip behaves as statically determinate for a further load increase. A supplementary illustration of the structural behaviour is given in Fig. 5.22, showing the time variation of the current moment in field M_{field} and at the supports $M_{support}$ and of the moment capacities in the same sections.

As mentioned, the complementary tests D21 and D22 of test series D were aimed to study if the plate strip may collapse under the design load for a sufficiently heavy fire exposure. For the two tests the opening factor was chosen to 0.06 $m^{1/2}$ and the fire load density to 1005 and 1506 $MJ \cdot m^{-2}$, respectively. The result from the test D21 is transferred to Appendix while the test D22 is analysed below. Fig. 5.23 illustrates the bending moment in the field and at the supports at the times 0, 1, 5 and 7.5 hours for this test. The negative moment capacity decreases from -18.6 to -14.9 kNm and the positive moment capacity in the field from +18.6 to 4.4 kNm at the time of 5 hours but then it is recovering and reaches after 7.5 hours 6.5 kNm. The heavy fire exposure has thus even influenced the moment capacity over the supports. The complete time-variation of these moments and moment capacities is shown in Fig. 5.24. As can be noticed, failure is not attained as the recovering of moment capacity in field enters

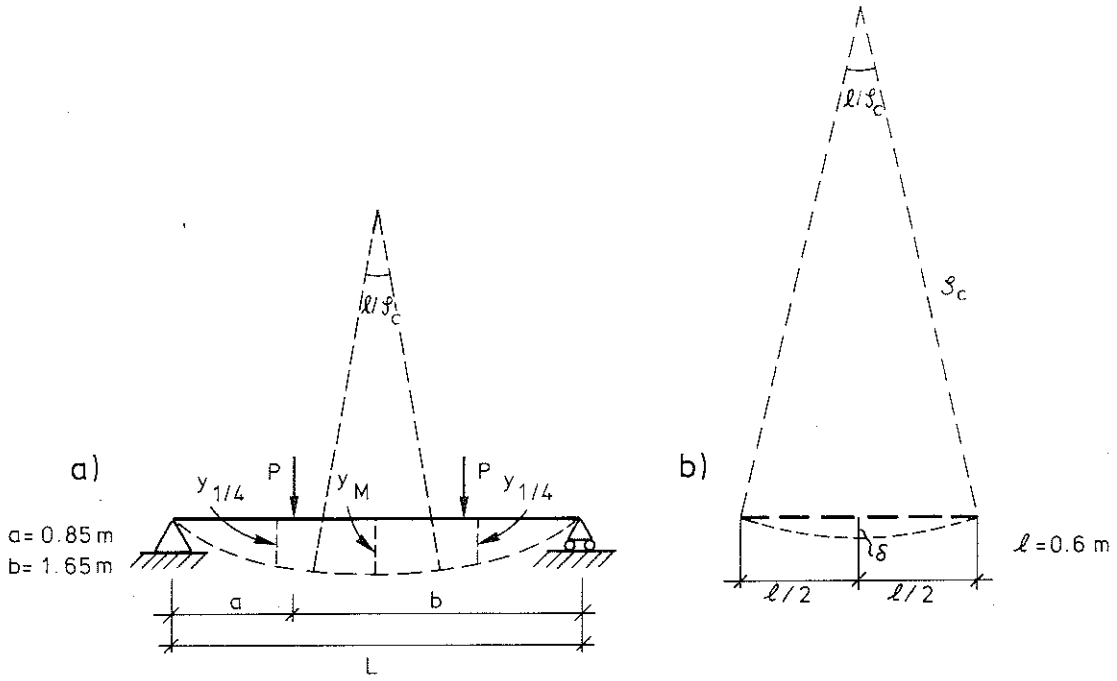

Figure 5.25 Notations for the flexural stiffness calculation.

after 4.75 hours. The temperature of the top reinforcing bars over the supports starts to decrease only after 7 hours, i.e. the recovering of the support moment capacity then begins at this time. The reserve load-bearing capacity for this test is, however, comparatively small and reaches at the times 4.75 and 6 hours the values 3.5 and 2.8 kNm, respectively. The conclusion may be, that the type of reinforced concrete structure used in this experiment and subject to a severe fire does not reach a collapse state, not even during the cooling phase. For a somewhat more severe fire exposure collapse had occurred, cf. Fig. 48 in Anderberg (1973).

5.6 Residual flexural stiffness and strength

The reserviceability of a fire-exposed load-bearing concrete structure and the extent of the subsequent repair of a fire-damaged structure are due to the residual load-bearing capacity, the residual flexural stiffness and the residual deformation state. The residual flexural stiffness has a great influence on the deformation behaviour, when loaded, and the remaining deflections can be decisive for the future use of the structure from a functional or an aesthetical point of view. This is the background and some of the reasons for investigating the residual load-bearing capacity and the residual flexural stiffness of the fire tested concrete plate strips.

The load-bearing capacity and the flexural stiffness after fire were examined for the strips simply supported and loaded up to fracture by two symmetrically placed concentrated loads, 0.8 m apart. This was also done for plate strips, not exposed to fire, in order to obtain the initial load-bearing capacity and the initial flexural stiffness.

The flexural stiffness was determined from three different types of measurements, viz. the curvature between the concentrated loads, the central deflection and the deflection in 1/4-section of the strip. The calculations were carried through by using well-known formulae for an elastic beam, illustrated below, see

Fig. 5.25.

A relationship between the moment M and the curvature ρ, measured on a length of 0.6 m symmetrical to the mid-section, gives the mean flexural stiffness $(EI)_c$ of that region, which also had a uniform fire-exposure in the main tests. The curvature follows the formula

$$\frac{1}{\rho_c} = \frac{M}{(EI)_c} \qquad 5.3$$

From geometrical considerations

$$2\rho_c \cdot \delta \simeq \frac{\ell^2}{4}$$

which gives

$$1/\rho_c = \frac{8\delta}{\ell^2} \qquad 5.4$$

and

$$(EI)_c = \frac{M_M \ell^2}{8\delta} \qquad 5.5$$

where M_M is the moment between the loads.

If EI is supposed to be constant over the whole length of the strip, the stiffness can be related to the deflection in the mid-section y_M by the following formula

$$y_M = \frac{P \cdot a(3L^2 - 4a^2)}{24(EI)_M} \qquad 5.6$$

giving

$$(EI)_M = \frac{0.66}{y_M} M_M \qquad 5.7$$

Analogously, the stiffness related to the deflection in the 1/4-section $y_{1/4}$ can be derived from the formula:

$$y_{1/4} = \frac{PL^3}{24(EI)_{1/4}} \left(1 - \frac{b^2}{L^2} - \frac{1}{16}\right) \qquad 5.8$$

giving

$$(EI)_{1/4} = \frac{0.468}{y_{1/4}} M_M \qquad 5.9$$

The stiffnesses, calculated in these different ways, the interrelationship

$$(EI)_c < (EI)_M < (EI)_{1/4}$$

both for an unexposed and an exposed plate strip. This is due to the moment distribution and in addition, for the exposed strip, to the nonuniform fire exposure along the plate strip, characterized by a temperature level, which is highest between the concentrated loads and decreasing towards the ends. It must be underlined, that the stiffnesses calculated in this manner are referred to a cracked state, as concerns the fire-exposed plate strips. Consequently, a load level should be chosen for the determination of the flexural stiffness, which is above that giving the cracking moment for an unexposed plate strip. The flexural stiffness values, reported in the following, are based on deflection values, generally obtained at about 0.8 M_{yield}, where M_{yield} denotes the yielding moment for the very plate strip.

For the unexposed plate strips, the flexural stiffnesses, evaluated from the formulae above, are:

$$(EI)_c^{unexp} = 0.64 \text{ MNm}^2$$

$$(EI)_M^{unexp} = 0.67 \text{ MNm}^2$$

$$(EI)_{1/4}^{unexp} = 0.70 \text{ MNm}^2$$

This interrelationship between the stiffnesses for the unexposed plate strips follows the correct pattern but for the plate strips

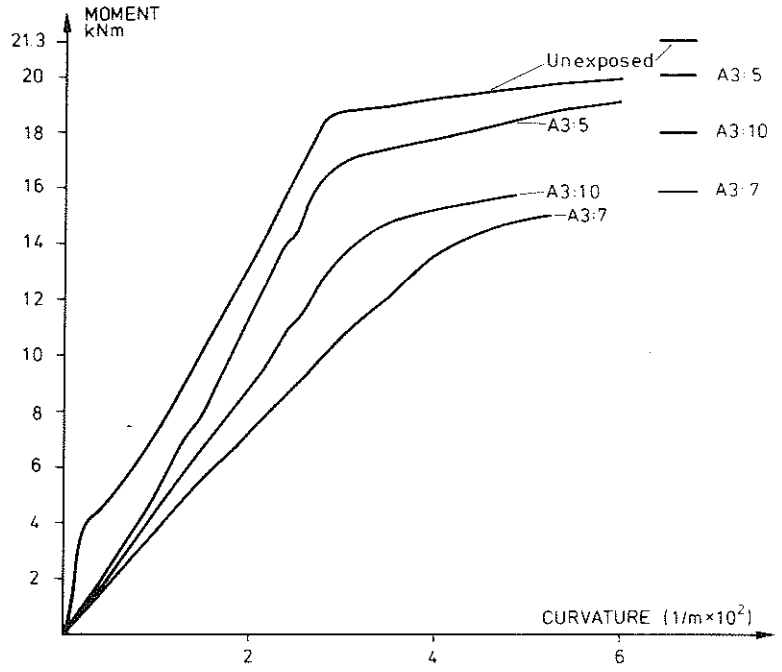

Figure 5.26 Moment curvature relationship of fire-tested plate strips, transversely loaded as simply supported at ambient temperature.

Test	Fire load ($MJ \cdot m^{-2}$)	Opening factor ($m^{1/2}$)
A3:5	502	0.06
A3:10	1005	0.08
A3:7	1005	0.06

A3:7 is tested upside down.

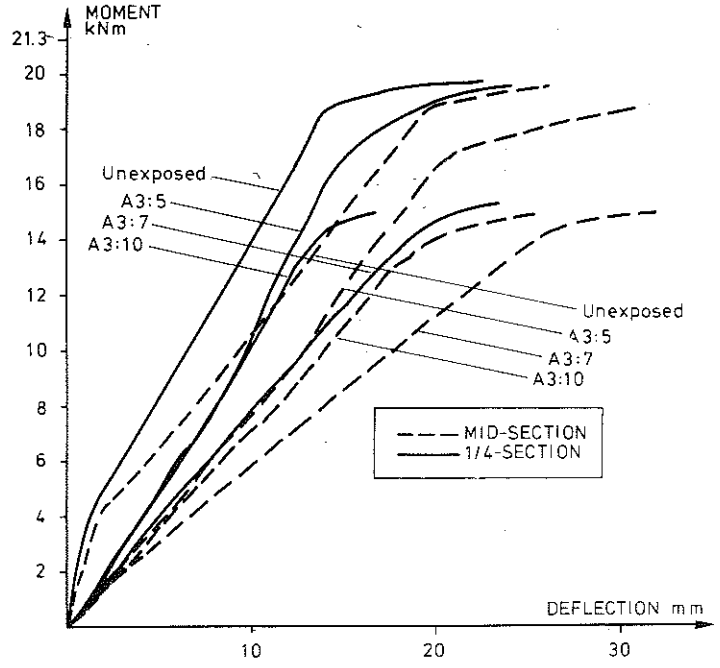

Figure 5.27 Moment deflection relationship of fire-tested plate strips, transversely loaded as simply supported at ambient temperature. Test characteristics in accordance with 5.26.

subjected to fire this is not always the case. The differences in residual deformed state from one strip to another influence the change in curvature and deflections due to a load increment. The calculated stiffness value is furthermore related to the value given for unexposed plate strips, which may have a relative deviation of 10%.

The estimated absolute error in the determination of $(EI)_c$ can be obtained from the following consideration:

Suppose that the deformation measurement has the error of $\delta = 2 \cdot 10^{-5}$ m. From the formulas 5.3 and 5.5 we obtain

$$\frac{1}{\Delta\rho_1} = \frac{8 \cdot 2 \cdot 10^{-5}}{0.6^2} = 0.44 \cdot 10^{-3} \quad 1/m$$

If we also consider an error in the applied load of $\Delta P = 0.20$ kN, it results in moment error, $\Delta M = 0.09$ kNm.
If $(EI)_c = 0.64$ MNm^2 we get

$$\frac{1}{\Delta\rho_2} = \frac{0.09 \cdot 10^{-3}}{0.64} = 0.14 \cdot 10^{-3} \quad 1/m$$

The total error in measured curvature may thus reach about $0.6 \cdot 10^{-3}$ 1/m, which must be born in mind in the study of the flexural stiffness values.

In Fig. 5.26 and 5.27 a principal illustration of the relationship between the moment and the curvature, the moment and the central deflection and the moment and the 1/4-section deflection is given for the plate strips of the tests A3:5, A3:10 and A3:7, which were investigated about five months after they had been subjected to fire. For comparison, the corresponding results from unexposed plate strips, given as mean values of two tests, are also drawn. The results for the plate strips A3:5 and 10, are intended to illustrate the decrease in the residual flexural stiffness and the load-bearing capacity when the fire load density is increased, while the strip A3:7, which is tested upside-down, shows a further decrease of both the stiffness and the load-carrying capa-

Table 5.8 Residual flexural stiffness and load-bearing capacity

Fire load density	Opening factor	Test	Flexural stiffness calculated from			Residual load-bearing capacity
			Curvature measurements mean value	Mid-section deflection mean value	1/4-section deflection mean value	mean value
$MJ \cdot m^{-2}$	$m^{1/2}$		%	%	%	%
251	0.01-0.08	A2:1-5	92	93	95	94
251	0.01	D9-10	-	95	100	90
251	0.04	D5-8	100	92	94	94
251	0.08	D1-3	-	94	96	94
502	0.04	B4,9-11	73	73	77	93
502	0.04	C1,5-8	84	84	84	98
502	0.04	D13, 15-16	-	83	84	91
502	0.06	A3:5	87	79	80	94
502	0.08	A3:8	98	85	89	92
502	0.08	D17-20	60-90	54-85	57-86	80-90
754	0.04,0.06	A3:2,6	76	72	73	84
1005	0.04	A3:3	63	64	68	80
1005	0.06	A3:10	72	70	75	84
1506	0.06	D22	-	-	-	76
2010	0.04	A1:10	60	66	64	70
251	0.01-0.08	D4,6,11, 12x)	-	59	60	84
754	0.08	A3:9x)	62	55	58	71
1005	0.06	A3:7x)	58	55	55	74

x) Plate strips loaded with negative moment.

city. This is due to the fact that the directly fire-exposed zone of concrete now acts as the compressive zone with a reduction in concrete strength. It is observed from the diagrams that there is an approximately linear relationship up to the moment level at which a smooth transition starts whenever the deformations strongly increase without any greater increase in moment. For the unexposed strip it is obvious that the appearance of the first cracks is attained at a moment of approximately 4 kNm whereupon the stiffness decreases. The yielding moment and the fracture moment then reach the values 18.8 and 21.3 kNm, respectively. The load-bearing capacity of the tests A3:5, 10 and 7 (q = 502, 1005 and 1005 $MJ \cdot m^{-2}$, respectively) attains the values 20, 17.9 and 15.7 kNm respectively, where the last value is referred to the plate strip tested upside-down.

The results of the experimental determination of the residual flexural stiffnesses, found above, and the load-bearing capacity are put together in Table 5.8, which in a condensed form illustrates the characteristic tendencies in the residual properties of the plate strips subjected to different fire exposures. From the table, it can be observed that the flexural stiffness and the load-bearing capacity decrease with increasing fire load density and reach values of 60 and 70% of the original value, respectively, at the very heavy fire load density of 2010 $MJ \cdot m^{-2}$. At normal conditions, when the fire load density is less than about 1000 $MJ \cdot m^{-2}$, the flexural stiffness and the load-carrying capacity have an approximate decrease within the range of 0 - 30% and 0 - 20%, respectively. If the plate strip is tested upside-down, the corresponding decrease is 0 - 45% and 0 - 30%, respectively.

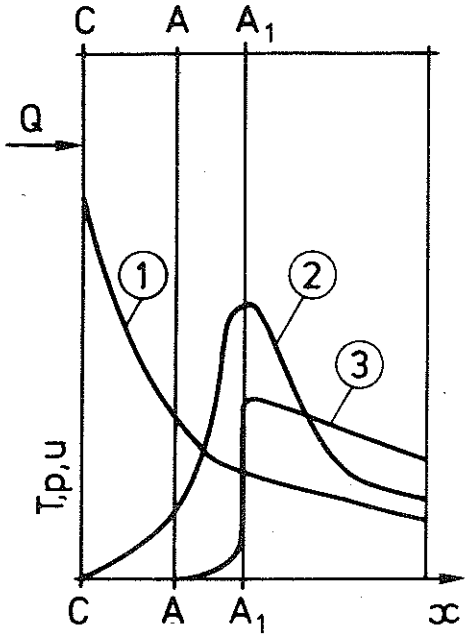

Figure 6.1 Principal temperature-, moisture- and vapour pressure conditions at heating of moist concrete.
C-C: Hot surface
A-A: Frontier of dried concrete
A1-A1: Frontier of vapourization
Q = Heat flow
① Temperature, T
② Vapour pressure, p
③ Moisture content, u
From Thelandersson (1974)

6 THEORETICAL STUDY

6.1 Thermal response of concrete structures

In concrete structures subjected to fire, two interrelated transport mechanicms are governing the thermal response. Theses mechanisms are the simultaneous heat and moisture flow which in a complicated manner are interdependent of each other. Owing to the vapourization of evaporable water above 100°C the moisture transport takes place in water phase as well as vapour phase and causes a continuous change in moisture distribution. When the capillary and adhesive forces and the steam pressure in the pores of concrete are developed, the temperature of evaporation is increased and sometimes reaches values of 150°C. The steam pressure primarily depends on the permeability, because the production of vapour may not exceed the transport and in order to keep this equilibrium, the vapour pressure is often consequently increased and so the mass transport. A qualitative illustration of the interrelated heat and moisture flow mechanisms is reproduced in Fig 6.1 according to Thelandersson (1974). The figure applies to the transient one-dimensional case and shows the distribution of temperature, T, vapour pressure, p, and moisture distribution, u at an arbitrary point of time, t, for a concrete wall, fire-exposed on one side. The transient state comprises three different types of zones, where the first zone close to the thermally exposed surface is dried out and the thickness of which is increasing all the time. This zone is followed by a narrow zone in which the vapourization takes place. In the third zone the moisture predominantly is in the phase of water. From a thermodynamical point of view, the simultaneous heat and moisture flow have to be analyzed analogously over a combination of partial differential equations.

For the present application the computation of transient temperature-time fields is based on a solution technique in which different approximations are made. A brief description is given below:

- The calculation of heat flow is based on the Fourier equation of heat conduction in non-transparent and non-porous material.

- Capillary moisture transport is neglected.
- Initial moisture content is successively vapourized on place as the steam temperature is reached.
- Other influences on the heat flow at current moisture state is regarded by making the thermal properties of concrete dependent on moisture content. This is however functionally seen an incorrect assumption.
- Vapour transport has no effect on temperature state.

The approximations mentioned above indicate a need for developing functionally pure analytical models for interrelated heat and moisture flow. In such an analysis the thermal properties are furthermore independent of moisture content.

Different numerical methods as finite difference and finite element approximations for computing the transient heat flow within a concrete structure have been developed and are widely used today. Such computations are based on the Fourier equation of heat conduction which in the three-dimensional case has the general form

$$\frac{\partial}{\partial x}\left(\lambda_x \frac{\partial T}{\partial x}\right) + \frac{\partial}{\partial y}\left(\lambda_y \frac{\partial T}{\partial y}\right) + \left(\lambda_z \frac{\partial T}{\partial z}\right) + Q = \rho c_p \frac{\partial T}{\partial t} \qquad 6.1$$

where T is the temperature, Q the external heat generation per unit volyme, λ_x, λ_y, and λ_z the anisotropic thermal conductivities in the x, y and z directions respectively, ρ the density, c_p the specific heat and t the time. In a fire engineering design of concrete structures the thermal material properties are temperature dependent which ordinarily cannot be neglected.

The basic equation (6.1) is connected to two different kinds of boundary conditions relevant for fire-exposed structures, viz.

a) The value of the temperature T is specified on the surface of the structure:

$$T = T_s \qquad 6.2$$

or

b) The heat flow characteristics are specified on the surface of the structure:

$$\lambda_x \frac{\partial T}{\partial x} l_x + \lambda_y \frac{\partial T}{\partial y} l_y + \lambda_z \frac{\partial T}{\partial z} l_z + q + \alpha(T - T_t) = 0 \qquad 6.3$$

where l_x, l_y, and l_z are the direction cosines of the outward normal to the boundary surface, q is prescribed heat transfer on the boundary per unit surface and $\alpha(T - T_t)$ the heat transfer per unit surface, α is the coefficient of heat transfer.

Despite the assumptions made, acceptable results for fire engineering application are obtained, if only the thermal properties used in equation (6.1) - the thermal conductivity and the product $\rho \cdot c_p$ or alternatively the enthalpy I_e given by the relation

$$\frac{\partial I_e}{\partial t} = \rho \cdot c_p \cdot \frac{\partial T}{\partial t} \qquad 6.4$$

or

$$I_e = \int_0^T \rho \cdot c_p dT \qquad 6.5$$

- are sufficiently well-known as concerns temperature and fictitious moisture dependence. It has been shown, however, that it is often very difficult to get reliable thermal material data. Measurements in different laboratories on "identical" specimens may often vary widely. Another way to find out these thermal properties is the procedure of optimization which is in progress today. This procedure means that <u>one</u> temperature dependent parameter is determined in such a way that the difference in measured and calculated temperatures has a minimum. If the state of temperature and the heat flow are measured simultaneously two thermal properties can indirectly be determined. However, by this method pure thermal properties are not found but these are a function of the state of moisture content and moisture movement.

As will be shown later in the application of the fire-exposed plate strip used in the experiment the theoretical determination

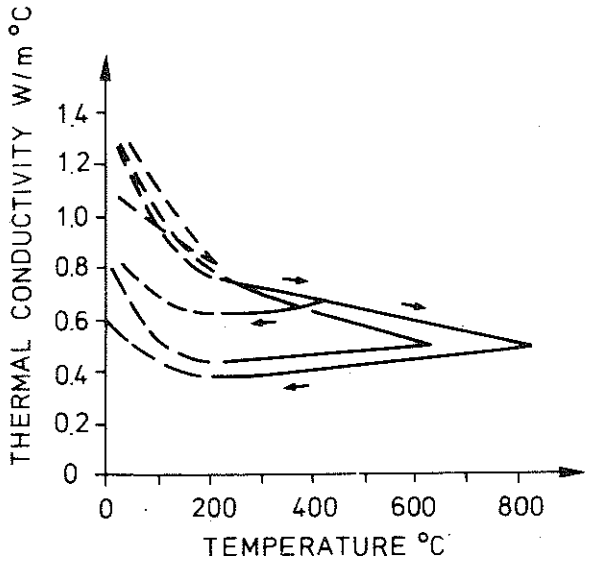

Figure 6.2 Thermal conductivity λ for granite aggregate concrete as a function of temperature under heating and subsequent cooling.
Cement aggregate 1:6, W/C = 0.7
From Ödeen & Nordström (1972)

Table 6.1 Thermal conductivity determined at room temperature at different laboratories (Stationary method). W/m°C

Laboratory	Size of test specimen	Moisture state	Concrete		
			P 400 + G 1	P 400 + L1 2	P 400 + LS1 3
1	65 x 65 x 10 cm reduced to 60 x 60 x 10 cm	Dry (105°C)	1.23	1.07	0.57
2	"	Dry (105°C)	1.72	1.19	0.77
3	"	Dry (105°C)	2.12 (1)	1.38 (1)	0.75 (1)
4	30 x 30 x 10 cm	Dry (105°C)	2.17 2.46 (1)	1.52 1.64 (1)	0.95 0.99 (1)
	"	Not dry Labo	2.55 2.98 (1)	1.77 1.96 (1)	1.15 1.23 (1)
	"	Saturated	3.13-3.25	3.13-3.25	4.99

(1) The value of λ is corrected as regards the resistance of contact between the hot and cold source

P 400 Portland Cement (class 400)

L1 Limestone from Tournaisis

LS1 Based on expanded state

G Gravel

From Collet (1975)

of the instationary temperature-time fields is very sensitive to the input of thermal properties.

6.1.1 Thermal properties of concrete

6.1.1.1 Thermal conductivity

In temperature calculations concrete is considered as an isotropic material, i.e. the thermal conductivity is invariant with respect to direction of heat flow. The thermal conductivity decreases with increasing temperature but during a subsequent cooling the change is not reversible. This is illustrated in Fig 6.2 for a granite aggregate concrete heated to different maximum temperature levels (Ödeen et al (1972)). Below 100°C the thermal conductivity is influenced by the moisture content, but it is very difficult to undertake well-defined measurements, due to the complicated interaction between moisture and heat flow. The initial thermal conductivity at room temperature increases almost linearly with moisture up to complete saturation. Also the type of aggregate will influence the conductivity.

As was mentioned in the previous section the test result on thermal properties may differ considerably from one laboratory to another. This is shown in a paper by Collet (1975) for the thermal conductivity determined at room temperature. Test results from four different laboratories on three different types of concrete are accounted for and these can be studied in Table 6.1. To the first three laboratories "identical" test specimens were sent and tested in dried state (exposed to 105°C) at room temperature. The deviation are thus remarkable and by comparing laboratory 1 to 3 for concrete 1 the value varies within 1.23 - 2.12 W/m°C.

In laboratory 4 the values seem to be even larger and for saturated specimens values of 3.25 W/m°C are obtained. These results, determined by a stationary method indicate that you have to be very careful before accepting data on thermal conductivity. In Collet (1975) is also described a non-stationary method used to investigate the thermal conductivity at elevated temperature. This method is of great interest but no comparisons have been made

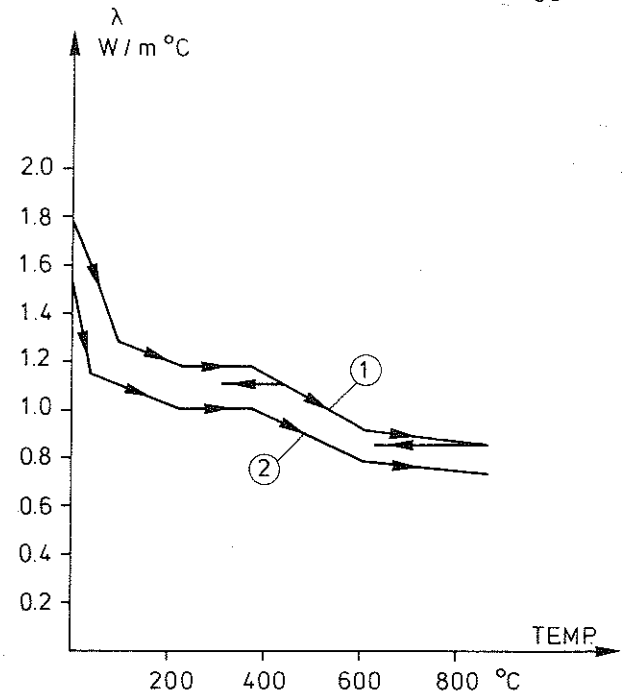

Figure 6.3 Thermal conductivity λ for quartizite aggregate concrete, used in the experiment, as function of temperature.
Curve (1) Measured curve used for temperature calculations (Initial moisture content u_o = 1.5%)
Curve (2) An assumed curve for comparative calculations.

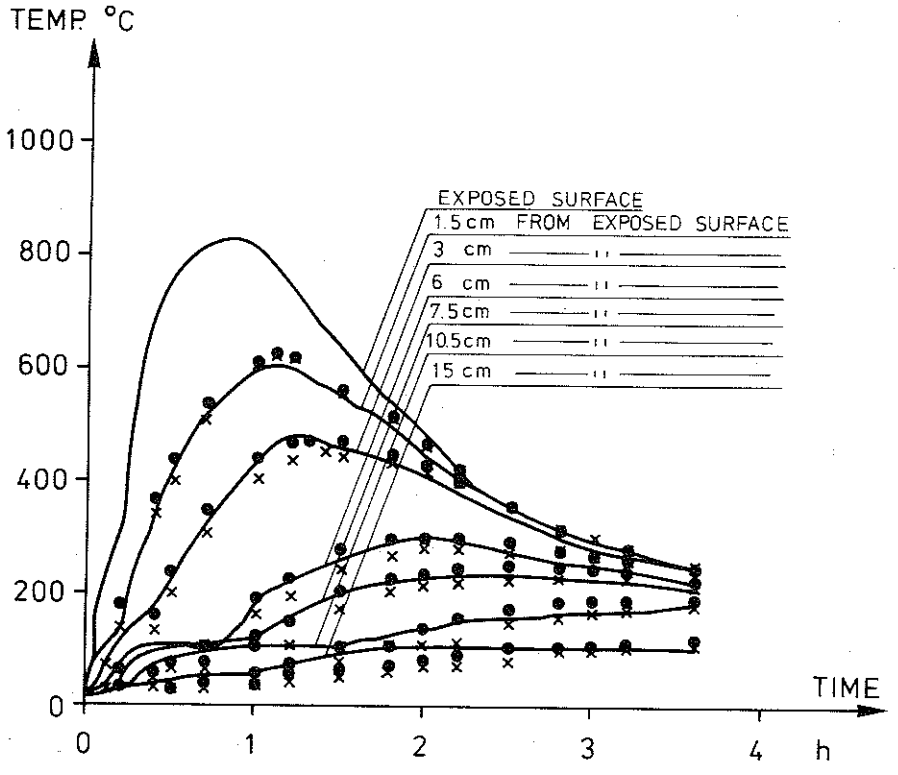

Figure 6.4 Temperature-time curves at different depths in mid-section of plate strip D17.
——— Measured curve
····· Calculated curve, measured λ-curve is used
x x x x Calculated curve, assumed λ-curve is used

so the reliability is not yet confirmed.

The thermal conductivity of the concrete used in the experiment for specimens in test series A3 and D is determined by Stålhane Pyk's method (1923) at the Central Laboratory of Höganäs AB. The curing condition of the specimens identical to the plate strip (cf. 4.3) and the initial moisture content was determined to 1.5%.

Curve (1) in Fig 6.3 illustrates the temperature dependence during heating and this is used as input in the temperature calculations. During cooling the curve branch is chosen to incline upwards 0.05 W/m^{o}C per 100^{o}C. As the appearance of the cooling branch of λ is dependent on the temperature level at which cooling starts it is difficult to define its variation, but this assumption of a linear relationship during cooling is an acceptable approximation for the calculations.

In order to illustrate the importance of having relevant data on the thermal conductivity when computing transient temperature-time fields an example will be presented. The calculation based on the measured λ-curve (1) and on the λ-curve (2) shown in Fig 6.3 will be compared with each other.

The heat flow is one-dimensional and the temperature calculations have as input measured surface temperatures taken from the mid-section of the plate strip D17. The influence of thermal conductivity on computed temperatures when keeping other parameters constant is illustrated in Fig 6.4, which shows the temperature-time-variation at different depths of the cross-section partly from the calculation and partly from the measurements. It is very obvious from the figure that a reduction in thermal conductivity of 13% gives a considerable decrease in calculated temperatures and in this case differences up to 40^{o}C or 20% may be noted.

6.1.1.2 Enthalpy

In the theoretical model capillary water-transport is omitted while the vapour is assumed to leave the structure without influencing the heat balance. The principal variation in moisture content with temperature is assumed to follow the curve in Fig. 6.5. The initial

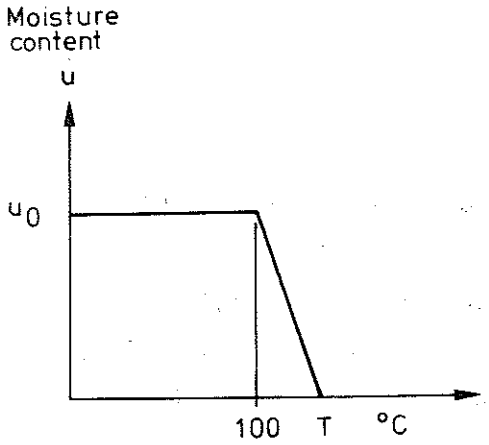

Figure 6.5 Principal variation of moisture content, u, vs temperature

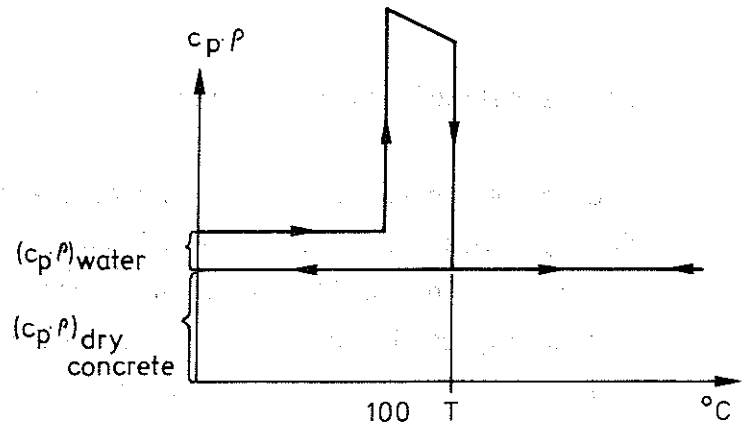

Figure 6.6 Principal variation of heat capacity, $c_p \cdot \rho$, vs temperature

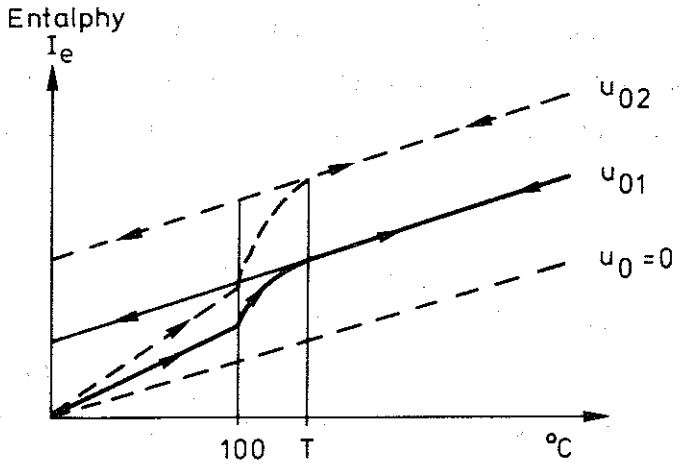

Figure 6.7 Principal variation of enthalpy, I_e, vs temperature

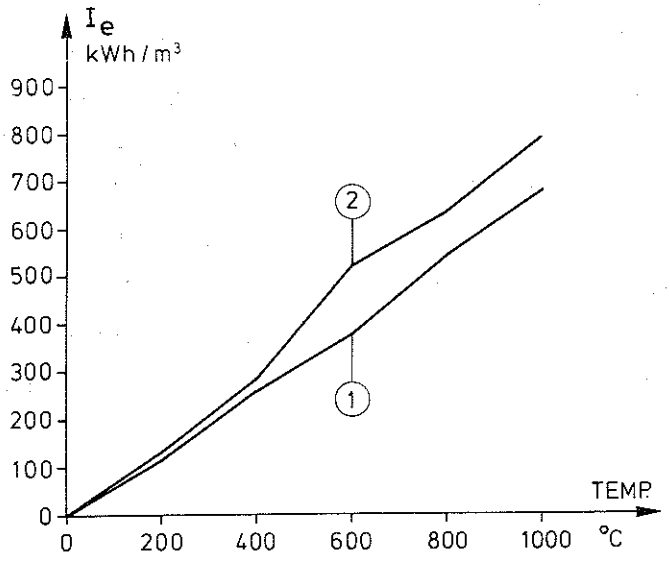

Figure 6.8 Enthalpy I_e for granite aggregate concrete vs temperature
Curve ① Measured under cooling (Ödeen et al (1972))
Curve ② Theoretical (Harmathy (1970))

moisture content is u_o and the water is supposed to be vapourized linearly between 100°C and T°C where T is dependent on dimensions of the structure, distribution and size of pores. In fire applications it is usually assumed that all the moisture evapourizes at the temperature 100°C and consequently the required heat renders a discontinous step in the enthalpy curve at this temperature.

The heat capacity is intended to consist of two parts, viz one part for the dry concrete and the other for the current moisture content i.e. $(c_p \cdot \rho)_{tot} = (c_p \cdot \rho)_{dry\ concrete} + (c_p \cdot \rho)_{water}$. The principal variation is illustrated in Fig 6.6 for both the heating and subsequent cooling phase.

As the enthalpy I_e is the integral of the heat capacity in respect to temperature, it can easily be calculated for different initial moisture contents of the concrete. The continous curve in Fig 6.7 indicates principally the variation in enthalpy at the moisture content $u_o = u_{o1}$ during heating as well as during cooling phase. The principal relationship is also shown for dry concrete $u_o = 0$ and at the moisture content $u_o = u_{o2}$.These illustrated curves are somewhat simplified, however, because the latent heat of various chemical reactions taking place during an initial heating is not considered. This latent heat, which is evaluated during heating of dry concrete is in Fig 6.8 illustrated as the difference between the curves. Curve (1) shows the enthalpy I_e versus temperature determined under cooling (Ödeen et al (1972)), and curve (2) gives the variation of the enthalpy theoretically determined on the basis of stochiometric calculations and simplified assumptions on the chemical reactions (Harmathy (1970)). Because no available methods of direct measurement exist regarding enthalpy during heating for example the effect of vapourization of moisture content and chemical reactions cannot be measured.

The enthalpy curve used for computation of temperature is chosen to be the same as has been practiced in connection with a manual concerning systematic determination of the temperature-time field for varying conditions of fire-exposure and structural characteristics. This manual is issued by the National Board of Physical Plan-

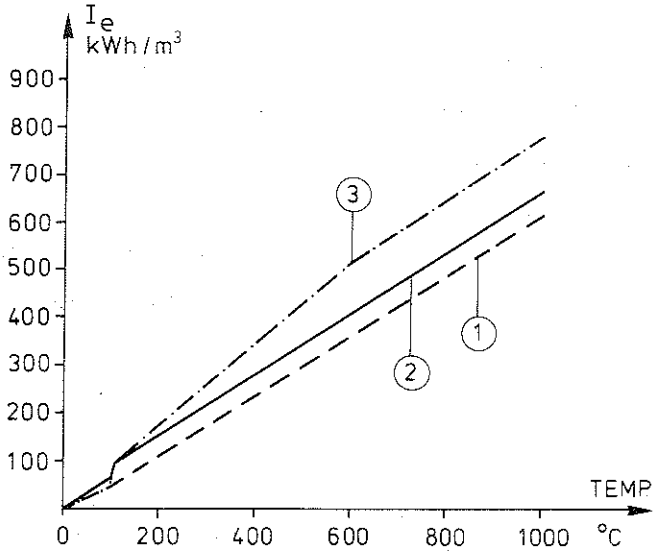

Figure 6.9 Different enthalpy curves used for sensitivity calculations
① Represents dry concrete
② Main curve, represents a moisture content of 1.5%
③ Latent heat due to chemical reactions is considered

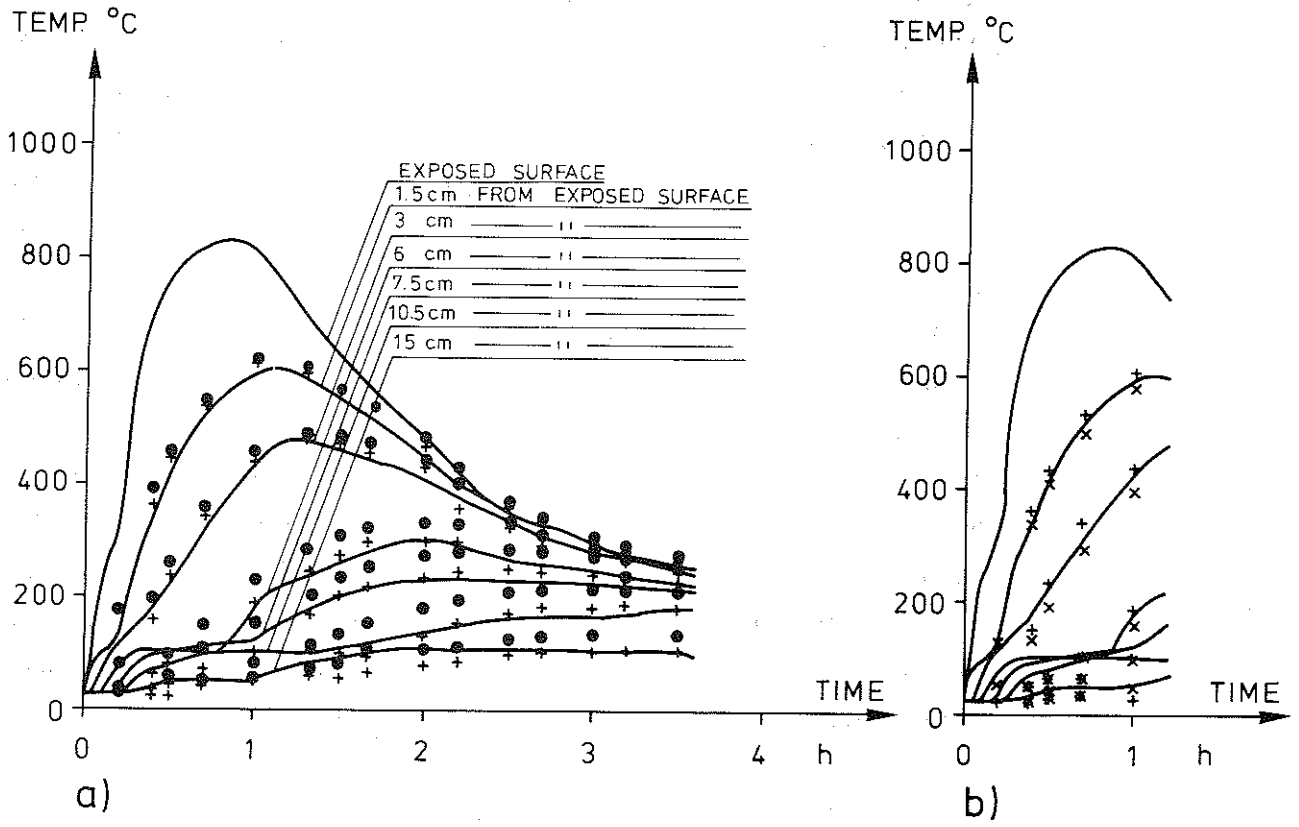

Figure 6.10 Temperature vs time at different depths in mid-section of plate strip D17
——— Measured curve
++++++++ Calculated curve, main curve of enthalpy used for temperature calculations
····· Calculated curve, dry concrete enthalpy curve used for temperature calculations
xxxxxxxx Calculated curve, Harmathy's enthalpy curve used for temperature calculations

ning and Building in Sweden. In Fig 6.9 this enthalpy curve relevant for concrete with the actual moisture content 1.5% is drawn as a full-line. The dashed curve represents initially dry concrete and the dash-dotted branch to the main curve intends to illustrate the latent heat due to chemical reactions during heating determined by Harmathy (1970). The influence of the chosen enthalpy curve on temperature calculation will be illustrated for the alternatives given in Fig 6.9. In the calculation the temperature dependence of thermal conductivity is pervadingly chosen in accordance with curve (1) in Fig 6.3. As can be noticed from Fig 6.10a the change in enthalpy curve regarding the effect of moisture in the concrete has an obvious result on calculated temperatures. Dry concrete has pervadingly higher temperatures, which as maximum attain 50°C which is equivalent to 50% increase at the depth of 7.5 cm after 1 hour. The effect of latent heat included in the main curve of enthalpy as shown in Fig 5.9 is illustrated in Fig 5.10b. In this comparison (only drawn during heating) the decrease in calculated temperatures due to the latent heat is not quite as much as was the case in Fig 5.10a but it amounts to 40°C or 10% at the depth of 3 cm after 1 hour. This calculation also gives too low temperatures so perhaps the effect of latent heat is overestimated, i.e. calculated increase in enthalpy is maybe greater than can be supposed. This remains of course to be proved.

6.1.2 Computer program calculating transient heat flow

The computer program based on the finite element method and used here for the purpose of predicting temperature distribution history for fire-exposed plate strips is developed from a program library constructed by Ulf Wickström at the Division of Structural Mechanics and Concrete Construction at Lund Institute of Technology. This program library consists of a supply of permanent system routines and problem-adapted routines, which must be constructed by the user. The program can be formed to solve one- as well as two-dimensional problems and in one-dimensional case also axi-symmetrical problems. All types of boundary conditions as pre-

scribed heat flow, heat transfer, prescribed temperature and adiabatic boundary may be inserted. The temperature dependence on the thermal properties is accordingly considered in the program and the current structure may even consist of different materials. The program package is constructed to be very general and the applications on transient heat flow are therefore wide. The temperature program will not be accounted for in detail, but characteristic features of it are described below.

In the one-dimensional case of transient heat flow the basic equation of heat conduction is in the form

$$\frac{\partial}{\partial x}\left(\lambda \frac{\partial T}{\partial x}\right) + Q = \rho c_p \frac{\partial T}{\partial t} \qquad 6.6$$

This heat balance equation can be transferred in the matrix format

$$k \cdot \bar{T} + P \frac{\partial T}{\partial t} = \bar{F} \qquad 6.7$$

where k = conductivity matrix
P = heat capacity matrix
$\bar{T}$ = temperature vector
$\bar{F}$ = external heat flow vector

In the numerical solution of equation (6.7) the forward difference method developed by Euler is used. As regards avoidance of convergence problems this method is the most appropriate one and gives the following solution chart:

$$\Delta t \cdot k_t \cdot T_t + P_t \cdot \Delta T_t = F_t \cdot \Delta t \qquad 6.8$$

the change in enthalpy is

$$\Delta I_i = P_t \cdot \Delta T_t = (F_t - k_t \cdot T_t)\Delta t \qquad 6.9$$

In order to avoid points of singularity of $c_p \cdot \rho$ a nominal heat capacity is introduced, viz $c_p \cdot \rho' = \frac{I_e}{T} = I_e'$. Furthermore, if it consists only of one material, the specific enthalpy i is defined as follows:

$$i = \frac{I_e}{V_{node}}$$, where V_{node} denotes the node volume.

As

$$i_{t+\Delta t} = i_t + \frac{\Delta I'}{V_{node}} \qquad 6.10$$

the temperature $T_{t+\Delta t}$ is directly determined through the known relationship between temperature and enthalpy. If, however, several materials are involved in the calculation an iteration procedure must be undertaken by the equation:

$$T_{t+\Delta t} = P^{-1}_{t+\Delta t} \cdot I_{t+\Delta t} \qquad 6.11$$

The time increment Δt is generally limited by the need for

a) acceptable accuracy in approximations of boundary conditions, heat conductivity and heat capacity matrices.

b) numerical instability which in the one-dimensional case means that

$$\Delta t \leq 0.4 \frac{c_p \cdot \rho}{\lambda} (\Delta x)^2 \qquad 6.12$$

and this well-known fact from finite difference approximation methods.

The efficiency of the computer program run on an Univac 1108 machine is illustrated by a certain calculation characterized below:

Boundary conditions: Surface temperatures are known on fire-exposed side and heat transfer is considered on unexposed side.

The smallest element length Δx = 0.0075 m, time of fire exposure = 5 hours, 52 time-steps and 11 nodes.

Execution time = constant x number of nodes x number of time-steps.

Result: 350 time-step iterations were needed or a mean time-step of 0.014 hours. Total execution time amounted to 6.5 seconds.

The flow chart of the computer program is presented in Table 6.2.

Table 6.2 Flow chart of computer program

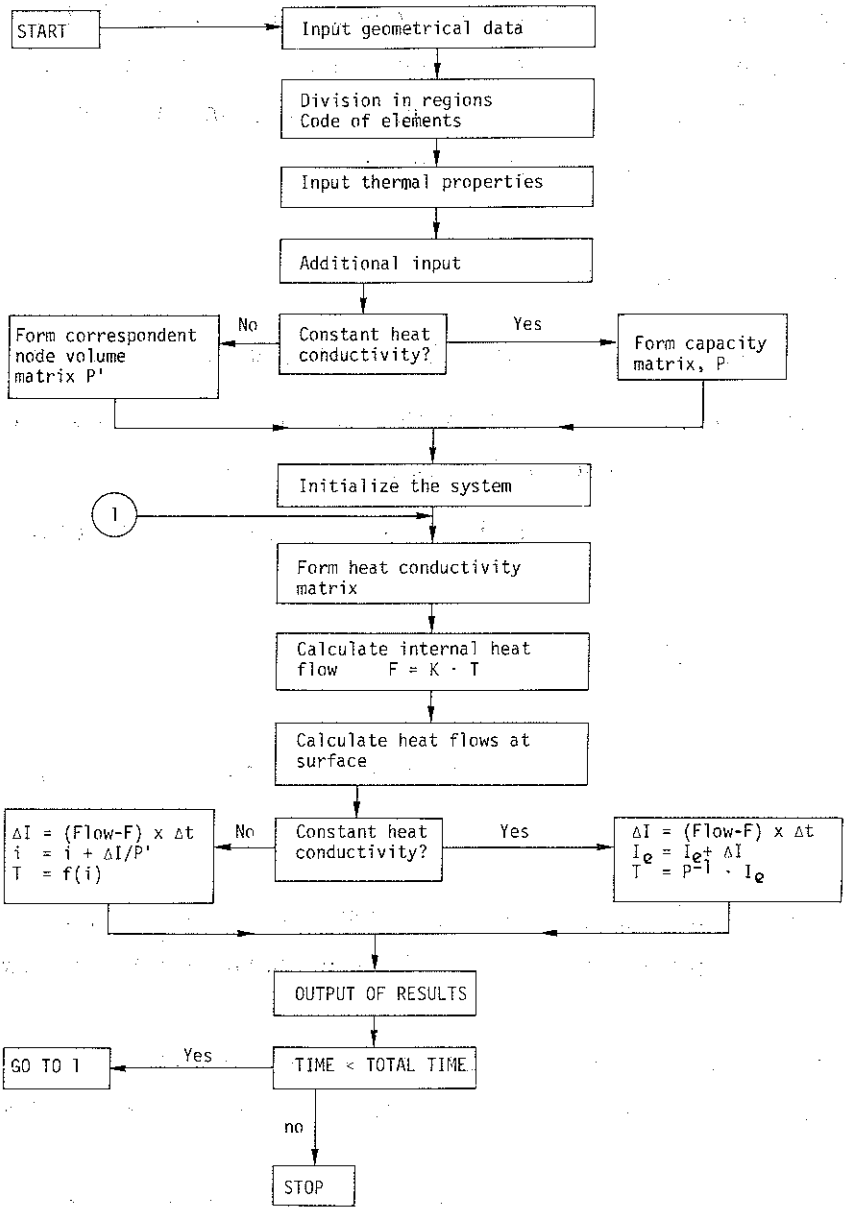

6.1.3 Measured and calculated transient temperature-time fields of fire-exposed plate strips

In a calculation of temperature-time fields it is of vital importance to simulate as well as possible the fire exposure, which serves as input in the evaluation. If that is successful you may have progress for further theoretical analysis of structural behaviour.

In the experimental investigation of the plate strips the fire exposure was subjected to one side and varied approximately symmetrical in longitudinal direction. Therefore, in the theoretical calculation, owing to symmetry only half the plate strip was studied, and the fire exposure was divided into four fire zones, see Fig 6.11a. Due to the division of the strip into comparatively large sections, where each section represents the mean temperature state for a certain length of the strip, the heat conduction in longitudinal direction is of secondary importance and therefore disregarded in the calculation i.e. we solve the one-dimensional heat conduction problem. The choice of division into four sections is based on considerations over the modelling of temperature distribution longitudinally and of course the need of division in structural analysis. For the latter purpose division into five (main calculations) segments has been used, which will be discussed later on.

Many attempts have been made in order to find or define the current coefficient of heat transfer in the furnace. As the heat transfer is varying both with temperature and the fire zone, no satisfactory results have been obtained. Therefore the measured surface temperatures have been used as input in the computations.

The boundary condition of the unexposed surface characterized by the coefficient of heat transfer, α, which consists of two parts convection, α_c, and radiation, α_r, where α_r is calculated from Stefan-Bolzmanns law with a resulting emissivity of 0.8. The convection part α_c is assumed constant $\alpha_c = 12\ W \cdot m^{-2} o \cdot C^{-1}$ due to a forced convection induced by a fan placed on the furnace during

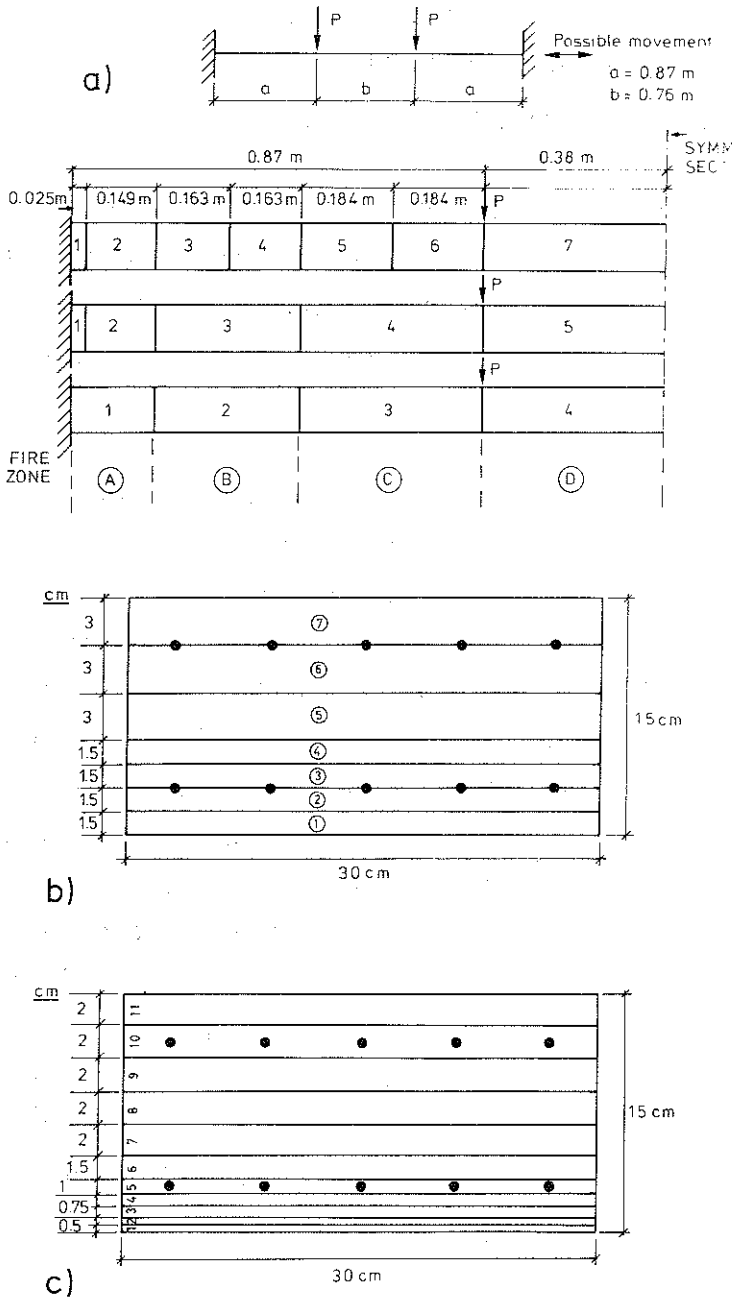

Figure 6.11 Geometrical idealization of plate strip
a) Segment
b) Cross-section, 7 concrete subslices
c) Cross-section,11 concrete subslices

the whole experiment. The value of convection has been determined by comparing measured and calculated surface temperatures on the unexposed side of the strips for different values of convection factor at the unexposed side. The thermal material data used in main temperature calculations is given by curve (1) in Fig 6.3 and full-line curve in Fig 6.9 for the thermal conductivity and enthalpy respectively. Initial moisture content is determined to 1.5%.

The geometrical idealization of a structure is often governed from the demand for accuracy in the structural analysis and so is also mainly the case here. In the main calculations the cross-section is divided into 7 subslices of concrete and 2 subslices of steel bars, illustrated in Fig 6.11b, but for control of the accuracy of the results, calculations also have been made with the cross-section divided into 11 concrete subslices and 2 steel subslices (see Fig 6.11c).

Five groups of tests have been theoretically analysed. One test from each group is chosen to represent the current temperature state. The different groups of tests illustrated in section 5 are D1 - 4, A2:5; D5 - 8, A2:3; D9 - 12, A2:1; D13 - 16, A1:12; D17 - 20, A3:8, and representative tests chosen are A2:5, A2:3, A2:1, D13 and D17 respectively. However, the test A3:8 was analysed separately as it differed too much from the tests D17 - 20. Results obtained in the computation are presented for the fire zones 1, 3 and 4, i.e. support section, 1/4-section and midsection. Due to the difficulty in placing the surface thermocouple exactly at the surface measured, the temperature is sometimes somewhat corrected by analysing tendencies in precalculated temperatures.

If corrections are made, this is indicated in the presentation. Computed temperature-time curves at different depths and comparisons with measured results are illustrated in Fig 6.12 - 6.13 for the tests mentioned above. As can be seen from the figures the calculated result is generally in good agreement with measured values under the heating as well as during the cooling phase.

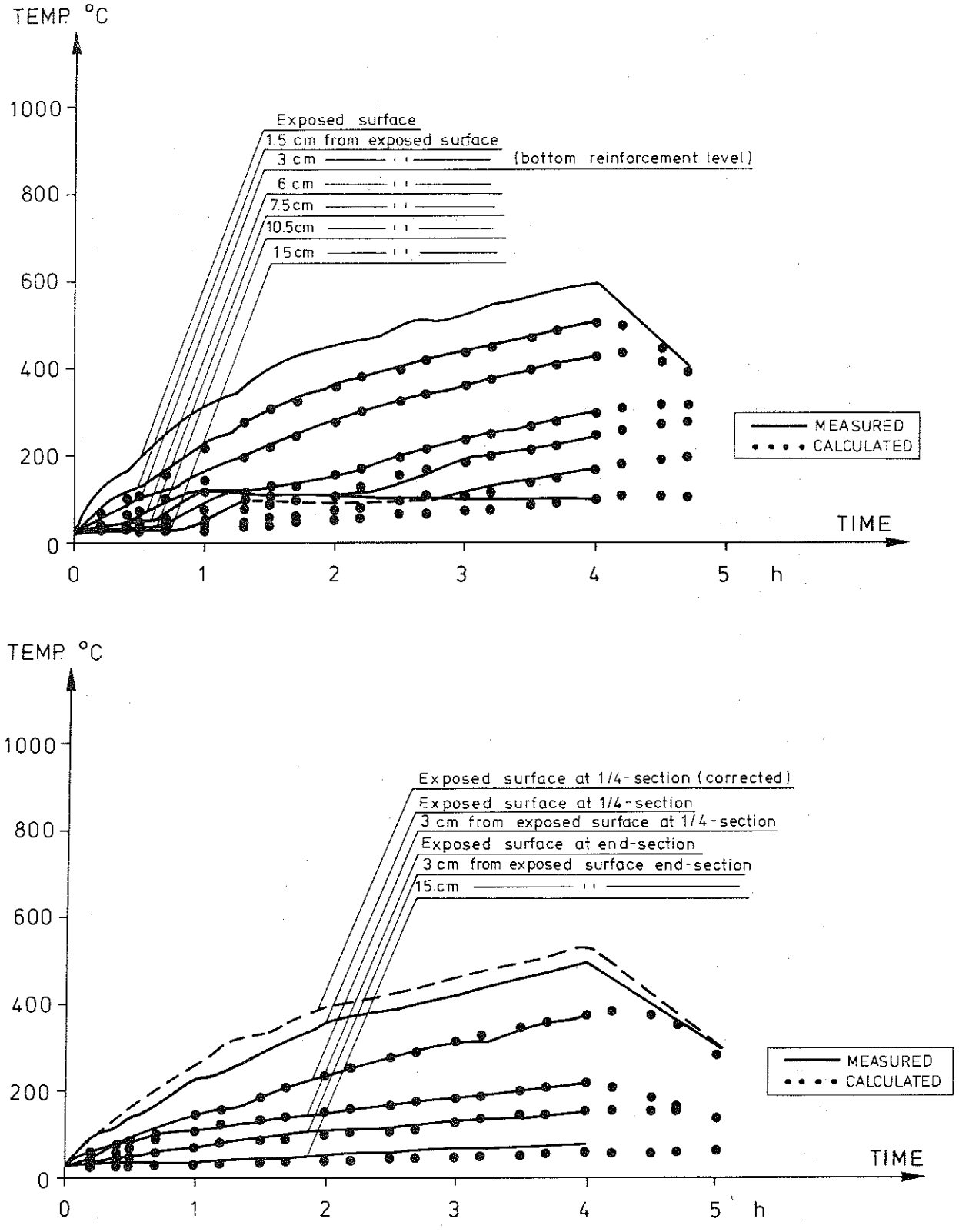

Figure 6.12 Temperature-time curves at different depths
Group 3: Test A2:1
a) Mid-section
b) 1/4-section

A characteristic feature in the comparison is the discrepancy at depths greater than 3 cm, often most pronounced during the first hour and as long as the temperature level is below 100°C at any depth. In these cases the measured temperatures are always higher than the calculated ones, partly dependent on the moisture transport and evaporation of water described in section 6.1, but also the development of cracks caused by the steep temperature gradient may facilitate the moisture transport. Also the concentrated amount of thermocouples attached in the mid-section may increase the risk of being exposed to unintended hot moisture flows. A partial result of these phenomena is indicated by a dashed envelop in Fig 6.13a, and can also be observed for the other tests. It may be noted from observations of the tests that moisture almost without exception started to drop out on unexposed surface just in mid-section and that it occurs mostly during the first 0.15 to 0.50 hours. These observations support the aforementioned theory of moisture flow influence, which is prevalent for calculated as well as measured results.

A calculation may also indicate if the location of a thermocouple is not in accordance with the prescribed depth as for example in test A3:8. The temperature state of this test in mid-section is illustrated in Fig 6.13a. In order to give better agreement to measurements at the depths 1.5 and 3 cm from exposed surface, the surface temperature is corrected in accordance with the figure. The computed temperatures at the depth of 1.5 cm are especially during heating above the measured curve but at the depth of 3 cm we notice the opposite. These circumstances indicate that the thermocouples prescribed to be placed at these depths were in reality moved 2 - 3 mm a fact which, however, during cooling has a much smaller effect on the correct results and therefore not that much noticed.

As the calculations of temperature-time fields have such a good agreement with the measured results for a wide range of different fire exposures characterized by these exemplified tests the final conclusions must be, that the accounted theoretical transient temperature-time fields are sufficiently reliable. If there are differences they are most probably due to an erroneous mea-

surement or a thermocouple not correctly located, at least when the temperature is above 100°C.

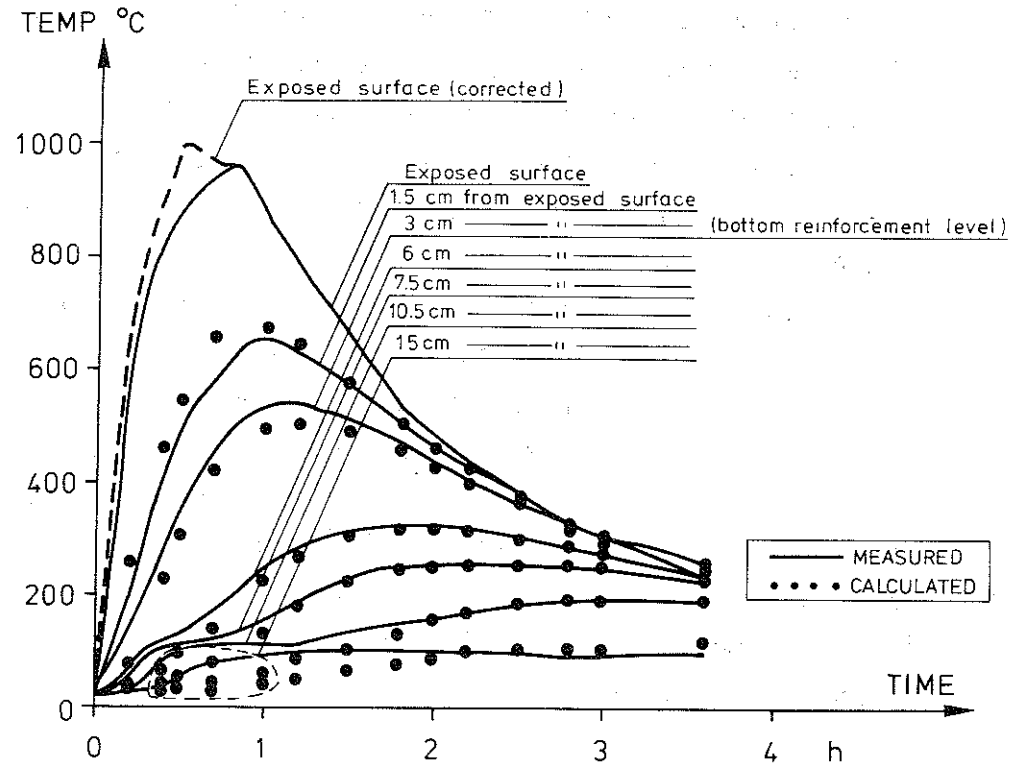

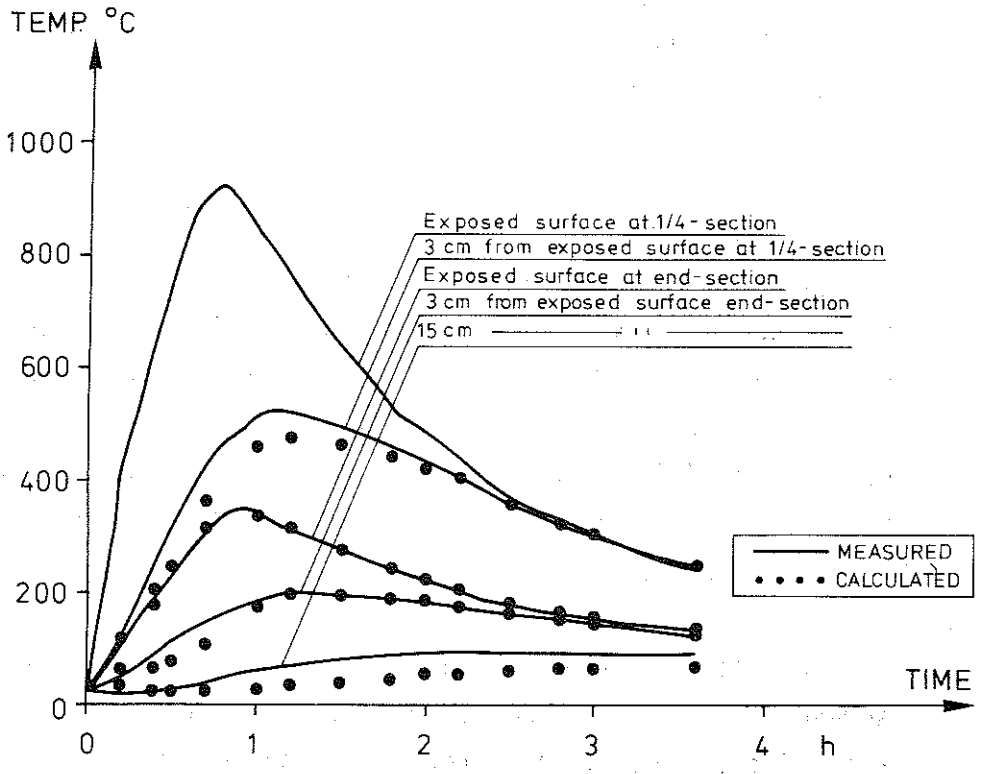

Figure 6.13 Temperature-time curves at different depths
Test A3:8
a) Mid-section
b) 1/4-section

6.2 Mechanical response of hyperstatic concrete structures

The success of predicting the structural behaviour of concrete constructions under transient thermal exposure depends in a decisive degree on the accuracy in temperature calculations as well as the knowledge about the real mechanical behaviour of the structural materials. The models of material behaviour used in calculations are based on experimental data obtained at transient as well as steady-state conditions. Such data are accounted for concrete in Anderberg & Thelandersson (1976), in which furthermore the constitutive model of concrete in compression is developed. Due to this progress in modelling more realistic material behaviour, viz. constitutive relationship between strain, stress, temperature and time is established, a wide step has been taken towards a better understanding and improved possibilities to predict the structural response to fire.

In this section the mechanical properties of concrete and steel and related transient material behaviour models used in the evaluation of structural response are presented briefly. A more thorough presentation as concerns stress and deformation characteristics of concrete at elevated transient temperature is given in Anderberg & Thelandersson (1976).

The theoretical analysis of structural response to fire is carried out by a computer program "FIRES-RC" originally constructed at University of California, Berkeley. This program is further developed by the author and the recent research on mechanical behaviour of structural materials under transient conditions is utilized. A brief description of the modified program is given.

Predicted and experimentally observed behaviour on fire-exposed reinforced concrete plate strips, fixed against rotation at both ends, but free to move longitudinally, is compared for a large number of tests during the whole fire process including the cooling phase. Some complementary calculations are also presented.

Finally the influence of restraint forces and moments on load-carrying capacity is briefly discussed on the basis of a theoretical analysis and observed behaviour.

6.2.1 Constitutive law of concrete

A complete constitutive law of concrete in compression as well as tension under transient, high temperature conditions is here described briefly. The constitutive equation of concrete in compression valid at first heating is originally presented in Anderberg & Thelandersson (1976) and all details behind that formulation are therefore not given in this paper.

The distinction of structural behaviour at changing temperature and stabilized temperature is thus fundamental. In the formulation of the computer-oriented model that is consequently regarded. In the model the total strain is seen as the sum of the following four strain components derived on a purely phenomenological basis.

Thermal strain, including shrinkage, measured on unstressed specimens under variable temperature.

Instantaneous stress-related strain, based on stress-strain curves obtained under stabilized temperature.

Creep strain, time-dependent strain recorded under constant stress at stabilized temperature.

Transient strain, stress-dependent and attributed to the effect of a virgin temperature increase.

Generally, the constitutive law for concrete can be expressed as follows:

$$\varepsilon^c = \varepsilon^c(\sigma(t), T(t), \tilde{\sigma}) \qquad 6.13$$

where

ε^c - total strain at time t
σ - stress
T - temperature
$\tilde{\sigma}$ - stress history

By dividing the total strain into strain components at a given time, t, the following mathematical relation is used:

$$\varepsilon^c = \varepsilon^c_{th}(T) + \varepsilon^c_{\sigma}(\tilde{\sigma}, \sigma, T) + \varepsilon^c_{cr}(\sigma, T, t) + \varepsilon^c_{tr}(\sigma, T) \qquad 6.14$$

where

ε^c_{th} - thermal strain

ε^c_{σ} - stress-related strain

ε^c_{cr} - creep strain

ε^c_{tr} - transient strain

The shrinkage, included in thermal strain, is developing below about 200°C and is properly time-dependent. That is, however, neglected in the model due to the application of the model at fire conditions i e rapid heating to elevated temperatures. Furthermore there exists an interrelationship between the stress-related and transient strain component, which will be shown later.

In a time-step calculation of the structural response to fire, equation 6.2 must be written in incremental form. The transformation of the equation is here only given in principal and the details behind are described later.

$$\Delta\varepsilon^c = \Delta\varepsilon^c_{th}(\Delta T) + \Delta\varepsilon^c_{\sigma}(\tilde{\sigma}, \sigma, T) + \Delta\varepsilon^c_{cr}(\sigma, T, \Delta t) + \Delta\varepsilon^c_{tr}(\sigma, \Delta T) \qquad 6.15$$

The solution technique of equation 6.15 in the structural program means that the total incremental strain, $\Delta\varepsilon^c$, is given and the current stress is to be evaluated. As not only the stress-related strain but also the transient and creep strain are stress dependent the calculation is complicated and therefore a simplification is introduced. When evaluating the incremental transient and creep strain at a given time the stress at the previous time-step is used, which is justified if the time-step, Δt, is chosen sufficiently small for the change in stress to be small.

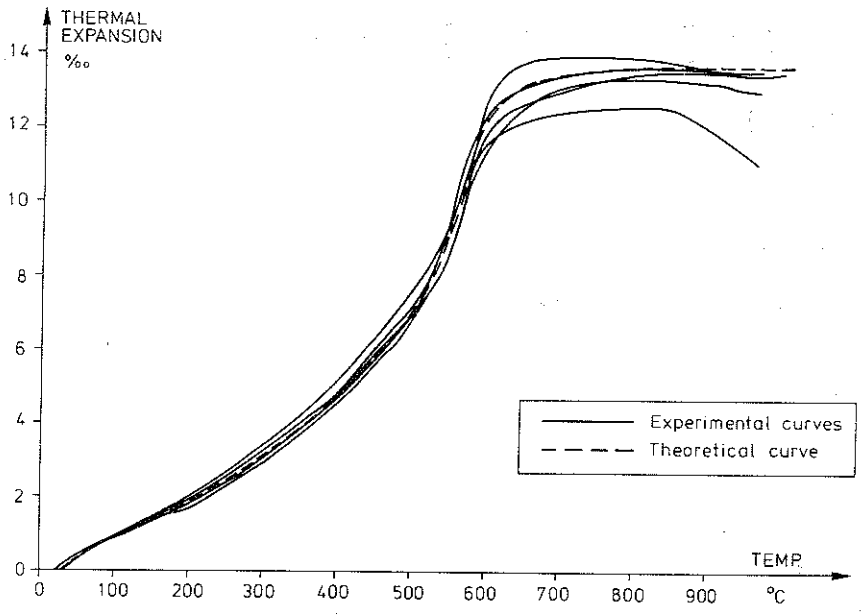

Figure 6.14 Thermal expansion of quartz aggregate concrete
W/C = 0.63
Test specimen (0.11x0.23x0.03 m^3) is water-cured for 5 days and the air-cured at 20°C for a relative air humidity of 50%.

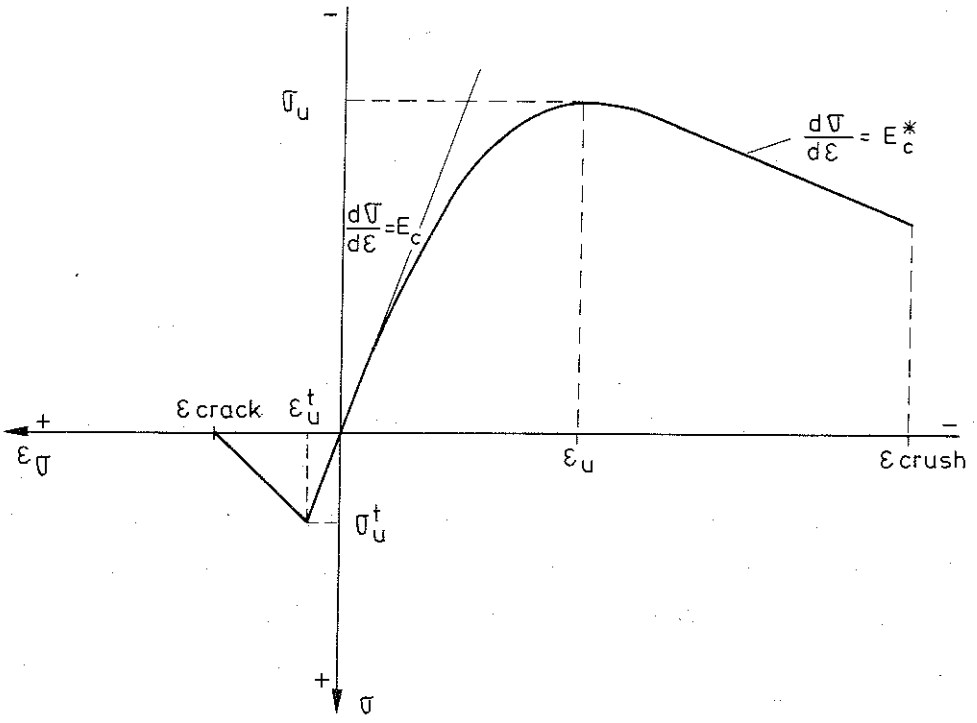

Figure 6.15 Theoretical stress-strain relation in principal.

6.2.1.1 Thermal strain model

The thermal strain during heating is a simple function of the temperature directly given by the measured thermal expansion curve. The curve used in the theoretical analysis of fire-exposed plate strips is based on measurements of four specimens casted from the same concrete mixture representative of plate strips in test series A2. The result is illustrated in Fig 6.14 and the dotted curve is estimated as the mean curve and chosen as representative in the calculations. It may also be underlined that drying shrinkage is included in the curve and no other consideration is made for that. This approximation is justified as the model mainly is used at rapid heating in the temperature range up to about 800°C, where the influence of moisture can be neglected.

Due to drying shrinkage and irreversible reactions occurring during heating as for instance the quartz inversion at 575°C, the thermal expansion during cooling is not quite reversible. The irreversible component is not insignificant for quartz aggregate concrete heated above the quartz inversion limit (Fischer 1970). However, as a first approximation, pending more complete experimental information, it may be justified to assume that the thermal expansion is fully reversible.

6.2.1.2 Stress-strain model

The calculation of the stress-related strain is based on the concept that at every state a stress-strain relation is valid for the material. This stress-strain relation should be such that it appropriately reflects the response of the material to a change in stress. From the behaviour known from testing this means that the stress-strain relation at a given time should depend on the current temperature and prehistory of stress, cf eq. 6.2.

The principal description of the stress-strain relation is illustrated in Fig 6.15. On compression side the curve consists of a parabolic branch followed by a linear descending branch until crushing occurs (Becker & Bresler (1974)). In tension zone the

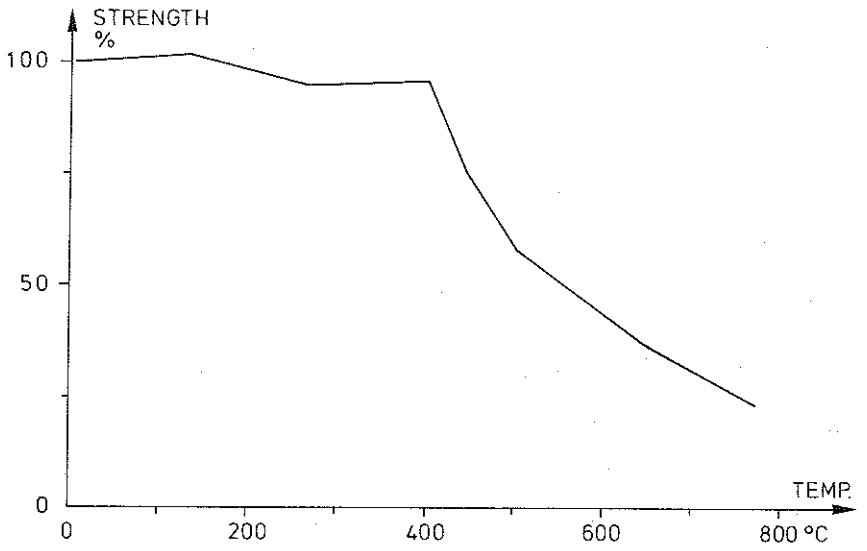

Figure 6.16 Compressive strength of quartz aggregate concrete as function of temperature

Mix proportions (weight units)

Cement	1
Water	0.6
Sand (< 8 mm)	2.88
Aggregate (8- 12 mm)	1.92

The specimens were water-cured for five days and then cured in 65% RH 20°C up to the time of testing. From Anderberg & Thelandersson (1976).

first linear portion up to maximum tensile strength is followed by a linearly descending branch. The stress-strain relation is uniquely defined by the following parameters indicated in the figure:

$\sigma_u(T)$ - compressive strength of concrete

$\varepsilon_u(T)$ - ultimate strain at which $\sigma = \sigma_u(T)$

$E_c^*(T)$ - slope of the second branch in compression zone

$\sigma_u^t(T)$ - tensile strength of concrete

ε_{crack} - formal strain at which cracking starts

The reason why the ultimate strain is preferred to the elastic modulus is due to the uncertainty in determining the latter parameter. In the following, these parameters are expressed as functions of temperature and stress-history.

Ultimate stress, σ_u

In this presentation different influences on compressive strength, such as petrographical composition and different types of aggregate, cement-aggregate mixture as well as age and storing condition will not be discussed. Here is only briefly mentioned results from Anderberg & Thelandersson (1976) on a quartz aggregate concrete almost identical to that used in the experiment. For a more detailed analysis the reader is referred to Anderberg & Thelandersson (1973).

The ultimate strength of concrete is a function of temperature but it is also to some extent dependent on the stress history. A somewhat higher strength is obtained for specimens heated under sustained low stress than for those unstressed during heating.

In view of the uncertainties inherent in any estimate of high-temperature strength of concrete it is reasonable to assume that σ_u is a unique function of temperature and that the influence of different prehistories of stress may be neglected. Its function of temperature is illustrated in Fig 6.16.

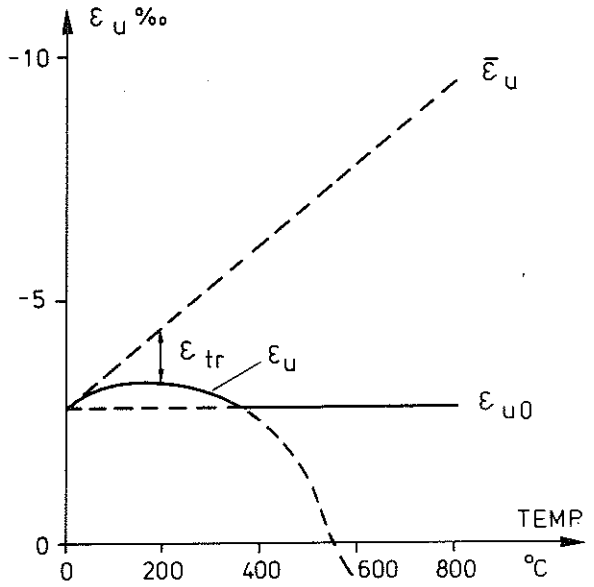

Figure 6.17 Theoretical model of ultimate strain

$\bar{\varepsilon}_u(T)$ - prehistory of stress equal to zero

ε_{uo} - ultimate strain at room temperature

$\varepsilon_u(T,\varepsilon^c_{tr})$ - prehistory of stress considered

The model is based on tests of quartzite aggregate concrete.

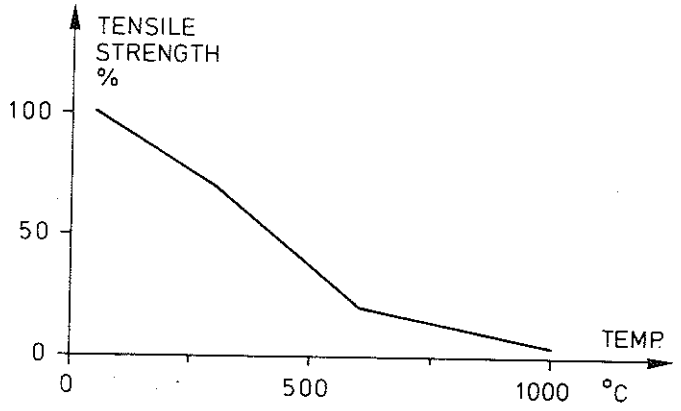

Figure 6.18 Tensile strength as function of temperature.
The curve is based on tests for flexural (Zoldners (1960)) and splitcylinder strength (Thelandersson (1972)).
Quartz aggregate concrete.

Ultimate strain, ε_u

The ultimate strain is temperature as well as stress history dependent

$$\varepsilon_u = \varepsilon_u(T, \tilde{\sigma}) \qquad 6.16$$

The influence of an arbitrary prehistory of stress can furthermore be expressed by the accumulated transient strain, ε^c_{tr} and we can write:

$$\varepsilon_u = \varepsilon_u(T, \varepsilon^c_{tr}) \qquad 6.17$$

When $\varepsilon_{tr} = 0$ i e the previous stress history is equal to zero, the ultimate strain based on experimental data is modelled as indicated in Fig 6.17 and

$$\varepsilon_u(T, 0) = \bar{\varepsilon}_u(T) \qquad 6.18$$

Noting that compressive strains are negative we can write:

$$\varepsilon_u(T, \tilde{\sigma}) = \text{MIN}[\varepsilon_{uo}, \bar{\varepsilon}_u(T) - \varepsilon^c_{tr}(T, \sigma)] \qquad 6.19$$

where

ε_{uo} - ultimate strain at ambient conditions

This means that the absolute value of the ultimate strain due to a prehistory of stress is always less or equal to $|\bar{\varepsilon}_u|$ but not reduced to less than $|\varepsilon_{uo}|$. This is illustrated in Fig 6.17 for a typical variation of ε_u.

Modulus of descending branch, E^*_c

The slope of the descending branch of the stress-strain curve is studied very little in literature. It can furthermore only be measured in a strain controlled test on the σ - ε relationship. The choice of this parameter is however not very important for the behaviour and E^*_c is given the constant value - 880 MPa in-

dependent of temperature and stress history. The final point on the descending branch defines the strain at which crushing occurs. The strain called ε_{crush} is supposed to increase approximately linearly from 5‰ at room temperature up to 15‰ at 1000°C. The prediction of the behaviour in the failure state cannot be done appropriately by this model. It is, however, necessary to consider a separate failure criteria depending on the structural problem in question. This is furthermore emphasized in Anderberg & Thelandersson (1976).

Tensile strength, σ_u^t

The tensile strength is supposed to be solely temperature dependent as shown in Fig 6.18. This curve is chosen on the basis of tests on flexural and split-cylinder strength presented by Zoldners (1960) and Thelandersson (1972) respectively. The tensile strength at room temperature is evaluated from the following formula:

$$\sigma_u^t = 0.28 \times (0.8 \times \sigma_{cube})^{2/3} \qquad 6.20$$

where

σ_{cube} - cube strength at room temperature (specimen size 0.15 x 0.15 m^2)

In the theoretical analysis of the plate strips σ_u^t is further reduced with 20% due to drying of the concrete. A representation cube strength is prevalently chosen to 40 MPa, which means a tensile strength equal to 2.3 MPa.

Cracking strain, ε_{crack}

In strain-rate controlled tests the stress-strain curve in tension has a shape similar to that in compression. This characteristic feature is shown by Evans & Marathe (1968) from which Fig 6.19 is taken. The elasto-plastic behaviour at room temperature is obvious which probably is more pronounced at elevated temperatures and consequently it ought to be considered in the theoretical model. As neither tensile nor flexural tests at elevated temperature are studied in literature in connection

with the determination of stress-strain curve in tension, the model chosen here is simplified. Two linear branches are chosen to describe the behaviour in tension as illustrated in Fig 6.15. The slope of the descending branch is determined by the tensile strength, σ_u^t, and the formal cracking strain, ε_{crack}, while the first linear portion coincides with the fictitious elastic modulus in compression, which is given from the derivation of chosen curve expression. The formal value of ε_{crack} is a measure of the deformability of concrete in tension and depends in a fundamental way on the degree of strain-rate control in real structure, for instance in actual plate strip. Such a condition does not exist in a pure tension test and thus ε_{crack} has to be based on flexural behaviour of the actual structure.

A representative value of ε_{crack} for a segment of the plate strip will be studied theoretically at room temperature. A moment-curvature relationship valid for a cross-section identical to that of the plate strip including reinforcing bars as shown in Fig 6.20 is calculated at different values of ε_{crack} and σ_u. The calculations can be directly compared with measurements on the moment-curvature relationship of the unexposed concrete plate strip, which is presented in 5.6. In that way a functionally correct determination of ε_{crack} can be carried through. This parameter takes into account the integrated effect of tensile carrying capacity between the real cracks within a segment of the structure.

The evaluation of the moment-curvature relation is carried out with a computer program published in Alemo (1976). The calculations are based on actual material properties used in the stress-strain law described above. In Fig 6.20a the moment-curvature relation is shown for four values of ε_{crack}, viz, 0.12, 0.40, 0.80 and 1.60‰, (ε_u^t = 0.11‰) at the compressive strength value of 32 MPa, which corresponds to σ_{cube} = 40 MPa. The curves imply an increasing cracking moment with increasing ε_{crack} from 3.5 to about 8 kNm. The level of cracking moment is not so distinct in the experimental curve (see section 5.6) as in the theoretical curves, but can be estimated to 4 kNm. It can also be

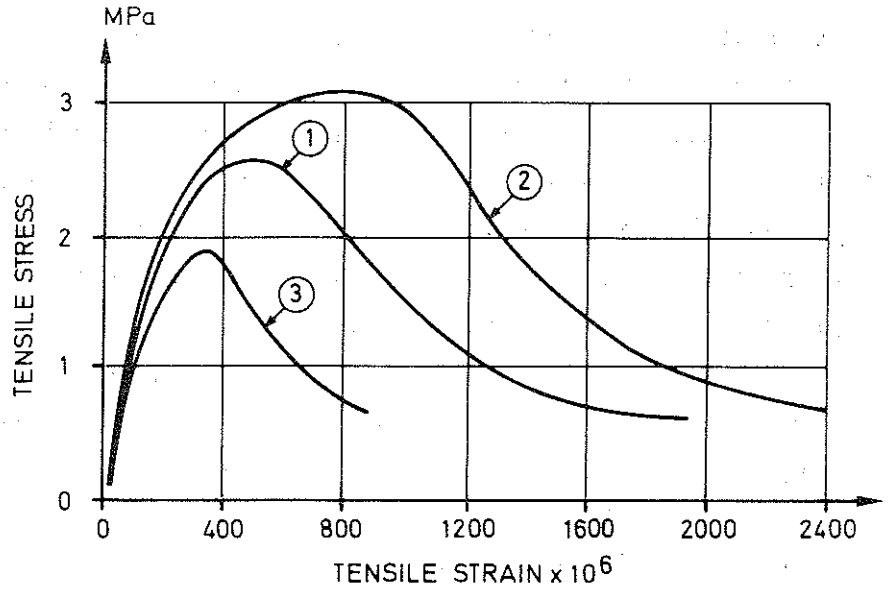

Figure 6.19 Stress-strain curves in tension from tests with controlled deformation (Evans & Marathe (1968)).

Curve	Mix	W/C	Age
①	1:1:2	0.45	65 days
②	1:2:4	0.60	270 days
③	1:3:6	0.90	70 days

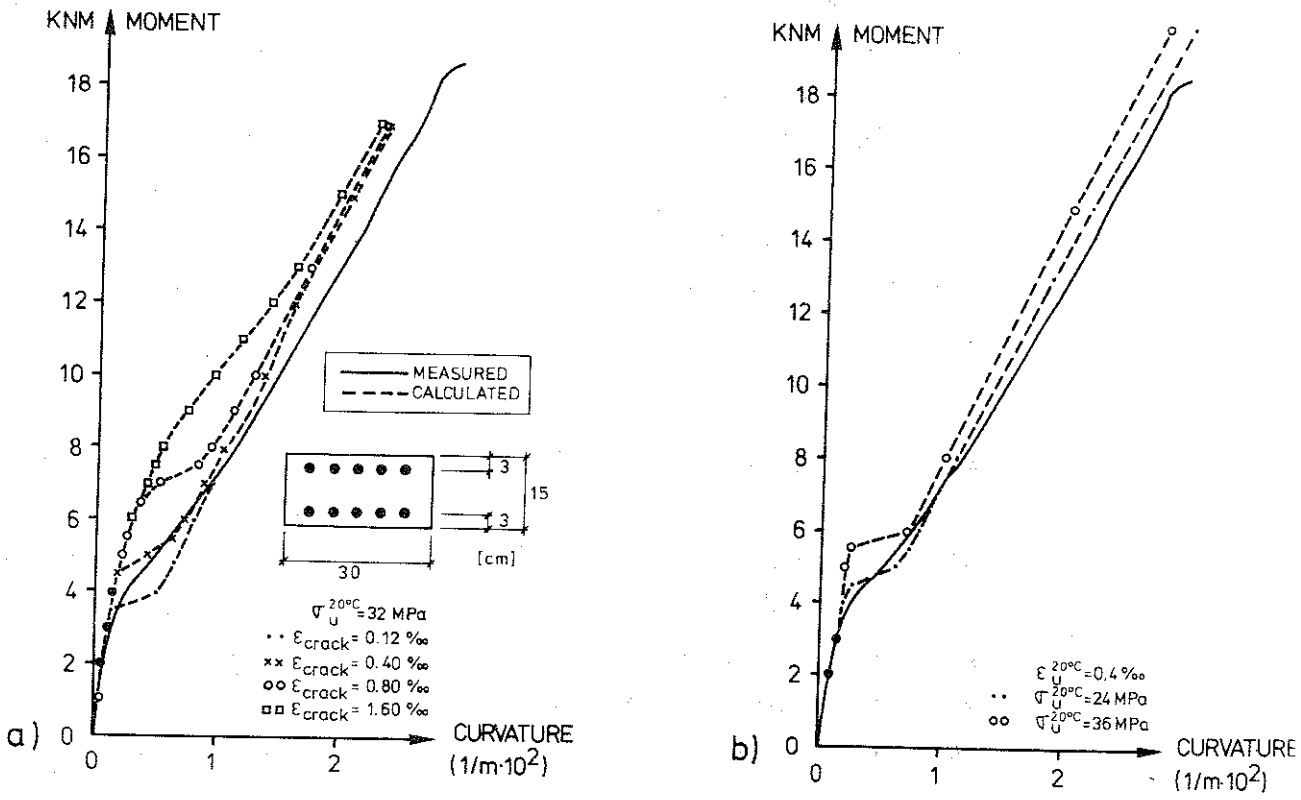

Figure 6.20 Moment-curvature relationship of unexposed plate strips.
Quartz aggregate concrete.
W/C = 0.63
Curing conditions see Fig. 6.14.
Measured curve cf. Fig. 5.26

noticed that the theoretical curves fit very well with the experimental one and the very best agreement is obtained when ε_{crack} = 0.4‰. Having in mind the uncertainties in the experimental determination of the moment-curvature relation (see section 5.6) and the discrepancy in the results obtained, the accordance is quite satisfactory. As the compressive strength of concrete varies from one plate strip to another (see Table 3.1) the influence of this parameter is also investigated. The moment-curvature relation is calculated at the values 24 and 36 MPa of compressive strength when keeping ε_{crack} constant at 0.4‰. The two values of strength represent actual measured minimum and maximum strength. The result, reproduced in Fig 6.20b indicates a cracking moment lying between 4.5 - 5.5 kNM. It is true that the measured cracking moment is only about 4 kNM but due to the age of the tested plate strips (1 1/2 year) the shrinkage has lowered the value and other uncontrolled circumstances may also influence the determination. Therefore it is justified to correct the value upwards and choose ε_{crack} equal to 0.4‰. How ε_{crack} is influenced by rising the temperature is unfortunately not clarified, and therefore it is chosen to be invariant with temperature. This assumption is insignificant in the theoretical analysis.

The parameters governing the complete stress-strain relation durig a first heating are presented. In order to make calculations during a cooling phase you have to define the influence of a subsequent cooling, too.

The stress-strain relation during cooling is studied very fragmentarily and only at room temperature after cooling. The knowledge is insufficient in order to establish any accurate theory. As a first approximation it is reasonable to assume that the stress-strain curve in compression used at the maximum temperature level is invariant during a subsequent cooling. Due to the complete lack of knowledge on tension side the same assumption means that the values of the five parameters σ_u, ε_u, E_c^*, σ_u^t and ε_{crack} respectively valid at the current maximum temperature are unchanged and also adequate during cooling. The sensitivity of other assumptions during cooling ought to be looked upon in future studies.

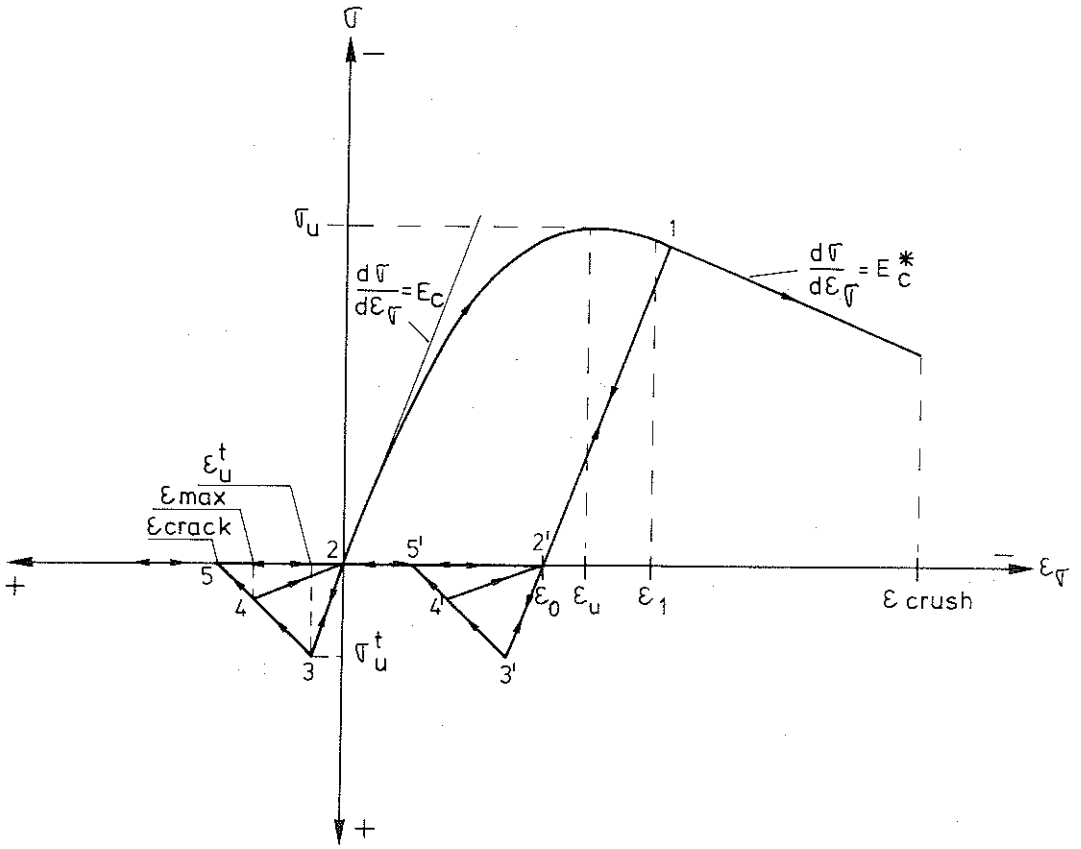

Figure 6.21 Complete stress-strain relationship for concrete

σ_u - compressive ultimate stress
σ^t_u - tensile ultimate stress
E^*_c - strain hardening modulus
ε_u - ultimate compressive strain
ε^t_u - ultimate tensile strain
ε_1 - strain at transition point
ε_o - permanent inelastic strain
ε_{crack} - formal cracking strain
ε_{max} - maximum tension strain
ε_{crush} - crushing strain
Index c is omitted.

The mechanical properties of concrete at elevated temperatures today are relatively satisfying, but there is still a need for investigating these characteristics especially during a subsequent cooling. As the material models during cooling are based on estimated properties this will accordingly influence the reliability of calculated structural behaviour.

The determination of all parameters necessary for the formulation of the stress-strain relation in principal at a given temperature and stress history is described. The complete model of the stress-strain law is characterized by a closed curve, which allows for an arbitrary loading and unloading process as illustrated in Fig 6.21.

In the structural computer program an iterative approach is used to determine the current stress at an assumed stress-related strain ε_σ^c. This analytical procedure is now formulated. The usual sign convention is used here, positive sign for stresses and strains in tension zone and negative for those in compression zone.

The boundary conditions of the parabolic curve are:

$$\sigma = \sigma_u \qquad \text{when } \varepsilon_\sigma^c = \varepsilon_u \tag{6.21a}$$

$$\frac{d\sigma}{d\varepsilon_\sigma} = 0 \qquad \text{when } \varepsilon_\sigma^c = \varepsilon_u \tag{6.21b}$$

$$\frac{d\sigma}{d\varepsilon_\sigma} = E_c^* \qquad \text{when } \varepsilon_\sigma^c = \varepsilon_1 \tag{6.21c}$$

where

ε_1 is the strain at transition between the parabolic branch and the linear second branch.

The parabolic curve is defined by the following equation:

1. $$\sigma = \sigma_u \frac{\varepsilon_\sigma^c}{\varepsilon_u}\left(2 - \frac{\varepsilon_\sigma^c}{\varepsilon_u}\right) \qquad 0 \geq \varepsilon_\sigma^c > \varepsilon_1 \tag{6.22}$$

From this equation the fictitious elastic modulus E_c and ε_1 (strain at the transition to the second branch) can be derived as follows:

$$E_c = 2 \frac{\sigma_u}{\varepsilon_u} \qquad 6.23$$

$$\varepsilon_1 = (1 - \frac{E_c^*}{E_c}) \varepsilon_u \qquad 6.24$$

The second portion of the stress-strain envelope in the compression zone yields the expression:

$$2. \quad \sigma = E_c^* \cdot \varepsilon_\sigma^c + \sigma^* \qquad \varepsilon_1 \geq \varepsilon_\sigma^c > \varepsilon_{crush} \qquad 6.25$$

where

$$\sigma^* = \sigma_u [1 - \frac{E^{*2}}{E_c}] \qquad 6.26$$

On the tension side the elasto-plastic behaviour is defined in the following way:

$$3. \quad \sigma = E_c \cdot \varepsilon_\sigma^c \qquad 0 \leq \varepsilon_\sigma^c < \varepsilon_u^t \qquad 6.27$$

where

ε_u^t is the strain when maximum tensile stress is reached

$$\varepsilon_u^t = \frac{\sigma_u^t}{E_c} \qquad 6.28$$

$$4. \quad \left.\begin{array}{ll} \sigma = E_c \cdot \varepsilon_u^t \dfrac{\varepsilon_{crack} - \varepsilon_\sigma^c}{\varepsilon_{crack} - \varepsilon_u^t} & \varepsilon_u^t \leq \varepsilon_\sigma^c < \varepsilon_{crack} \\ \sigma = 0 & \varepsilon_{crack} \leq \varepsilon_\sigma^c \end{array}\right\} \qquad 6.29$$

where

ε_{crack} is that strain at which cracking starts.

The four basic equations for the total stress-strain curve are presented above. Now an extension follows, which describes how any unloading process is considered in the model. This is prin-

cipally illustrated in Fig 6.21, in which arrows indicate in which direction we are allowed to follow the closed curve. The unloading on compression side starts at point 1 and ends at point 2, where the stress transfers into tension. The loop on tension side is indicated by 2 - 3 - 4 - 2 or 2' - 3' - 4' - 2' valid if a previous unloading has taken place on compression side. The last loop is thus transferred ε_o and identical to the virgin loop. The turning point 4 implies the unloading on tension side, which always leads to origin (2). Cracking is assumed to occur at point 5. However, cracked portions can be closed again on the branch 5 - 2 and then turn into compression.

The calculation of current stress is made in a time-step iteration where the incremental change between two time-steps is either a loading or an unloading process. The unloading branch on compression side is based on the plastic or permanent inelastic strain

$$\varepsilon_o^c = \varepsilon_\sigma^c - \frac{\sigma}{E_c} \qquad 6.30$$

which in a time-step iteration is calculated on the basis of the stress and strain at the end of previous time-step i - 1 and the fictitious elastic modulus given at time-step i - 1.

$$\varepsilon_{o,i-1}^c = \text{MIN}(\varepsilon_{o,i-2}^c,\ \varepsilon_{\sigma,i-1}^c - \frac{\sigma_{i-1}}{E_{c,i-1}}) \qquad 6.31$$

If unloading is prevalent for the time-step the stress is evaluated at the time-step from the following expression

$$\sigma_i = E_{ci}(\varepsilon_{\sigma,i}^c - \varepsilon_{o,i-1}^c) \qquad \varepsilon_\sigma^c \leq \varepsilon_o^c + \varepsilon_u^t \qquad 6.32$$

which thus is valid into the tension zone (cf Fig 6.21). The greater (in algebraic sense) of the stresses, obtained from equation 6.22 or 6.25 (depends on the magnitude of ε_σ^c) and 6.32, becomes the current state of stress.

In order to take into account a possible unloading on compression side, before entering the tension side, the descending branch in

tension zone must be extended for an arbitrary strain history. Equation 6.29 is therefore rewritten in a generalized form:

$$\sigma = E_c \cdot \varepsilon^t_{ult} \frac{\varepsilon_{crack} - \varepsilon^c_\sigma + \varepsilon^c_o}{\varepsilon_{crack} - \varepsilon^t_{ult}} \qquad 6.33$$

$$\varepsilon_{crack} + \varepsilon^c_o \geq \varepsilon^c_\sigma > \varepsilon^t_u + \varepsilon^c_o$$

The unloading branch on tension side always leads to origin or to ε^c_o depending on the prehistory in the stress-strain diagram which is indicated in Fig 6.21. Quantities necessary to store in order to formulate the current unloading branch are the maximum strain on tension side, ε_{max} and of course ε^c_o. The general formula will be:

$$\left.\begin{aligned} \sigma &= E_c \cdot \varepsilon^t_{ult} \frac{(\varepsilon_{crack} - \varepsilon_{max} + \varepsilon^c_o)(\varepsilon_{crack} - \varepsilon^c_\sigma + \varepsilon^c_o)}{(\varepsilon_{crack} - \varepsilon^t_{ult})^2} \\ & \qquad \varepsilon^t_{ult} + \varepsilon^c_o < \varepsilon^c_\sigma < \varepsilon^c_o + \varepsilon_{crack} \\ \sigma &= 0 \qquad \varepsilon^c_\sigma \geq \varepsilon^c_o \quad \text{and} \quad \varepsilon_{max} \geq \varepsilon_{crack} + \varepsilon^c_o \end{aligned}\right\} \quad 6.34$$

The analytical formulation of a complete stress-strain model is then completed, taking into account any arbitrary strain-history, i e any possible unloading where even the number of cycles is unlimited. The programming of the stress-strain law given as a subroutine in the main program is illustrated in Appendix. This subroutine is a further developement of that formulated in Becker & Bresler (1974).

6.2.1.3 Creep strain model

Constant temperature creep of concrete is measured under constant compressive stress as the time-dependent strain at a stabilized temperature level. Creep tests on concrete very similar to the type of concrete used in this investigation is presented in Anderberg et al (1976). In that paper an analytical expression of creep, based on these tests, is developed. This creep model is extended for use also at changes in temperature and stress by using the concept of the strain hardening rule. The model is expressed below:

1. The basic creep at constant temperature and stress is given by

$$\varepsilon_{cr}^{c} = \beta_o \frac{\sigma}{\sigma_u(T)} \left(\frac{t}{t_r}\right)^{p_1} \cdot e^{k_1 (T - 20)} \qquad 6.35$$

where

$\beta_o = -0.53 \cdot 10^{-3}$
$k_1 = 3.04 \cdot 10^{-3} \ {}^{o}C^{-1}$
$p_1 = 0.5$
$t_r = 3$ (hours)

2. Varying temperature and stress.

We start to assume that the creep at the time t_i is defined by:

$$\varepsilon_{cr}^{c}(t_i) = \beta_o \frac{\sigma_i}{\sigma_u(T_i)} \left(\frac{t_i}{t_r}\right)^{p_1} e^{k_1 (T_i - 20)} \qquad 6.36$$

where the index i refers to the time t_i.

We want to calculate the creep increment at the time t_{i+1} when the temperature is T_{i+1} and the stress σ_{i+1}. This can be done by using the principle of strain hardening which broadly speaking means that the creep rate depends on the actual temperature and stress and the accumulated creep strain. The principle is illustrated in Fig 6.22. Introduce the material time t_{im}, which gives the same creep at temperature T_{i+1} and stress σ_{i+1} as at temperature T_i and σ_i

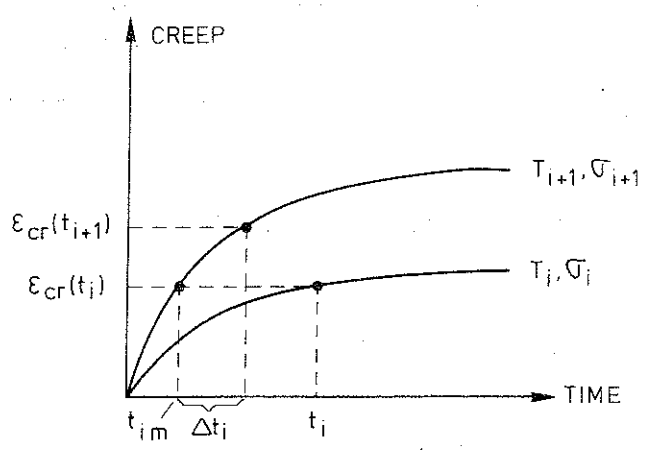

Figure 6.22 The principle of strain hardening rule applied on creep strain for concrete.

$$t_{im} = t_r \left(\frac{\varepsilon^c_{cr}(t_i)}{\beta_o \, e^{k_1 (T_{i+1} - 20)} \, \frac{\sigma_{i+1}}{\sigma_u(T_{i+1})}} \right)^{1/p_i} \qquad 6.37$$

At the material time $t_{i+1} = t_{im} + \Delta t_i$ the total creep in accordance to strain hardening rule will be

$$\varepsilon^c_{cr}(t_{i+1}) = \beta_o \frac{\sigma_{i+1}}{\sigma_u(T_{i+1})} \left(\frac{t_{i+1}}{t_r}\right)^{p_i} e^{k_1 (T_{i+1} - 20)} \qquad 6.38$$

The incremental creep strain is given by

$$\Delta\varepsilon_{cr}(t_i) = \varepsilon_{cr}(t_{i+1}) - \varepsilon_{cr}(t_i) \qquad 6.39$$

and by using the two first terms in the Taylor series we obtain instead

$$\Delta\varepsilon_{cr}(t_i) \approx \beta_o \frac{\sigma_{i+1}}{\sigma_u(T_{i+1})} \, e^{k_1 (T_{i+1} - 20)} \, \frac{t_{im}^{p_i - 1}}{t_r^{p_i}} \cdot p_i \cdot \Delta t_i \qquad 6.40$$

and

$$\varepsilon_{cr}(t_{i+1}) = \sum_{n=1}^{i} \Delta\varepsilon_{cr}(t_n) \qquad 6.41$$

This general expression is thus obtained by assuming the stress and temperature to be constant through each time-step. In the FIRES-RC program the stress at the actual time-step is not known when the incremental creep is evaluated. Therefore, the stress at the previous time-step is used, which simplifies the calculation. This is not regarded in the presented formulas.

The creep strain at tension is insignificant in the structural analysis. However, it is calculated in the same manner as in compression, pending on available experimental data. Probably

the creep formula used for concrete in torsion (Thelandersson (1975)) is more appropriate than that at compression.

6.2.1.4 Transient strain model

The transient strain, ε^c_{tr}, developes under compressive and probably tensile stress when the temperature increases. The strain is essentially permanent and irrecoverable and occurs only under the first heating.

In transient tests this strain component is often dominating and it is approximately independent of time (Thelandersson (1975) and Anderberg & Thelandersson (1976)). Furthermore it has a temperature dependence very similar to that of the thermal strain and the linear relation to compressive stress level yields the expression

$$\varepsilon^c_{tr} = - k_2 \frac{\sigma}{\sigma^c_{uo}} \varepsilon^c_{th} \qquad T \leq 500^oC \qquad 6.42$$

or in incremental form

$$\Delta\varepsilon^c_{tr} = - k_2 \frac{\sigma}{\sigma^c_{uo}} \Delta\varepsilon^c_{th} \qquad T \leq 500^oC \qquad 6.43$$

where

$k_2 = 2.35$ (determined for similar concrete mix as used for the plate strip)

It is likely that the kind of aggregate and concrete mix used are influencing the value of k_2. The variation of k_2 is in Anderberg & Thelandersson (1976) found, on the basis of published tests to vary from 1.8 to 2.35 for quartzite aggregate concrete.

However, the aforementioned relationship seems to be too conservative at temperatures above about 500°C, so it has to be complemented above this level. Due to an accelerated temperature effect on the transient strain the following expression is estimated on the basis of published tests studied in the last mentioned reference

$$\Delta\varepsilon^c_{tr} = 0.1 \cdot 10^{-3} \cdot \Delta T \cdot \frac{\sigma}{\sigma^c_{uo}} \qquad 500^oC < T \leq 800^oC \qquad 6.44$$

The transient strain under tensile stress is hitherto not investigated and due to its unimportance in structural analysis it is not regarded in the model. Probably a modification of the transient strain model used in torsion (Thelandersson (1975)) can be applied if desired.

6.2.2 Constitutive law of steel

The consititutive law of steel is far from that complicated as concerns concrete but has a more traditional definition. Only three components are involved, which are the same at steady state as well as at transient conditions.

Thermal strain, or thermal expansion, is measured on unstressed specimens under variable temperature.

Instantaneous stress-related strain, based on stress-strain curves obtained under stabilized temperature.

Creep strain, time-dependent strain recorded under constant stress at stabilized temperature.

The constitutive law of steel can thus be formulated in the following way:

$$\varepsilon^{S}(\sigma, T, t) = \varepsilon^{S}_{th}(T) + \varepsilon^{S}_{\sigma}(\sigma, T) + \varepsilon^{S}_{cr}(\sigma, T, t) \qquad 6.45$$

For use in the FIRES-RC program this expression is transformed for incremental calculation, i e

$$\Delta\varepsilon^{S} = \Delta\varepsilon^{S}_{th}(\Delta T) + \Delta\varepsilon^{S}_{\sigma}(\sigma, T) + \Delta\varepsilon^{S}_{cr}(\sigma, T, \Delta t) \qquad 6.46$$

6.2.2.1 Thermal strain model

The thermal strain of steel is generally expressed by the coefficient of thermal expansion, which in literature is presented both for structural and reinforcing steel. The temperature dependence of the coefficient seems to be very similar for the different

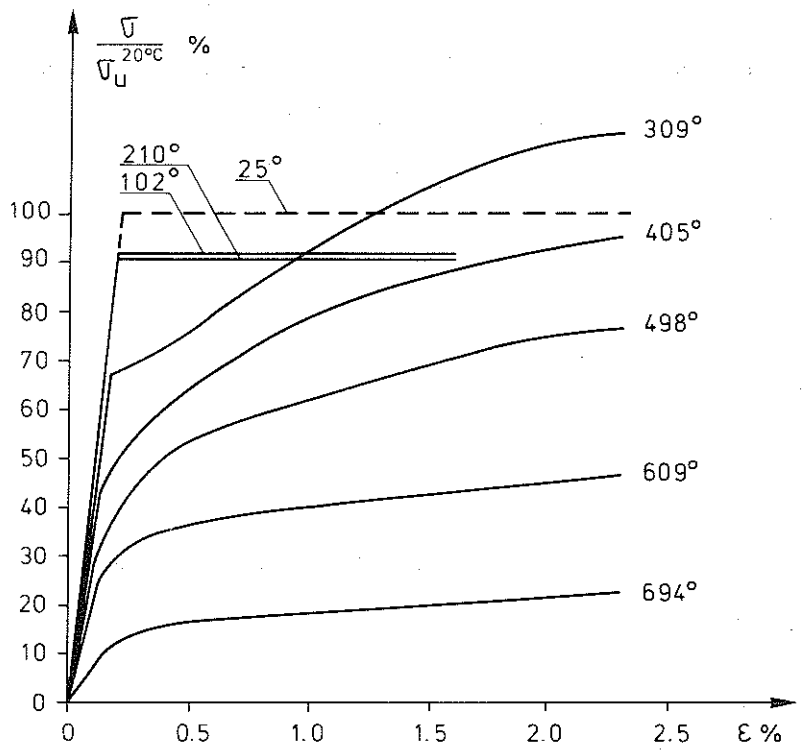

Figure 6.23 Stress-strain curves of reinforcing steel Ks 40 ϕ10 determined in tensile tests at elevated temperatures.
Yield stress measured at room temperature = 450 MPa
Rate of loading = 211 MPa/min
Ks 40 is an ordinary hot-rolled reinforcing steel.

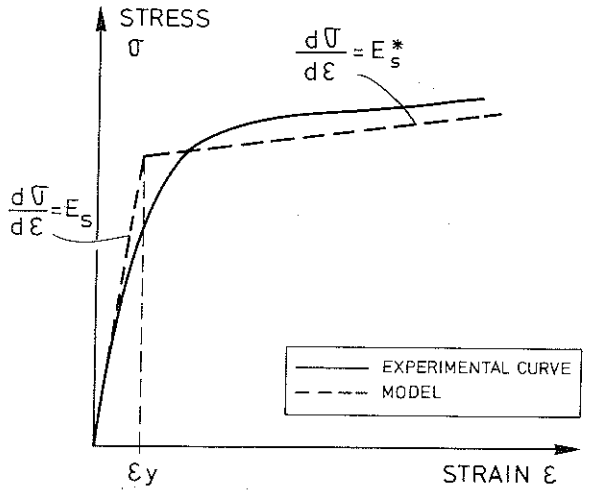

Figure 6.24 Model of stress-strain curve for steel in principal.

steels and a linear relationship is often used. The thermal expansion is furthermore investigated by the author for reinforcing steel KS 40, ϕ10 used in the experiment, and the coefficient at room temperature is determined to $12 \cdot 10^{-6}/^{o}C$ and at $800^{o}C$ to $20 \cdot 10^{-6}/^{o}C$ which is in a close accordance to an example model used in Bizri (1973). Thus

$$\varepsilon_{th}^{s}(T) = \int_{0}^{T} \zeta_{s}(T) \cdot dT \qquad 6.47$$

and

$$\Delta\varepsilon_{th}^{s}(\Delta T) = \zeta_{s}(T) \cdot \Delta T \qquad 6.48$$

where

$\zeta_{s}(T)$ - coefficient of thermal expansion

6.2.2.2 Stress-strain model

The stress-strain relationship at elevated temperatures for the actual steel is investigated in Krakau et al (1975). The stress-strain relationship in tension zone was determined at 9 temperature levels and the result is reproduced in Fig 6.23. The rate of loading during the tests was 211 MPa/min, i e the influence of creep strain on the stress-strain curve is negligible.

The yielding plateau is already at about $300^{o}C$ disappearing and the curves get a more smooth form and no marked yield stress can be defined. However, in the theoretical model the stress-strain curve is identified with two linear portions as shown in Fig 6.24. The slope of the first branch coincides with the elastic modulus, E_s, and the break point is denoted ε_y, which furthermore are temperature dependent. The slope of the second branch is called the strain hardening modulus E_s^* and is also varying with temperature. The fitting to the experimental curves has given a temperature dependence of the three parameters, E_s, ε_y and E_s^* as illustrated in Fig 6.25 - 6.27. Of course this modelling of the real stress-strain relation of steel is simplified. The fictitious parameters ε_y and E_s^* attain a somewhat irregular temperature depen-

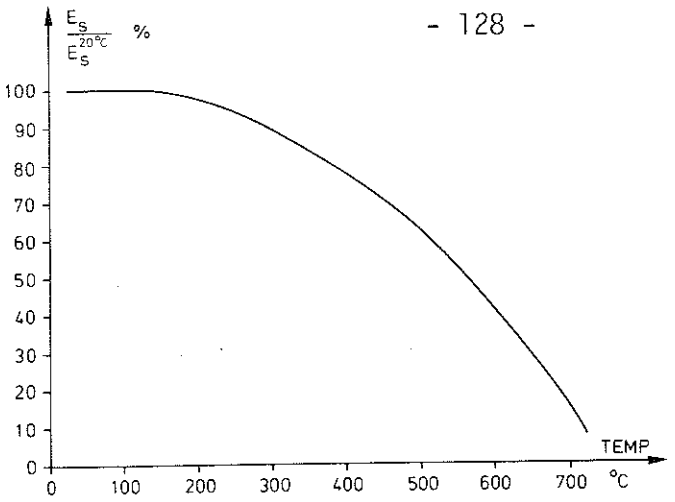

Figure 6.25 Temperature-dependence of elastic modulus for reinforcing steel Ks 40 ϕ10
$E_s^{20°C}$ = 210 GPa
Rate of loading = 211 MPa/min.

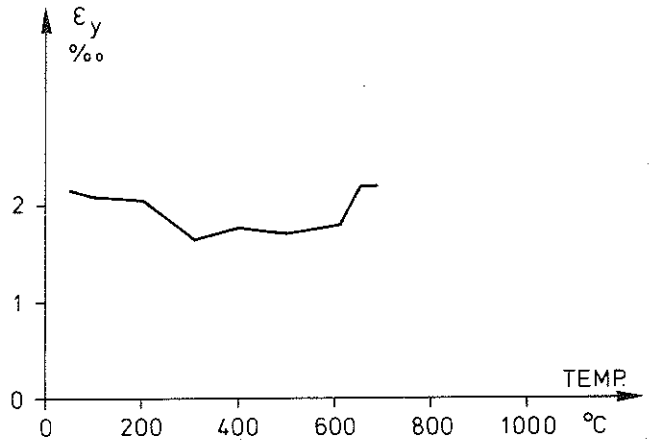

Figure 6.26 Temperature-dependence of ε_y as defined in the model for reinforcing steel Ks 40 ϕ10
Rate of loading = 211 MPa/min.

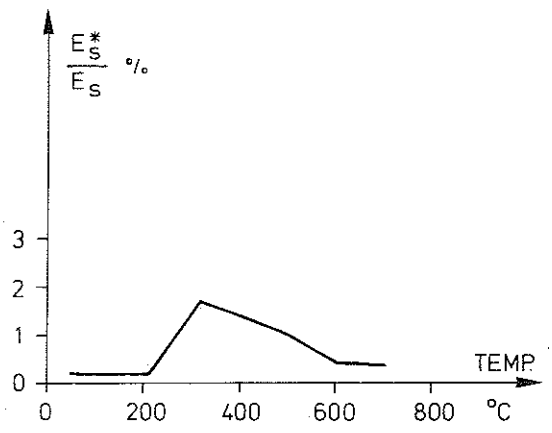

Figure 6.27 Temperature-dependence of strain hardening modulus, E_s^* as defined in the model for reinforcing steel Ks 40 ϕ10
$E_s^{20°C}$ = 210 GPa.

dence but for the structural analysis it is justified. An alternative and more accurate description of the stress-strain curve is illustrated in Fig 6.28 where a transition curve defined by the equation of the ellipse is used. It is furthermore supposed that the stress-strain relation in compression is identical to that in tension, and consequently this is also the case for the temperature dependent parameters necessary for the formulation of the model. During a subsequent cooling the mechanical properties for this type of reinforcing steel are supposed to be regained totally, which seems to be an adequate estimation of real conditions. The temperature dependence of the actual parameters is thus reversible. The stress-strain model used here for reinforcing steel is given in Becker & Bresler (1974). This model considers any given stress history including unloading processes. The stress-strain envelope shown in Fig 6.29 is constructed from the three aforementioned parameters, which are known at any temperature state including cooling. Arrows in the figure illustrate in which direction we may follow the closed curve.

The envelope is bounded by two parallel lines going through the points $(\varepsilon_y, \sigma_y)$ and $-(\varepsilon_y, \sigma_y)$ respectively (see Fig 6.29). The lines are formulated as follows:

$$\sigma_{ul} = \sigma_y + E_s^* \, (\varepsilon_\sigma^s - |\varepsilon_y|) \qquad 6.49$$

$$\sigma_\ell = -\sigma_y + E_s^* \, (\varepsilon_\sigma^s + |\varepsilon_y|) \qquad 6.50$$

By including the unloading process a third line is defined as intercepting the strain axis at point of plastic or permanent inelastic strain, ε_o^s, or $-\varepsilon_o^s$ depending on strain history with a slope equal to the modulus of elasticity. In an iterative calculation at the time-step i

$$\sigma_{E_i} = E_{s,i}(\varepsilon_{\sigma,i}^s - \varepsilon_{o,i-1}^s) \qquad 6.51$$

The plastic strain, ε_o^s, during time step i is calculated on the basis of the stress and strain at the end of the previous time-step, i - 1 and the elastic modulus given at time-step i - 1 and i.

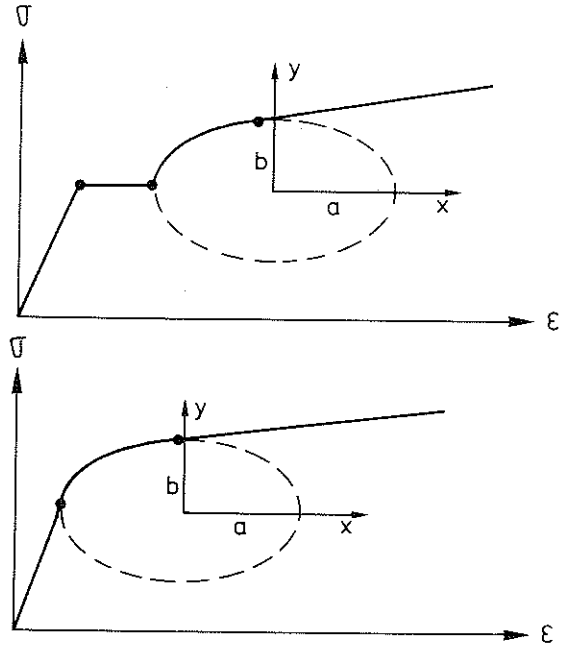

Figure 6.28 Refined modelling of stress-strain relationship of steel at elevated temperatures.

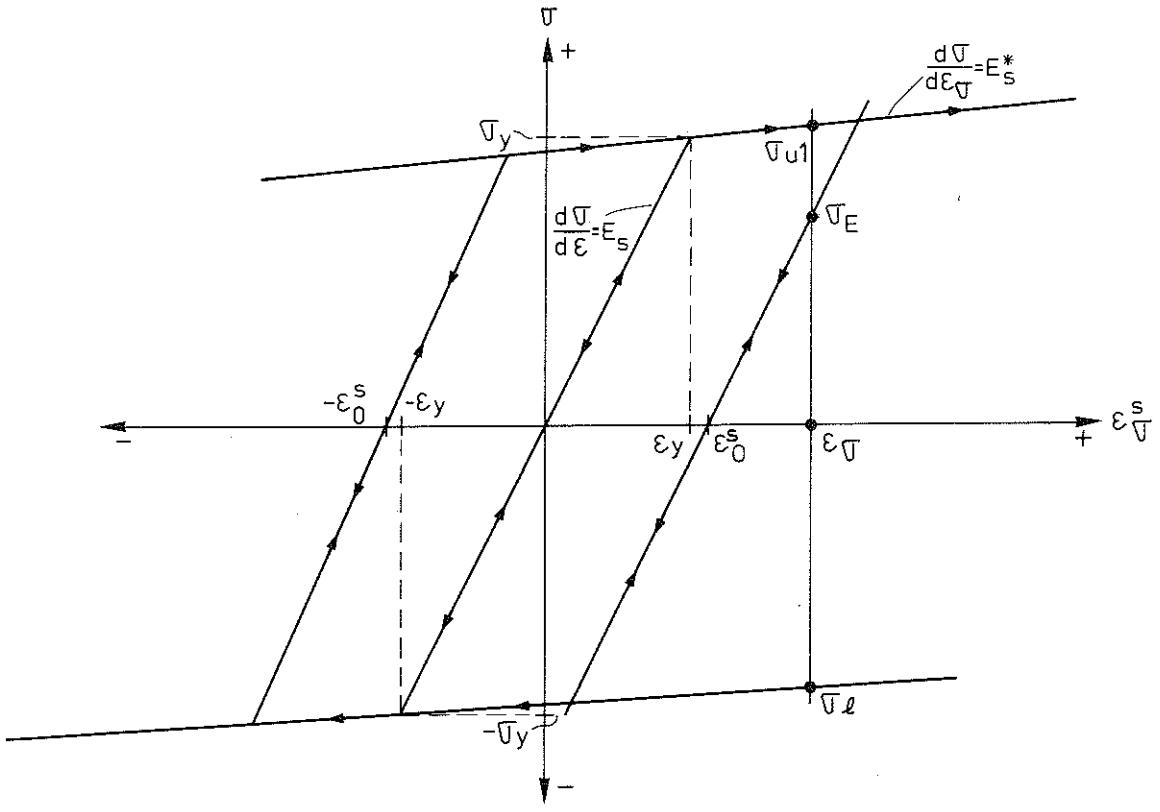

Figure 6.29 Complete stress-strain relationship for steel.

$$\varepsilon^{s}_{o,i-1} = \varepsilon^{s}_{\sigma,i-1} - \frac{\sigma_{i-1}}{(E_{s,i-1} + E_{s,i})/2} \qquad 6.52$$

When the three stresses σ_u, σ_ℓ and σ_E are calculated the actual state of stress is determined as follows

$$\sigma = \sigma_{ul} \qquad \text{if } \sigma_E > \sigma_{ul} \qquad 6.53a$$

$$\sigma = \sigma_\ell \qquad \text{if } \sigma_E < \sigma_{ul} \qquad 6.53b$$

else

$$\sigma = \sigma_E \qquad 6.53c$$

6.2.2.3 Creep strain model

The model for creep in reinforcing steel used in the calculation is based on a creep theory put forward by Dorn (1954), which considers the effect of variable temperatures. The extension of the model to be applicable to variable stress is based on the concept of strain hardening rule. The creep strain model is furthermore assumed to be identical in both tension and compression, but the creep is neglected at temperatures below 200°C.

The creep strain ε^{s}_{cr} is assumed to be dependent on the magnitude of stress and on the temperature-compensated time evaluated from the expression

$$\Theta = \int_0^t e^{-\frac{\Delta H}{RT}} dt \quad (h) \qquad 6.54$$

where

ΔH	- activation energy of creep	(J/mol)
R	- gas constant	(J/mol °Kelvin)
t	- time	(hours)

The relation between creep strain, ε^{s}_{cr}, and temperature-compensated time, Θ, at different stress levels illustrated in Fig 6.30

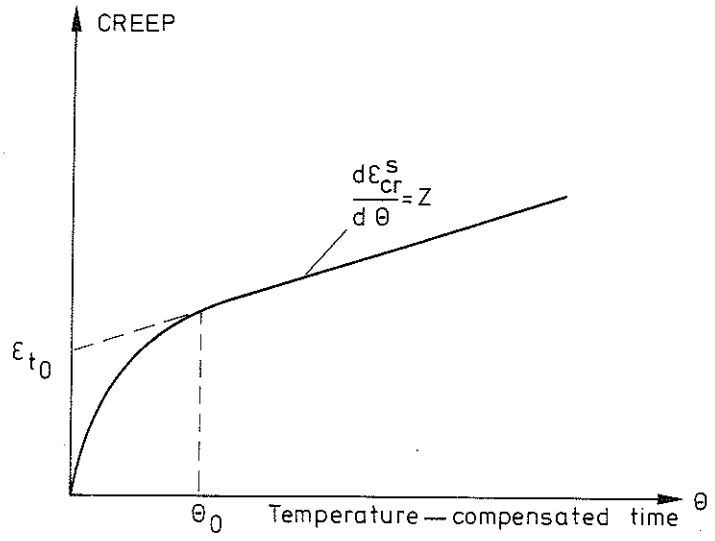

Figure 6.30 Principal creep curve for steel according to Dorn theory.

$$\Theta = \int_0^t e^{-\frac{\Delta H}{RT}} dt \quad (h)$$

is during the primary phase defined by a parabolic equation suggested by Plem (1975), which at Θ_o transfers to a linear slope into the secondary phase. The mathematical formulation for the creep strain at constant stress, where ε_{cr}^{s} in the continuation is replaced by ε_t, is

$$\left.\begin{aligned} \varepsilon_t &= \varepsilon_{to}\,(2\sqrt{\frac{Z\cdot\Theta}{\varepsilon_{to}}}) \qquad \text{when } 0 \leq \Theta < \Theta_o \\ \varepsilon_t &= \varepsilon_{to}\,(1 + \frac{Z\cdot\Theta}{\varepsilon_{to}}) \qquad \text{when } \Theta \geq \Theta_o \end{aligned}\right\} \qquad 6.55$$

where

$\Theta_o = \frac{\varepsilon_{to}}{Z}$; h

$Z = Z(\sigma)$ h^{-1}

$\varepsilon_{to} = \varepsilon_{to}(\sigma)$

Creep parameters necessary for the calculation are $\frac{\Delta H}{R}$, Z and ε_{to}, which are determined from conventional creep tests on the reinforcement steel Ks 40 (ϕ10). The following coefficients are derived for the actual steel (Krakau et al (1975)).

$$\frac{\Delta H}{R} = 45000^{o}K$$

$$Z(\sigma) = 140\cdot 10^{4}\cdot\sigma^{4.7} \qquad 0 \leq \sigma \leq 8 \text{ kPa}$$

$$Z(\sigma) = 258\cdot 10^{16}\cdot e^{0.00443\cdot\sigma} \qquad \sigma > 8 \text{ kPa}$$

$$\varepsilon_{to}(\sigma) = 2.62\cdot 10^{-6}\cdot\sigma^{1.0365}$$

The creep strain model formulated for varying temperatures at constant stress is extended to variable stress by using the strain hardening rule in a way analogous to that for concrete (cf. Fig 6.22).

Assume that at the temperature-compensated time Θ_i the accumulated creep strain is $\varepsilon_{t,i}(\Theta_i, \sigma_i)$.

The evaluation of the creep increment from Θ_i to Θ_{i+1} when the

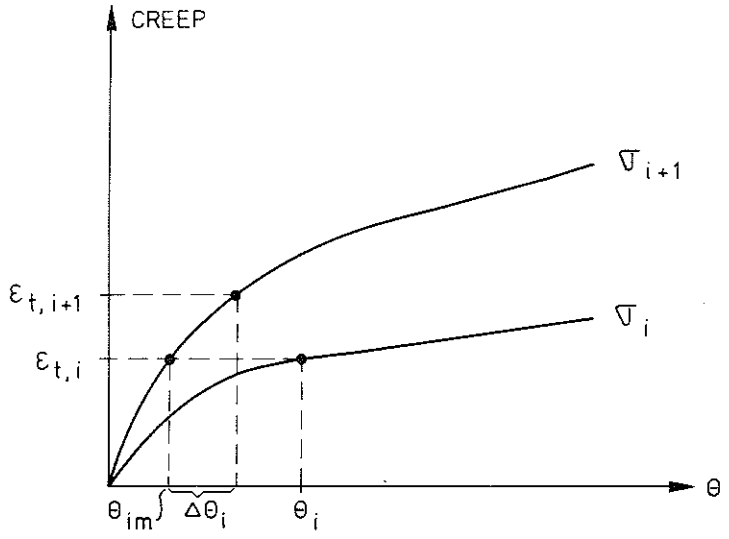

Figure 6.31 The principle of strain hardening rule applied on creep strain for steel.

stress is σ_{i+1} follows the principle shown in Fig 6.31. First we introduce the fictitious temperature-compensated time Θ_{im}, that would give the same creep $\varepsilon_{t,i}$ at the stress σ_i as at σ_{i+1}.

$$\left.\begin{aligned} \Theta_{im} &= \frac{\varepsilon_{t,i}^2}{4\varepsilon_{to}(\sigma_{i+1})\cdot Z(\sigma_{i+1})} && \text{if } \Theta_{im} < \Theta_o \\ \Theta_{im} &= \frac{\varepsilon_{t,i} - \varepsilon_{to}(\sigma_{i+1})}{Z(\sigma_{i+1})} && \text{if } \Theta_{im} \geq \Theta_o \end{aligned}\right\} \quad 6.56$$

At the temperature-compensated time $\Theta_{i+1} = \Theta_{im} + \Delta\Theta_i$ the incremental creep is calculated from

$$\left.\begin{aligned} \frac{d\varepsilon_t}{d\Theta} &= \frac{\varepsilon_t}{2\Theta} && 0 \leq \Theta < \Theta_o \\ \frac{d\varepsilon_t}{d\Theta} &= Z && \Theta_o \leq \Theta \end{aligned}\right\} \quad 6.57$$

which gives

$$\left.\begin{aligned} \Delta\varepsilon_{t,i} &= \frac{\Delta\Theta_i}{2\Theta_{im}}\,\varepsilon_{t,i} && 0 \leq \Theta \leq \Theta_o \\ \Delta\varepsilon_{t,i} &= \Delta\Theta_i \cdot Z && \Theta_o \leq \Theta \end{aligned}\right\} \quad 6.58$$

where

$$\Delta\Theta_i = e^{-\frac{\Delta H}{RT}} \cdot dt \qquad 6.59$$

The total strain yields

$$\varepsilon_{t,i+1} = \varepsilon_{t,i} + \Delta\varepsilon_{t,i} \qquad 6.60$$

6.2.3 Computer program calculating structural behaviour

A computer program evaluating the mechanical response to fire of reinforced concrete frames was published by Becker & Bresler within "Fire Research Group" at University of California, Berkeley in July 1974. This computer program named "FIRES-RC" and originally written for a CDC-6400 Computer is later reconstructed for use on a Univac 1108 Computer at Lund Computer Center. The FIRES-RC program is then further developed by the author and the current version can be considered as an extension and modification of the program originally constructed by the "Fire Research Group" at Berkeley. The recent research results on the mechanical behaviour of concrete at transient elevated temperature conditions presented in section 6.2.1 have been utilized and the new version of FIRES-RC is thus based on these new developments of material behaviour models. The transient thermal state during heating as well as during subsequent cooling phase used in the analysis is predicted by a separate temperature computer program (see section 6.1.2), used as input in the FIRES-RC program. As the original version of FIRES-RC is accounted for in detail in Becker & Bresler (1974), only a brief outline of the program will be given here.

In FIRES-RC a non-linear, direct stiffness method coupled with a time step integration is applied for the structural analysis. During the calculation procedure the boundary conditions as well as the external forces can be changed. The program is capable of providing a broad spectrum of response data including the time history of displacements, internal forces and moments, stresses and strains in concrete and in steel reinforcement. Furthermore, local cracking and crushing of concrete, which cause degradation in strength and stiffness, and yielding of the reinforcement are considered. The continually change and redistribution of forces and moments in a fire-exposed hyperstatic concrete structure is evaluated for each time-step by an iterative approach. This approach is used to find those incremental changes in the deformed shape of the structure, which are giving equilibrium between external and internal forces.

The equilibrium analysis is carried through under the assumption that secondary forces and moments are negligible. Thus, instability phenomena are not possible to solve with the current version of the program. The structure of the computer model, based on prismatic elements, furthermore limits the application to uniaxial stress states. Consequently, the influence of multiaxial stress components i.e. shear stresses are therefore disregarded. The support boundary conditions included in FIRES-RC, are idealized through the use of linear springs, which limits the potential use, i.e. the effect of a coupling between supports has to be neglected. Spalling of concrete cannot be modelled, due to the separation of the temperature and structural programs and due to the simplifying assumptions in the temperature computer program, as regards the moisture transport. This means that the cross-sections of the structure are presumed to be intact in the temperature calculations. Besides, no reliable analytical model exists at present, which describes the spalling phenomena in a functionally correct way.

The discretization of the geometry of the structure in the program is illustrated in principal in Fig. 6.11. The structure is divided into members (beams and columns), which in turn are substructured to a sequence of segments (maximum 6) per member. Each segment may have its own fire environment and is assumed in the calculation to be characterized by average values of the changes in the stress and deformation state. Furthermore, the cross-sections of the segments are subdivided into rectangular concrete and steel subslices (maximum 288 and 15, respectively). No slippage is allowed between adjacent subslices and initially plane cross-sections are presupposed to remain plane during the deformation of the structure.

Convergence problems may sometimes arise in the calculations, as described in the next section, although the time step is chosen as small as 0.025 h. This is probably due to the character of the iterative technique occasionally resulting in numeric instability. For faster convergence, it can be recommended to chose the start value of the incremental deformation at a new time-step calculation to 75% of that calculated at the previous time-step.

Table 6.3 Characteristics of the tests in the calculation schedule

Tests	Load level	Fire characteristics	Time step h	Time interval h
Group 1: A2:5 D2 D4 Bound.cond. (1)	P = 0 P = 1/2·P_{all} P = P_{all}	q = 251 MJ·m^{-2} $\frac{A\sqrt{H}}{A_t}$ = 0.08 $m^{1/2}$	0.025 0.05 0.10 0.20	0.0 - 0.5 0.5 - 1.0 1.0 - 2.3 2.3 - 3.2
Group 2: A2:3 D6 D8 Bound.cond. (1)	P = 0 P = 1/2 P_{all} P = P_{all}	q = 251 MJ·m^{-2} $\frac{A\sqrt{H}}{A_t}$ = 0.08 $m^{1/2}$	0.025 0.05 0.10 0.20	0.0 - 0.5 0.5 - 1.0 1.0 - 1.5 1.5 - 4.6
Group 3: A2:1 D11 Bound.cond. (1)	P = 0 P = 3/4 P_{all}	q = 251 MJ·m^{-2} $\frac{A\sqrt{H}}{A_t}$ = 0.01 $m^{1/2}$	0.05 0.10 0.20	0.0 - 0.5 0.5 - 2.0 2.0 - 5.0
Group 4: A1:12 D14 D16 Bound.cond. (1)	P = 0 P = 1/2 P_{all} P = P_{all}	q = 502 MJ·m^{-2} $\frac{A\sqrt{H}}{A_t}$ = 0.04 $m^{1/2}$	0.025 0.05 0.20	0.0 - 0.5 0.5 - 1.0 2.0 - 5.0
Group 5: A3:8 D18 D20 Bound.cond. (1)	P = 0 P = 1/2 P_{all} P = P_{all}	q = 502 MJ·m^{-2} $\frac{A\sqrt{H}}{A_t}$ = 0.08 $m^{1/2}$	0.01 0.02 0.05 0.10 0.20	0.0 - 0.1 0.1 - 0.32 0.5 - 1.0 1.0 - 3.0 3.0 - 3.6
Simply supported plate strip Bound.cond. (2)	P = 0	Dito group 4	Dito gr. 4	Dito gr. 4
Axially restrained simply supported plate strip Bound.cond. (3)	P = 0	"	"	"
Simultaneous rotational and axial restraint Bound.cond. (4)	P = 0 P = 1/2 P_{all}	" "	" "	" "

The amount of temperature data used as input in FIRES-RC is often very great. Therefore the temperature data is edited and stored on a file for a direct use in the program as well as material properties of concrete and steel. Furthermore, the program stores selected results on a file which later is directly plotted.

6.2.4 Calculations - comparisons with test results

The calculations accounted for in this section embrace a theoretical study of the structural behaviour of unilaterally fire-exposed plate strips in one span during a complete fire process, including the cooling phase. The following combinations of boundary conditions of the plate strips are studied:

(1) Hyperstatic plate strips, characterized by a complete rotational restraint at both ends and a free axial movement.

(2) Isostatic, simply supported plate strips.

(3) Hyperstatic plate strips, simply supported at both ends but restrained against axial movement

(4) Hyperstatic plate strips, restrained against rotation as well as axial movement at both ends.

The check of validity of the calculations is mainly related to five different groups of experimental tests having boundary conditions of type (1). These tests are chosen from the test series A1, A2, A3 and D according to Table 6.3, cf. also Table 4.4 and section 5.2. Each group of tests is characterized by its own fire exposure, specified in conformity with Fig. 4.2, and by various levels of concentrated lateral loads. Furthermore, a validity control is made also for a fire-exposed simply supported plate strip, boundary condition type (2), without any external load. The effect on the evaluated bending moment and deflections of a possible displacement of the longitudinal reinforcing bars is looked upon. Also the significance is demonstrated of using an adequate material behaviour model of concrete at transient elevated temperatures. The time-variation of the bending stiffness for a nil-loaded plate strip with boundary condition of type (1) is illustrated and checked against measurements.

As a complement to the validity control calculations described above the influence of an axial restraint of the plate strip is investigated theoretically [boundary conditions of type (3) and (4)], see Table 6.3.

The evaluation of the structural response is carried out by the computer program FIRES-RC, modified and extended as described in section 6.2.3. Results over time-history of bending restraint moment and deflections are analysed and compared with measurements. Examples of calculated strain and stress distributions over the cross-sections of the plate strip at selected times are presented.

6.2.4.1 Discretization

The fire exposure is divided into four fire zones (A, B, C and D) for each half of the plate strip, as shown in Fig. 6.11a, making use of the symmetry in the structural design of the plate strip, loading and fire exposure. Thus, only half the strip is studied and the discretization in the main calculations is chosen to 5 segments.

Segments 1 and 2 are located in the fire zone A, where segment 1 is only 0.025 m, and the position of the other three segments (3, 4 and 5) coincide with the fire zones B, C and D, respectively. Segment 1 is used for evaluating the stress and deformation state close to the support where yielding ordinarily starts, due to the rotational restraint and where consequently, a thin segment is required for getting an accurately calculated moment distribution. The concentrated load P is placed at the internal node between the segments 4 and 5. For comparisons, calculations have been carried out for the actual plate strip subdivided into 7 segments and with the same model of fire zones, but these calculations indicated that any noticeably improved accuracy could not be reached.

In the main calculations, the cross-section is divided into 7 concrete subslices and 2 steel subslices (bottom and top reinforcing bars), which is illustrated in Fig. 6.11b. The subslices are rectangular and cover the whole width of the plate strip which

is justified as the heat flow can be assumed one-dimensional. In order to make control calculations and to verify the chosen division as appropriate, alternatively 11 concrete and 2 steel subslices as indicated in Fig. 6.11c, were used. This control proved that the subdivision, chosen for the main calculations, was quite sufficient in this application.

Table 6.3 indicates the time discretization for the different calculations. For a very rapid increase in temperature, i.e. at the opening factor 0.08 $m^{1/2}$, the time step is as minimum chosen to 0.01 hours during the first time interval and then successively increased to 0.2 hours during the last time interval of the cooling phase. Although the time-step is that small, convergence problems may sometimes arise.

6.2.4.2 Validity of calculations

a) Main tests

Great restraint forces and moments, which continuously change, are very complex and important behaviour characteristics of fire-exposed hyperstatic concrete structures. For the actual structure of the main tests, the time variation of the bending restraint moment was calculated and is presented in Fig. 6.32 - 6.36, together with the midpoint deflections, for the tests belonging to the five groups, accounted for in Table 6.3. In the figures, the initial deflections caused by the load application at room temperature then are excluded, but these are reported in Table 5.3.

In Fig. 6.32 - 6.35, the calculated results from the respective group 1, 2, 3 and 5 are shown, where dashed curves refer to the calculations while full-line curves indicate the measurements. The measured curve of restraint moment represents the mean value of the measurements at two supports. Any possible unsymmetrical fire-exposure in the tests is not modelled in the calculations. A pervading feature of these calculated restraint moment curves is the somewhat slower rise during heating and greater maximum values, which furthermore are attained later than observed in

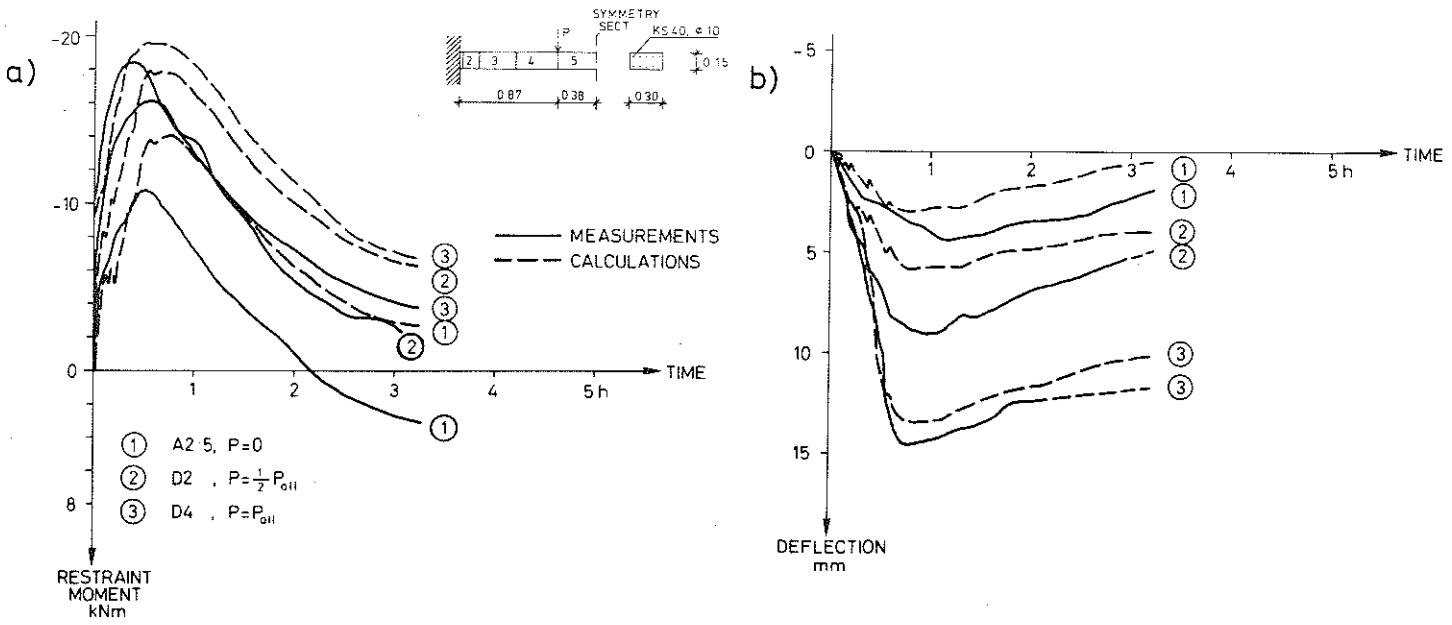

Figure 6.32 Time history of
a) bending restraint moment and
b) midpoint deflection
Fire process characteristics $q = 251\ MJ \cdot m^{-2}$,
$A\sqrt{H}/A_t = 0.08\ m^{1/2}$

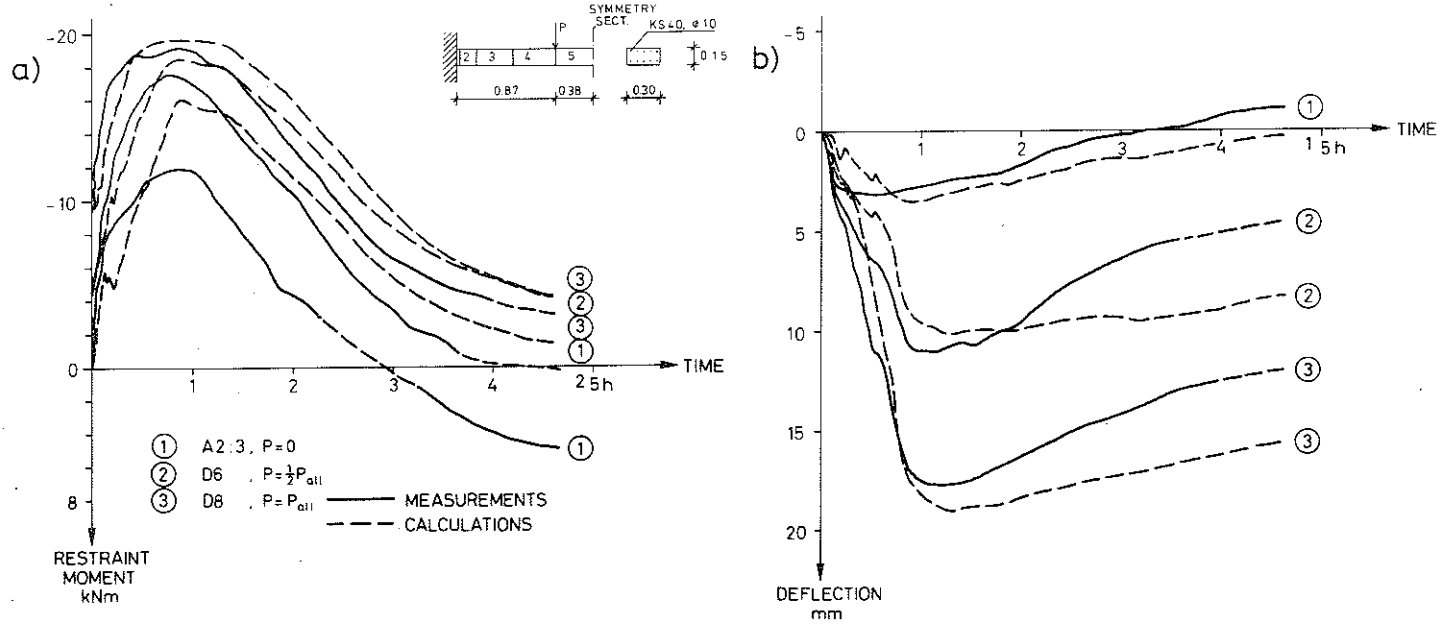

Figure 6.33 Time history of
a) bending restraint moment and
b) midpoint deflection
Fire process characteristics $q = 251\ MJ \cdot m^{-2}$,
$A\sqrt{H}/A_t = 0.04\ m^{1/2}$.

the experiments. During cooling the decline consequently comes later. In all nil-loaded tests, the cracking moment attained at the support sections can be observed at about 5 kNm as an interruption in the curve. In the tests A2:5 (Fig. 6.32) and A2:3 (Fig. 6.33), the maximum moment differs quite a lot in comparison with the measured value. The cause of this deviation is here solely due to the fire-exposure, nonuniform in longitudinal direction and stepwise divided into 4 fire zones in the calculations. This discretization may disturb the agreement. The accuracy in modelling the fire-exposure also ought to be more sensitive for the nil-loaded than for the loaded plate strips and therefore we cannot expect that good accordance between calculations and measurements. The observed tendency in somewhat higher restraint maximum moments in the calculations than in the tests can be a consequence of a possible deviation at the casting, from the prescribed placing of the reinforcement bars, primarily the top bars. This will be more thoroughly discussed further on in this section. Furthermore the scatter in the yielding stress of the reinforcement may give an influence. The yielding moment at a correct placement of the reinforcing bars is determined to 19.8 kNm for a cross-section of the strip, negligibly affected by heating. This is approximately valid for the support sections, when the heating period does not exceed about 2 hours. During cooling the less agreement may partly be reflected in the constitutive law of concrete as more roughly estimated material properties are used for the cooling phase. As was emphasized in section 5 the difference in measured restraint moment in two identically defined experiments may reach 10%. In view of this fact the calculated results are quite satisfactory.

The development of midpoint deflections in the tests referred to are also illustrated in Fig. 6.32 - 6.35. The calculated deflection curves, in which the contribution of the shear forces is neglected, verify a good concordance with the measurements for various fire environments and different load levels during heating as well as during the subsequent cooling phase. As found in the experimental investigation, the dispersion in the measured deflection may reach 20 - 30% for identically defined tests, which must be born in mind at these comparisons.

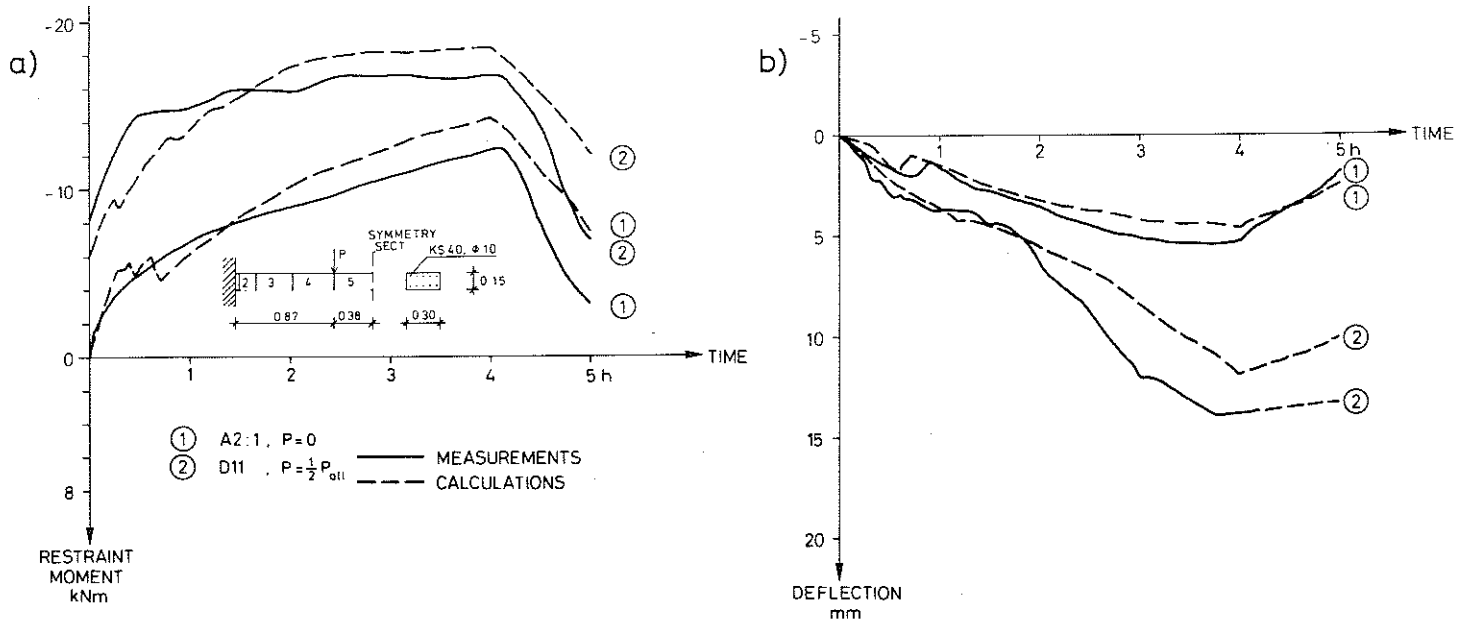

Figure 6.34 Time history of
a) bending restraint moment and
b) midpoint deflection
Fire process characteristics $q = 251\ MJ \cdot m^{-2}$,
$A\sqrt{H}/A_t = 0.01\ m^{1/2}$.

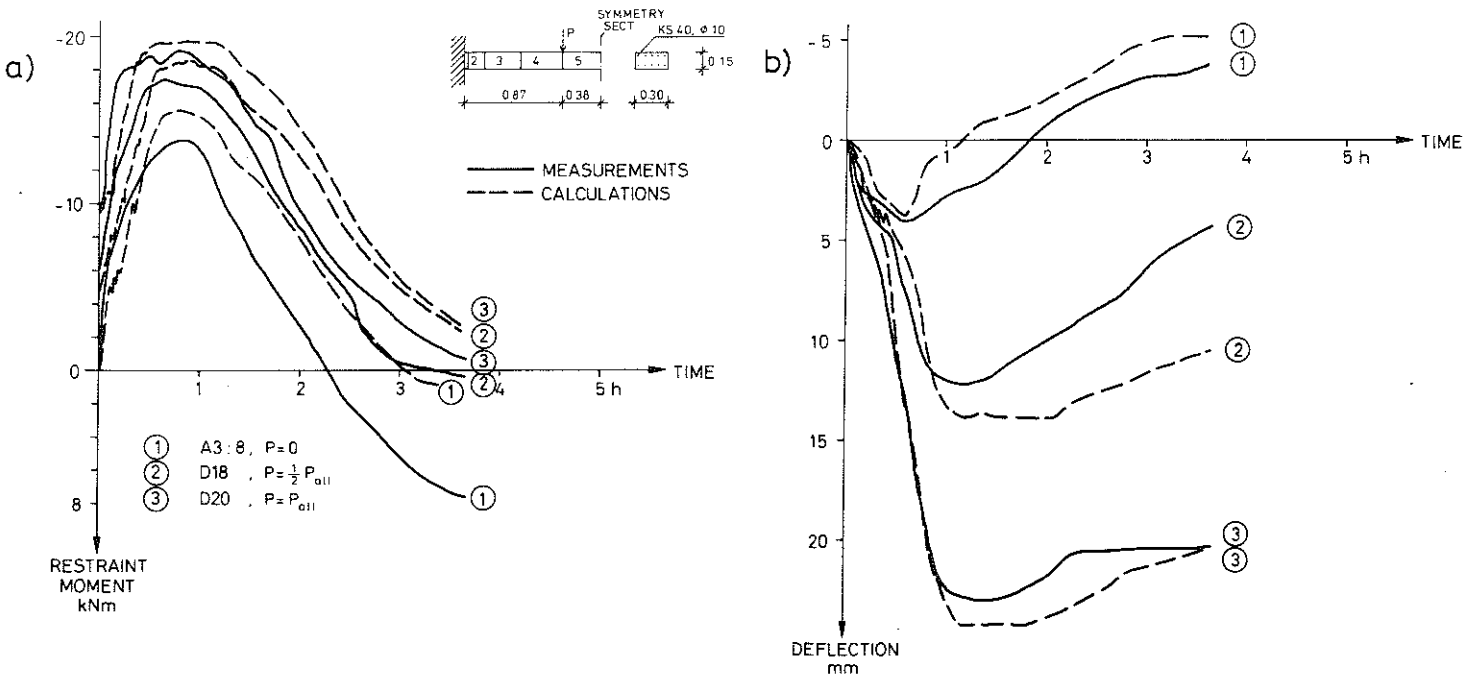

Figure 6.35 Time history of
a) bending restraint moment and
b) midpoint deflection
Fire process characteristics $q = 502\ MJ \cdot m^{-2}$,
$A\sqrt{H}/A_t = 0.08\ m^{1/2}$.

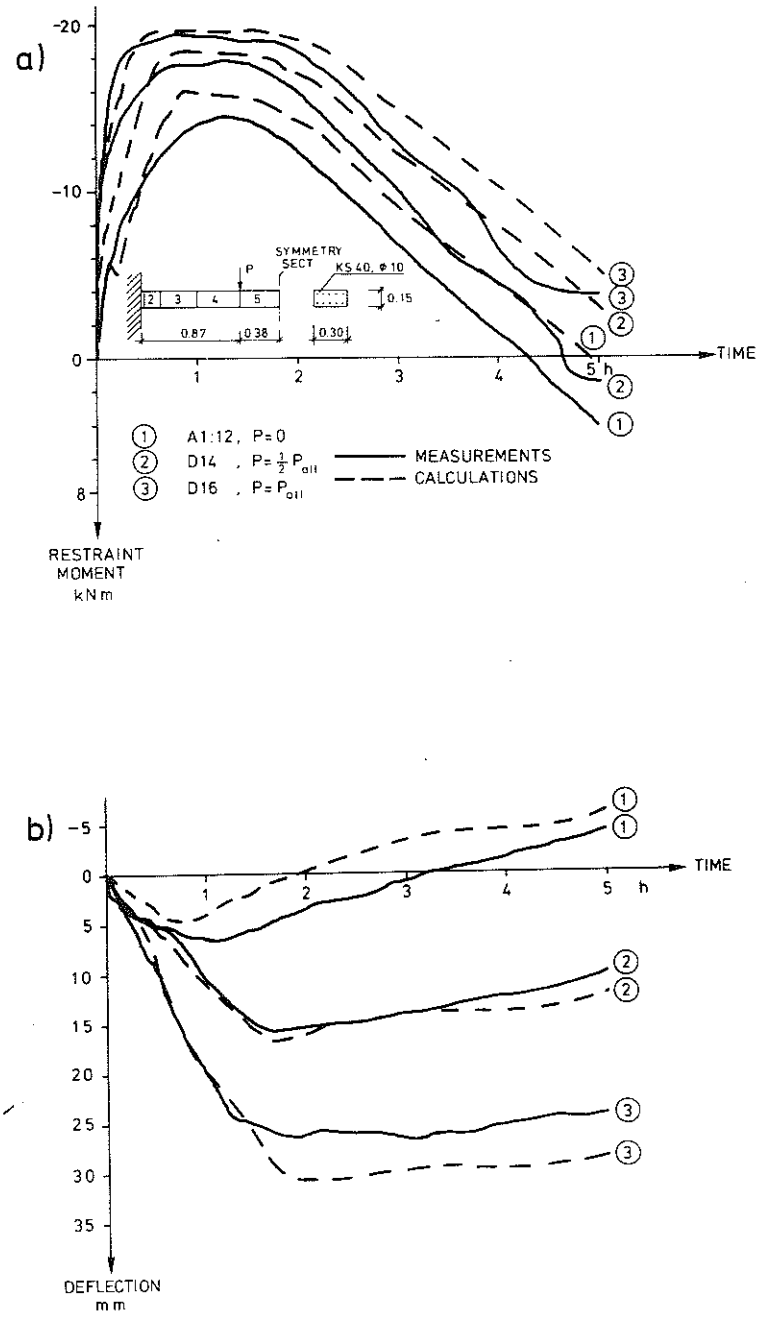

Figure 6.36 Time history of
a) bending restraint moment and
b) midpoint deflection
Fire process characteristics $q = 502\ MJ \cdot m^{-2}$, $A\sqrt{H}/A_t = 0.04\ m^{1/2}$.

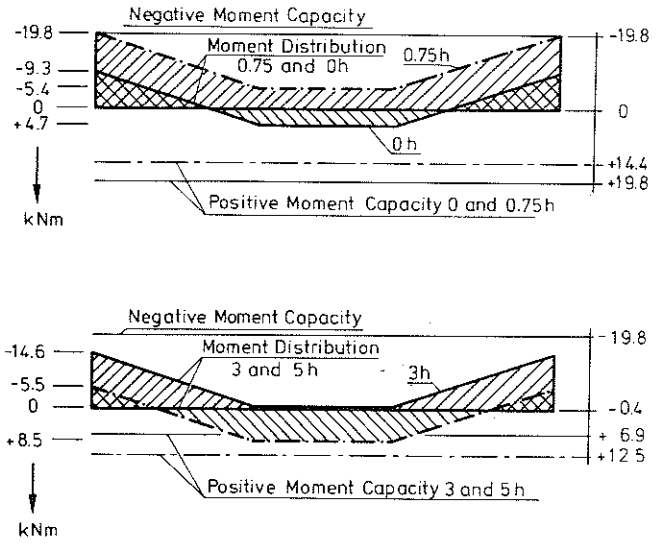

Figure 6.37 Calculated bending moment distribution and bending moment capacity for the test D16.

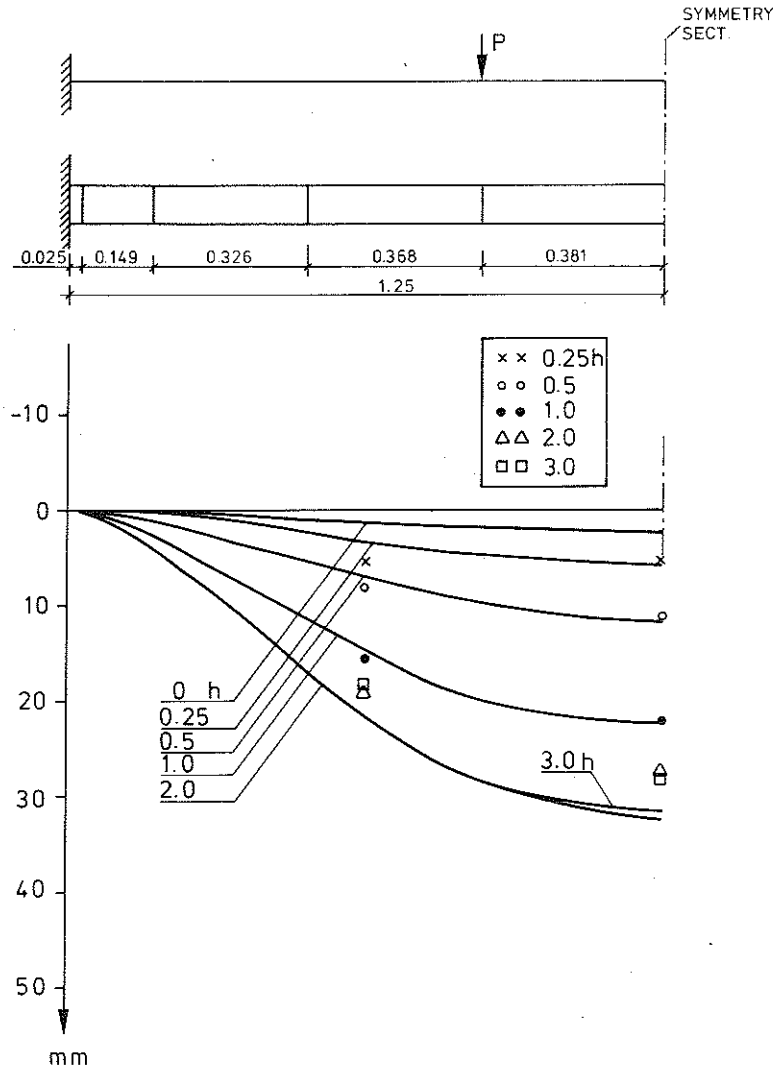

Figure 6.38 Deflection curve at different times of the plate strip D16. Measured values are also indicated.

The tests D13 - 16 and A1:12 belonging to group 4 and not yet illustrated are exemplified in the calculations for the three load levels P = 0, P = 1/2 P_{all} and P = P_{all} (Fig. 6.36). The fire exposure has a duration of the heating period of about 2 hours, a fire load density of 502 $MJ \cdot m^{-2}$ and an opening factor of 0.04 $m^{1/2}$. The agreement in these tests between the calculated and measured values is extraordinary good for the restraint bending moment as well as for the deflections during the whole fire process, including cooling, at all load levels. The structural behaviour is further illustrated for the test D16 in Fig. 6.37, giving the calculated moment distribution along the plate strip at different times and corresponds to Fig. 5.21, based on test results. Fig. 6.38 is showing the calculated deflection curve and measured deflections in midpoint and 1/4-point sections at corresponding times.

Calculated stress and strain distribution

A more detailed analysis of the structural response to fire will now be presented for the tests A1:12 and D16 in terms of calculated strain and stress distribution over the cross-sections at the support and for the segment 5. This illustration comprises the distribution of all strain components which together constitute the evaluated behaviour, viz. thermal strain (ε^c_{th}), transient strain (ε^c_{tr}), creep strain (ε^c_{cr}), instantaneous stress-related strain (ε^c_σ) and finally the total strain (ε^c) at selected times, as well as the resulting stress distribution for the concrete and steel subslices. In the calculations, a mean value of the current strain and stress is used for each subslice and therefore the distributions are drawn in a stepwise way.

For the test conditions A1:12, the state of strain and stress in the cross-sections of the segments 1 and 5 is illustrated in Fig. 6.39, at five different times (0.5, 1, 2, 3 and 4 hours). In the figures the total strain distribution is also indicated as a dashed line giving the curvature of the section.

Cracking occurs in a subslice at a tensile strain of 0.4 % and this happens after 0.125 hours at the support section and after

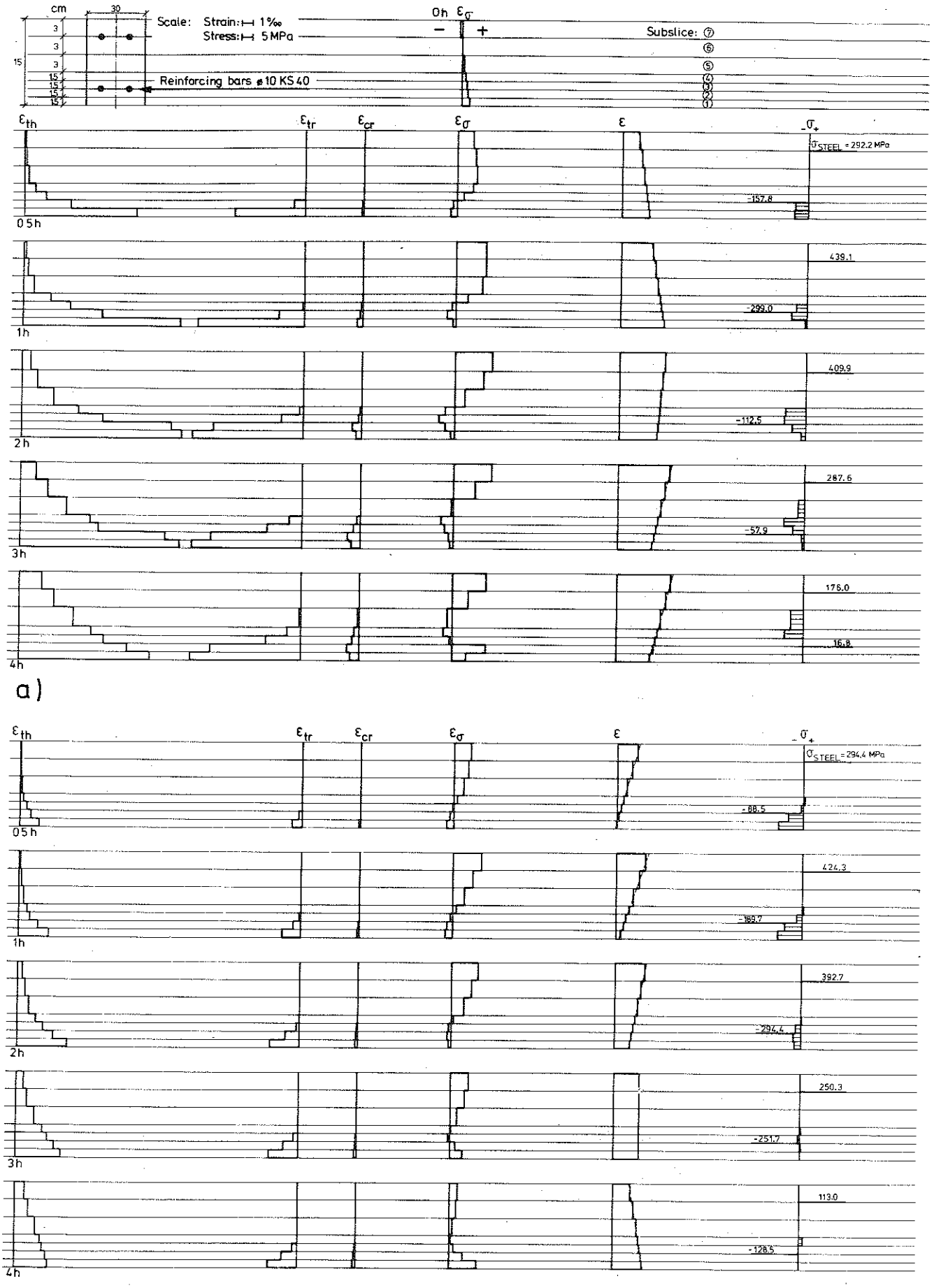

Figure 6.39 Cross-sectional strain and stress distribution of the plate strip A1:12 at different times.
a) segment 1 b) segment 5

ε_{th} - thermal strain ε_{σ} - stress-related strain

ε_{tr} - transient strain ε - total strain

ε_{cr} - creep strain σ - stress

Index c is omitted.

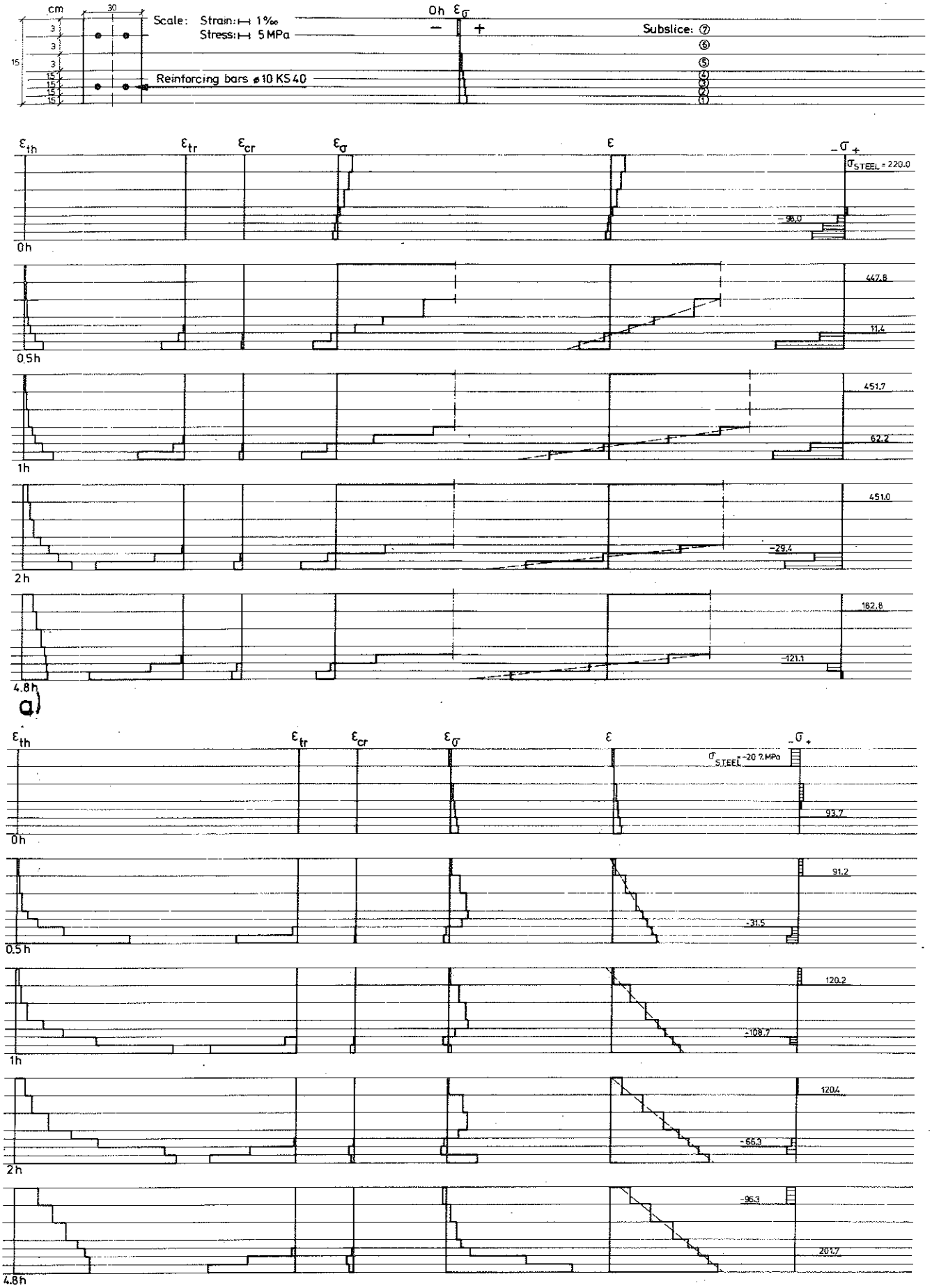

Figure 6.40 Cross-sectional strain and stress distribution of the plate strip D16 at different times.
a) segment 1 b) segment 5
Strain components, see Fig. 6.39.

0.175 hours at the section of the segment 5 in this calculation. At about the latter time, water was observed to penetrate up to the upper surface at the mid-section in the test, thus confirming the calculation. In the figures the total strain distribution is also indicated as a dashed line giving the curvature of the section.

Due to the imposed thermal gradient, excessive thermal strains, which successively in considerable extent are compensated by the transient strain (mainly) and the creep strain, are developing in portions close to the fire-exposed surface. This is mostly accentuated in the cross-section of segment 5, having a stronger fire exposure. Severe degradation due to cracking rapidly takes place in both sections illustrated and consequently the bottom as well as the top reinforcing bars and their thermal behaviour signify a dominating effect on the structural response of the plate strip. This typical behaviour is more emphasized during cooling and stresses are still more concentrated to the reinforcing bars. The slope of the total strain distribution indicates that the curvature is increasing during the first hour in both sections and then it starts to decrease, most rapidly in the midsection where it changes the sign already after 1.5 hours.

Simultaneously, a significant redistribution of the stresses takes place, which is particularly accentuated during cooling, when even previously cracked subslices (mid-section) transfer into compression. A cracking degradation of about 90% is attained at the support section 1 after 3.4 hours. Firstly after 3 hours, the curvature is zero at the end-section but the restraint moment is far from being zero. This is owing to the fact that considerable residual strains exist and a complex unloading process develops in the cross-section. The behaviour model can only describe this process very roughly and this may exert an influence on the calculated structural behaviour, especially during cooling, which is unsufficiently explored.

The additional effect of a simultaneous lateral load $P = P_{all}$ on the detailed behaviour is given in a similar way for the fire-exposed plate strip D16 in Fig. 6.40, showing the strain and stress

distribution for the end-section and the mid-section at the times 0, 0.5, 1.0, 3.4 and 4.8 hours. Due to the external load, the total restraint moment very quickly (after 2/3 hours according to Fig. 6.40a) reaches the yielding moment on the supports. After that, considerable rotations develop and consequently high compressive stresses as shown in Fig. 6.40a Furthermore, the curvature, observed from calculation sheets, reaches the value -0.45 m^{-1} after about 2 hours, and is then kept almost constant during cooling. For the mid-section, illustrated in Fig. 6.40b, the behaviour in principal is found similar to that for the nil-loaded plate strips previously discussed.

b) Test on simply supported plate strip

As a complementary validity control of the theoretical model, comparative studies also have been made for a simply supported and nil-loaded plate strip, boundary condition of type (2). This plate strip is tested for a fire exposure having a duration of the heating phase of about 2 hours, a fire load density of 502 $MJ \cdot m^{-2}$ and opening factor of 0.04 $m^{1/2}$. The temperature calculation is the same as that used for group 4. The evaluation of the mechanical response of this type of structure, solely exposed to transient high temperatures, coincides extremely good with the measured behaviour for the mid-point deflection, which is illustrated in Fig. 6.41.

Influence of unintended displacement of the longitudinal reinforcement

As mentioned previously, an unintended displacement of the longitudinal reinforcement at the casting of the plate strips may be one cause of the observed tendency in somewhat higher restraint maximum moments in the calculations than in the tests. Consequently a numerical study of this influence has been carried out. The study is based on an assumed lowering of the top reinforcement of 5 mm along the whole plate strip. Such a deviation from a prescribed position is inevitable in many practical cases, why its influ-

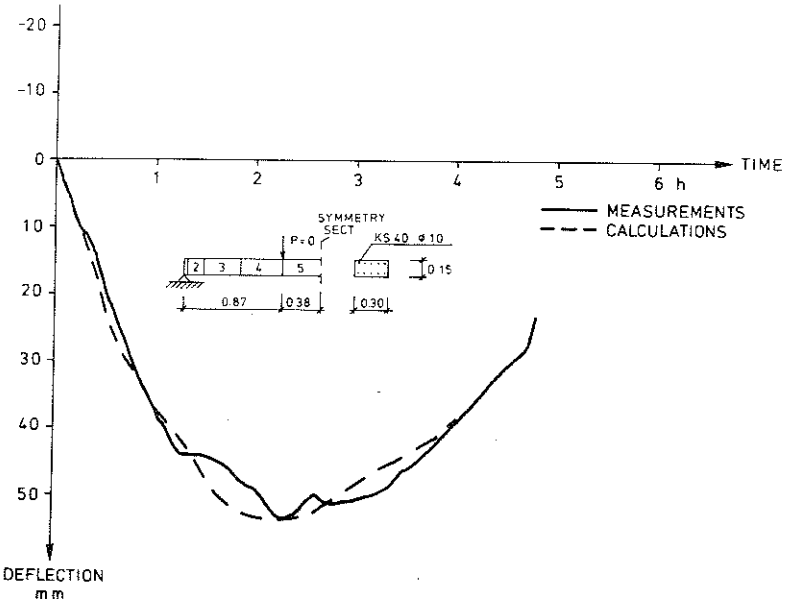

Figure 6.41 Deflection curve of simply supported and solely fire-exposed plate strip.
Fire process characteristics $q = 502\ MJ \cdot m^{-2}$, $A\sqrt{H}/A_t = 0.04\ m^{1/2}$.

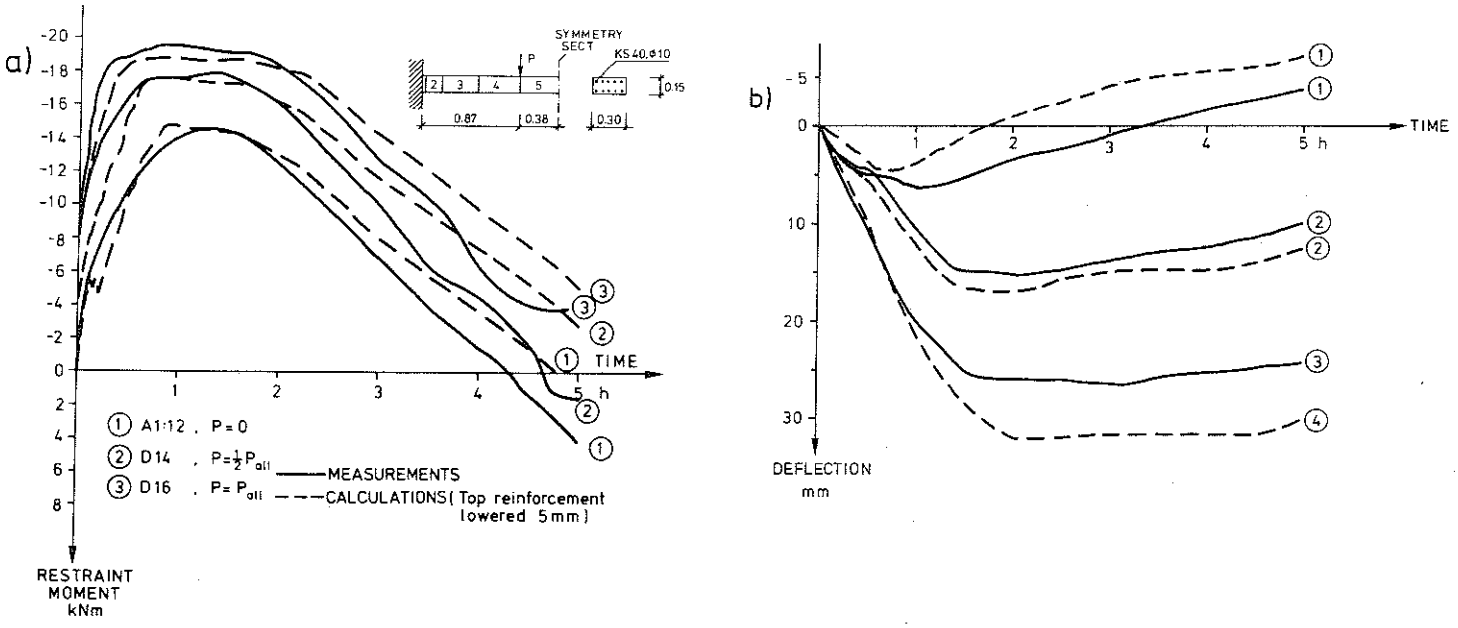

Figure 6.42 The influence of unintended displacement of top reinforcement on
a) bending restraint moment and
b) midpoint deflection
for the tests A1:12, D14 and D16, cf. Fig. 6.36.

ence on the fire behaviour is of great interest. The result of the calculations are illustrated in Fig. 6.42, which indicates a decrease in the maximum restraint moment of about 1 kNm and accordingly an increase in mid-point deflections of maximum 1 - 2 mm. The results, referring to the tests of group 4, also indicate an improved agreement between the measured and calculated support moments, cf. Fig. 6.36a.

The dimension of the plate strip and the real position of the reinforcing bars have been checked at the support-sections and the mid-section on a plate strip, arbitrarily selected. The total area of these three cross-sections was found on an average to be 1.5% less than prescribed and the top as well as the bottom reinforcement was pervadingly placed too low. On an average the displacement amounted to 6.5 and 1 mm, respectively. Deviations of this magnitude from the theoretical cross-section are probably a pervading feature of most plate strips. If the calculations, presented here, had been corrected for an unintended displacement of the reinforcement, primarily the top reinforcement, the evaluated curves of bending restraint moments and deflections would probably have been a little more close to the measured ones.

Influence of varying material behaviour models

In order to illustrate the significance of using an adequate material behaviour model of concrete at transient temperature conditions, further computations were done for the test conditions A1:12 and D14. In a comparative study then the very important strain component in the constitutive law of concrete, viz. the transient strain, was disregarded in the calculations, giving results as reported in Fig. 6.43. As this strain component is of vital importance for the deformability of concrete, the bending restraint moment will therefore increase considerably for both the nil-loaded and the loaded structure. The deflection curve will also deviate considerably from that calculated by applying a more correct material behaviour model. In connection to these comparative calculations it may be noted that a traditional use of an incomplete material behaviour model, not taking into account the transient strain, often gives

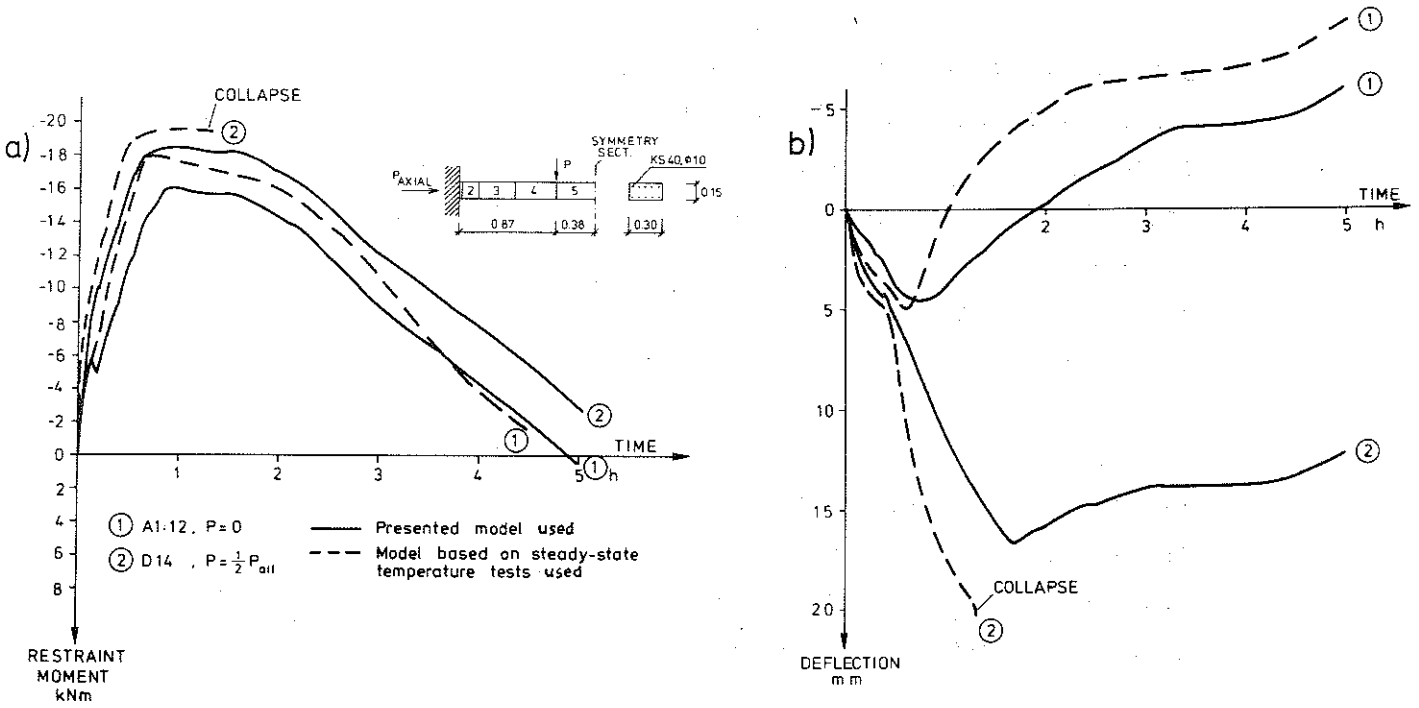

Figure 6.43 Influence of varying material behaviour models on
a) bending restraint moment
b) midpoint deflection.

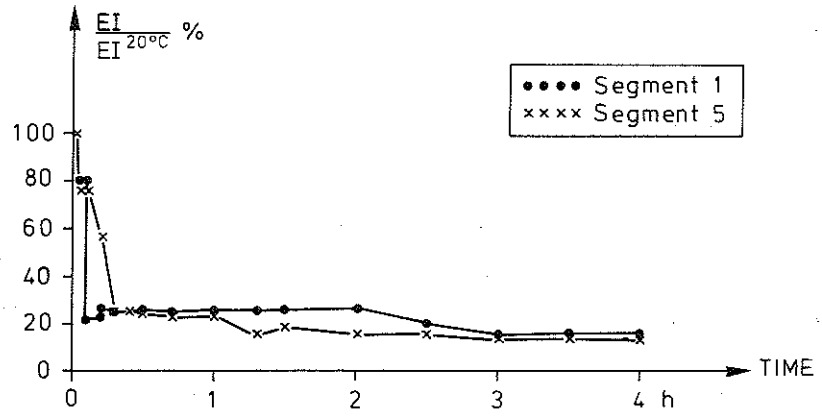

Figure 6.44 Calculated flexural stiffness during fire of the nil-loaded plate strip A2:3.

rise to difficulties to find the equilibrium state, resulting in no convergence and for the loaded strip D14 even in collapse after 1.3 hours. This collapse is due to crushing of concrete in the compressive zone at the support sections. In this calculation, also some subslices very quickly were exposed to strains which lie on the descending branch of the stress-strain diagram of the concrete on the compression side. These results show very obiously how drastically an incomplete material model law can destroy the calculations carried through by computer programs which in themselves can be very advanced and sophisticated. In general, it can be stated that if the material behaviour model is not based on transient temperature conditions when evaluating the mechanical response to fire, every type of restraint gives unrealistic great restraint forces and moments, however limited by the yielding moment. Furthermore, in such calculations the deflections are normally far from reality.

Flexural stiffness

In the experimental investigation, the flexural stiffness of nil-loaded plate strips during fire was determined by a repeated procedure of an instantaneous application of a small transverse load. However, the intention only was to illustrate the principal change in the stiffness. For comparison, the flexural stiffness was calculated as a function of time in segment 1 and 5 for which the test A2:3 is illustrated in Fig. 6.44. As can be observed from the figure, there is a rapid drop in stiffness during the first 6 minutes in both cross-sections and later on the stiffness continuously decreases to 15 and 14% for the sections of segment 1 and 5, respectively. If this figure is compared with the corresponding measurements, presented in Fig. 5.20, we notice that the principal decrease in stiffness well follows the calculated decrease but the values are somewhat too high. Regarding that the uncertainty is very great in the experimental procedure for determining the flexural stiffness from additional deflections, the agreement between measured and calculated values is satisfactory.

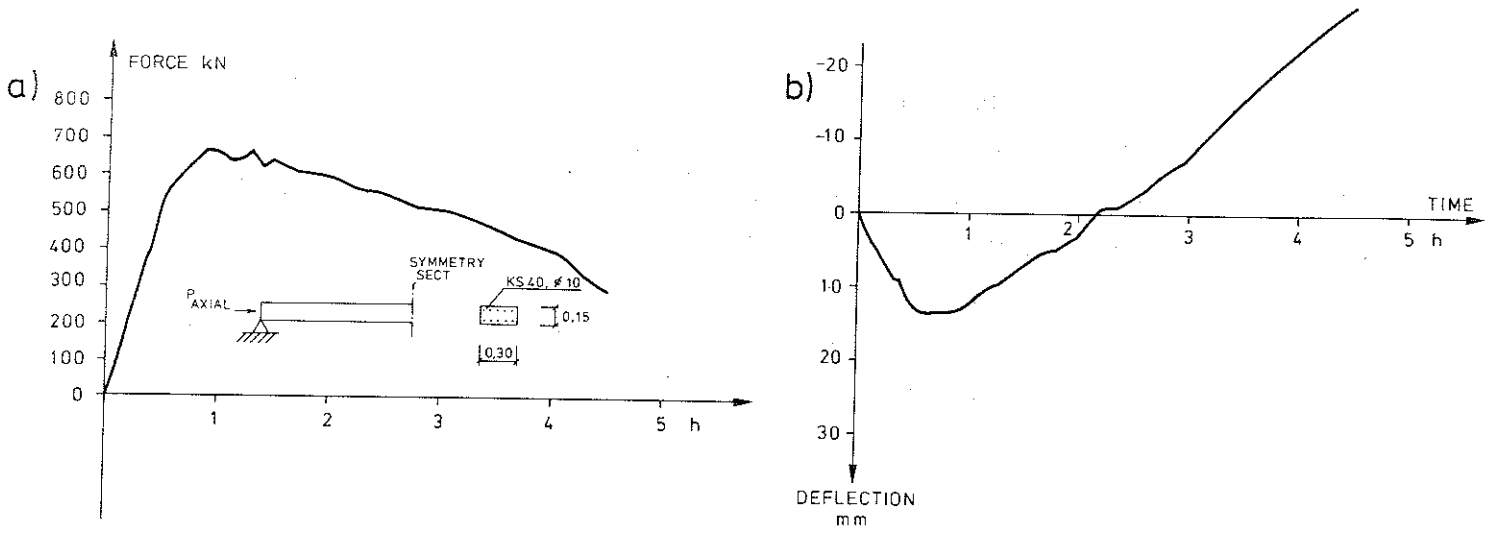

Figure 6.45 Structural behaviour of a simply supported and nil-loaded plate strip restrained against axial movement
a) thermal axial force
b) midpoint deflection.
Fire process characteristics in accordance with Fig. 6.41.

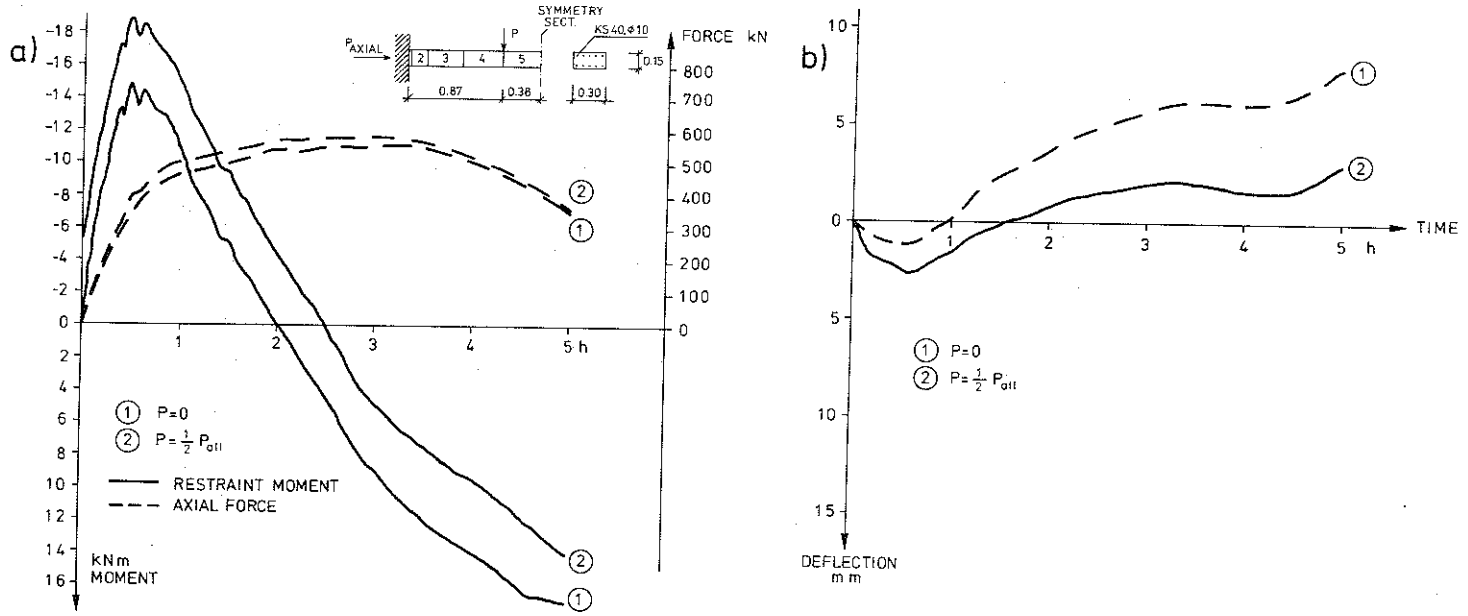

Figure 6.46 Structural behaviour of a nil-loaded and loaded plate strip restrained against rotation as well as longitudinal movement at both ends
a) bending restraint moment and axial force
b) midpoint deflection.
Fire process characteristics $q = 502\ MJ \cdot m^{-2}$, $A\sqrt{H}/A_t = 0.04\ m^{1/2}$.

6.2.4.3 Further calculations

For a complemetary illustration of the structural behaviour of a fire-exposed, hyperstatic plate strip, calculations were carried out for on one hand a simply supported, axially restrained plate strip, boundary condition (3), on the other hand a plate strip with a rotational as well as an axial restraint on both supports, boundary condition (4), see Table 6.3.

The structural behaviour of the fire-exposed, simply supported plate strip, axially restrained and without any external load, is shown in Fig. 6.45 in terms of the axial restraint force and the mid-section deflection. The fire-exposure is identical to that of group 4, which enables direct comparisons to the simply supported plate strip, studied above and illustrated in Fig. 6.41. The additional effect of an axial restraint results in a quite different behaviour of the strip. A considerable axial force due to the imposed thermal deformation arises and increases to a maximum value of 660 kN after about 1 hour. This axial force can be compared with the ultimate force of the cross-section at ambient conditions, viz. 1.440 kN. Consequently, the deformation process is quite different and after reaching the maximum deflection value it starts to decrease considerably in pace with the axial force and passes later on to an upwards deflection. This behaviour is mainly due to the decreasing load-carrying capacity in portions near the fire-exposed surface of the plate strip.

In order to illustrate how an axial restraint added to the rotational restraint on a fire-exposed plate strip changes the structural behaviour in terms of bending restraint moment, axial force and mid-point deflection, two complementary calculations are presented. The tests A1:12 ($P = 0$) and D14 ($P = 1/2\ P_{all}$), supplemented with an axial restraint, are analyzed and the results can be studied in Fig. 6.46. The calculated time-history of the restraint moment for the two tests are in conformity with each other and the difference between the curves is approximately the same as the initial value due to the lateral load in test

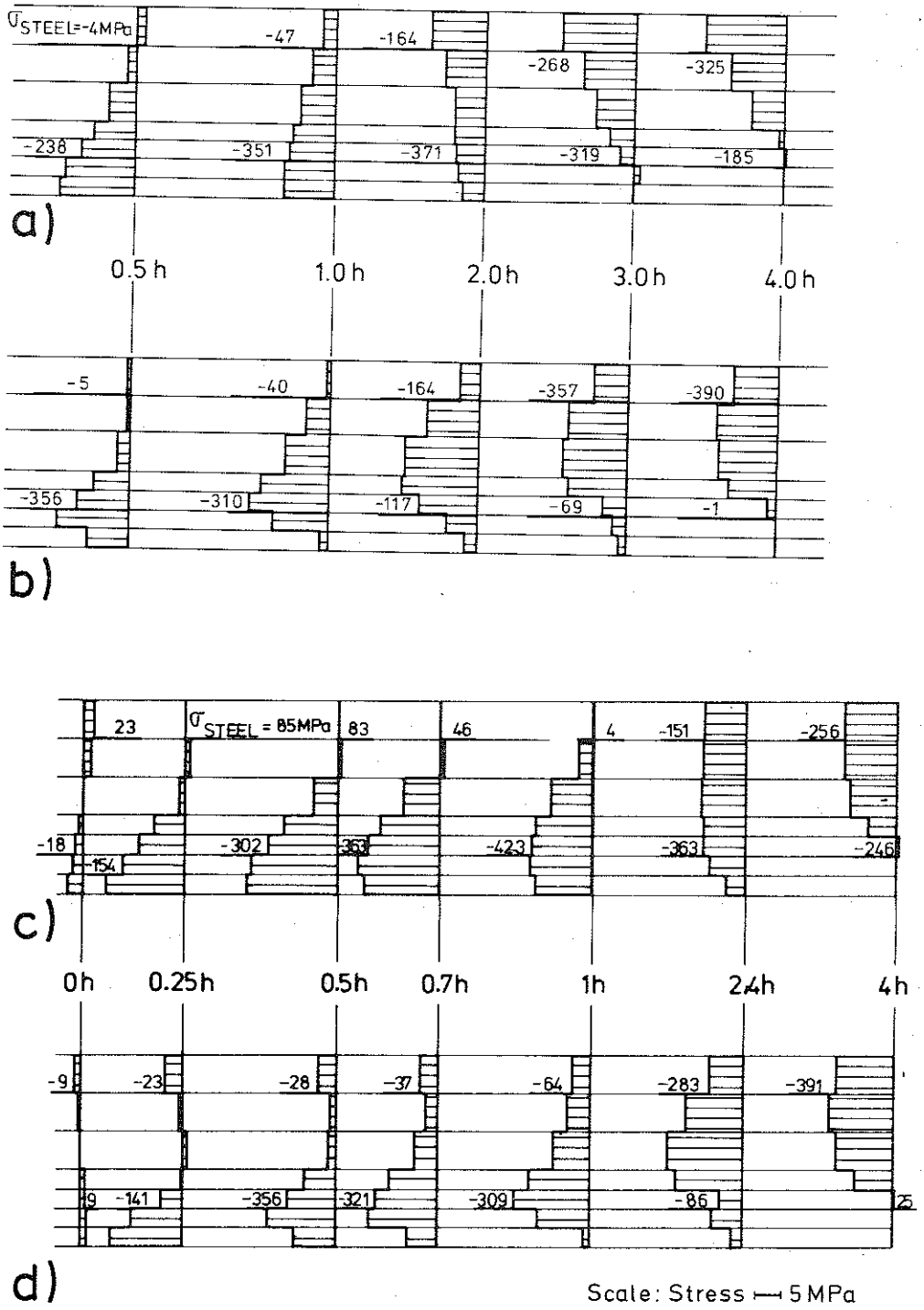

Figure 6.47 Cross-sectional stress distribution of plate strips accounted for in Fig. 6.46.
a) Section 1, P = 0
b) Section 5, P = 0
c) Section 1, P = 1/2 P_{all}
d) Section 5, P = 1/2 P_{all}

D14. After a rapid increase in the moment, the maximum value is attained after o.5 hours, which then is followed by a descending branch which reaches great positive values. It may be noted that for the nil-loaded case a positive moment of 18.5 kNm is attained after 5 hours, which can be compared with 14 kNm for the loaded strip. This drastic change in restraint moment compared with what was observed for the original tests A1:12 and D14 - cf. Fig. 6.36a - is a result of the axial restraint. As the figure shows the development of the axial force is very alike for the two tests and in some degree also the deflection curve which indicates an approximate independence of the external load. For the restraint moment, it seems to be justified to treat the thermal restraint forces and moments separated from those caused by the external load, if the yielding state is not attained. The sum of these components of restraint forces and moments is approximately equal to the total forces and moments of the structure at fire. The axial force amounts to about 560 kN as maximum, or 39% of ultimate compressive load at ambient conditions. The mid-point deflection is very small in comparison with that attained in the original tests A1:12 and D14, which again is a consequence of the axial restraint. The nil-loaded strip attains a somewhat more accentuated upwards deflection during cooling than the loaded one owing to the load.

The changed mode of behaviour excessed by the additional axial restraint can be further analyzed from the time variation of the stress distribution at different cross-sections of the plate strip. This is illustrated in Fig. 6.47 for the end- and mid-section of the plate strip for the tests A1:12 and D14, supplemented with an axial restraint. The rapid decrease of the restraint moment, after attained maximum value illustrated in Fig. 6.46 is due to excessive transient strains which compensate the thermal strains and the decrease in compressive strength above 400^{o}C for concrete subslices close to the fire-exposed surface. This is verified by the figure showing an almost complete unloading of the subslice (1) in the mid-section of the nil-loaded as well as the loaded plate strip after 0.7 - 1

hours. The ability of the cross-section to redistribute stresses is apparent from the figure.

The structural behaviour at fire of hyperstatic plate strips, theoretically predicted above, comprises several differentiated fire processes, including cooling, and different loading levels and restraint conditions. The theoretical results seem to coincide sufficiently well to the observed behaviour in tests for an arbitrary case, so the computer model can be considered to be fully validated. The computer model opens improved possibilities to a better understanding of the principal fire behaviour of different types of reinforced concrete structures and will then, hopefully be a valuable tool in further studies within the research field.

6.2.5 Restraint forces and moments - influence on load-carrying capacity

Restraint forces and moments in hyperstatic concrete structures at fire cause excessive compressive strains in different portions of the cross-sections due to steep temperature gradients. It is therefore of vital importance to know if the deformability of concrete at elevated temperatures is sufficient so that the cross-section can be fully utilized before the crushing strain is reached in any portion of the cross-section. Fundamental questions are: Can the limit state approach be used when evaluating the load carrying capacity at fire exposure? Are the stresses sufficiently redistributed before the collapse occurs, for making the stress distribution in the limit state independent of the imposed thermal strains?

For continuous beams, which are the main subject for the present study, a limit state approach requires that the rotational capacity of the structure is greater than the need of rotation. This means that a complete moment redistribution and a reduction to zero of the thermally induced moments is enabled in all plastic hinges. When restraints against rotation are applicated, the yielding moment often is reached at a comparatively early stage of the fire exposure. It also should be noted that the rotations induced by the thermal gradients are required for a complete moment redistribution therefore can be greater than at ambient conditions. The performance of a fire-exposed hyperstatic structure, as concerns the conditions for a limit state stress distribution is very substantial when considering functional demands and structural fire safety problems. These problems will now be somewhat elucidated on the basis of the present study by some exemplifyings.

In the experimental investigation, 81 tests were carried out at various fire exposures and external load levels. Although the yielding moment was reached over the support in most tests at a comparatively early stage and consequently extreme rotations took place, within the support regions, however no failure occurred.

In all tests, the rotational capacity was sufficient for enabling the hyperstatic plate strips to survive a complete fire process. It is quite evident, that the rotational capacity and the deformability of a reinforced concrete structure on the whole increase considerably at elevated temperatures, but, as mentioned, also the need of rotation and stress redistribution. The calculations indicate that the test D16 has attained the greatest strains and rotations at support. Therefore this plate strip is of special interest to analyse further in terms of maximum total strains, stress-related strains and curvature. The maximum stress-related strain of concrete in compression was reached at the bottom surface, subslice No. 1, of segment (1) after 1 hour fire exposure, amounting to -3.3‰, which shall be compared with the total strain -5.1‰. At the same time, the curvature of this cross-section is evaluated to 0.31 m^{-1}. The simultaneous strain in the top reinforcement amounts to 29.4‰. Then, the stress-related strain successively decreases and amounts to -2.8‰ after 2.4 hours and -1.7‰ after 4.8 hours with the correspondent total strains -7.2 and -8.3‰, respectively. The tensile strain in the top reinforcement is at these times as much as 43 and 42‰, and the curvature 0.45 and 0.46 m^{-1}, respectively. These values illustrate a considerable deformability of the cross-section as influenced by a bending moment. From the test D22, it may be added that, although the sum of the moment capacity at the supports and in the field of the plate strip was almost exhausted, the rotational capacity was satisfactory, as failure did not occur.

Cross-sections influenced by a restraint bending moment as well as a restraint axial force as exemplified in section 6.2.4 for a plate strip with a simultaneous restraint against rotational and longitudinal movements at the supports show up a remarkable ability to redistribute the internal stresses.

The computations referred imply that the limit state approach may be justified to applicate in a determination of the load-carrying capacity of fire-exposed hyperstatic concrete beams and frames. For a final judging of this problem, further systematic investigations are necessary primarily more directly oriented against a detail study of the rotational capacity and the ultimate state behaviour.

The load-carrying capacity is determined for the hyperstatic plate strips cooled down to room temperature. This load-carrying capacity may be influenced by crack formation and chemical decomposition of the concrete at elevated temperature, altered properties of the reinforcement steel by yielding at high temperature. Additional stresses are then caused by restraint moments and forces. The load-carrying capacity is ascertained for the plate strips as simply supported, i.e. isostatic. This means that the bending moment capacity of the mid-section is decisive for the load-carrying capacity of the plate strip. In some cases the occurrence of shear failure also have to be considered. Built-in residual deformations and stresses may have little influence as the measured decrease in load-carrying capacity after cooling (see section 5.6) normally lies between 0 and 10%, which exceeds what is obtained in a simple theoretical calculation. In such a calculation the maximum temperatures are reconstructed and the ultimate strength of concrete is based on the rough assumption that the strength is invariant during cooling (cf. section 6.2.1.2). The accounted study doesn't give information about any possible influence of built-in restraint forces and moments on residual load-carrying capacity of the hyperstatic plate strip after cooling down to ambient conditions. However, in the opinion of the author, this influence is very limited or even insignificant, but further studies on the residual load-carrying capacity are needed in order to judge this statement.

7 ANALYTICAL PREDICTION MODELS AND A RATIONAL, THEORETICAL DESIGN OF FIRE-EXPOSED CONCRETE STRUCTURES

A reliable analytical prediction of the thermal response and the mechanical behaviour of fire-exposed concrete structures leads to the development of a rational fire engineering design, comprising simplified methods and systematical design diagrams and tables, facilitating the practical application. This paper will hopefully form a basis of and contribute to such a development. Essential components in such a rational design procedure are:

- Design principals:

  Functional demands and fire safety considerations, including a probabilistic determination of design load and design fire load density.
  Influence of detection, warning-communication and extinguishment systems.
- Determination of fire environment.

  Thermal exposure on interior and exterior structures.
- Thermal properties of materials at elevated temperatures.
- Determination of transient temperature fields of the structure.

  Influence of moisture transfer and vapourization.
- Mechanical properties of materials at transient elevated temperatures.
- Evaluation of design load-carrying capacity at fire.

  Sections influenced by bending moment and axial force.
  Interaction diagrams.
  Hyperstatic beams, frames, arches and plates. Consideration of restraint moments and forces. Use of limit state approach.
  Rotational capacity.
  Questions concerning shear, torsion, anchorage and bond at elevated temperatures.
  Instability problems, second order theory.
  Walls and high beams.
  Special problems in conjunction with prestressed concrete structures.
- Spalling. Estimation of risks and possible consequences of spalling under different conditions.
- Estimation of residual load-carrying capacity and residual state of stress and deformation.

8 SUMMARY AND CONCLUSIONS

The thermal and mechanical response of hyperstatic concrete structures under fire exposure conditions is studied both experimentally and theoretically. In the study differentiated fire processes, including the subsequent cooling phase, are considered and laboratory tests were performed under well-defined conditions.

In the first stage, the objective of the project was to derive computer models, which enable to predict the thermal and mechanical behaviour and the load-carrying capacity of hyperstatic, continuous beams and frames of reinforced concrete in fire environments. The validity of the computer programs for on one side the thermal analysis and on the other side the structural analysis should be confirmed by extensive comparisons with observed behaviour in a great number of tests in which the fire development as well as the lateral load are varied within a wide range. In a second stage, the aim was to present a thorough, functionally based understanding of the fire response of hyperstatic concrete structures to be used for practical purposes. This means that the present study may form a basis for a development of a rational design procedure of fire-exposed concrete structures.

The experimental part of the project is mainly focused on a fundamental study of a pure type of a hyperstatic structure, viz. a reinforced concrete plate strip thermally exposed on one side and restrained against rotation at both ends, while axial displacement is free to take place.

The experimental program embraces 81 tests divided into 6 different test series (A1, A2, A3, B, C and D). The tests are carried out at varying fire processes, concrete compositions (B and C), age of the specimens at testing (B and C) and lateral loads (D). All tests except those belonging to test series D are nil-loaded plate strips. For the tests in series D, the loading consists of two symmetrically placed transverse concentrated loads. Different combinations of the opening factor (0.01 - 0.08 $m^{1/2}$) and

the fire load density (31 - 2010 $MJ \cdot m^{-2}$) have determined the characteristic fire exposure, including the subsequent cooling phase.

The experimental investigation comprises a continuous registration of temperature-gradients, deformations, cracking formations and restraint bending moments. These measurements are carried through at a fire exposure merely and at a combined influence of a fire and lateral load respectively until the residual state after cooling is reached.

Furthermore the flexural stiffness during fire exposure was investigated for some nil-loaded plate strips by measuring the deflection response to an instantaneous application of a lateral load. As a complementary study on the residual state, the residual flexural rigidity and load-carrying capacity of the plate strips were determined about 5 months after the fire test. From that study a decrease was observed in the flexural stiffness and load-carrying capacity varying from 0 to 30% and 0 to 20% resepectively when the fire load density is in the range of 31 - 1000 $MJ \cdot m^{-2}$.

The evaluation of the thermal response is carried out by a finite element computer program, created from a program library consisting of a supply of permanent system routines and problem adapted routines, which must be constructed by the user. The program is formed for the one-dimensional case but can easily be extended to two dimensions. It can also solve axi-symmetrical problems and comprises various boundary conditions as prescribed heat flow, temperature and adiabatic state.

The program considers the temperature dependence of the thermal properties, viz. the thermal conductivity and the enthalpy even during cooling and the structure may consist of many different materials. The storage of program routines is constructed with wide possibilities and consequently general applications.

The prediction of the temperature distribution history for the

fire-tested concrete plate strips was in all cases in a good accordance with measurements during the heating as well as during the subsequent cooling phase. As the temperature-time fields serve as input in the structural analysis program, these have successfully contributed to further progress in the calculations of the mechanical response.

A theoretical study of the mechanical behaviour of concrete structures at fire is in a decisive manner dependent on a realistic material behaviour model of concrete as well as reinforcing steel. During the last years it has been found that data obtained on concrete at steady-state conditions cannot solely be used to predict the real behaviour during transient temperature circumstances. A realistic behaviour model of concrete, valid at transient states, has recently been developed at Lund Institute of Technology and is utilized in the presented computations. In this model described by a constitutive equation, the total strain is seen as the sum of four strain components derived on a purely phenomenological level. These components are:

Thermal strain, including shrinkage, measured on unstressed specimens under variable temperature.

Instantaneous stress-related strain, based on stress-strain curves obtained under stabilized temperature.

Creep strain, time-dependent strain recorded under constant stress at stabilized temperature.

Transient strain, stress-dependent and attributed to the effect of a virgin temperature increase.

Complete material behaviour models of concrete and steel taking into account the history of temperature and stress as well as any arbitrary process of unloading in the stress-strain diagram are also given in the paper.

The mechanical response is evaluated by a computer program separated from the thermal analysis program. This program is a reconstruction and further development of a computer program

("FIRES-RC") derived by Becker & Bresler at the University of California, Berkeley 1974 and written for a CDC-6400 Computer. The current version used on a Univac 1108 Computer can be seen as an extension and modification of the program constructed in Berkeley. The program is based on a non-linear, direct stiffness method of the structural analysis coupled with a time step integration. An iterative approach is used in finding the incremental changes in the deformed shape, which results in equilibrium between the external and internal forces. The new development of more realistic behaviour models of the structural materials, mentioned above, is an essential new contribution in the program.

The computer program is capable to evaluate the detailed structural behaviour of fire exposed reinforced concrete frames. The presented study is however limited to a structural member in accordance to the experimental investigation.

The calculations accounted for are referred to four different combinations of boundary conditions for the plate strip, viz.

(1) Complete rotational restraint at both ends and a free axial movement.

(2) Simply supported.

(3) Simply supported but restrained against axial movement.

(4) Complete restraint against rotation as well as axial movements at both ends.

The check of the validity of the analytical models is mainly related to five different groups of experimental tests with boundary conditions of type (1). Each group of the tests is characterized by its own fire exposure and various levels of the symmetrically applied transverse concentrated loads. Extensive comparisons with observed behaviour in terms of time-history of the bending restraint moment and the deflections have verified the analytical predictions. Furthermore, the simply supported plate strip, boundary condition type (2), without any static load is compared with an identical experimental test in order to further illustrate the validity.

The effect of an unintentional, small displacement of the reinforcing bars are looked upon. Also the significance of the material behaviour model of concrete at transient high temperature conditions is demonstrated. The flexural stiffness as function of time for a nil-loaded plate strip, boundary condition type (1), thermally exposed, is illustrated and checked against measurements. The agreement was found qualitatively good.

In an analytical study, the thermal exposure has to be modelled in an accurate way and the geometric discretization of the structure must be chosen with care. Furthermore, the material models are constructed less complex than the real performance. The validity of the simplifications made is justified by the good agreement obtained in the comparisons between the analytical results and the experimental data.

As a complement to the calculations described above, the influence of an axial restraint of the plate strip is investigated theoretically for the boundary conditions of type (3) and (4). These computations furthermore contributed to illustrate the influence of restraint forces and moments on the structural behaviour and the load-carrying capacity.

The present study illustrates the capability of the analytical models to predict a quite realistic fire response of hyperstatic concrete structures. This is in a decisive degree owing to the fact that realistic material behaviour models, valid under transient thermal exposures, have been used. Computer calculations may hopefully in a near future facilitate the development of a design concept of fire-exposed concrete structures, based on functionally requirements and performance criteria. Important components in such a rational design procedure is summarized in the paper.

Some general conclusions of the study are:

1. Material behaviour models based on experimental data, obtained at steady state conditions, applicated in the prediction of the structural response to fire of concrete structures result

in unrealistic great thermal restraint forces and moments (if less than the yield moment) and sometimes in an erroneous collapse state.

2. The material behaviour models and the computer model give a good prediction of the mechanical behaviour and load-carrying capacity at fire of iso- as well as hyperstatic reinforced concrete structures.

3. Thermal restraint forces never exceed 45% of the load-carrying capacity at ambient conditions, in analyzed fire-exposed hyperstatic concrete plate strips, axially restrained.

4. The influence of restraint forces and moments on the load-carrying capacity of a fire-exposed, hyperstatic concrete structure depends on the deformation capacity of concrete at high temperatures.

5. The current study indicates the limit state design to be applied as a consequence of the fact that in no test or calculation the rotation demand exceeded the rotation capacity. The same indication also has been noted previously by Gustaferro. For a gerenal conclusion, further studies are necessary.

6. From calculations and tests performed it seems to be justified to treat the thermal restraint forces and moments separated from those caused by an external load, as long as the yielding moment has not been reached at any cross-section. The sum of these components is approximately equal to the total forces and moments of the structure at fire.

REFERENCES

Alemo, J., The Effects of Imposed Deformations on the Behaviour of Loaded Concrete Structures. Division of Structural Mechanics and Concrete Construction, Lund Institute of Technology, Bulletin 53, Lund, 1976.

Anderberg, Y., Mörnstad, M. & Sjödahl, S., Grundläggande studium av statisk obestämd armerad betongkonstruktions beteende vid brandpåverkan. (A fundamental experimental study of the structural behaviour of a statically undeterminate reinforced concrete structure subjected to fire). Graduate work at Division of Structural Mechanics and Concrete Construction, Lund Institute of Technology, Lund 1969.

Anderberg, Y., Fire-Exposed Hyperstatic Concrete Structures. National Swedish Institute for Building Research, Document D1, Stockholm, 1973.

Anderberg, Y., Thelandersson, S., Stress and Deformation Characteristics of Concrete at High Temperatures. 1. General Discussion and Critical Review of Literature. Division of Structural Mechanics and Concrete Construction, Lund Institute of Technology, Bulletin 34, Lund, 1973.

Anderberg, Y., Pettersson, O., Thelandersson, S., Wickström, U., A Differentiated Design of Fire Exposed Concrete Structures. Presented at FIP VII Congress, New York, 1974.

Anderberg, Y., Thelandersson, S., "Stress and Deformation Characteristics of Concrete at High Temperatures. 2. Experimental Investigation and Material Behaviour Model", Lund Institute of Technology, Division of Structural Mechanics and Concrete Construction, Bulletin 54, Lund, 1976.

ASTM Committee E-20., Manual on the use of Thermocouples in Temperature Measurements, STP 470, 1970.

Becker, J., Bresler, B., "FIRES-RC, A Computer Program for the Fire Response of Structures - Reinforced Concrete Frames", University of California, Berkeley, Fire Research Group, Report No. UCB FRG 74-3, July 1974.

Bizri, H., Structural Capacity of Reinforced Concrete Columns Subjected to Fire Induced Thermal Gradients, University of California, Berkeley, Report No. UC SESM 73-1, January 1973.

Bernow, S., Kristoffersson, R. & Paulsson, B., Grundläggande studium av statisk obestämd armerad betongkonstruktions beteende vid brandpåverkan. (A Fundamental Experimental Study of the Structural Behaviour of Statically Undeterminate Reinforced Concrete Structure Subject to Fire). Graduate work at Division of Structural Mechanics and Concrete Construction, Lund Institute of Technology, Lund, 1972.

Carlson, C.C., Selvaggio, S.L. & Gustaferro, A.H., A Review of Studies of the Effects of Restraint on the Fire Resistance of re-stressed Concrete. Symposium on Fire Resistance of Prestressed Concrete (International Federation for Prestressing, F.I.P.). Braunschweig, Germany, 1965.

Christiansson, P., Minidator-Datalogg (Minicomputer-Datalogging), Division of Building Technology, Lund Institute of Technology, Oct. 1973.

Collet, Y., Conductivite Thermique du Materiau Beton. (Thermal Conductivity for Concrete). Groupe de Travail "Beton Leger de Structure" et "Comportement du Materiau Beton en Fonction de la Temperature", Avril 1975.

Denker, C., Isberg, B. & Lewis-Johnsson, T., Grundläggande studium av statisk obestämd armerad betongkonstruktions beteende vid brandpåverkan. (A Fundamental Experimental Study of the Structural Behaviour of Statically Undeterminate Reinforced Concrete Structure Subject to Fire). Graduate work at Division of Structural Mechanics and Concrete Construction, Lund Institute of Technology, Lund, 1970.

Ehm, H. & von Postel, R., Versuche an Stahlbetonkonstruktionen mit Durchlaufwirkung unter Feuerangriff. Symposium on fire resistance of prestressed concrete. (International Federation for Prestressing, F.I.P.). Braunschweig, June 1965, Wiesbaden-Bauverlag, 1966.

Ernstsson, H.E., Helgesson, L., Hjort, B. & Nohlin, I., Grundläggande studium av statisk obestämd armerad betongkonstruktions beteende vid brandpåverkan. (A Fundamental Experimental Study of the Structural Behaviour of Statically Undeterminate Reinforced Concrete Structure Subject to Fire). Graduate work at Division of Structural Mechanics and Concrete Construction, Lund Institute of Technology, Lund, 1971.

Evans, R.M., Marathe, M.S., Microcracking and Stress Strain Curves for Concrete in Tension. RILEM bulletin, No. 1, Jan. - Febr. 1968, pp 61-64.

FIP, Guides to Good Practice - FIP/CEB Recommendations for the Design of Reinforced and Prestressed Concrete Structural Members for Fire Resistance. FIP/1/1, June 1975.

Fischer, R., Über das Verhalten von Zementmörtel und Beton bei Höheren Temperaturen. Deutscher Asuschuss für Stahlbeton, Heft 214, 1970.

Gustaferro, A.H., Temperature Criteria at Failure. Fire Test Performance, ASTM STP 464, American Society for Testing and Materials, pp. 68-84, 1970.

Gustaferro, A.H., Abrams, M.S. & Sales, E.A.B., Fire Resistance of Prestressed Concrete Beams. Study C. Structural Behaviour during Fire Tests. Portland Cement Association, 1971.

Haksever, A., Rechnerische Untersuchung des Tragverhaltens von einfach statisch unbestimmten Stahlbetonrahmen unter Brandbeanspruchung. Technische Universität Braunschweig, Braunschweig, 1975.

Harmathy, T.Z., Thermal Properties of Concrete at High Temperatures. Journal of Materials, ASTM, Vol. 5, No. 1, March 1970.

Harmathy, T.Z., A New Look at Compartment Fires. Part 1, Fire Technology, Vol. 8, No. 3, August 1972 and Part 2, Fire Technology, Vol. 8, No. 4, November 1972.

Issen, L.A., Gustaferro, A.H. & Carlson, C.C., Fire Tests on Concrete Members: An Improved Method for Estimating Thermal Restraint Forces. Fire Test Performance, ASTM, STP 464, American Society for Testing and Materials, 1970, pp. 153-185.

ISO., "Fire Resistance Tests - Elements of Building Construction", International Standard 834, 1975-11-01.

Klingsch, W., Traglastberechnung thermisch belasteter Stahlbetondruckglieder unter Anwendung einer zwei- und dreidimensionalen Diskretisierung. Technische Universität Braunschweig, Braunschweig, 1975.

Magnusson, S.E., Thelandersson, S., "Temperature-Time Curves for the Complete Process of Fire Development. A Theoretical Study of Wood Fuel Fires in Enclosed Spaces", Acta Polytechnica Scandinavica, Ci 65, Stockholm, 1970.

Magnusson, S.E., Thelandersson, S., "Comments on Rate of Gas Flow and Rate of Burning for Fires in Enclosures", Lund Institute of Technology, Division of Structural Mechanics and Concrete Construction, Bulletin 19, Lund, 1971.

Magnusson, S.E., Thelandersson, S., "A Discussion of Compartment Fires", Fire Technology, Vol. 10, No. 3, August 1974.

Magnusson, S.E., Pettersson, O., Thor, J., "Fire Engineering Design of Steel Structures (Brandteknisk dimensionering av stålkonstruktioner)", Manual, issued by the Swedish Institute of Steel Construction, Stockholm, 1974 - English edition, Lund and Stockholm, 1976.

Paulsen, O., "On Heat Transmission in Fire Test Furnaces (Om varmeovergang i brandprøveovne)", Technical University of Denmark, Laboratory for Heat and Climate Technology, Copenhagen, 1975.

Pettersson, O., Brandteknisk dimensionering av spännbetongkonstruktioner (Fire Engineering Design of Prestressed Concrete Structures). Lecture given at Den Norkse Ingeniörförening, Oslo, 1971.

Pettersson, O., Principles of Fire Engineering Design and Fire Safety of Tall Buildings. ASCE-IABSE International Conference on Planning and Design of Tall Buildings, Lehigh University, Pa., August 21-26, 1972, Summary Report of Technical Committee 8. - Slightly modified and published as Bulletin 31, Division of Structural Mechanics and Concrete Construction, Lund Institute of Technology, Lund, 1973.

Pettersson, O., Theoretical Design of Fire Exposed Structures. Division of Structural Mechanics and Concrete Construction, Lund Institute of Technology, Bulletin 51, Lund, 1976.

Plem, E., Theoretical and Experimental Investigations of Point Set Structures. Swedish Council for Building Research, Document D9:1975, Lund, 1975.

Saito, H., Behaviour of End Restrained Concrete Member in Fire. BRI Research Paper, No. 32, March 1968.

Salse, E.A.B., Gustaferro, A.H., "Structural Capacity of Concrete Beams during Fires as Affected by Restraint and Continuity", 5th CIB Congress, Proceeding, Paris, 1971.

Selvaggio, S.L. & Carlsson, C.C., Effect of Restraint on Fire Resistance of Prestressed Concrete. Symposium on Fire Test Methods, ASTM STP 344, 1963, p. 1.

Selvaggio, S.L. & Carlsson, C.C., Restraint in Fire Tests of Concrete Floors and Roofs. Symposium on Fire Test Methods - Restraint and Smoke, ASTM STP 422, 1967, p. 21.

Stålhane-Pyk., Elektrovärmeinstitutet 1923-1933.

Thelandersson, S., Effect of High Temperatures on Tensile Strength of Concrete. Nordisk Betong 1972:2.

Thelandersson, S., "Concrete Structures at Elevated Temperatures (Betongkonstruktioner vid höga temperaturer - en översikt)", Lund Institute of Technology, Division of Structural Mechanics and Concrete Construction, Bulletin 43, Lund, 1974.

Thelandersson, S., Mechanical Behaviour of Concrete under Torsional Loading at Transient, High-Temperature Conditions. Division of Structural Mechanics and Concrete Construction, Lund Institute of Technology, Bulletin 46, Lund, 1974.

Thomas, P.H., "Some Problem Aspects of Fully Developed Room Fires", presented at Symposium on "Fire Standards and Safety", 5-6 April 1976, Washington, 1976.

Zoldners, N.G., Effect of High Temperatures on Concrete Incorporating Different Aggregates. ASTM Proceedings Volume 60, 1960.

Ödeen, K., Nordström, Å., Termiska egenskaper hos betong vid höga temperaturer. (Thermal Properties of Concrete at High Temperatures). Cement och Betong 1972:1, Stockholm.

MAIN SYMBOLS

Latin

a	constant	m
A	total area of the window and door openings	m^2
A_s	steel reinforcement area	m^2
A_t	total interior area of the surfaces bounding the fire compartment, opening areas included	m^2
b	constant	m
c_p	specific heat capacity	$MJ \cdot kg^{-1} \cdot {}^oC^{-1}$
E	elastic modulus	$MN \cdot m^{-2}$
E^*	strain hardening modulus	$MN \cdot m^{-2}$
EI	flexural stiffness	MNm^2
F	external heat flow vector	-
ΔH	activation energy of creep	$J \cdot mol^{-1}$
H	mean value of the heights of the window and door openings, weighed with respect to each individual opening area	m
H_ν	effective heat value of combustible material ν within the fire compartment	$MJ \cdot kg^{-1}$
I	moment of inertia	m^4
I_e	enthalpy	$MJ \cdot m^{-3}$
i	specific enthalpy	$MJ \cdot m^{-6}$
K	conductivity matrix	-
k_1	constant	${}^oC^{-1}$
k_2	diemnsionless constant	-
L	length of the plate strip	m
M	moment	kNm
m_ν	total weight of combustible material ν	kg
P	lateral concentrated load	kN
P_{all}	the allowable load at ambient conditions according to Swedish Concrete Standards	kN
P_1	wire forces	kN
p	vapour pressure	$kN \cdot m^{-2}$
p_1	dimensionless constant	-
Q	external heat generation per unit volume	$MJ \cdot m^{-3}$
q	heat transfer	$MJ \cdot m^{-2}$
R	gas constant	$J \cdot mol^{-1} \cdot {}^oKelvin^{-1}$
T	temperature	${}^oC$
t	time	hours

t_d	duration of heating phase	hours
t_r	constant	hours
u	moisture content	%
y	deflection	m
Z	defined in section 6.2.2.3	s^{-1}

Greek

β_o	dimensionless constant	-
α	coefficient of heat transfer	$W \cdot m^{-2} \cdot {}^oC^{-1}$
δ	deflection defined in Fig. 5.25	m
θ	temperature-compensated time	hours
θ_o	temperature-compensated time defined in Fig. 6.30	hours
θ_{im}	fictitious temperature-compensated time	hours
ε	total strain	‰
ε_{th}	thermal strain	‰
ε_σ	stress-related strain	‰
ε_{cr}	creep strain	‰
ε_{tr}	transient strain	‰
ε_u	ultimate strain at which $\sigma = \sigma_u$	‰
$\bar{\varepsilon}_u$	defined in equation 6.18	‰
ε_{crush}	crushing strain	‰
ε_1	strain at the transition point in the stress-strain relationship for concrete	‰
ε_o	permanent inelastic strain	‰
ε_u^t	ultimate tensile strain	‰
ε_{max}	maximum tensile strain	‰
ε_{crack}	strain at which carcking occurs	‰
ε_y	strain at which yielding occurs for steel	‰
ε_t	creep strain for steel	‰
ε_{to}	defined in section 6.2.2.3	‰
λ	thermal conductivity	$W \cdot m^{-1} \cdot {}^oC^{-1}$
ζ_s	coefficient of thermal expansion for steel	$^oC^{-1}$
ρ	density	$kg \cdot m^{-3}$
σ_{cube}	cube strength of concrete	$MN \cdot m^{-2}$
σ_u	ultimate compressive stress	$MN \cdot m^{-2}$
σ_u^t	ultimate tensile stress	
$\tilde{\sigma}$	stress history	-
σ_y	yield stress of steel	$MN \cdot m^{-2}$
ϕ	diameter	mm
$1/\rho_c$	curvature	m^{-1}

ρc_p	heat capacity	$MJ \cdot m^{-3} \cdot {}^oC^{-1}$
$\rho' c_p$	nominal heat capacity	$MJ \cdot m^{-3} \cdot {}^oC^{-1}$

Indices

c	concrete
s	steel
o	room temperature
x,y,z	directions

APPENDIX

A. Results from measurements

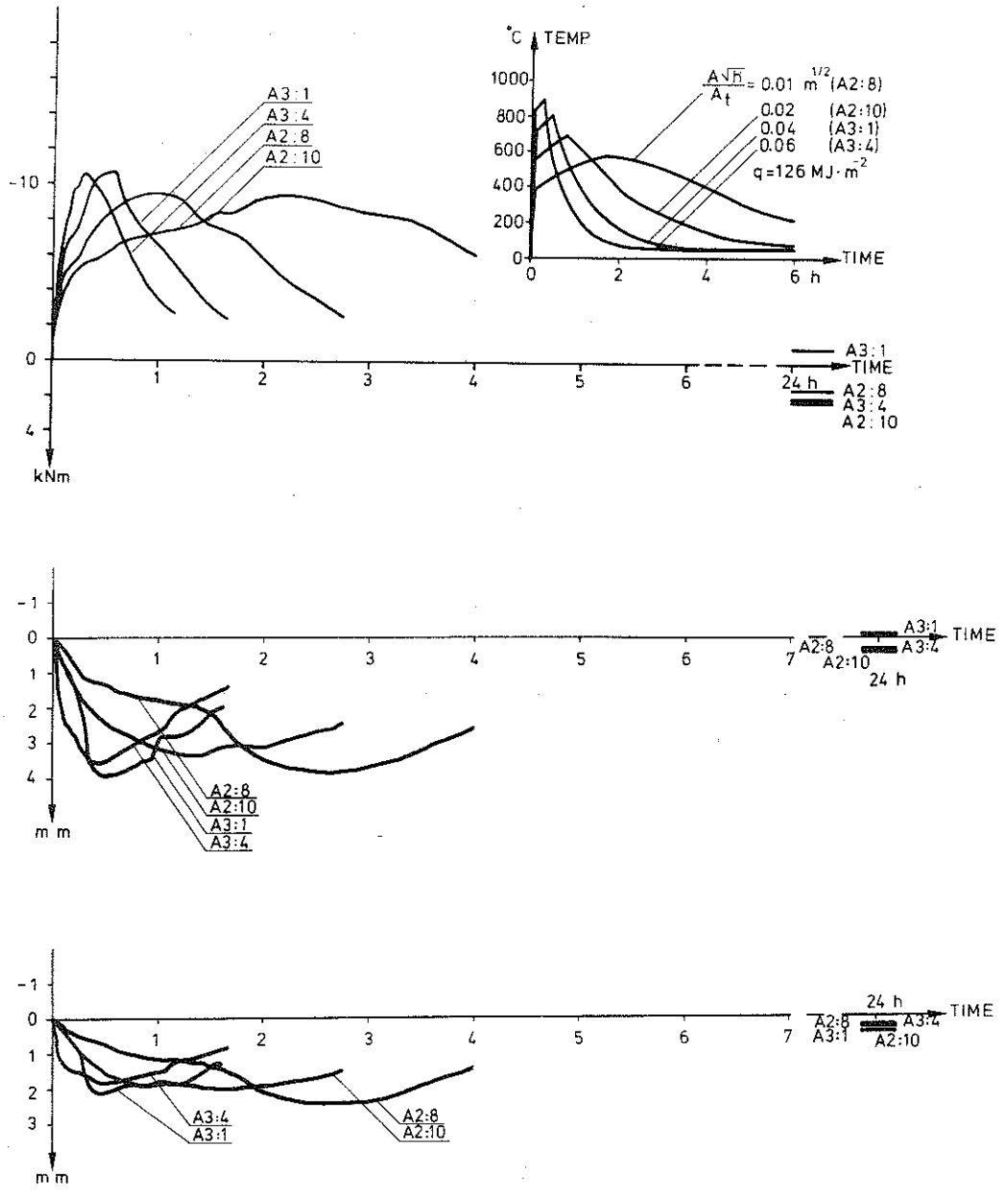

Figure A1 a) Bending restraint moment and deflection process at b) mid-section and c) 1/4-section. Fire load density 126 $MJ \cdot m^{-2}$. Opening factor within the range 0.01 - 0.06 $m^{1/2}$. The corresponding furnace temperature-time curves are inserted.

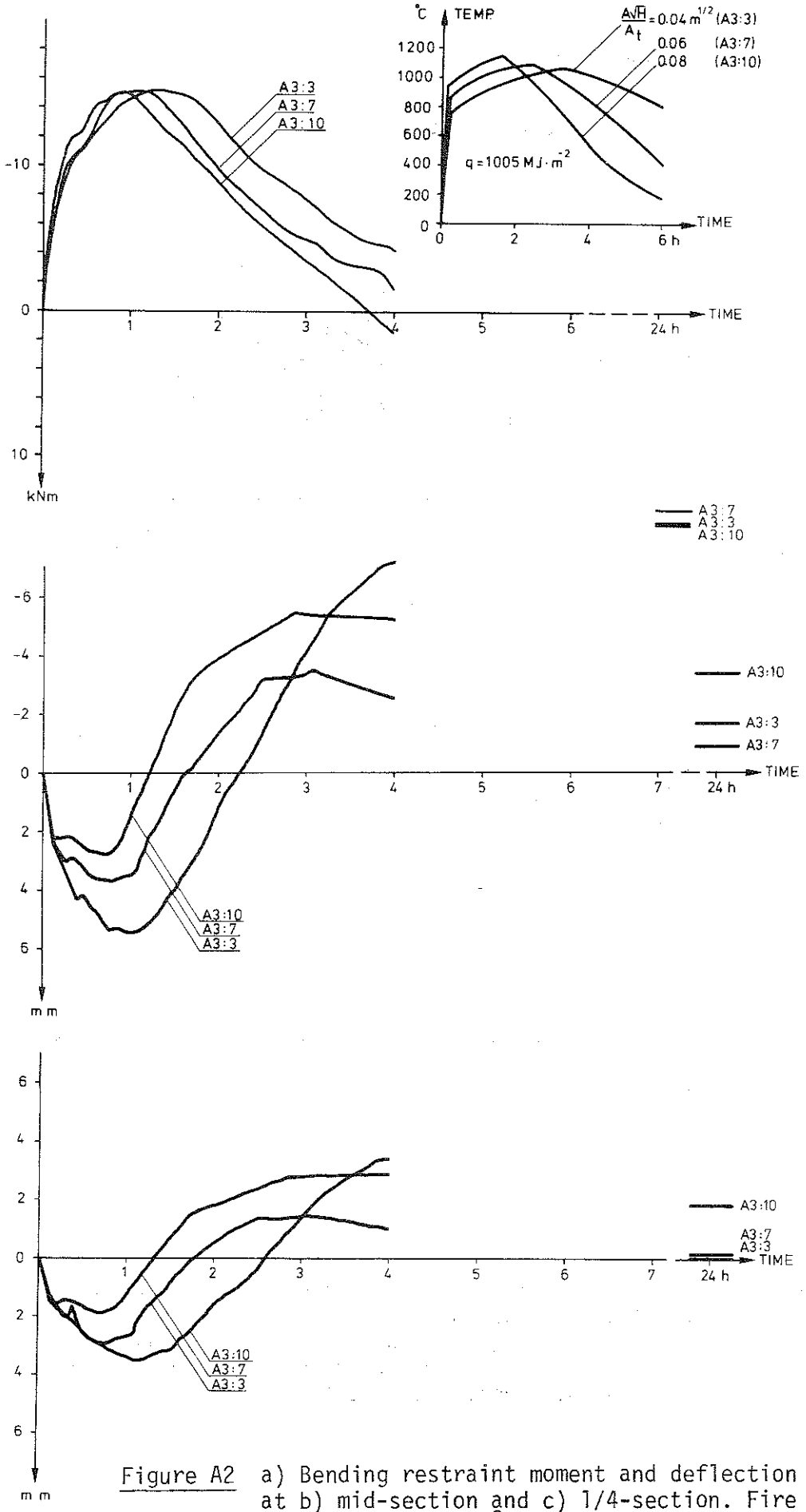

Figure A2 a) Bending restraint moment and deflection process at b) mid-section and c) 1/4-section. Fire load density 1005 $MJ \cdot m^{-2}$. Opening factor within the range 0.04 - 0.08 $m^{1/2}$. The corresponding furnace temperature-time curves are inserted.

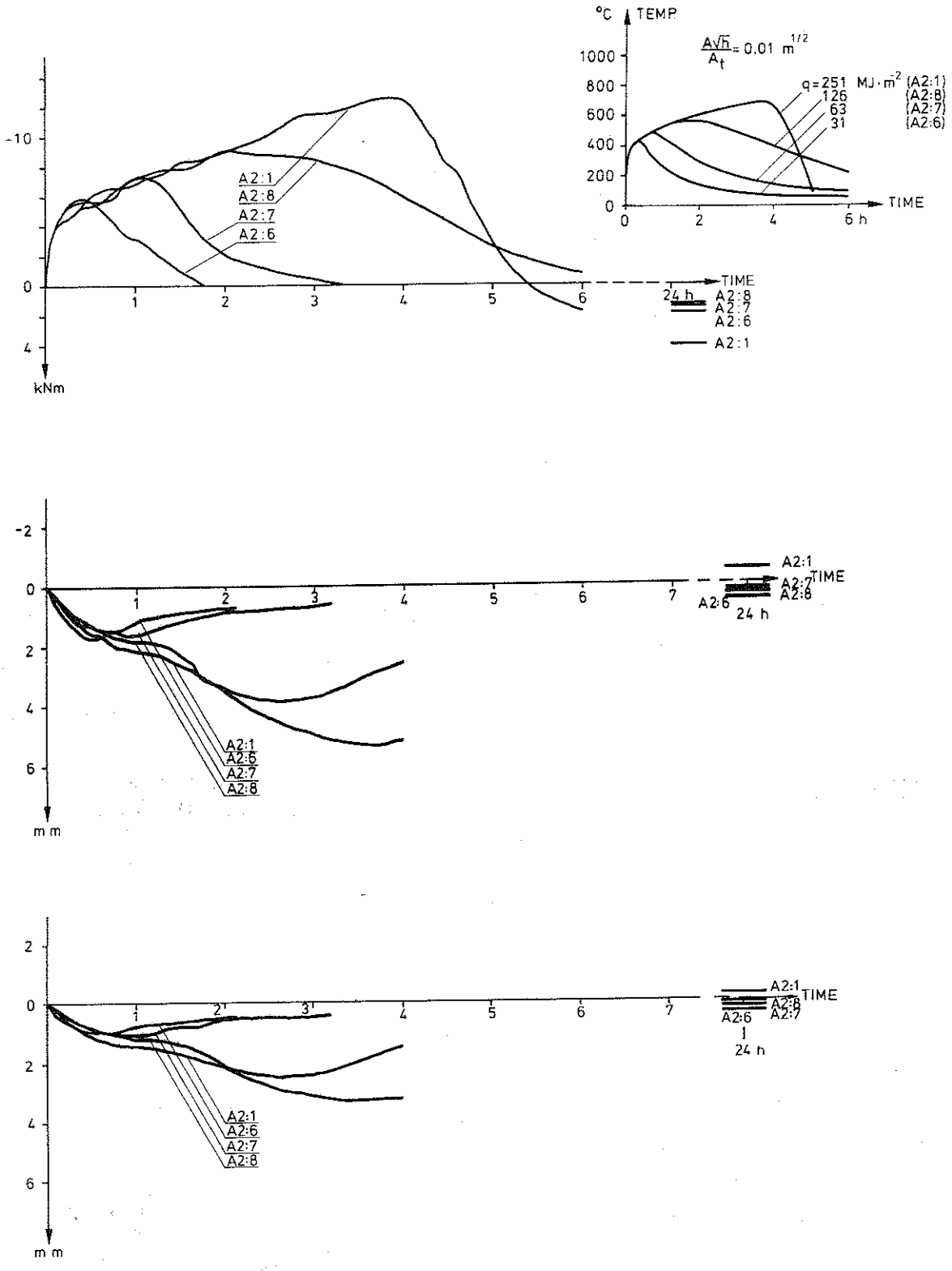

Figure A3 a) Bending restraint moment and deflection process at b) mid-section and c) 1/4-section. Opening factor 0.01 $m^{1/2}$. Fire load density within the range 31 - 251 $MJ \cdot m^{-2}$. The corresponding furnace temperature-time curves are inserted.

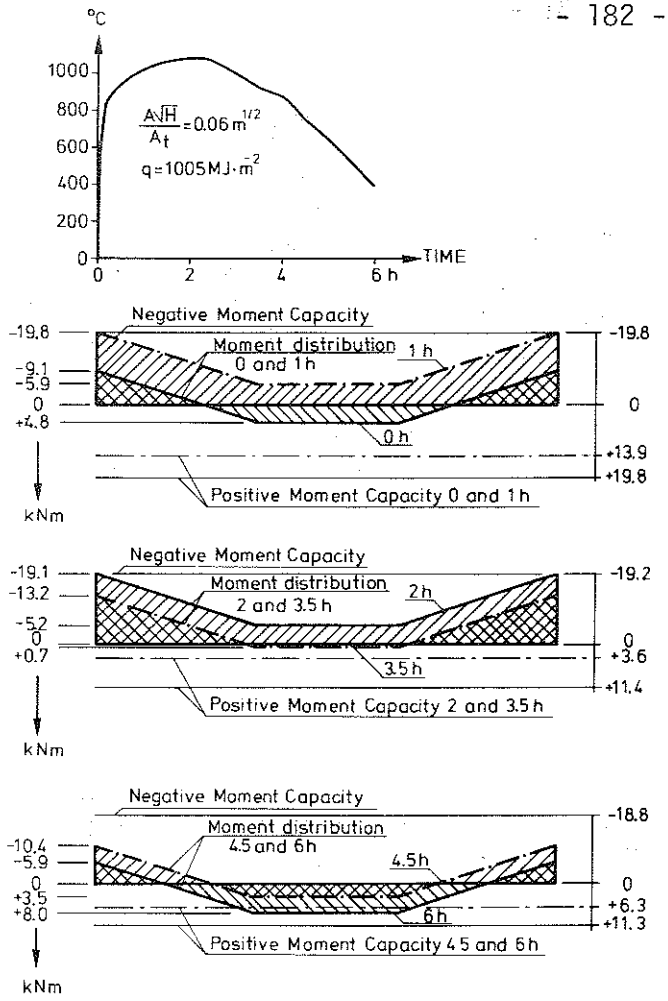

Figure A4 Bending moment distribution and bending moment capacity during fire exposure for the test D21. Fire load density 1005 MJ·m^{-2}. Opening factor 0.06 m$^{1/2}$. Load level : P = P_{all}. The corresponding furnace temperature-time curve is inserted.

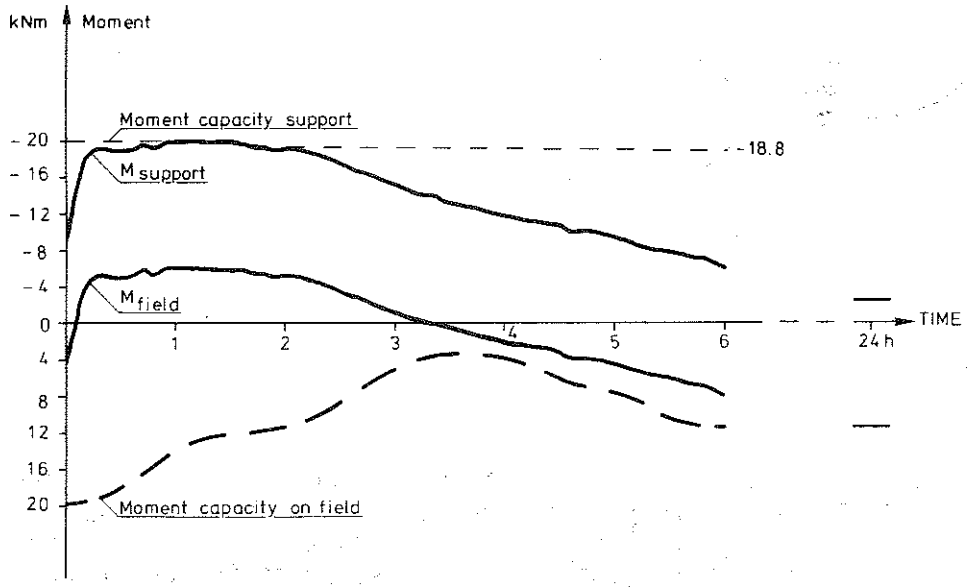

Figure A5 Time variation of current bending moment and calculated moment capacity at supports and in field for the test D21. See further Fig. A4.

B. Temperature calculations

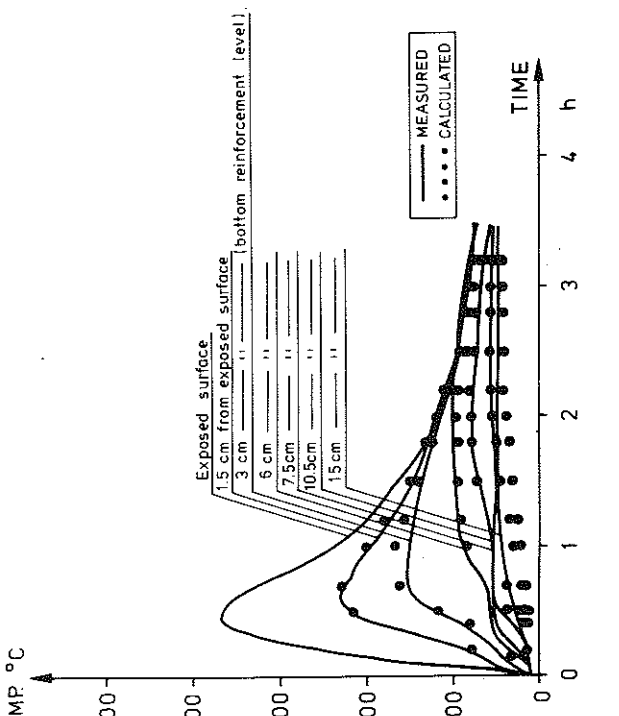

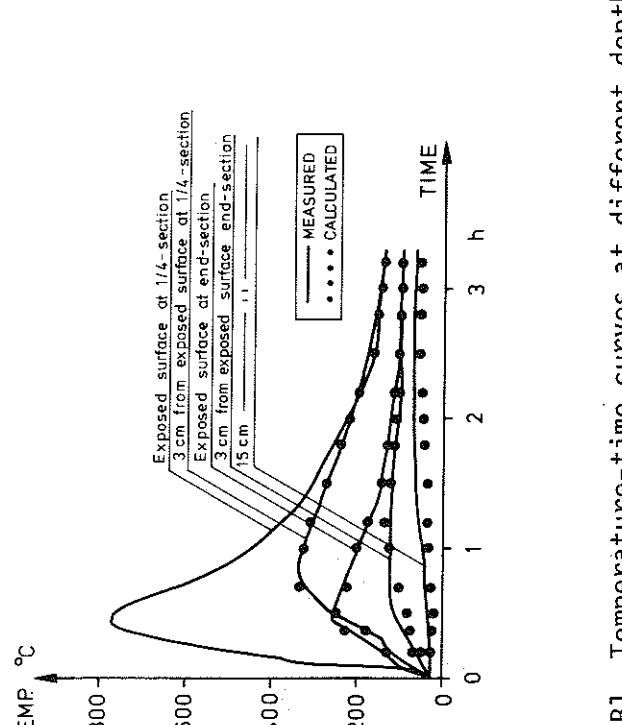

Figure B1 Temperature-time curves at different depths
Group 1 : Test A2:5
a) mid-section
b) 1/4-section.

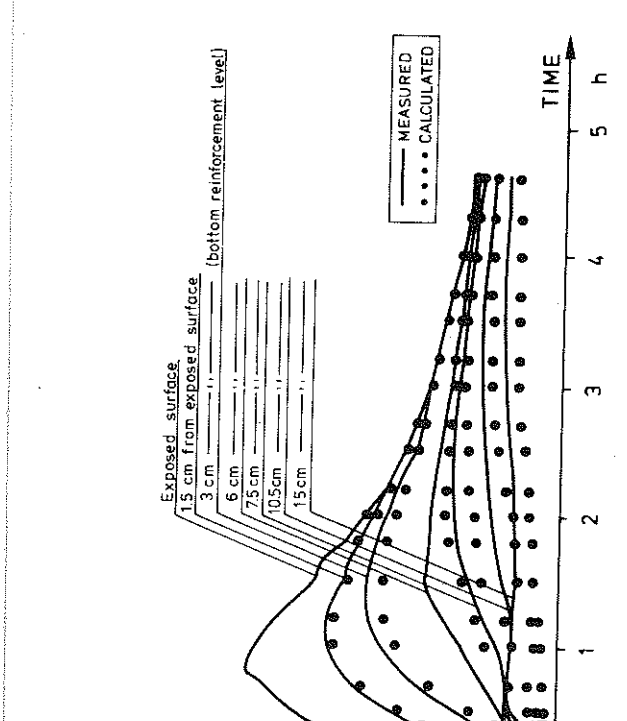

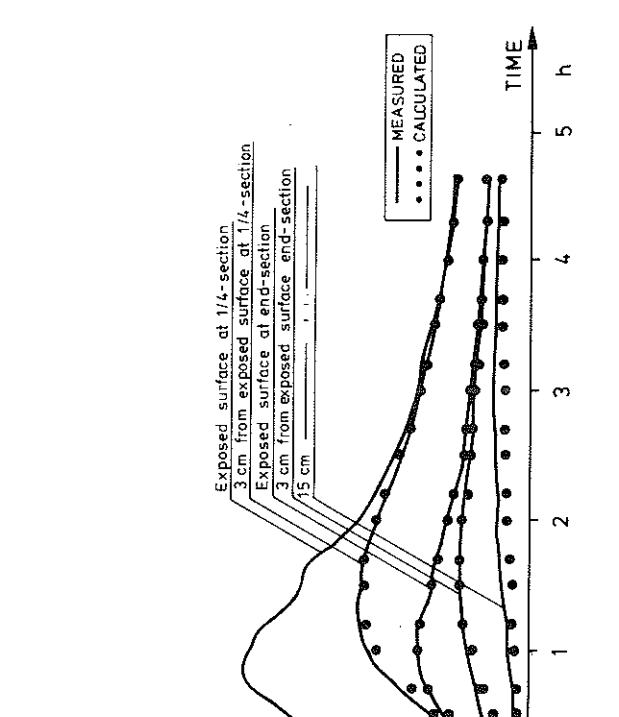

Figure B2 Temperature-time curves at different depths
Group 2 : Test A2:3
a) mid-section
b) 1/4-section.

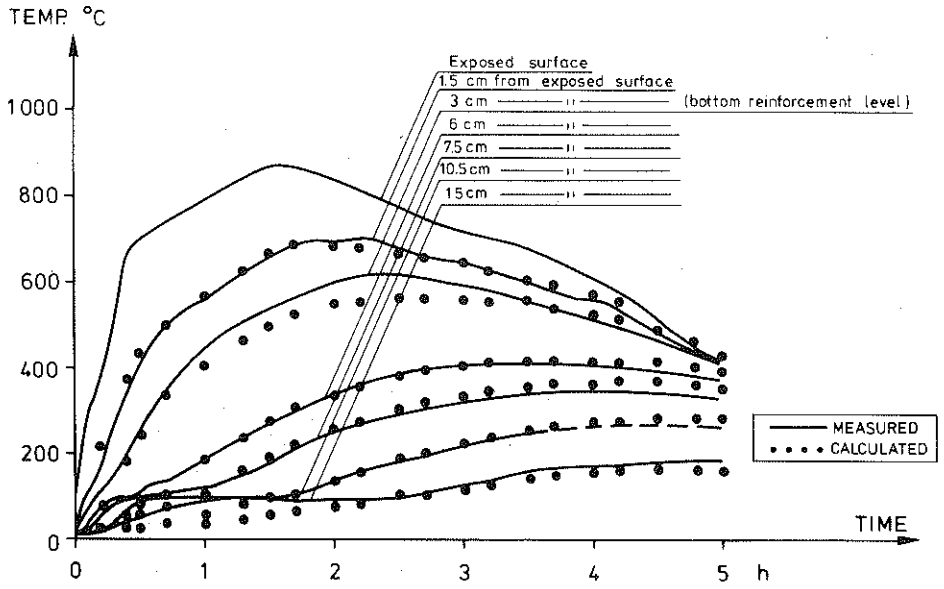

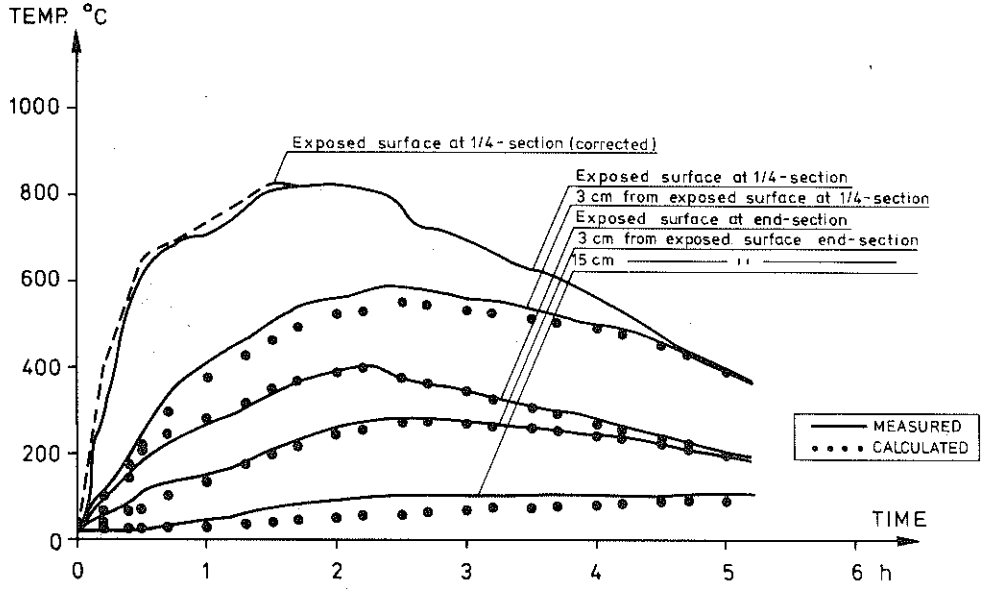

Figure B3 Temperature-time curves at different depths
Group 4 : Test D13
a) mid-section
b) 1/4-section.

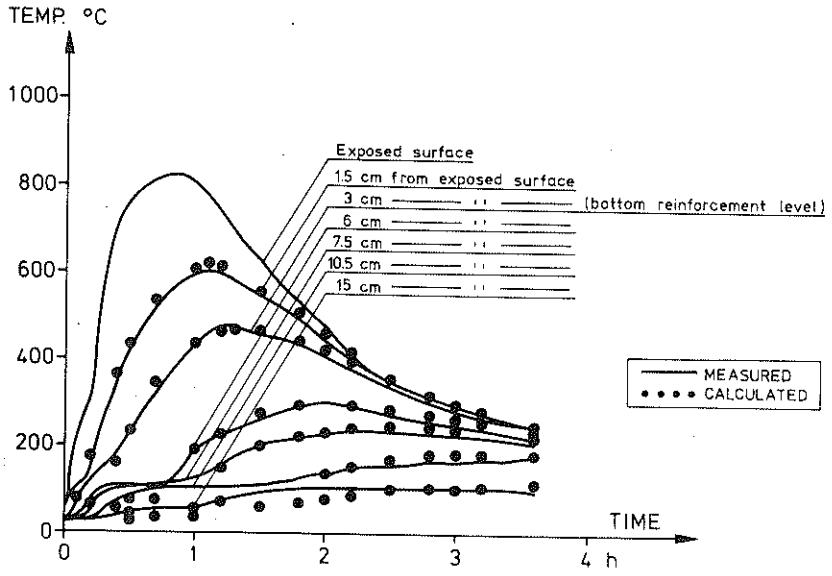

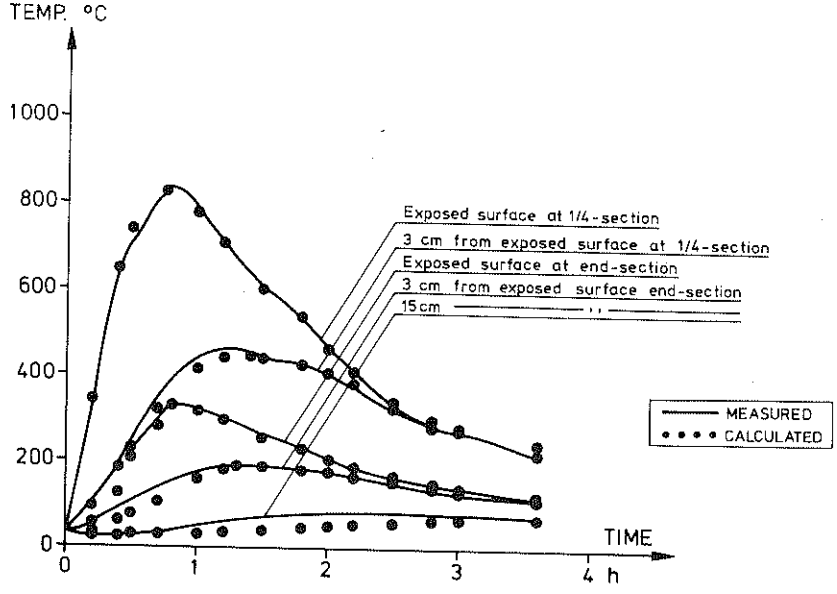

Figure B4 Temperature-time curves at different depths
Group 5 : Test D17
a) mid-section
b) 1/4-section.

C. SUBROUTINE IN FIRES-RC OVER THE STRESS-STRAIN RELATIONSHIP FOR CONCRETE

```
      FUNCTION STR(E,FC,EC,EO,FT,EMAX)
C
C
C     ELASTO-PLASTIC STRESS-STRAIN LAW ON BOTH COMPRESSION AND
C     TENSION SIDE INCLUDING UNLOADING.
C
C
C     COMPRESSIVE STRESS IS CALCULATED FROM A PARABOLIC STRESS-
C     STRAIN RELATION FOLLOWED BY A LINEAR DESCENDING BRANCH.
C
C     TENSILE STRESS IS CALCULATED FROM A TWOLINEAR RELATIONSHIP
C     INCLUDING A DESCENDING BRANCH.
C     UNLOADING BRANCH LEADS TO ORIGIN
C
C     E-STRESS RELATED STRAIN
C     FC-COMPRESSIVE STRENGTH
C     EC-INITIAL MODULUS
C     EO-INELASTIC STRAIN
C     ESTAR-SLOPE OF DESCENDING BRANCH
C     FT-TENSILE STRENGTH
C     EMAX-MAXIMUM TENSILE STRAIN
C
C     CALCULATE STRESS
C
      IF (E-EO-FT/EC.GE.0)  GO TO 116
      IF (E-EO) 120,100,105
  100 STR=0.0
      GO TO 155
C
C     TENSILE STRESS
C
C 105 STR=(E-EO)*EC
      GO TO 155
C
  116 C=0.4*10**-3
      IF (E.LE. C+EC)  GO TO 118
      STR=0.0
      GO TO 155
C
C     STRESS IS ON DESCENDING BRANCH OF STRESS-STRAIN CURVE
C
  118 STR=0.99*FT*((C-E+EO)/(C-FT/EC))
      IF(EMAX.LE.E)  GO TO 155
C
C     STRESS IS ON UNLOADING BRANCH OF STRESS-STRAIN CURVE
C
      STRU=0.99*FT*((C-EMAX+EO)/(C-FT/EC))
      STR=STRU*((E-EO)/(EMAX-EO))
      GO TO 155
C
C
```

```
C          COMPRESSIVE STRESS
C
      120  E1=FC/EC
           E1=E1+E1
           R=ESTAR/EC
           E2=E1*(1.0-R)
           DE=E+E2
           IF (DE) 130,130,140
C
C          STRESS IS ON ESTAR PROTION OF STRESS-STRAIN CURVE
C
      130  STR=FC*(1.0-R*R)
           STR=STR+ESTAR*DE
           GO TO 150
C
C          STRESS IS ON PARABOLIC PORTION OF STRESS-STRAIN CURVE
C
      140  B=0.5*EC/E1
           STR=EC+B*E
           STR=STR*E
C
C          CALCULATE LINEAR ELASTIC STRESS WITH ORIGIN AT EO
C
      150  S=EC*(E-EO)
C
C          IF UNLOADING CHOOSE LARGER STRESS
C
           IF (S.GT.STR) STR=S
C
C
           EO=MIN(EO,E-STR/EC)
      155  CONTINUE
           RETURN
           END
```